EMOTION REGULATION AND PROCESSING - EDITOR'S PICK 2021

EDITED BY: Nuno Sousa
PUBLISHED IN: Frontiers in Behavioral Neuroscience

frontiers Research Topics

frontiers

ISSN 1664-8714
ISBN 978-2-88971-172-7
DOI 10.3389/978-2-88971-172-7

About Frontiers

Frontiers is more than just an open-access publisher of scholarly articles: it is a pioneering approach to the world of academia, radically improving the way scholarly research is managed. The grand vision of Frontiers is a world where all people have an equal opportunity to seek, share and generate knowledge. Frontiers provides immediate and permanent online open access to all its publications, but this alone is not enough to realize our grand goals.

Frontiers Journal Series

The Frontiers Journal Series is a multi-tier and interdisciplinary set of open-access, online journals, promising a paradigm shift from the current review, selection and dissemination processes in academic publishing. All Frontiers journals are driven by researchers for researchers; therefore, they constitute a service to the scholarly community. At the same time, the Frontiers Journal Series operates on a revolutionary invention, the tiered publishing system, initially addressing specific communities of scholars, and gradually climbing up to broader public understanding, thus serving the interests of the lay society, too.

Dedication to Quality

Each Frontiers article is a landmark of the highest quality, thanks to genuinely collaborative interactions between authors and review editors, who include some of the world's best academicians. Research must be certified by peers before entering a stream of knowledge that may eventually reach the public - and shape society; therefore, Frontiers only applies the most rigorous and unbiased reviews.
Frontiers revolutionizes research publishing by freely delivering the most outstanding research, evaluated with no bias from both the academic and social point of view. By applying the most advanced information technologies, Frontiers is catapulting scholarly publishing into a new generation.

What are Frontiers Research Topics?

Frontiers Research Topics are very popular trademarks of the Frontiers Journals Series: they are collections of at least ten articles, all centered on a particular subject. With their unique mix of varied contributions from Original Research to Review Articles, Frontiers Research Topics unify the most influential researchers, the latest key findings and historical advances in a hot research area! Find out more on how to host your own Frontiers Research Topic or contribute to one as an author by contacting the Frontiers Editorial Office: frontiersin.org/about/contact

EMOTION REGULATION AND PROCESSING - EDITOR'S PICK 2021

Topic Editor:
Nuno Sousa, University of Minho, Portugal

Citation: Sousa, N., ed. (2021). Emotion Regulation and Processing - Editor's Pick 2021. Lausanne: Frontiers Media SA. doi: 10.3389/978-2-88971-172-7

Table of Contents

frontiers in Behavioral Neuroscience

ORIGINAL RESEARCH
published: 16 April 2019
doi: 10.3389/fnbeh.2019.00077

Intracerebroventricular Ghrelin Administration Increases Depressive-Like Behavior in Male Juvenile Rats

Thomas M. Jackson[1], *Tim D. Ostrowski*[2] *and David S. Middlemas*[1]*

[1]Department of Pharmacology, Kirksville College of Osteopathic Medicine, A.T. Still University of Health Sciences, Kirksville, MO, United States, [2]Department of Physiology, Kirksville College of Osteopathic Medicine, A.T. Still University of Health Sciences, Kirksville, MO, United States

Major depressive disorder (MDD) is arguably the largest contributor to the global disease and disability burden, but very few treatment options exist for juvenile MDD patients. Ghrelin is the principal hunger-stimulating peptide, and it has also been shown to reduce depressive-like symptoms in adult rodents. We examined the effects of intracerebroventricular (icv) injection of ghrelin on depressive-like behavior. Moreover, we determined whether ghrelin increased neurogenesis in the hippocampus. Ghrelin (0.2-nM, 0.5-nM, and 1.0-nM) was administered acutely by icv injection to juvenile rats to determine the most effective dose (0.5-nM) by a validated feeding behavior test and using the forced swim test (FST) as an indicator of depressive-like behavior. 0.5-nM ghrelin was then administered icv against an artificial cerebrospinal fluid (aCSF) vehicle control to determine behavioral changes in the tail suspension test (TST) as an indicator of depressive-like behavior. Neurogenesis was investigated using a mitogenic paradigm, as well as a neurogenic paradigm to assess whether ghrelin altered neurogenesis. Newborn hippocampal cells were marked using 5′-bromo-2′-deoxyuridine (BrdU) administered intraperitoneally (ip) at either the end or the beginning of the experiment for the mitogenic and neurogenic paradigms, respectively. We found that ghrelin administration increased immobility time in the TST. Treatment with ghrelin did not change mitogenesis or neurogenesis. These results suggest that ghrelin administration does not have an antidepressant effect in juvenile rats. In contrast to adult rodents, ghrelin increases depressive-like behavior in male juvenile rats. These results highlight the need to better delineate differences in the neuropharmacology of depressive-like behavior between juvenile and adult rodents.

Keywords: depression, ghrelin, intracerebroventricular, neurogenesis, juvenile

OPEN ACCESS

Edited by:
Gregg Stanwood, Florida State University, United States

Reviewed by:
Axel Steiger, Max-Planck-Institut für Psychiatrie, Germany
Devon L. Graham, Florida State University College of Medicine, United States

***Correspondence:**
David S. Middlemas
dmiddlemas@atsu.edu

Received: *24 December 2018*
Accepted: *28 March 2019*
Published: *16 April 2019*

Citation:
Jackson TM, Ostrowski TD and Middlemas DS (2019) Intracerebroventricular Ghrelin Administration Increases Depressive-Like Behavior in Male Juvenile Rats. Front. Behav. Neurosci. 13:77. doi: 10.3389/fnbeh.2019.00077

INTRODUCTION

Juveniles with depression manifest a different array of symptoms than adults, which is one significant reason that major depressive disorder (MDD) may be underdiagnosed in juveniles (Yorbik et al., 2004). It has been reported that approximately 2.5% of children and 9.8% of adolescents are diagnosed with MDD. Moreover, selective serotonin reuptake inhibitors have

efficacy in juvenile patients, whereas other classes of antidepressant drugs do not have demonstrated efficacy in juvenile patients (Hazell et al., 1995, 2002). The neuropharmacology of antidepressant drugs is clearly different in juvenile and adult patients.

Ghrelin is a peptide hormone that has been found to have an acute antidepressant effect in adult rodents (Carlini et al., 2012), which is correlated with an increase of hippocampal neurogenesis (Moon et al., 2009). In humans, some weak antidepressive effects of ghrelin in male depressed patients were reported (Kluge et al., 2011). Neurogenesis is a potential mechanism that could be involved in antidepressant drug action as antidepressant drugs have been shown to increase neurogenesis in adult rodents (Malberg et al., 2000). In adult rodents, neurogenesis is required for some of the antidepressant effects of antidepressant drugs such as imipramine and fluoxetine (Santarelli et al., 2003). Antidepressant drugs increase neurogenesis in the hippocampus of nonhuman primates (Perera et al., 2007). Also, an increase in the rate of hippocampal neurogenesis was observed in human progenitor cells treated with antidepressant drugs (Belmaker and Agam, 2008; Anacker et al., 2011).

Ghrelin has been recognized as the most potent endogenous stimulant of the hunger sensation (Bali and Jaggi, 2016). Recent studies have linked ghrelin to the etiology of depression, as treatment with ghrelin has been shown to decrease depressive-like symptoms related to anhedonia (Wang et al., 2015). Acute ghrelin administration has also been shown to reverse depressive-like behavior in adult rodents (Carlini et al., 2012). The receptors for ghrelin, the type 1a growth hormone secretagogue receptors, have been discovered to exist not only in the hypothalamus and pituitary, but also in the entire hippocampus (Hornsby et al., 2016). Treatment with ghrelin in adult rodents increased neuronal proliferation in the hippocampus by 50% (Moon et al., 2009).

Only selective serotonin reuptake inhibitors (SSRIs; one of five drug classes approved for treatment of depression in adults) have been demonstrated effective and only two are approved by the FDA to treat juvenile MDD. Considering the lack of antidepressant drugs available for juveniles, this study aimed to determine whether the brain-gut peptide ghrelin effectively reduces depressive-like symptoms in juvenile rats, as it does acutely in adult rodents (Carlini et al., 2012; Liu et al., 2015). In this study, we used behavioral testing to examine any changes in depressive-like behavior with the treatment of ghrelin. We also quantified hippocampal mitogenesis and neurogenesis to determine whether ghrelin influences the juvenile nervous system in the same way as the adult system.

MATERIALS AND METHODS

Experimental Design

Male juvenile Sprague-Dawley rats post-natal day (PND $<$ 18) were housed with their mothers in cages under regulated temperature (21 $\pm$ 1°C), humidity (46%), and light conditions (12 h light/dark cycle) at A.T. Still University's Kirksville College of Osteopathic Medicine (KCOM). Rats age PND 18–36 were housed individually. All care and procedures involving rats were approved by the KCOM Institution Animal Care and Use Committee (IACUC). The KCOM animal care program is accredited by the Association for Assessment and Accreditation for Laboratory Animal Care (AAALAC), has an assurance (Assurance Number A3058-01) with the Office of Laboratory Animal Welfare (OLAW), and has a license (Customer No. 1495, Registration No. 43-R-0012) from the U.S. Department of Agriculture (USDA). The KCOM animal care program also has an Occupational Health and Safety Program (OHSP) supervised by the IACUC.

The first set of rats (n = 24) was randomly divided into an artificial cerebrospinal fluid (aCSF) treated group (n = 6) and 200-pmol (n = 6), 500-pmol (n = 6), and 1-nmol (n = 6) ghrelin treated groups. All groups underwent the forced swim test (FST) at the end of the treatment cycles (PND 29) to assess the effects of the treatments on depressive-like behavior (Katz, 1982; Martínez-Mota et al., 2011). The second set of rats (n = 16) was divided into a fluoxetine (5-mg/kg) treatment group and a phosphate-buffered saline (PBS) control group. These rats were subjected to the tail suspension test (TST) to determine if the TST could successfully be used in juvenile rat studies. The third set of rats (n = 32) was randomly divided into a mitogenic paradigm group (n = 16) and a neurogenic paradigm group (n = 16). Each of these groups was further divided into an aCSF treated group (n = 8) and a ghrelin treated group (n = 8).

For the last set of rats, behavioral assessments were conducted 6 and 7 days prior to euthanasia. Each group underwent the FST (PND, 29) and the TST (PND 30; timelines, **Figure 1**) to assess the effects of the treatments. The mitogenic group received 5′-bromo-2′-deoxyuridine (BrdU) injections three times daily for 2 days, beginning the first day of behavioral assessment, as part of the preparation for newborn cell visualization. The neurogenic group received BrdU injections twice daily for 3 days, beginning the day of drug treatment, in preparation to visualize newborn neurons. Euthanasia occurred at PND 36. The rats were anesthetized with sodium pentobarbital, then euthanized by thoracotomy, jugular exsanguination, and transcardial perfusion. Death was confirmed by respiratory and cardiac system cessations. At PND 36, the brains were removed and frozen; then, 30 μm slices were made using a cryostat (Leica CM 1900). Immunohistochemistry of brain slices was performed using primary antibodies for BrdU (for both mitogenic and neurogenic paradigms) and NeuN (for the neurogenic paradigm), with fluorescently labeled secondary antibodies excited at 594 and 488-nm, respectively. Brain slices were examined using a confocal microscope to identify differences in the number of BrdU positive cells in the hippocampal dentate gyrus for the mitogenic paradigm group and differences in colocalization of BrdU and NeuN in the neurogenic paradigm group.

Ghrelin Administration Protocol

Acyl-ghrelin (0.2-nM, 0.5-nM, and 1.0-nM; Abbiotec, San Diego, CA, USA) dissolved in (aCSF: 123-mM NaCl, 1.14-mM $CaCl_2$,

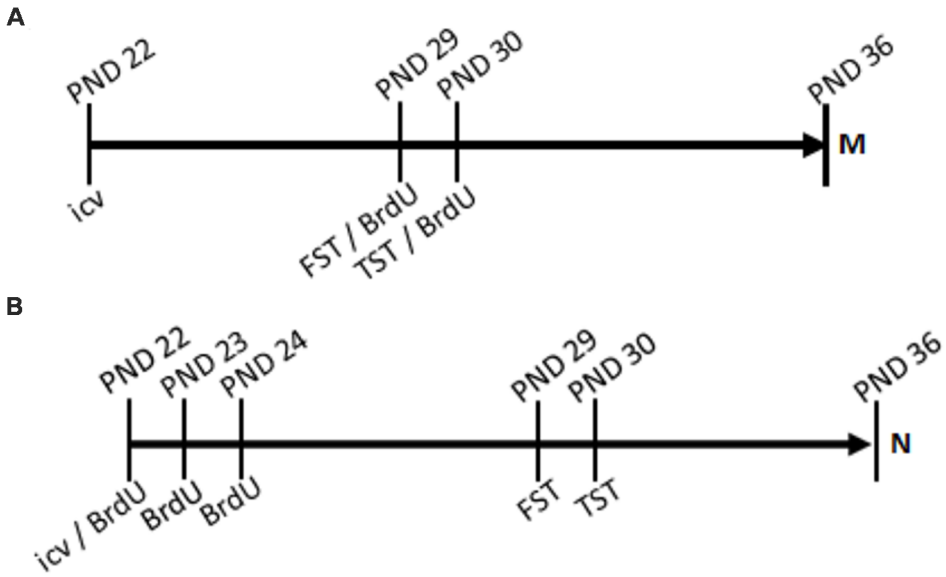

FIGURE 1 | Timelines. Treatment of ghrelin or artificial cerebrospinal fluid (aCSF) control was administered by intracerebroventricular (icv) injection acutely at post-natal day 22 (PND 22). In the mitogenic paradigm **(A)**, 5′-bromo-2′-deoxyuridine (BrdU) was administered by intraperitoneal (ip) injection three times daily for two consecutive days, PND29 and PND30. In the neurogenic paradigm **(B)**, BrdU was administered twice daily for three consecutive days, PND22, PND23, and PND24.

3.03-mM KCl, 1.90 -mM $MgCl_2$, 25.0-mM $NaHCO_3$, 0.50-mM NaH_2PO_4, 0.25-gmM Na_2HPO_4) was administered by icv injection via stereotaxic surgery. Rats (PND 21) were fasted overnight prior to surgery (for the dose response experiment), and they were anesthetized with isoflurane (5%; Piramal Group, Mumbai, India) prior to surgery (PND 22; **Figure 1**). Dexamethasone (2-mg/kg, s.q.; AuroMedics Pharma, LLC, Dayton, NJ, USA) was administered to the rats to prevent immunological responses that could cause the brain to swell. The rats were then placed in a stereotaxic frame (David Kopf Instruments, Tujunga, CA, USA) with ear bars to hold the head in a stable position, and isoflurane was reduced to 2% for maintenance of anesthetization. The skull was exposed, and, using an atlas of stereotaxic coordinates (Khazipov et al., 2015) and a p21 juvenile rat brain map, the lateral ventricles were located at 0.9-mm posterior and 1.5-mm lateral (on each side) from Bregma, and 3.6-mm deep from the surface of the brain. This was the site of injection with ghrelin or aCSF (control). Following closure of the incision, rats were injected with baytril (7-mg/kg, i.m.; Norbrook Laboratories, Down, Northern Ireland) to prevent infection, buprenorphine (50-μg/kg, s.q.; Reckitt Benckiser Pharmaceuticals, Richmond, VA, USA) to manage pain, and saline (2-mL, 0.9%, s.q.; Hospira, Inc., Lake Forest, IL, USA) to restore physiologic fluid balance (DeVos and Miller, 2013). Treatment occurred on PND 22, and the rats were caged individually and allowed to recover until PND 29, when they began to undergo behavioral assessment.

Feeding Behavior Test

Food was withheld for 8 h prior to ghrelin injection. Thirty minutes after recovery from anesthesia, all animals had food available *ad libitum*. Food intake was the difference between the weight of food given and the food left prior by weight after a 2 h period.

Forced Swim Test

A modified version of the FST was used to determine the behavioral effect of each injection and therefore the effectiveness of the target agent (acyl-ghrelin) as a potential antidepressant (Lucki, 1997; Porsolt et al., 1977; Borsini and Meli, 1988). Rats underwent the FST 1 week after the treatment with ghrelin, on PND 29 (1 week before euthanasia). Behaviors were assessed in the FST to determine each rat's change in behavior following treatment. The efficacy of the interventions was demonstrated by an increase in the time spent swimming and/or climbing and a decrease in time spent immobile (Reed et al., 2008) compared to the aCSF vehicle control group. Swimming behavior was characterized by actively maneuvering around the container. Climbing behavior was characterized by moving the forepaws against the wall of the container in an effort to escape. Immobility behavior was characterized by floating and only making the movements necessary to keep the head above water and prevent drowning. An increase in the time spent immobile (lack of physical effort to survive) was an indicator of hopelessness, a behavioral symptom that is characteristic of a depressive state. An increase in the time spent immobile was an indicator of depressive-like behavior, as this was indicative of the characteristic depressive symptom of hopelessness (lack of physical effort to survive).

Fluoxetine Protocol

Fluoxetine (5-mg/kg; Sigma Aldrich, St. Louis, MO, USA) dissolved in PBS was administered by intraperitoneal (ip)

injection to the hypogastric region. Fluoxetine is one of only two antidepressant drugs (the other being escitalopram) that is FDA approved for treatment of depression in juvenile patients. Behavioral tests with fluoxetine were used as a positive control for observing an antidepressant effect.

Tail Suspension Test

On PND 30 (1 day after the FST, and 6 days before euthanasia), we performed the TST. In the TST, we employed a short-term stressor—suspension by the tail via surgical tape—to assess the long-term behavioral effect of the administered ghrelin. Suspension by the tail occurred for 6 min at a time, and any struggle by the rat to escape was considered unperturbed, "non-depressed" behavior. Attempts to escape were characterized by the rat moving its feet as if to run away, attempting to climb its tail to the site of suspension, twisting and swinging to try and free itself from the tape, and scratching or biting the tape to try and free its tail. Immobility—when the rat hung limply, making no effort to escape the stressor—was considered depressive-like behavior (Steru et al., 1985). Immobility time was counted visually in 1-min intervals over the course of the 6-min test. An increase in time spent immobile was indicative of the depressive-like symptom of anhedonia, or a state of hopelessness (Carlini et al., 2012). The effectiveness of the intervention was assessed as less time spent immobile by the ghrelin (or fluoxetine)-treated group than by the aCSF (or PBS) control group.

BrdU Administration Protocol

BrdU is a thymidine analogue that incorporates into the DNA during the synthesis phase of the cell cycle. Thus, it marks newborn cells and is used as a label for mitogenesis (Taupin, 2007). Rats received i.p. injections of BrdU (Sigma-Aldrich, St. Louis, MO, USA) dissolved in PBS (11.9 mM phosphates, 137 mM sodium chloride, 2.7 mM potassium chloride; Fischer Scientific, Houston, TX, USA; Wojtowicz and Kee, 2006). These injections were administered at a fixed volume of 5 μL/g three times daily for two consecutive days, beginning the day of the FST (PND 29–30) for the mitogenic paradigm group, and for the neurogenic paradigm group, rats received the BrdU injections at a volume of 2.5 μL/g twice daily for three consecutive days, beginning the day of drug treatment (PND 22–24; **Figure 1**). Since the process of neurogenesis takes approximately 5 to 7 days to occur, the neurogenic group received BrdU earlier in the treatment schedule so that the neurons visualized would be the differentiated newborn cells whose DNA was traced by BrdU upon proliferation.

Transcardial Perfusion

The brains of the rats were collected using the transcardial perfusion protocol as described by Wojtowicz and Kee (2006). The rats were anesthetized by IP injection of 50 mg/kg of sodium pentobarbital (PND 36). We determined complete anesthetization by observing corneal, foot withdrawal, and tail squeeze reflexes. Once complete anesthetization was determined, the rats were then sacrificed. The thoracic wall was bluntly dissected to expose the heart. A needle was injected into the left ventricle, and the jugular veins were severed to allow an outflow of fluids. The brains were then flushed via transcardial perfusion with 35 mL of PBS. Then, the brains were perfusion-fixed with 35 mL of 4% paraformaldehyde in PBS. Once the brains were removed, they were weighed and subsequently placed in 4% paraformaldehyde for 24 h. We then transferred the brains to a vial of 30% sucrose and PBS solution for 3 days or until they sank to the bottom of the vial (van Praag et al., 2005). Finally, the brains were frozen by placing them on dry ice (Sartori et al., 2004) and then were stored at −80°C.

Stereotaxic Slicing Protocol

Whole brains were sliced into 30 μm coronal sections using a cryostat (Leica CM 1900) set at a temperature of −22°C. The brains were sliced through the dentate gyrus of the hippocampus. Prior to slicing, we used the Atlas of the Postnatal Rat Brain in Stereotaxic Coordinates (Khazipov et al., 2015) for orientation purposes. A total of 96 slices were obtained for each rat brain, slices were stored at 4°C in PBS with 0.1% sodium azide, and every 12th slice was used for immunohistochemistry (eight slices).

Immunohistochemistry

Newly differentiated (newborn) neurons in the dentate gyrus of the dorsal hippocampus were identified by immunohistochemistry. Fluorescent antibodies allowed us to visualize cells containing BrdU and NeuN (a neuronal nuclear marker; Wojtowicz and Kee, 2006). BrdU was administered to mark newborn cells; NeuN is an endogenous protein present in neuronal nuclei. The assay for BrdU and NeuN allowed for the visualization of newborn cells and those that had differentiated into neurons. The brain slices were washed in PBS three times for 5 min each. Brain slices were then incubated in 1-M hydrochloric acid at 45°C for 1 h. Then, the brain slices were washed six times, for 5 min each, with PBS and incubated in a blocking solution (PBS, 0.3% Triton X-100, 2% equine serum; Invitrogen Corporation, Carlsbad, CA, USA) for 1 h. Once the blocking solution was removed, the brain slices were placed in a 1:4,000 solution of primary antibody (rat anti-BrdU, Batch No. 1015, Bio-Rad Laboratories, Hercules, CA, USA; mouse anti-NeuN, Lot #2950736, EMD Millipore Corporation, Temecula, CA, USA) in blocking solution. The slices were then incubated for 24 h at 4°C. Brain slices were washed three times for 5 min each with PBS, and they were then incubated with secondary antibodies (Alexa Fluor 594 donkey anti-rat, Lot# 1870948, Invitrogen, Carlsbad, CA, USA; Alexa Fluor 488 goat anti-mouse, Lot #1834337, Invitrogen, Carlsbad, CA, USA) diluted at 1:1,000 in PBS with 0.3% Triton x-100 for 2 h. Slices were washed three times for 5 min each in PBS and then mounted with Permount Toluene Solution (Lot #155508, Fisher Scientific, Waltham, MA, USA) onto microscope slides.

Confocal Microscopic Imaging

Newborn neuron survival was assessed using confocal microscopy (Leica DMI 6000B confocal laser scanning microscope). Colocalization of the signal from BrdU and NeuN constituted neurogenesis. We analyzed colocalized fluorescence using the Leica LAS Advanced Fluorescent software. Visual

thresholds were set for $BrdU^+$ (red) and $NeuN^+$ (green) signals; the overlap two signals (white), represented cells positive both for BrdU and NeuN.

Data Analysis

One-way ANOVA tests with Tukey post-tests were used to determine whether there was a difference in the feeding behavior test and the FST. To determine whether a change in immobility time was correlated with a change in mitogenesis or neurogenesis, a two-tailed Pearson product-moment correlation coefficient was performed. Analysis of all experiments comparing aCSF control and ghrelin treatment groups was performed using an unpaired two-tailed *t*-test. *P*-values < 0.05 were considered significant. Data were analyzed using GraphPad Prism software.

RESULTS

Tail Suspension Test Validation

The TST is a behavioral test that has been used exclusively in mouse studies. To determine whether or not the TST could be used to measure depressive-like behavior in juvenile rats, we used fluoxetine as a positive control; fluoxetine is one of two FDA-approved antidepressant treatments for human juveniles. It was found that the fluoxetine-treated group spent less time immobile in the TST than the saline control group (data not shown, $p < 0.05$, Mean $\pm$ SD; control 92 $\pm$ 1.2, Fluoxetine 71 $\pm$ 7.2). Showing that fluoxetine produced a measurable effect validated that the TST can be used to assess depressive-like behavior in juvenile rats. This was contrasted to Fluoxetine in the FST in juvenile rats ($p > 0.05$, Mean $\pm$ SD; control 18 $\pm$ 32, fluoxetine 7 $\pm$ 8). This led to using the TST in the mitogenic and neurogenic experiments, as the TST has less variability in young adolescent rats then the FST.

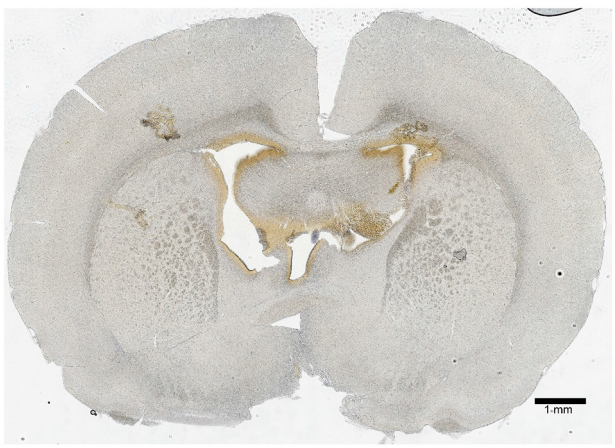

FIGURE 2 | Icv injection validation. A 50-μm coronal section 0.9-mm posterior from Bregma was imaged to show the site of icv injection. The lateral ventricles were located 1.5-mm lateral from Bregma (on both sides), and the injection was made at a depth of 3.6-mm from the surface of the brain. The hole-like structures in the central region of the section show the ventricle system, and the brown coloration is residue from a tryptophan blue control injection. The scale bar represents a length of 1-mm of brain tissue.

Intracerebroventricular Injection Validation

A PND 21 brain map (Paxinos and Watson) was used initially to approximate the location of the lateral ventricles; then, the surgery was performed with injection of tryptophan blue in aCSF to visualize the locations of injection (brown stain; **Figure 2**). It was determined that the proper stereotaxic coordinates for icv injection of PND 22 rats were 0.9-mm posterior and 1.5-mm lateral (both sides) from Bregma, and 3.6-mm deep from the surface of the brain.

Ghrelin Dose-Response on a Feeding Behavior and the Forced Swim Tests

To determine the most effective dose of ghrelin, a feeding behavior test and the FST were performed. Four groups were treated with 0, 0.2, 0.5-nM, and 1 nM ghrelin respectively (**Figure 3**, $p = 0.02$). From this result, it was determined that the 0.5-nM concentration was the most effective dose of acyl-ghrelin for eliciting the hunger sensation. In the FST, the 0.2-nM ($p < 0.0001$) and 0.5-nM ($p = 0.008$) groups demonstrated significant increases in immobility time (**Figure 4**). Contrary to adult rodents, treatment with ghrelin in juvenile rats did not yield changes indicative of an antidepressant-like effect.

Also, there was no significant difference in both feeding behavior and immobility time in the FST among the 1-nM group; perhaps this was due to desensitization of ghrelin receptors. Therefore, the 0.5-nM concentration was used throughout the remainder of the experiments.

To assess whether injection of ghrelin had a lasting effect on feeding behavior, the change in weight of the juvenile rats from the day of icv injection surgery (PND 22) to the day

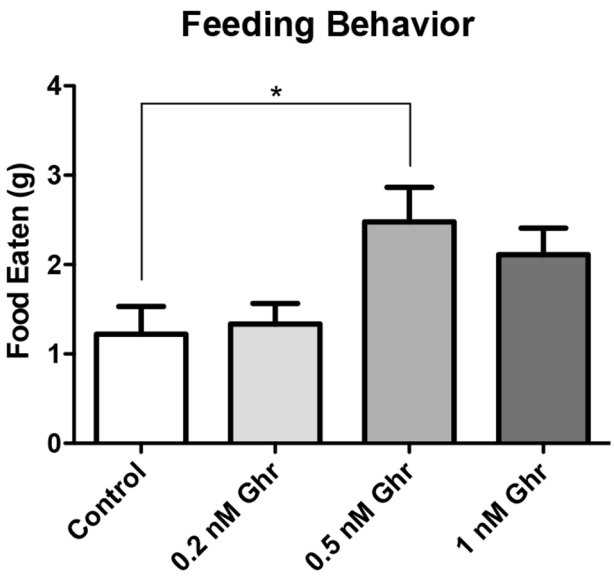

FIGURE 3 | Dose response: feeding behavior test. Weight of food consumed within 2 h following recovery from anesthetization (PND2). Values expressed as mean + SEM (one way ANOVA, $p = 0.02$, Tukey's Multiple Comparison Test, $^*p < 0.05$).

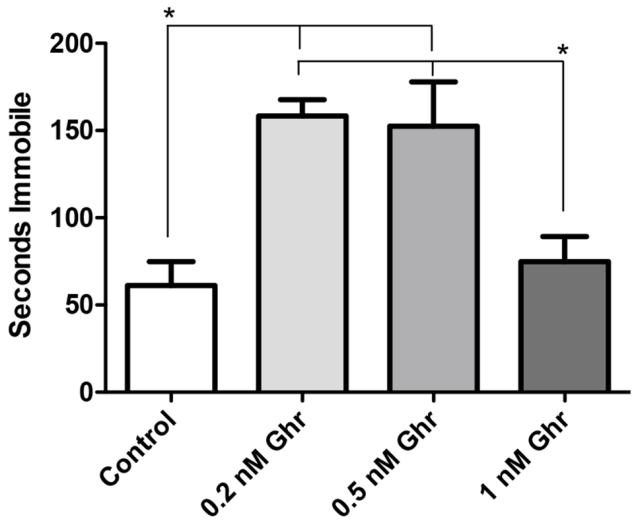

FIGURE 4 | Dose response: forced swim test (FST). Time spent immobile in the FST. Values expressed as mean + SEM (one way ANOVA, $p < 0.01$), Tukey's Multiple Comparison Test, $^*p < 0.05$.

of behavioral testing (PND 29) was compared between the control and ghrelin treated groups (**Figure 5**). Also, curves were generated to depict the progression of rat weights every 2 days from PND 22 to PND 29 (**Figure 5**). It was found that there was no significant difference between control and ghrelin ($p = 0.4724$) in terms of weight change. Also, the weight curves were virtually parallel, indicating that the only difference between ghrelin and control rats was the average weights per group, a difference consequent of randomized placement into groups. This analysis demonstrated that the acute effect of ghrelin—the stimulation of the hunger sensation and therefore the drive to consume food—did not persist beyond the time period between icv injection and the end of the feeding behavior test, and furthermore did not affect long-term feeding behavior of the rats. Also, the half-life of acyl-ghrelin is approximately 29 min (Akamizu et al., 2004), which is yet another indication that the acute effect of ghrelin would not be present beyond the day of administration.

TST and Mitogenesis

To quantify any changes in the proliferation of neural stem cells in the dorsal hippocampal dentate gyrus, BrdU was injected 7 and 8 days after ghrelin administration to determine if ghrelin altered the basal mitogenic rate (**Figure 1**). We performed

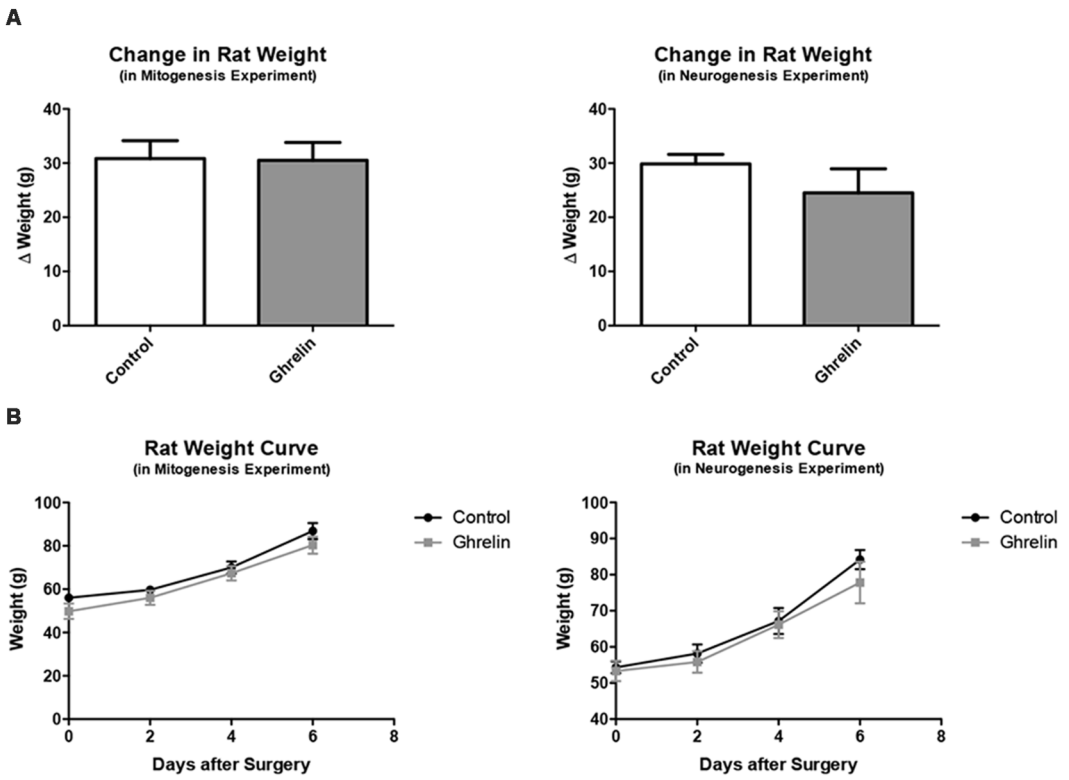

FIGURE 5 | Rat weights for mitogenesis experiment. **(A)** For the mitogenesis and neurogenesis experiments, we compared the change in weights from the day of surgery (PND 22) to 1 week following surgery (PND 29) for both the control ($n = 6$) and ghrelin treated ($n = 6$) groups **(A)**. Values are expressed as mean ± SEM ($p > 0.05$). **(B)** We also compared the weights of control and ghrelin-treated groups every 2 days from the day of surgery to 1 week following surgery (two way repeated measures ANOVA, $p > 0.05$).

immunohistochemistry and visualized coronal sections of rat brains using confocal microscopy. Cells positive for BrdU (newly proliferated neural stem cells) appeared red; cells positive for NeuN (neurons) appeared green; with the overlay of the two signals, cells that were positive for both BrdU and NeuN (newborn neurons) appeared white. The TST showed that ghrelin-treated rats spent more time immobile than aCSF vehicle-treated rats (p = 0.04; **Figure 6A**). There was no significant difference in mitogenesis (quantity of newly formed cells in the hippocampal dentate gyrus) between the control and 0.5-nM ghrelin treatment groups (p = 0.74; **Figure 6B**). There was also no correlation with a linear regression line between the TST immobility time and mitogenesis (**Figure 6C**; control p = 0.46, ghrelin p = 0.63). These results demonstrated that ghrelin did not increase hippocampal mitogenesis; so, treatment with ghrelin did not yield changes indicative of an antidepressant-like effect.

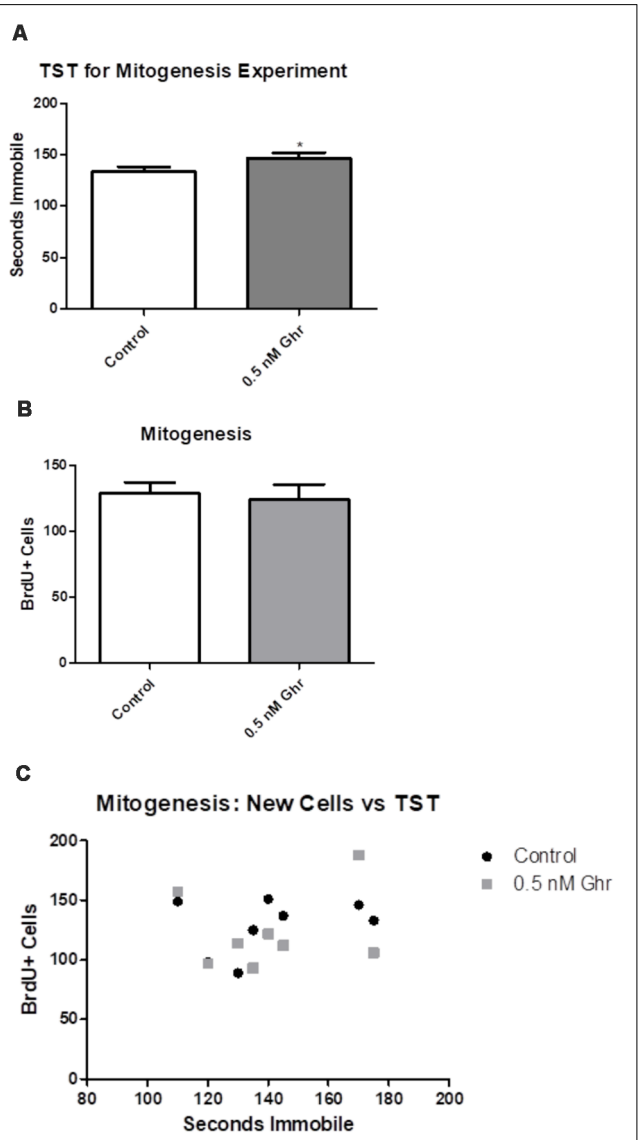

FIGURE 6 | Mitogenesis and the tail suspension test (TST). Behavioral tests as conducted for the mitogenic paradigm. **(A)** TST for the mitogenic paradigm. Values expressed as mean + SEM (*$p < 0.05$). **(B)** Number of cells that contained BrdU, as quantified using confocal microscopy. Values expressed as mean + SEM (*$p < 0.05$). **(C)** Linear comparison of the TST to the number of BrdU positive cells.

TST and Neurogenesis

To quantify any changes in neurogenesis in the hippocampal dentate gyrus, BrdU was injected initially in the neurogenic paradigm to assess if there was a difference in neurogenesis (**Figure 1**). We performed immunohistochemistry and visualized coronal brain sections using confocal microscopy (**Figure 7**); we also assessed behavior in the TST. The TST showed that ghrelin-treated rats spent more time immobile than the aCSF vehicle-treated rats (p = 0.04; **Figure 8A**). There was no significant difference in the neurogenic ratio (percentage of newly formed hippocampal cells that differentiated into neurons) between the control and 0.5-nM ghrelin treatment groups (**Figure 8B**; p = 0.67). There was also no correlation with a linear regression line between the TST immobility time and neurogenesis (**Figure 8C**; control p = 0.30, ghrelin p = 0.73). These results indicated that treatment with ghrelin did not yield changes in the hippocampus indicative of an antidepressant-like effect.

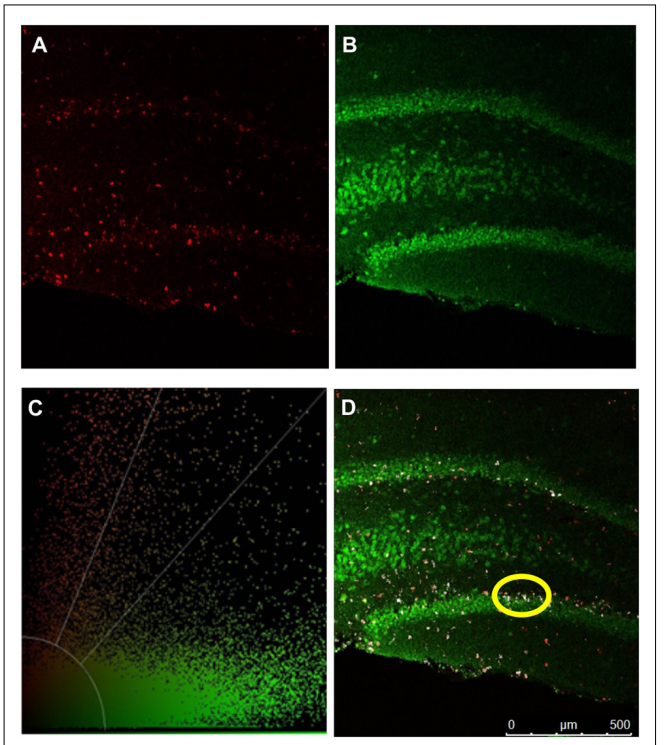

FIGURE 7 | Confocal microscopy. Confocal microscopy was used to quantify mitogenesis and neurogenesis in the hippocampal dentate gyrus. IHC detection of BrdU and NeuN are depicted in pseudocolored images. **(A)** BrdU positive cells (red). **(B)** NeuN positive (green) cells. **(C)** Threshold of color intensities. **(D)** An overlap of **(A,B)**. Cells that have colocalized signal from both BrdU labeling and NeuN expression are depicted in white (example circled in yellow).

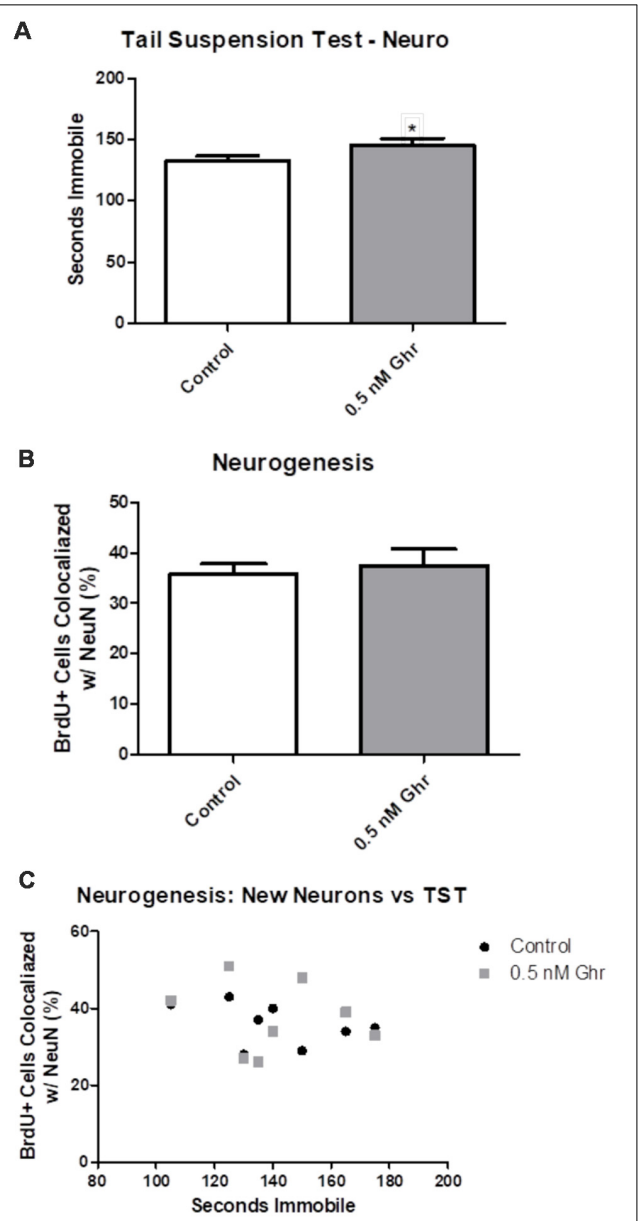

FIGURE 8 | Neurogenesis and the TST. **(A)** TST for the neurogenic paradigm. **(B)** Number of cells that contained both BrdU and NeuN, as quantified using confocal microscopy. **(C)** Linear comparison of the TST to the percentage of BrdU positive cells that were co-localized with NeuN. Values expressed as mean + SEM (*$p < 0.05$).

DISCUSSION

Ghrelin is a hunger-stimulating brain-gut peptide that has been implicated as a potential antidepressant in studies involving adult rodents. In adult rodent studies, acute treatment with ghrelin was shown to decrease depressive-like behavior, indicated by decreases in immobility time in behavioral tests. Treatment with ghrelin was also shown to increase hippocampal mitogenesis (neural precursor cell proliferation) and neurogenesis in adult rodents. It is hypothesized that immobility time in the FST mimics the depressive-like behaviors of despondency and anhedonia (Marks et al., 2009). However, we found that acute icv administration of ghrelin increased depressive-like behavior in male, juvenile rats using the FST. Moreover, this finding was reproduced using the TST, that icv administration of ghrelin increases depressive-like behavior in male juvenile rats.

Although acute administration of ghrelin in adult rats has antidepressant effects (Carlini et al., 2012), chronic infusion over weeks increases depression-like behavior in adult rats (Hansson et al., 2011). Ghrelin is involved in activation of the HPA axis, which correlates with the increase in depressive-like behavior observed with chronic ghrelin infusion (Spencer et al., 2015). There are also other methods for chronic central administration of ghrelin (Choi et al., 2013). We have found that a single administration of ghrelin increases depressive-like behavior a week later in juvenile rats. Sustained effects like this on emotional behavior are not unprecedented. Single administration of either ketamine or brain-derived neurotrophic factor have long-lasting antidepressant effects in rats (Hoshaw et al., 2005; Browne and Lucki, 2013). It will be interesting to further explore the acute and chronic effects of ghrelin in a juvenile rat model, and especially to determine if the effects of ghrelin are long lived.

The TST revealed an increase in immobility time in the ghrelin-treated group, as compared to the control group. The TST was validated in juvenile rats using fluoxetine, which is predicted to be an antidepressant drug in juvenile rats using the FST (Yoo et al., 2013). Fluoxetine produced a significant decrease in depressive-like behavior in the TST. As an increase in immobility time in the TST is an indicator of increased depressive-like behavior (Cryan et al., 2005), these experiments demonstrated that treatment with ghrelin increases depressive-like behavior in juvenile rats. This is contrary to the effect of ghrelin in adult rodents, where it has been shown to decrease depressive-like behavior (Carlini et al., 2012; Wang et al., 2015). These differences may be attributable to developmental differences in neural pathways related to the mechanism of action of antidepressant drugs. The norepinephrine system, for example, is not fully developed in rats until sexual maturation is achieved—at about PND 49 (Bylund and Reed, 2007; Sengupta, 2013). The norepinephrine system is necessary in the mechanism of action of nearly all classes of antidepressants—the serotonin-norepinephrine reuptake inhibitors, the tricyclic antidepressants, the monoamine oxidase inhibitors, and the atypical antidepressants. The only class that does not function through the noradrenergic system, the selective serotonin reuptake inhibitors, are notably the only antidepressant drugs that effectively reduce depressive symptoms in juvenile patients. Indeed, the only two antidepressant drugs that are FDA approved for treatment of juveniles, fluoxetine and escitalopram, are selective serotonin reuptake inhibitors. It is hypothesized that many antidepressant drugs work in adults but not in juveniles because the serotonergic system develops before the noradrenergic system, and most antidepressant drugs function through noradrenergic stimulation (Murrin et al., 2007). This could also explain the developmental difference seen in the effect of ghrelin on depressive-like behavior and

on hippocampal mitogenesis and neurogenesis since it has been shown that many effects of ghrelin are produced through alpha-1 and beta-2 stimulation of the noradrenergic system (Date et al., 2006).

Antidepressant-like activity of drugs in adult rodents is correlated with increased hippocampal mitogenesis (David et al., 2009) and Ghrelin has been found to increased mitogenesis in adult mice (Moon et al., 2009). However, we found that treatment with ghrelin did not alter mitogenesis in the hippocampal dentate gyrus in male, juvenile rats. There was no significant difference between the control group and the ghrelin-treated group in terms of the number of new cells formed in the hippocampal dentate gyrus. Moreover, we found that there was also no significant difference between the control and ghrelin-treated groups on juvenile rat hippocampal neurogenesis. This investigation focused on the dorsal hippocampus because previous work revealed chronic fluoxetine treatment of juvenile male rats increased mitogenesis. However, there is evidence that ghrelin-mediated feeding behavior may involve the ventral hippocampus (Kanoski et al., 2013). These results are opposite the observations in adult rodent studies. Ghrelin increased mitogenesis and neurogenesis in adult rodents, but it did not affect mitogenesis or neurogenesis in juvenile rats.

Based on previous studies demonstrating that acute icv administration of ghrelin had antidepressant effects in adult rats, and moreover, increased hippocampal neurogenesis, we hypothesized that administration of acyl-ghrelin to juvenile rats would also have an antidepressant effect and increase hippocampal neurogenesis. However, our findings indicate just the opposite, that ghrelin increases depressive-like behavior in juvenile rats. This is more in line with the effects of chronic ghrelin infusion in adult rats over weeks, where ghrelin increases depression-like behavior (Hansson et al., 2011). Using the FST, ghrelin did not have an antidepressant-like effect in juvenile rats, as there was an increase in depressive-like behavior in the dose-response experiment. Also, using the TST, ghrelin was demonstrated to actually have increased depressive-like behavior in juvenile rats; that is, there was an increase in immobility time among the ghrelin-treated rats. There were no significant differences in cell proliferation or the generation of new neurons, respectively, in the hippocampal dentate gyrus. This further demonstrated that ghrelin, unlike the selective serotonin reuptake inhibitors, does not increase hippocampal neurogenesis in male, juvenile rats. It will be interesting to test whether the chronic ghrelin administration decreases hippocampal neurogenesis. These results highlight the urgent need to better understand the differences between depression in juveniles and adults in order to develop better treatment options for juvenile patients with MDD.

ETHICS STATEMENT

All care and procedures involving rats were approved by the KCOM Institution Animal Care and Use Committee (IACUC). The KCOM animal care program is accredited by the Association for Assessment and Accreditation for Laboratory Animal Care (AAALAC), has an assurance (Assurance Number A3058-01) with the Office of Laboratory Animal Welfare (OLAW), and has a license (Customer No. 1495, Registration No. 43-R-0012) from the US Department of Agriculture (USDA). The KCOM animal care program also has an Occupational Health and Safety Program (OHSP) supervised by the IACUC.

AUTHOR CONTRIBUTIONS

TJ completed most of the experiments under collaborative supervision by TO and DM.

FUNDING

This study was supported by an Institutional Graduate Program Committee grant (850-617) and a Warner Fermaturo grant (501-501) from AT Still University.

ACKNOWLEDGMENTS

We would like to thank Dr Yingzi Chang and Dr William Sexton; the ATSU-KCOM Graduate Program Committee; and Erica Stanley and Zhiping Jia.

REFERENCES

Akamizu, T., Takaya, K., Irako, T., Hosoda, H., Teramukai, S., Matsuyama, A., et al. (2004). Pharmacokinetics, safety and endocrine and appetite effects of ghrelin administration in young healthy subjects. *Eur. J. Endocrinol.* 150, 447–455. doi: 10.1530/eje.0.1500447

Anacker, C., Zunszain, P. A., Carvalho, L. A., and Pariante, C. M. (2011). The glucocorticoid receptor: pivot of depression and of antidepressant treatment?. *Psychoneuroendocrinology* 36, 415–425. doi: 10.1016/j.psyneuen.2010.03.007

Bali, A., and Jaggi, A. S. (2016). An integrative review on role and mechanisms of Ghrelin in stress, anxiety and depression. *Curr. Drug Targets* 17, 495–507. doi: 10.2174/1389450116666150518095650

Belmaker, R. H., and Agam, G. (2008). Major depressive disorder. *N. Engl. J. Med.* 358, 55–68. doi: 10.1056/NEJMra073096

Borsini, F., and Meli, A. (1988). Is the forced swimming test a suitable model for revealing antidepressant activity? *Psychopharmacology* 94, 147–160. doi: 10.1007/bf00176837

Browne, C. A., and Lucki, I. (2013). Antidepressant effects of ketamine: mechanisms underlying fast-acting novel antidepressants. *Front. Pharmacol.* 4:161. doi: 10.3389/fphar.2013.00161

Bylund, D., and Reed, A. (2007). Childhood and adolescent depression: why do children and adults respond differently to antidepressant drugs? *Neurochem. Int.* 51, 246–253. doi: 10.1016/j.neuint.2007.06.025

Carlini, V. P., MacHado, D. G., Buteler, F., Ghersi, M., Ponzio, M. F., Martini, A. C., et al. (2012). Acute ghrelin administration reverses depressive-like behavior induced by bilateral olfactory bulbectomy in mice. *Peptides* 35, 160–165. doi: 10.1016/j.peptides.2012.03.031

Choi, H. J., Ki, K. H., Yang, J. Y., Song, J. A., Baek, W. Y., Kim, J. H., et al. (2013). Chronic central administration of ghrelin increases bone mass through a mechanism independent of appetite regulation. *PLOS One* 8:e65505. doi: 10.1371/journal.pone.0065505

Cryan, J. F., Mombereau, C., and Vassout, A. (2005). The tail suspension test as a model for assessing antidepressant activity: review of pharmacological and genetic studies in mice. *Neurosci. Biobehav. Rev.* 29, 571–625. doi: 10.1016/j.neubiorev.2005.03.009

Date, Y., Shimbara, T., Koda, S., Toshinai, K., Ida, T., Murakami, N., et al. (2006). Peripheral ghrelin transmits orexigenic signals through the noradrenergic pathway from the hindbrain to the hypothalamus. *Cell Metab.* 4, 323–331. doi: 10.1016/j.cmet.2006.09.004

David, D. J., Samuels, B. A., Rainer, Q., Wang, J.-W., Marsteller, D., Mendez, I., et al. (2009). Neurogenesis-dependent and -independent effects of fluoxetine independent an animal model of anxiety/depression. *Neuron* 62, 479–493. doi: 10.1016/j.neuron.2009.04.017

DeVos, S. L., and Miller, T. M. (2013). Direct intraventricular delivery of drugs to the rodent central nervous system. *J. Vis. Exp.* 75:e50326. doi: 10.3791/50326

Hansson, C., Haage, D., Taube, M., Egecioglu, E., Salomé, N., and Dickson, S. L. (2011). Central administration of ghrelin alters emotional responses in rats: behavioural, electrophysiological and molecular evidence. *Neuroscience* 180, 201–211. doi: 10.1016/j.neuroscience.2011.02.002

Hazell, P., O'Connell, D., Heathcote, D., and Henry, D. (2002). Tricyclic drugs for depression in children and adolescents. *Cochrane Database Syst. Rev.* 2:CD002317. doi: 10.1002/14651858.CD002317

Hazell, P., O'Connell, D., Heathcote, D., Robertson, J., and Henry, D. (1995). Efficacy of tricyclic drugs in treating child and adolescent depression: a meta-analysis. *BMJ* 310, 897–901. doi: 10.1136/bmj.310.6984.897

Hornsby, A. K. E., Redhead, Y. T., Rees, D. J., Ratcliff, M. S. G., Reichenbach, A., Wells, T., et al. (2016). Short-term calorie restriction enhances adult hippocampal neurogenesis and remote fear memory in a Ghsr-dependent manner. *Psychoneuroendocrinology* 63, 198–207. doi: 10.1016/j.psyneuen.2015.09.023

Hoshaw, B. A., Malberg, J. E., and Lucki, I. (2005). Central administration of IGF-I and BDNF leads to long-lasting antidepressant-like effects. *Brain Res.* 1037, 204–208. doi: 10.1016/j.brainres.2005.01.007

Kanoski, S. E., Fortin, S. M., Ricks, K. M., and Grill, H. J. (2013). Ghrelin signaling in the ventral hippocampus stimulates learned and motivational aspects of feeding via PI3K-Akt signaling. *Biol. Psychiatry* 73, 915–923. doi: 10.1016/j.biopsych.2012.07.002

Katz, R. J. (1982). Animal model of depression: pharmacological sensitivity of a hedonic deficit. *Pharmacol. Biochem. Behav.* 16, 965–968. doi: 10.1016/0091-3057(82)90053-3

Khazipov, R., Zaynutdinova, D., Ogievetsky, E., Valeeva, G., Mitrukhina, O., Manent, J.-B., et al. (2015). Atlas of the postnatal rat brain in stereotaxic coordinates. *Front. Neuroanat.* 9:161. doi: 10.3389/fnana.2015.00161

Kluge, M., Schüssler, P., Dresler, M., Schmidt, D., Yassouridis, A., Uhr, M., et al (2011). Effects of ghrelin on psychopathology, sleep and secretion of cortisol and growth hormone in patients with major depression. *J. Psychiatr. Res.* 45, 421–426. doi: 10.1016/j.jpsychires.2010.09.002

Liu, W., Wang, H., Wang, Y., Li, H., and Ji, L. (2015). Metabolic factors-triggered inflammatory response drives antidepressant effects of exercise in CUMS rats. *Psychiatry Res.* 228, 257–264. doi: 10.1016/j.psychres.2015.05.102

Lucki, I. (1997). The forced swimming test as a model for core and component behavioral effects of antidepressant drugs. *Behav. Pharmacol.* 8, 523–532. doi: 10.1097/00008877-199711000-00010

Malberg, J. E., Eisch, A. J., Nestler, E. J., and Duman, R. S. (2000). Chronic antidepressant treatment increases neurogenesis in adult rat hippocampus. *J. Neurosci.* 20, 9104–9110. doi: 10.1523/jneurosci.20-24-09104.2000

Martínez-Mota, L., Ulloa, R. E., Herrera-Pérez, J., Chavira, R., and Fernández-Guasti, A. (2011). Sex and age differences in the impact of the forced swimming test on the levels of steroid hormones. *Physiol. Behav.* 104, 900–905. doi: 10.1016/j.physbeh.2011.05.027

Marks, W., Fournier, N. M., and Kalynchuk, L. E. (2009). Repeated exposure to corticosterone increases depression-like behavior in two different versions of the forced swim test without altering nonspecific locomotor activity or muscle strength. *Physiol. Behav.* 98, 67–72. doi: 10.1016/j.physbeh.2009.04.014

Moon, M., Kim, S., Hwang, L., and Park, S. (2009). Ghrelin regulates hippocampal neurogenesis in adult mice. *Endocr. J.* 56, 525–531. doi: 10.1507/endocrj.k09e-089

Murrin, L. C., Sanders, J. D., and Bylund, D. B. (2007). Comparison of the maturation of the adrenergic and serotonergic neurotransmitter systems in the brain: implications for differential drug effects on juveniles and adults. *Biochem. Pharmacol.* 73, 1225–1236. doi: 10.1016/j.bcp.2007.01.028

Perera, T. D., Coplan, J. D., Lisanby, S. H., Lipira, C. M., Arif, M., Carpio, C., et al. (2007). Antidepressant-induced neurogenesis in the hippocampus of adult nonhuman primates. *J. Neurosci.* 27, 4894–4901. doi: 10.1523/JNEUROSCI.0237-07.2007

Porsolt, R. D., Le Pichon, M., and Jalfre, M. (1977). Depression: a new animal model sensitive to antidepressant treatments. *Nature* 266, 730–732. doi: 10.1038/266730a0

Reed, A. L., Happe, H. K., Petty, F., and Bylund, D. B. (2008). Juvenile rats in the forced-swim test model the human response to antidepressant treatment for pediatric depression. *Psychopharmacology* 197, 433–441. doi: 10.1007/s00213-007-1052-0

Santarelli, L., Saxe, M., Gross, C., Surget, A., Battaglia, F., Dulawa, S., et al. (2003). Requirement of hippocampal neurogenesis for the behavioral effects of antidepressants. *Science* 301, 805–809. doi: 10.1126/science.1083328

Sartori, S. B., Burnet, P. W. J., Sharp, T., and Singewald, N. (2004). Evaluation of the effect of chronic antidepressant treatment on neurokinin-1 receptor expression in the rat brain. *Neuropharmacology* 46, 1177–1183. doi: 10.1016/j.neuropharm.2004.02.013

Sengupta, P. (2013). The laboratory rat: relating its age with human's. *Int. J. Prev. Med.* 4, 624–630.

Spencer, S. J., Emmerzaal, T. L., Kozicz, T., and Andrews, Z. B. (2015). Ghrelin's role in the hypothalamic-pituitary-adrenal axis stress response: implications for mood disorders. *Biol. Psychiatry* 78, 19–27. doi: 10.1016/j.biopsych.2014.10.021

Steru, L., Chermat, R., Thierry, B., and Simon, P. (1985). The tail suspension test: a new method for screening antidepressants in mice. *Psychopharmacology* 85, 367–370. doi: 10.1007/bf00428203

Taupin, P. (2007). BrdU immunohistochemistry for studying adult neurogenesis: paradigms, pitfalls, limitations, and validation. *Brain Res. Rev.* 53, 198–214. doi: 10.1016/j.brainresrev.2006.08.002

van Praag, H., Shubert, T., Zhao, C., and Gage, F. H. (2005). Exercise enhances learning and hippocampal neurogenesis in aged mice. *J. Neurosci.* 25, 8680–8685. doi: 10.1523/jneurosci.1731-05.2005

Wang, P., Liu, C., Liu, L., Zhang, X., Ren, B., and Li, B. (2015). The antidepressant-like effects of estrogen-mediated ghrelin. *Curr. Neuropharmacol.* 13, 524–535. doi: 10.2174/1570159x1304150831120650

Wojtowicz, J. M., and Kee, N. (2006). BrdU assay for neurogenesis in rodents. *Nat. Protoc.* 1, 1399–1405. doi: 10.1038/nprot.2006.224

Yoo, S. B., Kim, B.-T., Kim, J. Y., Ryu, V., Kang, D.-W., Lee, J.-H., et al. (2013). Adolescence fluoxetine increases serotonergic activity in the raphe-hippocampus axis and improves depression-like behaviors in female rats that experienced neonatal maternal separation. *Psychoneuroendocrinology* 38, 777–788. doi: 10.1016/j.psyneuen.2012.08.013

Yorbik, O., Birmaher, B., Axelson, D., Williamson, D. E., and Ryan, N. D. (2004). Clinical characteristics of depressive symptoms in children and adolescents with major depressive disorder. *J. Clin. Psychiatry* 65, 1654–1659. doi: 10.4088/jcp.v65n1210

Conflict of Interest Statement: The authors declare that the research was conducted in the absence of any commercial or financial relationships that could be construed as a potential conflict of interest.

frontiers in Behavioral Neuroscience

ORIGINAL RESEARCH
published: 30 April 2019
doi: 10.3389/fnbeh.2019.00087

Optogenetic Stimulation of the Basolateral Amygdala Increased Theta-Modulated Gamma Oscillations in the Hippocampus

*Nathan S. Ahlgrim[1] and Joseph R. Manns[2]**

[1] Graduate Program in Neuroscience, Emory University, Atlanta, GA, United States, [2] Department of Psychology, Emory University, Atlanta, GA, United States

The amygdala can modulate declarative memory. For example, previous research in rats and humans showed that brief electrical stimulation to the basolateral complex of the amygdala (BLA) prioritized specific objects to be consolidated into long term memory in the absence of emotional stimuli and without awareness of stimulation. The capacity of the BLA to influence memory depends on its substantial projections to many other brain regions, including the hippocampus. Nevertheless, how activation of the BLA influences ongoing neuronal activity in other regions is poorly understood. The current study used optogenetic stimulation of putative glutamatergic neurons in the BLA of freely exploring rats to determine whether brief activation of the BLA could increase in the hippocampus gamma oscillations for which the amplitude was modulated by the phase of theta oscillations, an oscillatory state previously reported to correlate with good memory. BLA neurons were stimulated in 1-s bouts with pulse frequencies that included the theta range (8 Hz), the gamma range (50 Hz), or a combination of both ranges (eight 50-Hz bursts). Local field potentials were recorded in the BLA and in the pyramidal layer of CA1 in the intermediate hippocampus. A key question was whether BLA stimulation at either theta or gamma frequencies could combine with ongoing hippocampal oscillations to result in theta-modulated gamma or whether BLA stimulation that included both theta and gamma frequencies would be necessary to increase theta–gamma comodulation in the hippocampus. All stimulation conditions elicited robust responses in BLA and CA1, but theta-modulated gamma oscillations increased in CA1 only when BLA stimulation included both theta and gamma frequencies. Longer bouts (5-s) of BLA stimulation resulted in hippocampal activity that evolved away from the initial oscillatory states and toward those characterized more by prominent low-frequency oscillations. The current results indicated that one mechanism by which the amygdala might influence declarative memory is by eliciting neuronal oscillatory states in the hippocampus that benefit memory.

Keywords: hippocampus, amygdala, memory, optogenetics, oscillations, theta, gamma

OPEN ACCESS

Edited by:
Bahar Güntekin, Istanbul Medipol University, Turkey

Reviewed by:
James R. Hinman, Boston University, United States
James Lafayette McGaugh, University of California, Irvine, United States

****Correspondence:***
Joseph R. Manns
jmanns@emory.edu

Received: *11 February 2019*
Accepted: *11 April 2019*
Published: *30 April 2019*

Citation:
Ahlgrim NS and Manns JR (2019) Optogenetic Stimulation of the Basolateral Amygdala Increased Theta-Modulated Gamma Oscillations in the Hippocampus. Front. Behav. Neurosci. 13:87. doi: 10.3389/fnbeh.2019.00087

INTRODUCTION

The basolateral complex of the amygdala (BLA) is a key modulatory region of hippocampus-dependent memory (McGaugh, 2002). Direct activation of the BLA via pharmacological manipulations (Roozendaal et al., 2008; Barsegyan et al., 2014) or brief electrical stimulation (Bass et al., 2012, 2014; Bass and Manns, 2015; Inman et al., 2018) improved performance in memory tasks not designed to be overtly emotional, such as object recognition memory tasks. Indeed, in one recent study with human participants, direct electrical stimulation targeting the BLA improved recognition memory for neutral object images despite participants reporting that they could not detect the stimulation (Inman et al., 2018). These experiments built on prior work in rodents demonstrating that the BLA mediated the influence of emotional arousal on memory performance in tasks such as inhibitory avoidance (McIntyre et al., 2002, 2005; McReynolds et al., 2010, 2014b; Holloway-Erickson et al., 2012; Huff et al., 2013). Thus, existing research suggests that activation of the BLA can modulate memory for the better and can be engaged by emotional arousal or by direct intervention.

The BLA is thought to modulate memory in part by influencing memory processes in other brain regions (McGaugh, 2002; Roozendaal et al., 2003, 2006). In particular, the BLA sends direct glutamatergic projections to the hippocampus and to regions such as the entorhinal and perirhinal cortices that in turn project to the hippocampus (Pitkänen et al., 2000). Inactivating the hippocampus via local infusion of muscimol blocked the object recognition memory improvement triggered by electrical stimulation of the BLA (Bass et al., 2014), whereas pharmacological manipulations of the BLA such as local infusion of adrenergic agonists led to increased markers of synaptic plasticity in the hippocampus (McIntyre et al., 2005; McReynolds et al., 2014a). In addition, electrical stimulation of the BLA increased slow gamma oscillatory activity in the hippocampus (Bass and Manns, 2015). Many brain regions receive inputs from the BLA (Sah et al., 2003), but for modulation of hippocampus-dependent memory, the current data suggest one key region influenced by the BLA is the hippocampus itself. Understanding these mechanisms will help characterize how the brain prioritizes important memories (Manns and Bass, 2016).

One possible mechanism by which the BLA could beneficially modulate memory is by eliciting oscillatory network states that favor memory in the hippocampus and associated areas. In particular, theta (6–10 Hz in rats) oscillations are related to behavioral states (Montoya et al., 1989; Sheremet et al., 2019) and memory (Buzsáki, 2005; McNaughton et al., 2006; Buzsaki and Moser, 2013). In addition, hippocampal slow gamma oscillations (30–55 Hz in rats) at encoding correlated with later retrieval success (Sederberg et al., 2007; Jutras et al., 2009; Trimper et al., 2017). The amplitude of slow gamma oscillations in the hippocampus fluctuates and is modulated by the phase of theta, one type of phase-amplitude cross-frequency coupling (hereby referred to as theta–gamma comodulation). The degree of theta–gamma comodulation is also a strong correlate of memory performance (Tort et al., 2009; Shirvalkar et al., 2010; Trimper et al., 2014). Indeed, recent studies using electrical stimulation to the BLA to enhance object recognition memory have used an electrical pulse frequency meant to simulate theta-modulated gamma oscillations (bursts of 50 Hz stimulation every 1/8th of a second; Bass et al., 2012, 2014; Bass and Manns, 2015; Inman et al., 2018). These results indicated that stimulating the BLA with a theta-modulated gamma pulse frequency was capable of improving memory performance, but the findings did not answer whether stimulating at theta or gamma frequencies alone would suffice to elicit in the hippocampus neuronal oscillations resembling those that correlate with good memory. For example, stimulating the BLA at 50 Hz alone could in principle lead to slow gamma (i.e., 50 Hz) oscillations in the hippocampus for which the amplitude would be modulated by the phase of the endogenous hippocampal theta oscillations.

The current experiment with freely moving rats asked if stimulating the BLA at theta and gamma frequencies could elicit in the hippocampus neuronal oscillations resembling those previously found to correlate with good memory performance. A key question was whether BLA stimulation that combined theta and gamma frequencies was needed to amplify hippocampal theta–gamma comodulation, which is known to be important for good memory. The current experiment utilized optogenetic rather than electrical stimulation of the BLA for several reasons. First, the use of a cell-type specific (CaMKII) promoter for the vector delivering the opsin (channelrhodopsin; ChR2) allowed for stimulation restricted to putative glutamatergic projection neurons in the BLA. Second, use of a blue light-sensitive opsin allowed for a control stimulation condition that used near-infrared light pulses outside the excitation spectrum of the opsin. Third, optical stimulation avoided electrophysiological recording artifacts induced by electrical stimulation. Stimulation was delivered in 1-s bouts at 8 Hz to emulate theta, at 50 Hz to emulate slow gamma, and at 50 Hz bursts every 1/8th second to emulate theta-modulated gamma (50/8 Hz). Included for comparison were conditions in which 1 s of 20 Hz stimulation was delivered using either blue (experimental) and near-infrared (control) light. BLA stimulation with blue light in all conditions elicited oscillatory activity in the hippocampus, but only BLA stimulation at 50/8 Hz elicited in CA1 a pattern of activity that appeared to reflect theta–gamma comodulation similar to what has been observed in studies to positively correlate with good object memory (Tort et al., 2009; Shirvalkar et al., 2010; Trimper et al., 2014).

MATERIALS AND METHODS

Subjects

Six adult male Long-Evans rats, between 400 and 500 g, were housed individually (12-h light/dark cycle; stimulation during light phase). All animals were given free access to water and were food restricted, maintaining at least 90% of their free-feeding body weight. All procedures involving rats were approved by the Institutional Animal Care and Use Committee at Emory University.

Surgery and Drive Positioning

Rats underwent a single stereotaxic surgery for infusion of the viral vector and implantation of combined optical fiber and tetrode recording assembly. Rats were anesthetized with isoflurane (1–3% in oxygen at 1.0 L/min) and received preoperative (0.03 mg/kg buprenorphine) and postoperative (0.05 mg/kg buprenorphine, 1.0 mg/kg meloxicam) analgesia. Additional care and nutrition were given as needed. A single craniectomy was created above the BLA and intermediate third of the hippocampus (coordinate range: 2.6–5.9 mm posterior and 2.8–5.5 mm lateral to Bregma; Paxinos and Watson, 1998) for a unilateral infusion and implantation in the right hemisphere. The viral vector containing channelrhodopsin and reporter fluorophore [AAV_5-CaMKII-hChR2(H134R)-EYFP; University of North Carolina Vector Core] was infused using a stereotaxic frame (Kopf Instruments) and syringe pump (Hamilton Company). The virus was infused through a 33-gauge needle into the BLA (coordinates: 3.5 mm posterior, 5.1 mm lateral, 8.9 mm ventral to Bregma) at 150 nL/min for a total volume of 500 nL. The needle was left in place for 10 min before withdrawal to allow the virus to diffuse into the surrounding tissue.

After withdrawal of the needle, the recording assembly containing a fixed optical fiber with a ceramic ferrule (200/230 nm, 0.66 NA; Plexon, Inc.) and independently moveable nichrome tetrodes was implanted. Tetrodes were spun with 12.5 nichrome wire (California Fine Wire or Sandvik) and plated with gold to reduce the impedance to approximately 200 kΩ at 1 kHz. The optical fiber was fixed in the recording assembly so that it was positioned directly above the BLA (coordinates: 3.5 mm posterior, 5.1 mm lateral, 8.4 mm ventral to Bregma) with the base of the recording assembly at the surface of the exposed brain. Tetrodes targeting the BLA were glued to the optical fiber to target 0.25–0.75 mm below the fiber tip. Tetrodes targeting the hippocampus were each controlled by a separate driver. They were targeted at the intermediate third of the hippocampus (coordinates range: 4.5–5.9 mm posterior, 2.9–5.4 lateral mm to Bregma), since the intermediate CA1 receives direct projections from the BLA (Pikkarainen et al., 1999; Pitkänen et al., 2000; Petrovich et al., 2001) and has been shown to be involved in memory enhancement by brief electrical stimulation to the BLA (Bass et al., 2014; Bass and Manns, 2015). The rat was grounded by a wire attached to a stainless-steel screw, which was implanted in the skull midline over the cerebellum. This ground screw also served as the reference for LFP recordings. After a minimum of 1-week recovery, tetrodes were slowly lowered into the pyramidal cell layer of the CA1 over the following weeks (recording tetrodes in BLA were fixed to the optical fiber). No tetrodes were moved within 24 h of stimulation and recording.

Optogenetic Stimulation

Testing occurred no sooner than 4 weeks post-surgery to allow sufficient time for viral transfection and opsin expression. All stimulation occurred on awake rats as they freely explored a 30-cm diameter circular recording platform bordered by an approximately 7-cm wall. Stimulation events were triggered by the experimenter no less than 10 s apart. Stimulation was never dependent on a particular behavioral state other than ensuring that the rat was awake throughout the experiment; the experimenter was not directly observing the animal during stimulation. Light was produced by a compact LED at 465 nm (blue) or 740 nm (near-infrared) (Plexon, Inc.). The blue LED produced light within the excitation spectrum of channelrhodopsin, and the near-infrared LED produced light outside of the excitation spectrum, a method documented to act as a reliable control (Blumberg et al., 2016; Klavir et al., 2017). The LED was connected to the optical fiber's ferrule on the recording assembly by an armored patch cable (200/230 nm, 0.5 NA) and ceramic coupler (Plexon, Inc.).

Stimulation included several parameter conditions, the order of which was randomized across rats. All rats experienced a least 20 bouts of each condition. Rats received stimulation in the following conditions: (1) 1-s blue light at 8 Hz, (2) 1-s blue light at 20 Hz, (3) 1-s blue light at 50 Hz, (4) 1-s blue light in bursts of four 50 Hz pulses every 1/8th second (50/8 Hz), (5) 5-s blue light at 50 Hz, (6) 5-s blue light at 50/8 Hz, and (7) 1-s near-infrared light at 20 Hz. Stimulation parameters were chosen to mimic theta (8 Hz), slow gamma (50 Hz), theta–gamma comodulation (50/8 Hz), and a frequency (20 Hz) known to reliably evoke responses from ChR2(H134R). All light pulses were of 5 ms duration. Power at the optical fiber tip was approximately 11 mW for the blue LED and 7 mW for the near-infrared LED.

Histology

Prior to euthanasia, the location of each tetrode was marked by passing 20–40 μA current for 10–30 s through a single wire of the tetrode. Rats were injected with an overdose (0.5 mL) of Euthanasia-III Solution (Med-Pharmex) after being anesthetized with isoflurane. They were then transcardially perfused with isotonic saline followed by neutral buffered formalin 10% (Harleco). Brains were extracted, post-fixed in neutral buffered formalin 10% for 24 h, and submerged in a 30% sucrose solution until saturated. Brains were sectioned on a freezing stage microtome at 40 μM thickness and stored in 0.1 M phosphate buffer. All sections were mounted on slides coated with gelatin and chromium potassium sulfate dodecahydrate (Fisher Scientific). For verification and localization of virus expression, slides were covered with Vectashield with DAPI (Vector Laboratories), and cover slipped. Expression of channelrhodopsin was inferred by the expression of the conjugated fluorophore, observed on an epifluorescence microscope for regional expression and on a confocal microscope for cell body and fiber identification. BLA tetrodes were localized by staining for acetylcholinesterase, which robustly stains the basal nucleus of the BLA. Hippocampal tetrodes were localized under light microscopy following a Nissl stain (cresyl violet).

Data Acquisition and Analysis

Local field potentials (LFPs) were recorded from tetrodes in the BLA and hippocampus with a sampling rate of 1.5 kHz and were filtered from 1 to 400 Hz. The LFP from one tetrode in the pyramidal layer of CA1 and one tetrode in the BLA was used for each rat. Spiking data were not analyzed due to too few well-isolated single units. All data were obtained with the

NSpike data acquisition system[1]. Analyses were performed in MATLAB (MathWorks) using custom scripts and the Chronux toolbox (Bokil et al., 2010). Power of the BLA and CA1 LFPs was estimated using a multitaper fast Fourier transform similar to previous reports (Bass and Manns, 2015; Trimper et al., 2017). The modulation index (MI) for phase-amplitude cross-frequency coupling (i.e., comodulation) was calculated as previously described (Tort et al., 2009).

For all analyses, results were averaged within a rat across all trials of a given condition, and then the data from all rats were averaged. For some analyses, a rat's data from a single stimulation condition were normalized prior to averaging across rats to demonstrate more clearly the impact of stimulation. In particular, for analyses of average stimulation-evoked LFPs in the time domain, LFPs from 4 s before stimulation onset to 5 s after stimulation offset were Z-transformed based on the mean and standard deviation of each single trial sweep. For spectral analyses in the frequency domain, FFT analyses were conducted on the raw LFPs. Absolute power is shown in spectrograms. However, for plots of moving-window spectrograms, estimates of power were normalized (Z-transformed) to a pre-stimulation baseline period (from −2 to −1 s before the onset of stimulation) to visualize more clearly the impact of stimulation.

Statistical significance was determined using a random permutation approach in which LFP data from the stimulation and baseline periods were randomly shuffled 1,000 times. All analyses were recalculated for each random shuffle, and statistical significance was defined as metrics falling outside the 95th percentile of the distribution obtained from the random shuffles. More specifically, power plotted in spectrograms was analyzed with a cluster-based permutation in which clusters were defined as frequency ranges in which the power values were greater than 2.5 standard deviations above or below the mean of the data. Only clusters spanning more than 1 Hz were considered. The random cluster permutation distribution included only the largest cluster from each random permutation. Clusters (frequency ranges) in the original data that were outside the 95th percentile of the random cluster distribution were labeled as statistically significant. This cluster-based approach was used because it preserves the overall alpha level (Maris and Oostenveld, 2007). For 5-s stimulation conditions, the same cluster-based random permutation approach was used for each second of stimulation. Power during seconds 1–5 were compared against baseline activity (−2 to −1 s before stimulation) independently to determine how the response to stimulation developed over time. Changes in comodulation were analyzed in a pre-determined theta–gamma range (6–10 Hz phase frequency, 30–55 Hz amplitude frequency). A random permutation analysis of variance was used to determine the significance of the effect of stimulation condition on the pre-defined theta–gamma comodulation. Specifically, the variance was defined as summed variance to the mean across stimulation conditions. The mean was the average comodulation index across conditions, and the variance was the difference between the comodulation during an individual condition and the mean. The random permutation was constructed by shuffling the condition labels for each stimulation bout. The resulting variance from the mean of the shuffled data populated the random permutation distribution. The effect of stimulation condition on comodulation was considered significant if the variance of the original data fell outside the 95th percentile of that distribution.

[1] nspike.sourceforge.net

RESULTS

Histological Verification of Stimulation and Recording Locations

Postmortem histological analysis verified placement of the optical fiber dorsal to the BLA, expression of channelrhodopsin in the BLA, and location of recording tetrodes in the BLA and CA1 of the intermediate hippocampus. **Figure 1** shows a schematic of the stimulation and recording approach as well as example histology. The tip of all unilaterally implanted optical fibers was confirmed to be positioned 0.2–0.6 mm dorsal to the BLA. In all six rats, the viral vector transfected cell bodies in the BLA, as evidenced by punctate expression of the fluorophore conjugated to the opsin (**Figure 1D**). Expression in the amygdala was restricted to the BLA. In two rats, the viral vector spread to a modest degree into the adjacent piriform cortex. However, the off-target neurons were largely outside the cone of light (with a 0.66 numerical aperture, light was emitted from the optical fiber at 29.0°), since the majority of labeled neurons in the piriform cortex were in the dorsal endopiriform nucleus (Paxinos and Watson, 1998). Thus, the impact of light stimulation was largely restricted to neurons in the BLA in all rats. In all rats, fluorophore-labeled fibers were visible in the temporal half of the hippocampus, particularly in the lacunosum-moleculare layer of CA1 and subiculum (**Figure 1E**), consistent with past studies showing projections from the BLA to hippocampus terminating in this specific area (Pitkänen et al., 2000; Wang and Barbas, 2018). Analyses of neural data focused on LFPs recorded from single electrodes in the BLA and CA1 in order to align the current results with past results from humans and rats (Bass et al., 2012, 2014; Bass and Manns, 2015; Inman et al., 2018) and because too few well-isolated single neurons were recorded to permit spiking analyses. All six rats had at least one tetrode positioned in the basolateral nucleus, and five rats had at least one tetrode positioned in the pyramidal layer of the CA1. The pyramidal layer was selected as a target layer to allow for comparison with past studies (Trimper et al., 2014; Bass and Manns, 2015), and because it could be localized at the time of recording by the presence of putative pyramidal neuron spiking. Analyses of LFP data from the BLA thus included six rats, whereas analyses of data from CA1 included five rats.

Effects of 1-s Optogenetic BLA Stimulation on BLA and CA1 LFPs

Figure 2 shows the mean normalized (Z-transformed) LFP in the BLA and CA1 during 1-s bouts of optical stimulation of the BLA. Stimulation was delivered up to 70 times per condition (mean number of stimulations per condition = 39.9; range = 20–70)

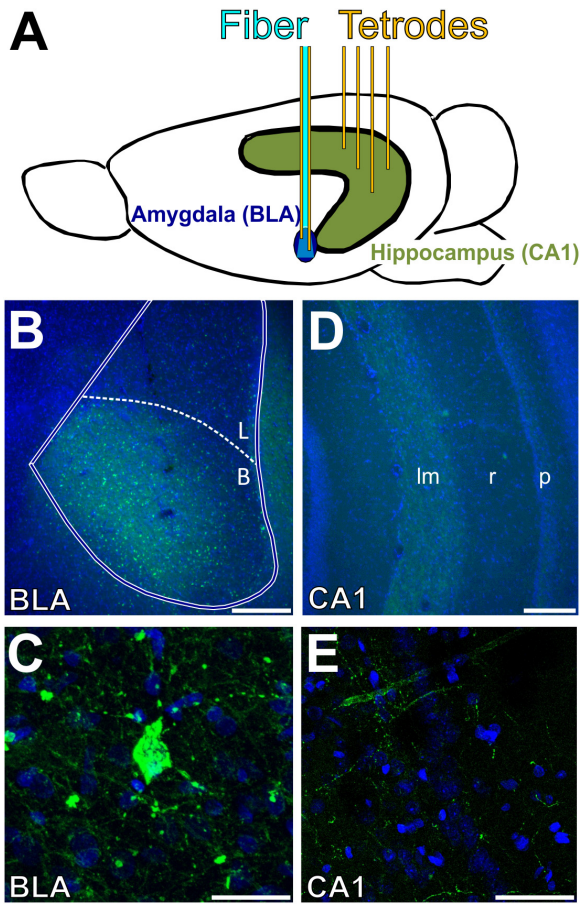

FIGURE 1 | Location of opsin expression, optogenetic stimulation, and tetrode recording. **(A)** Tetrodes (yellow) were lowered into the CA1 subregion of the intermediate hippocampus (green) and basolateral amygdala (blue). An optical fiber (cyan) was lowered to 0.25–0.75 mm above the target depth in the BLA. **(B–E)** Images of coronal sections of the BLA **(B,C)** and intermediate hippocampus **(D,E)**. Nuclei are shown in blue (DAPI), and eYFP expression (conjugated to the opsin) is shown in green. **(B)** CaMKII^{+} neurons were transfected in the basal nucleus of the amygdala. **(C)** The opsin was preferentially expressed in the cell bodies of the BLA. **(D)** Projections from the BLA also expressed the viral vector in the lacunosum-moleculare layer of CA1 in the intermediate hippocampus. **(E)** Hippocampal expression of the opsin was restricted to axonal projections; no cells were labeled in the hippocampus. Scale bars are 250 μm in **(B,D)**, and 30 μm in **(C,E)**. BLA, basolateral complex of the amygdala; B, basal nucleus; L, lateral nucleus; lm, lacunosum-moleculare; r, radiatum; p: pyramidale.

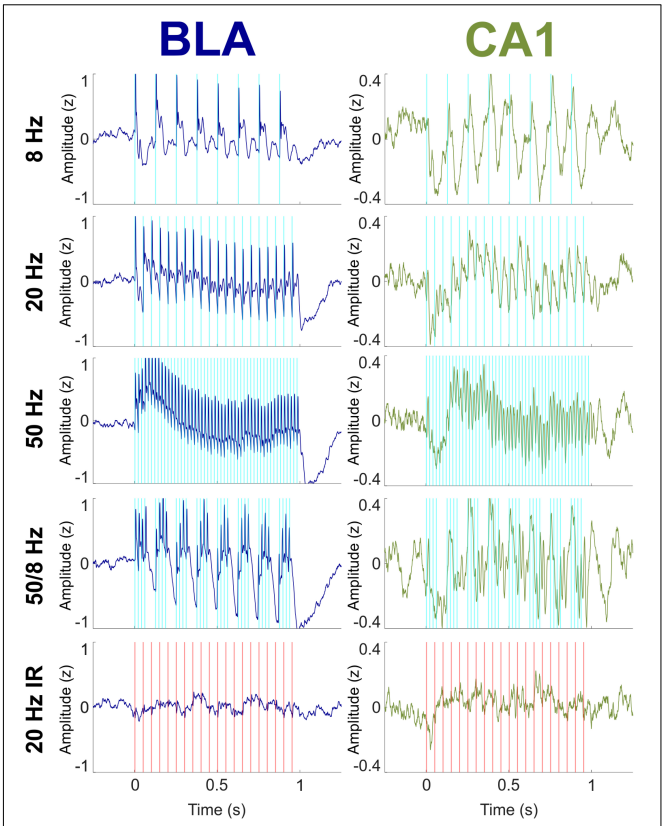

FIGURE 2 | Effects on BLA and CA1 LFPs of optogenetic BLA stimulation with blue (experimental) light at 8, 20, 50, and 50/8 Hz and with near infrared (IR; control) light at 20 Hz. LFPs were Z-transformed within conditions for each rat and then averaged across all rats. **(Left)** Evoked responses in the BLA (blue) tracked stimulation at all frequencies. **(Right)** LFPs in the CA1 (green) tracked stimulation at all frequencies with more regular oscillatory activity than what was seen in the BLA.

over the course of multiple recording sessions for each rat (mean number of recording sessions per rat = 2.83; range = 1–4). The optical stimulation was a blue 465-nm light delivered at 8, 20, or 50 Hz, or as bursts of four 50-Hz pulses delivered every 1/8th second ("50/8 Hz"). A control condition consisted of 1 s of 20-Hz near-infrared 740-nm light to the BLA, a wavelength known to be outside the excitation spectrum of channelrhodopsin (Mattis et al., 2012). Optical stimulation with blue light in the 8, 20, 50, and 50/8 Hz conditions evoked large responses of the same frequencies in the LFPs in the BLA (*Z*-scores ranged from about −1 to +1 across conditions) and moderate responses of the same frequencies in the LFPs in CA1 (*Z*-scores ranged from about −0.4 to +0.4 across conditions). Evoked responses in both regions appeared to cease soon after termination of stimulation in each condition. The control 20-Hz near-infrared optical stimulation did not evoke appreciable responses in either the BLA or CA1. These results suggest that optical stimulation of the BLA with blue light was capable of evoking frequency-matched responses in both the BLA and CA1 and that the evoked responses were a direct result of activation of the opsin, not an optoelectronic artifact or an artifact of the recording system.

Although the overall responses to 1 s of light stimulation were similar in the BLA and CA1, a closer inspection highlighted important differences between the regions. **Figure 3** shows mean normalized evoked responses in the BLA and CA1 to individual pulses of light delivered to the BLA. Averaged across all blue light stimulation conditions, the latency from onset of the first light pulse in each bout of stimulation to the initial peak of evoked response was 6.67 ms in the BLA, which reflects the response time of the opsin to light stimulation (Mattis et al., 2012). The latency to the initial peak was 12.7 ms in CA1 (**Figure 3A**), a 6.03 ms difference, suggesting

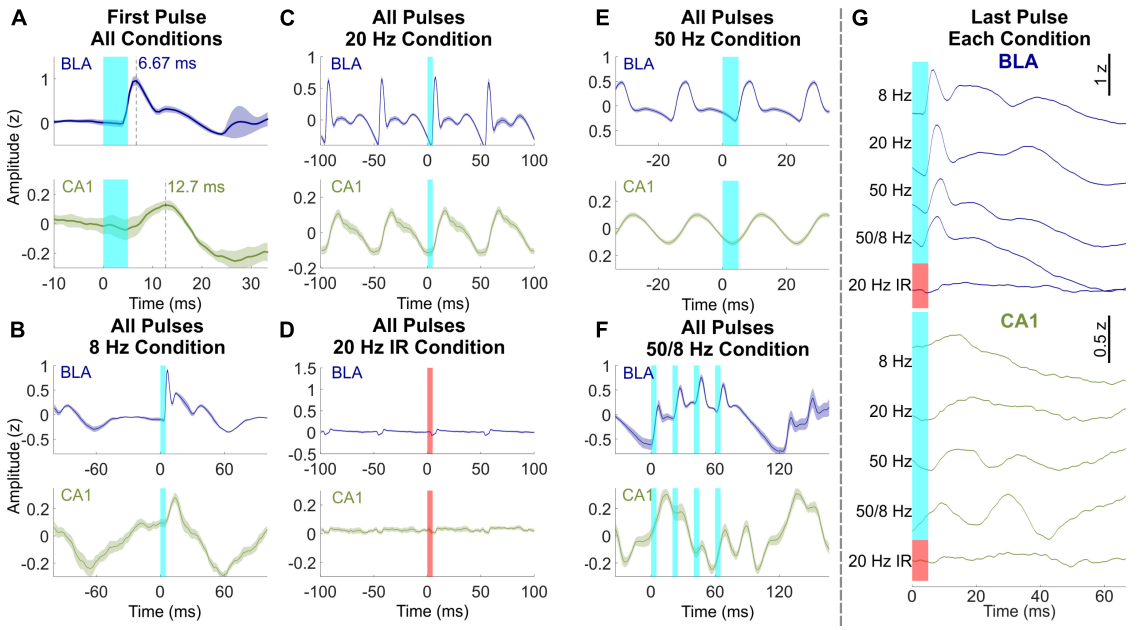

FIGURE 3 | Effects of BLA stimulation pulses differed between BLA and CA1. **(A)** Response latencies to the first light pulse of all conditions in the BLA (blue, top) and CA1 (green, bottom). Time to LFP peak response was 6.67 ms in the BLA and 12.7 ms in CA1. **(B–F)** Averaged LFP across all light pulses within the 8 Hz, 20 Hz, 20 Hz near-infrared, 50 Hz, and 50/8 Hz stimulation conditions, respectively (averaged across bursts of 50 Hz pulses for **F**). Responses in the BLA were characterized by fast activity that was similar across conditions, whereas oscillatory activity in CA1 was dependent on stimulation frequency. Maximal gamma activity preferentially occurred at the peak of theta in the BLA and trough of theta in CA1. **(G)** Response in the BLA and CA1 after the last pulse of each condition. 50/8 Hz stimulation produced persistent gamma in CA1 after termination of stimulation.

that the responses recorded in CA1 were neither triggered directly by the light nor conducted passively by brain volume but instead were evoked by monosynaptic connections from the BLA. Averaging across all light pulses separately for each condition shows additional differences between the responses in the BLA and CA1 (e.g., averaging across all 8 pulses in the 8 Hz condition). BLA LFPs were characterized by evoked responses of the same width (approximately 9 ms) in the 8, 20, 50, and 50/8 Hz conditions (**Figures 3B–F**). The initial evoked responses were followed by smaller responses in the fast gamma range (60–120 Hz), which is a prominent frequency band in the amygdala (Amir et al., 2018; Feng et al., 2019). In contrast, CA1 LFPs during stimulation with blue light displayed a more continuous waveform that had a sawtooth shape for 8 and 20 Hz conditions and a sinusoidal shape for 50 Hz stimulation (**Figures 3B–D**). For the 50/8 Hz condition, LFPs in the BLA and CA1 both showed 8 Hz and 50 Hz components in the shape of the response to the four 50-Hz pulses delivered every 1/8th second (**Figure 3F**). However, the 8 Hz response was out of phase between the BLA and CA1, and the 50-Hz response was delayed by at least a full 50 Hz cycle in CA1 compared to the BLA. Thus, the 50 Hz responses were largest on the rising slope of the 8 Hz wave in the BLA but largest on the falling slope of the 8 Hz wave in CA1. The differences in LFP responses between the BLA and CA1 suggested that stimulation of the BLA modulated activity within the hippocampus above and beyond a simple recapitulation of the stimulation effects in BLA. LFPs in both regions showed a small artifact during 20 Hz near-infrared stimulation, but the artifacts were the opposite polarity and occurred at a shorter delay as compared to those produced by blue light stimulation (**Figure 3D**).

A final comparison of waveforms between the BLA and CA1 during BLA stimulation focused on the average normalized response following the last light pulse in each bout of stimulation (**Figure 3G**). LFPs in the BLA following the last pulse of light were similar to the previous analyses of LFPs averaged across all light pulses in a condition (**Figures 3B–F**), and LFPs averaged across the first light pulse of each condition (**Figure 3A**). For example, for each condition, the delay of initial peak responses of the BLA LFP following the final BLA pulse was similar (range = 6.67–8.67 ms) to the average delay in response to the first pulse (6.67 ms) and was followed by fast, small amplitude activity in each case. In contrast, LFPs responses in CA1 following the last pulse of light differed across stimulation conditions. The times to initial peak response in CA1 following the final BLA pulse were 14.0, 19.3, 16.0, and 9.33 ms for 8, 20, 50, and 50/8 Hz conditions, respectively. In addition, a full extra cycle of slow gamma activity persisted in CA1 following the last pulse of 50/8 Hz stimulation and, to a lesser extent (and with different timing) following the last pulse of 50 Hz stimulation. The frequency-dependent persistent activity in CA1 supports the characterization of responses in the CA1 as oscillations rather than concatenated evoked responses, particularly for the 50/8 Hz stimulation condition.

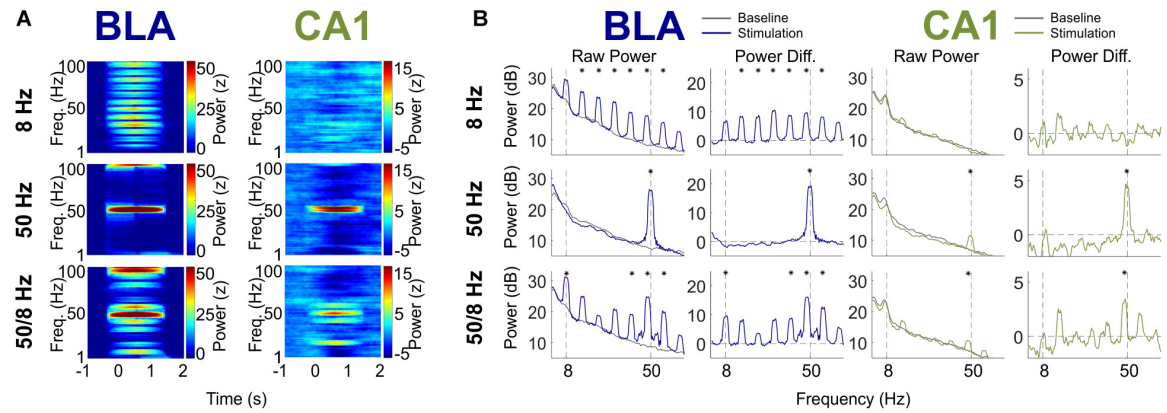

FIGURE 4 | BLA and CA1 LFP Power in response to optogenetic BLA stimulation. **(A)** Moving window spectrogram of power around the stimulation event. Power was normalized to the baseline period for clarity. **(B)** Spectrogram of power during stimulation, displayed as absolute decibels (left) and with the baseline period subtracted (right). Asterisks indicate frequency clusters that differed significantly between stimulation and baseline periods.

Effects of 1-s Optogenetic BLA Stimulation on Power Spectra in the BLA and CA1

Figure 4 shows the power spectra for the 8, 50, and 50/8 Hz conditions following a multitaper fast Fourier transform (FFT) of the BLA and CA1 LFP traces (see section "Materials and Methods" for analysis details, including testing for statistical significance). The results are shown as normalized (Z-transformed) moving window power spectrograms as well as standard power spectrograms to illustrate and statistically evaluate changes in the theta and gamma frequency ranges during stimulation relative to a pre-stimulation baseline. The moving window power spectrograms were calculated using a 1-s sliding window, so power values for a given timepoint contain information from the preceding and following 0.5 s. For LFPs from the BLA, BLA stimulation in the 8 and 50 Hz conditions resulted in increased power in the 8 and 50 Hz frequency ranges (plus harmonics), respectively. The increase in 50 Hz power was statistically significant for the 50 Hz condition, and the increase in power in the 8 Hz harmonic ranges (peaks at 16, 24, 32, 40, 48, and 56 Hz) was statistically significant for the 8 Hz condition. Stimulation in the 50/8 Hz condition resulted in statistically significantly increased BLA power at 8, 40, 48, and 56 Hz. In contrast to the results from BLA LFPs, CA1 LFPs showed power with prominent peaks in the 8 Hz range during the baseline in all conditions but did not show increased power in the 8 Hz range for any stimulation condition. The lack of increase in 8 Hz CA1 power in the 8 Hz stimulation condition contrasts with the clear entrainment of CA1 LFPs at 8 Hz during 8 Hz stimulation (see **Figure 2** top right panel, and **Figure 3B**). Thus, the phase but not the amplitude of ongoing hippocampal theta oscillations appeared to be modulated by 8 Hz BLA stimulation. Stimulation in both the 50 Hz and 50/8 Hz conditions resulted in significantly increased CA1 power in the slow gamma range. However, the peak frequency of CA1 power increase was 50 Hz during 50 Hz stimulation yet 48.7 Hz during 50/8 Hz stimulation, which is closer to a harmonic (48 Hz) of the underlying 8 Hz pattern than 50 Hz. Thus, the 8 Hz entrainment of CA1 LFPs during 8 Hz stimulation and the slightly shifted peak slow gamma power increase in the 50/8 Hz (48.7 Hz rather than 50 Hz) both suggest that the 8 Hz component of BLA stimulation in the 8 Hz and 50/8 Hz conditions did influence CA1 LFPs. Nevertheless, the only statistically significant power increases in CA1 during BLA stimulation in 8, 50, and 50/8 Hz conditions were in the slow gamma range (∼50 Hz).

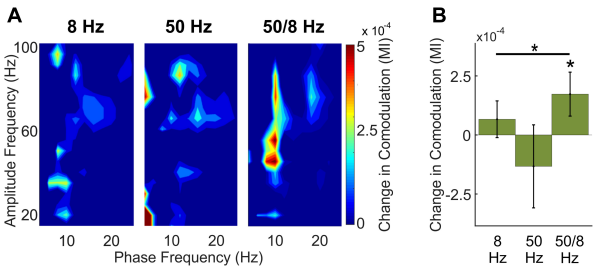

FIGURE 5 | Comodulation within CA1 across BLA stimulation conditions. **(A)** Comodulogram during 1-s BLA stimulation with the baseline period subtracted for clarity. **(B)** Total theta-modulated-slow gamma during stimulation relative to baseline for each stimulation conditions. Asterisks indicate that theta–gamma comodulation was significantly increased during 50/8 Hz stimulation and that theta–gamma comodulation was significantly different across conditions.

Theta–Gamma Comodulation During Optogenetic Stimulation

A key question was whether optogenetic stimulation of putative BLA glutamatergic projection neurons could increase gamma oscillations in the hippocampus for which the amplitude was modulated by the phase of theta oscillations—the type of phase-amplitude cross-frequency coupling (here referred to in brief as comodulation) known to be important for memory (Tort et al., 2009; Shirvalkar et al., 2010; Trimper et al., 2014). **Figure 5** shows comodulation in CA1 during BLA stimulation

relative to baseline in the 8, 50, and 50/8 Hz conditions. Only stimulation in the 50/8 Hz condition statistically significantly ($p < 0.05$ per a random permutation analysis; see section "Materials and Methods") increased theta–gamma comodulation relative to baseline [mean modulation index (MI) = 0.67×10^{-4}, -1.33×10^{-4}, and 1.73×10^{-4}, for 8, 50, and 50/8 Hz conditions, respectively]. In addition, the stimulation condition was a statistically significant factor ($p < 0.05$ per a random permutation analysis) in theta–gamma comodulation across 8, 50, and 50/8 Hz conditions (see section "Materials and Methods" for analysis details). Thus, theta-modulated gamma oscillations were increased in CA1 only when BLA stimulation included both theta and gamma frequencies.

Temporal Effects of Optogenetic Stimulation

The final question was whether longer bouts of BLA stimulation might elicit larger or different responses as compared to 1 s of simulation. **Figure 6** shows activity in the BLA and CA1 during 5 s of BLA stimulation in the 50 Hz and 50/8 Hz conditions ($n = 3$ for these data). The BLA LFPs did not appreciably change over the 5 s of BLA stimulation in either condition. In contrast, CA1 LFPs substantially changed from the first to the fifth second of stimulation, such that prominent fast oscillatory activity at the beginning of stimulation was almost completely replaced by slow oscillatory activity by the end of stimulation. For the 50 Hz stimulation condition, the 50 Hz CA1 oscillations in the first second returned to baseline levels and were largely replaced by slow oscillations in the 8 and 16 Hz ranges by the fifth second of stimulation. For the 50/8 Hz condition, CA1 oscillations in the 48-Hz range decreased moderately and CA1 oscillations in 8 and 16 Hz ranges increased markedly from the first to fifth second of BLA stimulation. In the BLA, 5-s BLA stimulation at 50 Hz stimulation evoked statistically significant increases in gamma power for each of the 5 s. In addition, 5-s BLA stimulation at 50/8 Hz stimulation evoked statistically significant increases in both theta (plus harmonics) and gamma power for each of the 5 s of stimulation. Thus, longer bouts of BLA stimulation resulted in temporally static responses in BLA LFPs but temporally dynamic responses in CA1 LFPs. It is unclear why the 5-s BLA stimulation resulted in different hippocampal activity as compared to 1 s of BLA stimulation. In any case, the present results suggest that brief (less than 2 s) optogenetic 50/8 Hz stimulation of the BLA would be most likely to elicit hippocampal oscillatory states thought to be beneficial to memory.

DISCUSSION

Brief optogenetic stimulation of the BLA at 8, 20, 50, and 50/8 Hz reliably elicited responses at matching frequencies in LFPs recorded in the BLA and CA1 in freely exploring rats. However, stimulation responses in CA1 differed from responses in the BLA in several ways. As compared to the responses in the BLA, the responses in CA1 across conditions were delayed by approximately 6 ms, displayed more continuous (sinusoidal or sawtooth) waveforms, and showed dynamic oscillatory changes across longer bouts (5 s) of stimulation. Thus, CA1 LFPs showed responses during BLA stimulation that broadly resembled neuronal oscillations, whereas BLA LFPs showed responses that resembled concatenated evoked responses. Moreover, the responses in CA1 LFPs to BLA stimulation differed between the 8, 50, and 50/8 Hz stimulation conditions, which were the focus of the current study. In particular, BLA stimulation in the 50 and 50/8 Hz conditions led to increased power close to 50 Hz in CA1, but none of the 8, 50, and 50/8 Hz conditions led to increased CA1 power in the 8 Hz range, despite 8 Hz BLA stimulation clearly entraining the phase of the ongoing 8 Hz theta oscillation in the hippocampus. A key finding was that 1 s of 50/8 Hz BLA stimulation preferentially increased in CA1 LFPs 50 Hz oscillations for which the amplitude was modulated by the phase of the 8 Hz oscillations, a type of phase-amplitude cross-frequency coupling (theta–gamma comodulation) known to be important for good memory. Thus, artificial stimulation of the BLA appears to be capable of increasing in the hippocampus neuronal oscillations that resemble endogenous oscillatory states that are thought to benefit memory formation. The results are discussed in more detail below.

BLA Projections to CA1 Were Among Many Potential BLA Projections Activated by Stimulation

The BLA includes the basal, lateral, and accessory basal nuclei (Sah et al., 2003). Neurons in these nuclei send axons to regions essential for declarative memory, including the hippocampus, entorhinal cortex, and perirhinal cortex, as well as to many other regions of the brain and to other amygdalar nuclei (Pitkänen et al., 1995, 2000; Savander et al., 1996; Sah et al., 2003). Thus, optogenetic stimulation of putative glutamatergic BLA projection neurons could have influenced neuronal activity in the hippocampus both directly and indirectly. One potential pathway mediating the indirect effects of BLA stimulation on the hippocampus is the pathway from perirhinal cortex to entorhinal cortex to hippocampus (Burwell and Amaral, 1998; Witter and Amaral, 2004). For example, activation of the amygdala is thought to facilitate information transfer from the perirhinal cortex to the entorhinal cortex, which in turn would influence the input to the hippocampus (Kajiwara et al., 2003; Paz et al., 2006). In addition, stimulation of the BLA-entorhinal cortex pathway was previously found to enhance hippocampal-dependent memories (Wahlstrom et al., 2018). Additional support for the importance of this perirhinal-entorhinal pathway comes from past studies showing that BLA stimulation modulated hippocampal LTP in the dentate gyrus (Abe, 2001; Akirav and Richter-Levin, 2002; Vouimba and Richter-Levin, 2005), which receives input from the entorhinal cortex but not from the BLA (Pitkänen et al., 2000; Witter and Amaral, 2004). As such, the BLA likely normally engages indirect pathways to influence hippocampal activity and to modulate memory.

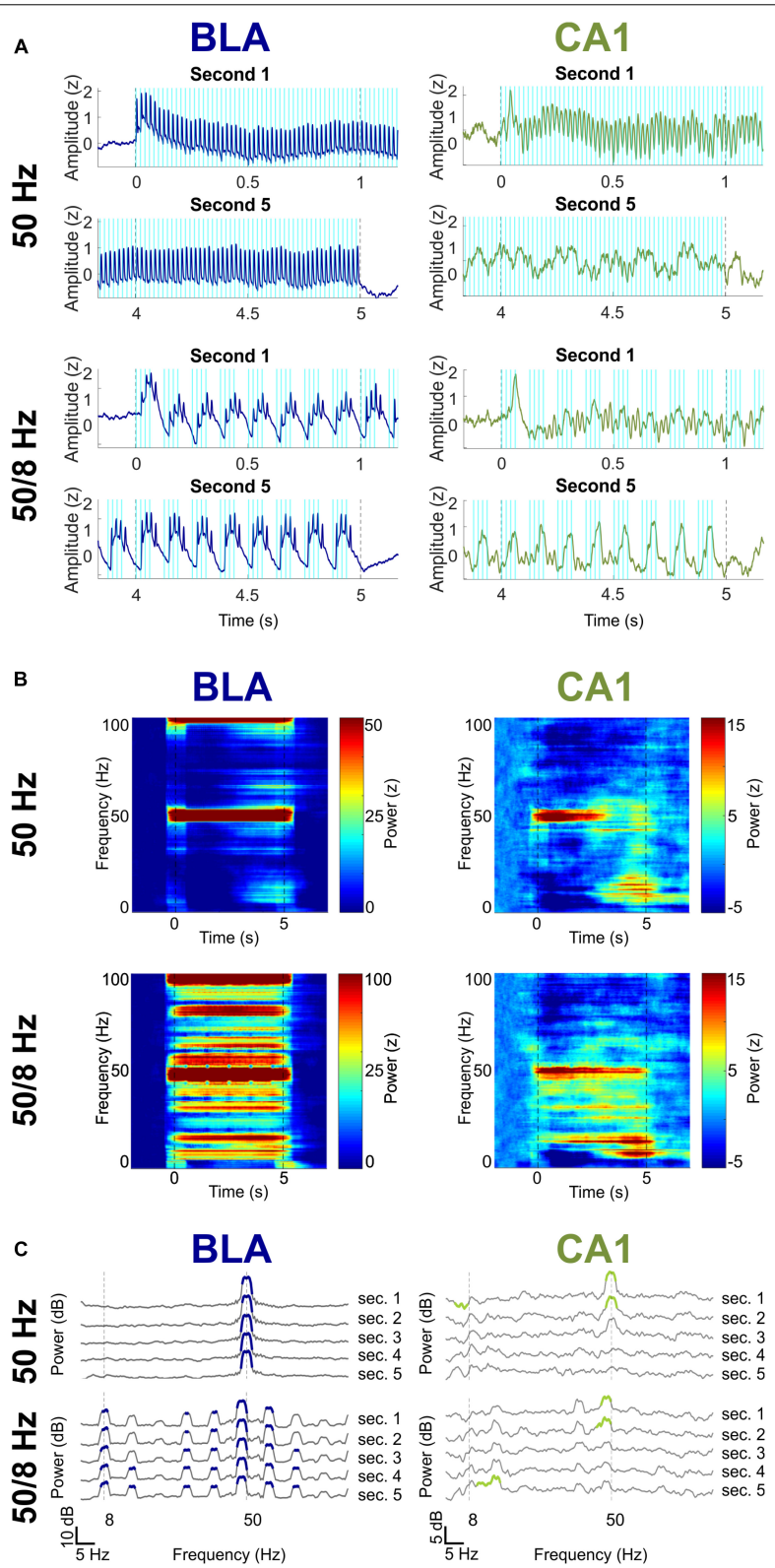

FIGURE 6 | Effects of 5-s 50 and 50/8 Hz stimulation on the BLA (blue) and CA1 (green). **(A)** Averaged BLA and CA1 LFPs in the first and last seconds of 5-s BLA stimulation. LFPs were Z-transformed and averaged across rats. **(B)** Moving window power spectrogram during 50 and 50/8 Hz 5-s stimulation, normalized to the baseline period for clarity. **(C)** Power spectrogram of second 1 (top) to second 5 (bottom), normalized against the baseline period. Frequency ranges that differed significantly between stimulation and baseline are highlighted in blue (BLA) and green (CA1).

Nevertheless, the current results indicated that direct BLA-CA1 projections were an important pathway through which optogenetic stimulation of BLA neurons influenced hippocampal activity. Infusions of the viral vector specifically targeted neurons in the posterior portion of the basal nucleus in the BLA, a region previously found to have strong direct projections to CA1 (Pitkänen et al., 2000). Postmortem histology in the present study confirmed expression of the opsin and reporter fluorophore in cell bodies in this nucleus as well as in fibers in the lacunosum-moleculare layer of intermediate CA1, consistent with the laminar profile of past anatomical studies of direct basal nucleus projections to CA1 (Pitkänen et al., 2000; Wang and Barbas, 2018). Thus, CA1 recording tetrodes were positioned near the soma (in pyramidale) of pyramidal neurons likely receiving synaptic inputs on their apical dendrites (in lacunosum-moleculare) from opsin-containing BLA neurons. Further, the short delay (6.03 ms) observed between BLA and CA1 responses to initial pulses of BLA stimulation strongly supported the involvement of this monosynaptic pathway. Previous studies have also shown that manipulation of this direct pathway was sufficient to drive behavioral changes (Rei et al., 2015; Huff et al., 2016). Taken together, the results suggested that the direct projection from BLA to CA1—although only one of many BLA projections—was important for the hippocampal responses increased by optogenetic BLA stimulation.

BLA Stimulation Modulated Neuronal Oscillations in CA1

The pattern of CA1 LFP activity in response to BLA stimulation reflected more than a concatenation of depolarizing events. Instead, CA1 LFPs responded to 1-s BLA stimulation in a manner more characteristic of neuronal oscillations, evidence for synaptic transmission that included (but was not limited to) direct BLA to CA1 projections. Specifically, LFP activity in CA1 during each of the 1-s BLA stimulation conditions showed rhythmic sinusoidal or sawtooth waveforms that corresponded to the stimulation frequency. In contrast, LFP activity in the BLA showed a sharp evoked response to each light pulse that was disconnected from preceding responses and was unrelated to stimulation frequency. One possible source of the differences between responses in BLA and CA1 LFPs was that the CA1 LFP responses may have been shaped by the low-pass frequency filtering that occurs during synaptic transmission, particularly in the case of synapses on the distal portion of apical dendrites of pyramidal neurons (Buzsáki et al., 2012), as was likely in the present study. Indeed, it is possible that synaptic transmission between regions is generally important in translating the effects of artificial stimulation to effects more reminiscent of endogenous activity. Nevertheless, the emergence of rhythmic oscillatory activity in CA1 LFPs likely also reflected circuit dynamics in the hippocampus. Possible examples include local excitatory-inhibitory interactions between CA1 pyramidal neurons and interneurons (Buzsáki and Wang, 2012) and rhythmic inputs to the hippocampus from a number of brain regions (Buzsáki, 2002). Thus, direct BLA to CA1 projections were likely key to initiating CA1 LFP responses to stimulation, but the emergence of oscillatory activity in CA1 also likely depended on other intra-hippocampal and extra-hippocampal influences on CA1 activity.

One of these main influences appeared to be ongoing theta oscillations in the hippocampus. Theta (∼8 Hz) oscillations in the hippocampus are prominent and are thought to emerge from a number of influences, including pacemaker inputs from medial septum and entorhinal cortex, from periodic activity of local interneurons, and from resonance properties of pyramidal neurons (Buzsáki, 2002). In the present study, theta power in CA1 LFPs was high at baseline, and neither 1-s BLA stimulation at 8 Hz nor at 50/8 Hz increased theta power in CA1 despite producing a large increase in theta power in BLA LFPs. However, the phase of CA1 theta oscillations appeared to reset and become strongly entrained to the 8 Hz component of both 8 and 50/8 Hz BLA stimulation. That is, hippocampal oscillations in the theta band were still modulated by BLA stimulation, even without significant increases in CA1 theta power.

Theta-Modulated 50-Hz BLA Stimulation Was Necessary to Increase Theta-Modulated Gamma Oscillations in CA1

A main question motivating the present study was whether BLA stimulation combining theta and gamma frequencies was needed to increase in the hippocampus gamma oscillations for which the amplitude was modulated by the phase of theta, the type of theta–gamma comodulation that is normally observed in the hippocampus (Bragin et al., 1995; Buzsaki et al., 2003). An alternate possibility was that continuous 50 Hz BLA stimulation would interact with endogenous hippocampal theta oscillations to also produce theta-modulated gamma oscillations. Another possibility was that 8 Hz BLA stimulation would modulate extant hippocampal gamma oscillations. Finally, it had been possible that 50/8 Hz BLA stimulation would misalign with existing theta and gamma oscillations in the hippocampus and not result in theta-modulated gamma oscillations in CA1. In short, it was possible that all or none of the stimulation conditions of interest would increase theta–gamma comodulation in the hippocampus. Nevertheless, the results of the current study showed that theta–gamma comodulation within CA1 was significantly increased during 50/8 Hz stimulation but not 50 Hz stimulation or 8 Hz stimulation. The results are important because hippocampal gamma oscillations are normally modulated by theta phase and because hippocampal theta–gamma comodulation is a neural state previously observed to correlate with successful encoding and retrieval of hippocampal memory (Tort et al., 2009; Shirvalkar et al., 2010; Trimper et al., 2014). Indeed, one hypothesis about amygdala-mediated declarative memory enhancement is that activation of the BLA elicits theta-modulated gamma oscillations in the hippocampus, which in turn promotes spike-timing dependent plasticity for recently active synapses (Manns and Bass, 2016).

Comparing the Effects of Optogenetic BLA Stimulation to Those of Electrical BLA Stimulation

Several previous studies in rats (Bass et al., 2012, 2014; Bass and Manns, 2015) and humans (Inman et al., 2018) observed improved 24-h recognition memory performance for neutral objects when the initial presentation of the objects was immediately followed by 1 s of 50/8 Hz electrical stimulation of the BLA. One of the studies in rats (Bass and Manns, 2015) also recorded neuronal activity in the intermediate hippocampus at the time of stimulation and observed increased coherence (both field-field and spike-field) between CA3 and CA1 in the slow gamma range (theta–gamma comodulation was not reported). The similarity in increased hippocampal gamma oscillations between this prior study and the present study suggests that activation of the BLA via either electrical or optogenetic stimulation can elicit oscillatory states in the hippocampus that favor memory. Nevertheless, the mechanisms of BLA activation likely differed between optogenetic and electrical stimulation. For example, optogenetic stimulation in the present study more preferentially depolarized glutamatergic cell bodies in the transfected area (though the depolarization of any neuron may have been stochastic rather than deterministic for the 50-Hz stimulation; Cardin et al., 2009; Weitz et al., 2015), whereas electrical stimulation in prior studies would have stimulated all neuron types as well as fibers of passage (Histed et al., 2009). Perhaps reflecting these differences, electrical pulses delivered to the BLA in the prior study (Bass and Manns, 2015) resulted in initial evoked responses in the hippocampus after a delay (24 ms) that suggested a polysynaptic effect of stimulation rather than the monosynaptic effect thought to be important in the present study. One possibility is that electrical stimulation of the BLA more strongly engaged the BLA-perirhinal/entorhinal-hippocampus pathway, whereas optogenetic stimulation of the BLA more strongly engaged the BLA-hippocampus pathway. If so, the results would suggest that activation of either pathway would be sufficient to produce memory-promoting oscillatory states in the hippocampus characterized by slow gamma oscillations.

CONCLUSION

The ability of 50/8 Hz optogenetic BLA stimulation to elicit theta–gamma comodulation in the hippocampus provides important insights into how the amygdala may modulate the hippocampus to prioritize memories with affective salience. Memory modulation should benefit some memories more than others if important moments are to be remembered better than unimportant moments. Thus, amygdala stimulation will likely need to be temporally specific to prioritize memories effectively. Indeed, consideration of temporal specificity will be important for any possible future therapeutic interventions and may be one explanation for the mixed results of past memory studies targeting amygdala activity (Agren, 2014; Taylor and Torregrossa, 2015). In addition, previous experiments have shown that the effects of direct hippocampal stimulation can depend on the neural state immediately prior to stimulation, which is possibly why closed-loop stimulations of the hippocampus have sometimes enhanced memory (Berger et al., 2011; Hampson et al., 2012, 2018; Ezzyat et al., 2017), whereas open-loop stimulations (i.e., delivered irrespective of ongoing activity) typically impair memory (Lacruz et al., 2010; Jacobs et al., 2016). In contrast to these studies of direct hippocampus stimulation, 50/8 Hz electrical stimulation of the BLA has reliably improved memory even when stimulation onset was not dependent on ongoing neuronal activity (Bass et al., 2012, 2014; Bass and Manns, 2015; Inman et al., 2018), perhaps because BLA stimulation was able to reset the phase of ongoing theta oscillations, as observed with optogenetic BLA stimulation in the present study. Finally, the anatomical specificity of BLA stimulation will be an additional important consideration moving forward. Future experiments using optogenetic stimulation of specific BLA projections (e.g., BLA to hippocampus) will be required to determine how projection-specific stimulation of the BLA might differentially impact hippocampal activity or memory performance. Indeed, it is an open question as to whether the glutamatergic neuron-specific optogenetic stimulation used in the present study would result in similar memory enhancement as observed in past studies using electrical stimulation of the BLA.

DATA AVAILABILITY

The datasets generated for this study are available on request to the corresponding author.

ETHICS STATEMENT

This study was carried out in accordance with the recommendations of Institutional Animal Care and Use Committee at Emory University. The protocol was approved by the Institutional Animal Care and Use Committee at Emory University.

AUTHOR CONTRIBUTIONS

NA designed and performed the experiments, analyzed the data, and wrote the manuscript. JM designed the experiments, analyzed the data, and wrote the manuscript.

FUNDING

This work was supported by National Institute of Mental Health (NIMH) 5R01MH100318.

ACKNOWLEDGMENTS

We thank David Reis for assistance with histology and microscopy.

REFERENCES

Abe, K. (2001). Modulation of hippocampal long-term potentiation by the amygdala: a synaptic mechanism linking emotion and memory. *Jpn. J. Pharmacol.* 86, 18–22. doi: 10.1254/jjp.86.18

Agren, T. (2014). Human reconsolidation: a reactivation and update. *Brain Res. Bull.* 105, 70–82. doi: 10.1016/j.brainresbull.2013.12.010

Akirav, I., and Richter-Levin, G. (2002). Mechanisms of amygdala modulation of hippocampal plasticity. *J. Neurosci.* 22, 9912–9921. doi: 10.1523/jneurosci.22-22-09912.2002

Amir, A., Headley, D. B., Lee, S. C., Haufler, D., and Pare, D. (2018). Vigilance-associated gamma oscillations coordinate the ensemble activity of basolateral amygdala neurons. *Neuron* 97, 656–669.e7. doi: 10.1016/j.neuron.2017.12.035

Barsegyan, A., McGaugh, J. L., and Roozendaal, B. (2014). Noradrenergic activation of the basolateral amygdala modulates the consolidation of object-in-context recognition memory. *Front. Behav. Neurosci.* 8:160. doi: 10.3389/fnbeh.2014.00160

Bass, D. I., and Manns, J. R. (2015). Memory-enhancing amygdala stimulation elicits gamma synchrony in the hippocampus. *Behav. Neurosci.* 129, 244–256. doi: 10.1037/bne0000052

Bass, D. I., Nizam, Z. G., Partain, K. N., Wang, A., and Manns, J. R. (2014). Amygdala-mediated enhancement of memory for specific events depends on the hippocampus. *Neurobiol. Learn. Mem.* 107, 37–41. doi: 10.1016/j.nlm.2013.10.020

Bass, D. I., Partain, K. N., and Manns, J. R. (2012). Event-specific enhancement of memory via brief electrical stimulation to the basolateral complex of the amygdala in rats. *Behav. Neurosci.* 126, 204–208. doi: 10.1037/a0026462

Berger, T. W., Hampson, R. E., Song, D., Goonawardena, A., Marmarelis, V. Z., and Deadwyler, S. A. (2011). A cortical neural prosthesis for restoring and enhancing memory. *J. Neural Eng.* 8:046017. doi: 10.1088/1741-2560/8/4/046017

Blumberg, B. J., Flynn, S. P., Barriere, S. J., Mouchati, P. R., Scott, R. C., Holmes, G. L., et al. (2016). Efficacy of nonselective optogenetic control of the medial septum over hippocampal oscillations: the influence of speed and implications for cognitive enhancement. *Physiol. Rep.* 4:e13048. doi: 10.14814/phy2.13048

Bokil, H., Andrews, P., Kulkarni, J. E., Mehta, S., and Mitra, P. P. (2010). Chronux: a platform for analyzing neural signals. *J. Neurosci. Methods* 192, 146–151. doi: 10.1016/j.jneumeth.2010.06.020

Bragin, A., Jando, G., Nadasdy, Z., Hetke, J., Wise, K., and Buzsaki, G. (1995). Gamma (40-100 hz) oscillation in the hippocampus of the behaving rat. *J. Neurosci.* 15, 47–60. doi: 10.1523/jneurosci.15-01-00047.1995

Burwell, R. D., and Amaral, D. G. (1998). Perirhinal and postrhinal cortices of the rat: interconnectivity and connections with the entorhinal cortex. *J. Comp. Neurol.* 391, 293–321. doi: 10.1002/(sici)1096-9861(19980216)391:3<293::aid-cne2>3.0.co;2-x

Buzsáki, G. (2002). Theta oscillations in the hippocampus. *Neuron* 33, 325–340. doi: 10.1016/s0896-6273(02)00586-x

Buzsáki, G. (2005). Theta rhythm of navigation: link between path integration and landmark navigation, episodic and semantic memory. *Hippocampus* 15, 827–840. doi: 10.1002/hipo.20113

Buzsáki, G., Anastassiou, C. A., and Koch, C. (2012). The origin of extracellular fields and currents — eeg, ecog, lfp and spikes. *Nat. Rev. Neurosci.* 13, 407–420. doi: 10.1038/nrn3241

Buzsaki, G., Buhl, D. L., Harris, K. D., Csicsvari, J., Czeh, B., and Morozov, A. (2003). Hippocampal network patterns of activity in the mouse. *Neuroscience* 116, 201–211. doi: 10.1016/s0306-4522(02)00669-3

Buzsaki, G., and Moser, E. I. (2013). Memory, navigation and theta rhythm in the hippocampal-entorhinal system. *Nat. Neurosci.* 16, 130–138. doi: 10.1038/nn.3304

Buzsáki, G., and Wang, X.-J. (2012). Mechanisms of gamma oscillations. *Annu. Rev. Neurosci.* 35, 203–225. doi: 10.1146/annurev-neuro-062111-150444

Cardin, J. A., Carlen, M., Meletis, K., Knoblich, U., Zhang, F., Deisseroth, K., et al. (2009). Driving fast-spiking cells induces gamma rhythm and controls sensory responses. *Nature* 459, 663–667. doi: 10.1038/nature08002

Ezzyat, Y., Kragel, J. E., Burke, J. F., Gorniak, R., Rizzuto, D. S., Kahana, M. J., et al. (2017). Direct brain stimulation modulates encoding states and memory performance in humans. *Curr. Biol.* 27, 1251–1258.

Feng, F., Headley, D. B., Amir, A., Kanta, V., Chen, Z., Paré, D., et al. (2019). Gamma oscillations in the basolateral amygdala: biophysical mechanisms and computational consequences. *eNeuro* 6:ENEURO.0388-18. doi: 10.1523/ENEURO.0388-18.2018

Hampson, R. E., Song, D., Chan, R. H., Sweatt, A. J., Riley, M. R., Gerhardt, G. A., et al. (2012). A nonlinear model for hippocampal cognitive prosthesis: memory facilitation by hippocampal ensemble stimulation. *IEEE Trans. Neural Syst. Rehabili. Eng.* 20, 184–197. doi: 10.1109/tnsre.2012.2189163

Hampson, R. E., Song, D., Robinson, B. S., Fetterhoff, D., Dakos, A. S., Roeder, B. M., et al. (2018). Developing a hippocampal neural prosthetic to facilitate human memory encoding and recall. *J. Neural Eng.* 15:036014. doi: 10.1088/1741-2552/aaaed7

Histed, M. H., Bonin, V., and Reid, R. C. (2009). Direct activation of sparse, distributed populations of cortical neurons by electrical microstimulation. *Neuron* 63, 508–522. doi: 10.1016/j.neuron.2009.07.016

Holloway-Erickson, C. M., McReynolds, J. R., and McIntyre, C. K. (2012). Memory-enhancing intra-basolateral amygdala infusions of clenbuterol increase arc and camkiiα protein expression in the rostral anterior cingulate cortex. *Front. Behav. Neurosci.* 6:17. doi: 10.3389/fnbeh.2012.00017

Huff, M. L., Emmons, E. B., Narayanan, N. S., and LaLumiere, R. T. (2016). Basolateral amygdala projections to ventral hippocampus modulate the consolidation of footshock, but not contextual, learning in rats. *Learn. Mem.* 23, 51–60. doi: 10.1101/lm.039909.115

Huff, M. L., Miller, R. L., Deisseroth, K., Moorman, D. E., and LaLumiere, R. T. (2013). Posttraining optogenetic manipulations of basolateral amygdala activity modulate consolidation of inhibitory avoidance memory in rats. *Proc. Natl. Acad. Sci. U.S.A.* 110, 3597–3602. doi: 10.1073/pnas.1219593110

Inman, C. S., Manns, J. R., Bijanki, K. R., Bass, D. I., Hamann, S., Drane, D. L., et al. (2018). Direct electrical stimulation of the amygdala enhances declarative memory in humans. *Proc. Natl. Acad. Sci. U.S.A.* 15, 98–103. doi: 10.1073/pnas.1714058114

Jacobs, J., Miller, J., Lee, S. A., Coffey, T., Watrous, A. J., Sperling, M. R., et al. (2016). Direct electrical stimulation of the human entorhinal region and hippocampus impairs memory. *Neuron* 92, 983–990. doi: 10.1016/j.neuron.2016.10.062

Jutras, M. J., Fries, P., and Buffalo, E. A. (2009). Gamma-band synchronization in the macaque hippocampus and memory formation. *J. Neurosci.* 29, 12521–12531. doi: 10.1523/JNEUROSCI.0640-09.2009

Kajiwara, R., Takashima, I., Mimura, Y., Witter, M. P., and Iijima, T. (2003). Amygdala input promotes spread of excitatory neural activity from perirhinal cortex to the entorhinal–hippocampal circuit. *J. Neurophysiol.* 89, 2176–2184. doi: 10.1152/jn.01033.2002

Klavir, O., Prigge, M., Sarel, A., Paz, R., and Yizhar, O. (2017). Manipulating fear associations via optogenetic modulation of amygdala inputs to prefrontal cortex. *Nat. Neurosci.* 20, 836–844. doi: 10.1038/nn.4523

Lacruz, M. E., Valentin, A., Seoane, J. J., Morris, R. G., Selway, R. P., and Alarcon, G. (2010). Single pulse electrical stimulation of the hippocampus is sufficient to impair human episodic memory. *Neuroscience* 170, 623–632. doi: 10.1016/j.neuroscience.2010.06.042

Manns, J. R., and Bass, D. I. (2016). The amygdala and prioritization of declarative memories. *Curr. Dir. Psychol. Sci.* 25, 261–265. doi: 10.1177/0963721416654456

Maris, E., and Oostenveld, R. (2007). Nonparametric statistical testing of eeg- and meg-data. *J. Neurosci. Methods* 164, 177–190. doi: 10.1016/j.jneumeth.2007.03.024

Mattis, J., Tye, K. M., Ferenczi, E. A., Ramakrishnan, C., O'Shea, D. J., Prakash, R., et al. (2012). Principles for applying optogenetic tools derived from direct comparative analysis of microbial opsins. *Nat. Methods* 9, 159–172. doi: 10.1038/nmeth.1808

McGaugh, J. L. (2002). Memory consolidation and the amygdala: a systems perspective. *Trends Neurosci.* 25, 456–461. doi: 10.1016/s0166-2236(02)02211-7

McIntyre, C. K., Hatfield, T., and McGaugh, J. L. (2002). Amygdala norepinephrine levels after training predict inhibitory avoidance retention performance in rats. *Eur. J. Neurosci.* 16, 1223–1226. doi: 10.1046/j.1460-9568.2002.02188.x

McIntyre, C. K., Miyashita, T., Setlow, B., Marjon, K. D., Steward, O., Guzowski, J. F., et al. (2005). Memory-influencing intra-basolateral amygdala drug infusions modulate expression of arc protein in the hippocampus. *Proc. Natl. Acad. Sci. U.S.A.* 102, 10718–10723. doi: 10.1073/pnas.0504436102

McNaughton, N., Ruan, M., and Woodnorth, M. A. (2006). Restoring theta-like rhythmicity in rats restores initial learning in the morris water maze. *Hippocampus* 16, 1102–1110. doi: 10.1002/hipo.20235

McReynolds, J. R., Anderson, K. M., Donowho, K. M., and McIntyre, C. K. (2014a). Noradrenergic actions in the basolateral complex of the amygdala modulate arc expression in hippocampal synapses and consolidation of aversive and non-aversive memory. *Neurobiol. Learn. Mem.* 115, 49–57. doi: 10.1016/j.nlm.2014.08.016

McReynolds, J. R., Holloway-Erickson, C. M., Parmar, T. U., and McIntyre, C. K. (2014b). Corticosterone-induced enhancement of memory and synaptic arc protein in the medial prefrontal cortex. *Neurobiol. Learn. Mem.* 112, 148–157. doi: 10.1016/j.nlm.2014.02.007

McReynolds, J. R., Donowho, K., Abdi, A., McGaugh, J. L., Roozendaal, B., and McIntyre, C. K. (2010). Memory-enhancing corticosterone treatment increases amygdala norepinephrine and arc protein expression in hippocampal synaptic fractions. *Neurobiol. Learn. Mem.* 93, 312–321. doi: 10.1016/j.nlm.2009.11.005

Montoya, C. P., Heynen, A. J., Faris, P. D., and Sainsbury, R. S. (1989). Modality specific type 2 theta production in the immobile rat. *Behav. Neurosci.* 103, 106–111. doi: 10.1037/0735-7044.103.1.106

Paxinos, G., and Watson, C. (1998). *The Rat Brain in Stereotaxic Coordinates*. Cambridge, MA: Academic Press.

Paz, R., Pelletier, J. G., Bauer, E. P., and Pare, D. (2006). Emotional enhancement of memory via amygdala-driven facilitation of rhinal interactions. *Nat. Neurosci.* 9, 1321–1329. doi: 10.1038/nn1771

Petrovich, G. D., Canteras, N. S., and Swanson, L. W. (2001). Combinatorial amygdalar inputs to hippocampal domains and hypothalamic behavior systems. *Brain Res. Brain Res. Rev.* 38, 247–289. doi: 10.1016/s0165-0173(01)00080-7

Pikkarainen, M., Rönkkö, S., Savander, V., Insausti, R., and Pitkänen, A. (1999). Projections from the lateral, basal, and accessory basal nuclei of the amygdala to the hippocampal formation in rat. *J. Comp. Neurol.* 403, 229–260. doi: 10.1002/(sici)1096-9861(19990111)403:2<229::aid-cne7>3.0.co;2-p

Pitkänen, A., Pikkarainen, M., Nurminen, N., and Ylinen, A. (2000). Reciprocal connections between the amygdala and the hippocampal formation, perirhinal cortex, and postrhinal cortex in rat: a review. *Ann. N. Y. Acad. Sci.* 911, 369–391. doi: 10.1111/j.1749-6632.2000.tb06738.x

Pitkänen, A., Stefanacci, L., Farb, C. R., Go, G. G., Ledoux, J. E., and Amaral, D. G. (1995). Intrinsic connections of the rat amygdaloid complex: projections originating in the lateral nucleus. *J. Comp. Neurol.* 356, 288–310. doi: 10.1002/cne.903560211

Rei, D., Mason, X., Seo, J., Graff, J., Rudenko, A., Wang, J., et al. (2015). Basolateral amygdala bidirectionally modulates stress-induced hippocampal learning and memory deficits through a p25/cdk5-dependent pathway. *Proc. Natl. Acad. Sci. U.S.A.* 112, 7291–7296. doi: 10.1073/pnas.1415845112

Roozendaal, B., Castello, N. A., Vedana, G., Barsegyan, A., and McGaugh, J. L. (2008). Noradrenergic activation of the basolateral amygdala modulates consolidation of object recognition memory. *Neurobiol. Learn. Mem.* 90, 576–579. doi: 10.1016/j.nlm.2008.06.010

Roozendaal, B., Griffith, Q. K., Buranday, J., de Quervain, D. J. F., and McGaugh, J. L. (2003). The hippocampus mediates glucocorticoid-induced impairment of spatial memory retrieval: dependence on the basolateral amygdala. *Proc. Natl. Acad. Sci. U.S.A.* 100, 1328–1333. doi: 10.1073/pnas.0337480100

Roozendaal, B., Okuda, S., Van der Zee, E. A., and McGaugh, J. L. (2006). Glucocorticoid enhancement of memory requires arousal-induced noradrenergic activation in the basolateral amygdala. *Proc. Natl. Acad. Sci. U.S.A.* 103, 6741–6746. doi: 10.1073/pnas.0601874103

Sah, P., Faber, E. S., Lopez De Armentia, M., and Power, J. (2003). The amygdaloid complex: anatomy and physiology. *Physiol. Rev.* 83, 803–834. doi: 10.1152/physrev.00002.2003

Savander, V., LeDoux, J. E., and Pitkänen, A. (1996). Interamygdaloid projections of the basal and accessory basal nuclei of the rat amygdaloid complex. *Neuroscience* 76, 725–735. doi: 10.1016/s0306-4522(96)00371-5

Sederberg, P. B., Schulze-Bonhage, A., Madsen, J. R., Bromfield, E. B., McCarthy, D. C., Brandt, A., et al. (2007). Hippocampal and neocortical gamma oscillations predict memory formation in humans. *Cereb. Cortex* 17, 1190–1196. doi: 10.1093/cercor/bhl030

Sheremet, A., Kennedy, J. P., Qin, Y., Zhou, Y., Lovett, S. D., Burke, S. N., et al. (2019). Theta-gamma cascades and running speed. *J. Neurophysiol.* 121, 444–458. doi: 10.1152/jn.00636.2018

Shirvalkar, P. R., Rapp, P. R., and Shapiro, M. L. (2010). Bidirectional changes to hippocampal theta-gamma comodulation predict memory for recent spatial episodes. *Proc. Natl. Acad. Sci. U.S.A.* 107, 7054–7059. doi: 10.1073/pnas.0911184107

Taylor, J. R., and Torregrossa, M. M. (2015). Pharmacological disruption of maladaptive memory. *Handb. Exp. Pharmacol.* 228, 381–415. doi: 10.1007/978-3-319-16522-6_13

Tort, A. B. L., Komorowski, R. W., Manns, J. R., Kopell, N. J., and Eichenbaum, H. (2009). Theta–gamma coupling increases during the learning of item–context associations. *Proc. Natl. Acad. Sci. U.S.A.* 106, 20942–20947. doi: 10.1073/pnas.0911331106

Trimper, J. B., Galloway, C. R., Jones, A. C., Mandi, K., and Manns, J. R. (2017). Gamma oscillations in rat hippocampal subregions dendate gyrus, ca3, ca1, and subiculum underlie associative memory encoding. *Cell Rep.* 21, 1–14. doi: 10.1016/j.celrep.2017.10.123

Trimper, J. B., Stefanescu, R. A., and Manns, J. R. (2014). Recognition memory and theta–gamma interactions in the hippocampus. *Hippocampus* 24, 341–353. doi: 10.1002/hipo.22228

Vouimba, R. M., and Richter-Levin, G. (2005). Physiological dissociation in hippocampal subregions in response to amygdala stimulation. *Cereb. Cortex* 15, 1815–1821. doi: 10.1093/cercor/bhi058

Wahlstrom, K. L., Huff, M. L., Emmons, E. B., Freeman, J. H., Narayanan, N. S., McIntyre, C. K., et al. (2018). Basolateral amygdala inputs to the medial entorhinal cortex selectively modulate the consolidation of spatial and contextual learning. *J. Neurosci.* 38, 2698–2712. doi: 10.1523/JNEUROSCI.2848-17.2018

Wang, J., and Barbas, H. (2018). Specificity of primate amygdalar pathways to hippocampus. *J. Neurosci.* 38, 10019–10041. doi: 10.1523/JNEUROSCI.1267-18.2018

Weitz, A. J., Fang, Z., Lee, H. J., Fisher, R. S., Smith, W. C., Choy, M., et al. (2015). Optogenetic fmri reveals distinct, frequency-dependent networks recruited by dorsal and intermediate hippocampus stimulations. *NeuroImage* 107, 229–241. doi: 10.1016/j.neuroimage.2014.10.039

Witter, M. P., and Amaral, D. G. (2004). "Hippocampal formation," in *The Rat Nervous System (Third edition)*, ed. G. Paxinos (San Diego, CA: Elsevier Academic Press), 635–704.

Conflict of Interest Statement: The authors declare that the research was conducted in the absence of any commercial or financial relationships that could be construed as a potential conflict of interest.

frontiers in Behavioral Neuroscience

ORIGINAL RESEARCH
published: 18 June 2019
doi: 10.3389/fnbeh.2019.00131

Loss of Glutamate Decarboxylase 67 in Somatostatin-Expressing Neurons Leads to Anxiety-Like Behavior and Alteration in the Akt/GSK3β Signaling Pathway

Shigeo Miyata[1], Ryota Kumagaya[2], Toshikazu Kakizaki[1], Kazuyuki Fujihara[1], Kaori Wakamatsu[2] and Yuchio Yanagawa[1]**

[1]*Department of Genetic and Behavioral Neuroscience, Graduate School of Medicine, Gunma University, Maebashi, Japan,*
[2]*Division of Molecular Science, Graduate School of Science and Technology, Gunma University, Kiryu, Japan*

Major depressive disorder (MDD) is a highly prevalent psychiatric disorder worldwide. Several lines of evidence suggest that the dysfunction of somatostatin (SOM) neurons is associated with the pathophysiology of MDD. Importantly, most SOM neurons are γ-aminobutyric acid (GABA) interneurons. However, whether the dysfunction of GABAergic neurotransmission from SOM neurons contributes to the pathophysiology of MDD remains elusive. To address this issue, we investigated the emotional behaviors and relevant molecular mechanism in mice lacking glutamate decarboxylase 67 (GAD67), an isoform of GABA-synthesizing enzyme, specifically in SOM neurons (SOM-GAD67 mice). The SOM-GAD67 mice exhibited anxiety-like behavior in the open-field test without an effect on locomotor activity. The SOM-GAD67 mice showed depression-like behavior in neither the forced swimming test nor the sucrose preference test. In addition, the ability to form contextual fear memory was normal in the SOM-GAD67 mice. Furthermore, the plasma corticosterone level was normal in the SOM-GAD67 mice both under baseline and stress conditions. The expression ratios of p-Akt^{Ser473}/Akt and p-GSK3β^{Ser9}/GSK3β were decreased in the frontal cortex of SOM-GAD67 mice. Taken together, these data suggest that the loss of GAD67 from SOM neurons may lead to the development of anxiety-like but not depression-like states mediated by modification of Akt/GSK3β activities.

Keywords: GABA, GAD, somatostatin, depression, anxiety, Akt, GSK3β

OPEN ACCESS

Edited by:
Denise Manahan-Vaughan,
Ruhr University Bochum, Germany

Reviewed by:
Etienne Sibille,
Centre for Addiction and Mental Health (CAMH), Canada
Mario U. Manto,
University of Mons, Belgium

****Correspondence:***
Shigeo Miyata
s_miyata@gunma-u.ac.jp
Yuchio Yanagawa
yuchio@gunma-u.ac.jp

Received: *26 March 2019*
Accepted: *04 June 2019*
Published: *18 June 2019*

Citation:
Miyata S, Kumagaya R, Kakizaki T, Fujihara K, Wakamatsu K and Yanagawa Y (2019) Loss of Glutamate Decarboxylase 67 in Somatostatin-Expressing Neurons Leads to Anxiety-Like Behavior and Alteration in the Akt/GSK3β Signaling Pathway. Front. Behav. Neurosci. 13:131. doi: 10.3389/fnbeh.2019.00131

INTRODUCTION

Major depressive disorder (MDD) affects approximately 10% of the population at some point in their life and is the leading cause of physical impairment, medical comorbidity, and mortality across the world (Penninx et al., 2013; Sato and Yeh, 2013). However, the current treatments are only partially effective, and patients fail to respond to trials with existing antidepressant agents targeting the monoaminergic systems (Fekadu et al., 2009; Kupfer et al., 2012). Clarifying the molecular biology of MDD is desired for developing innovative therapeutics.

Several lines of evidence indicate that the dysfunction of somatostatin (SOM)-expressing cells is likely associated with the pathophysiology of MDD (Fee et al., 2017). In the postmortem brain of patients with MDD, the expression levels of SOM were decreased in the dorsolateral prefrontal cortex (Sibille et al., 2011), the subgenual anterior cingulate cortex (Tripp et al., 2011) and the amygdala (Guilloux et al., 2012). In animal studies, mice subjected to chronic mild stress, an animal model of depression, demonstrated a decrease in the mRNA level of SOM in the prefrontal cortex (Banasr et al., 2017). On the other hand, mice with increased excitability in SOM neurons by deletion of the γ2-subunit of γ-aminobutyric $acid_A$ ($GABA_A$) receptors demonstrated anti-anxiety and anti-depressive behaviors (Fuchs et al., 2017). SOM knockout (KO) mice displayed a higher response to stress in plasma corticosterone levels (Zeyda et al., 2001; Lin and Sibille, 2015; Viollet et al., 2017). SOM KO mice displayed no change in emotional behaviors (Zeyda et al., 2001; Viollet et al., 2017) or mild anxiety-like behavior (Lin and Sibille, 2015). Lin and Sibille reported the anxiety-like/depression-like behaviors were pronounced after exposure to chronic mild stress (Lin and Sibille, 2015).

Importantly, most SOM-expressing cells in the central nervous system are GABA interneurons (Kosaka et al., 1988; Kubota et al., 1994; Esclapez and Houser, 1995; Gonchar and Burkhalter, 1997; Uematsu et al., 2008). Neuroimaging studies have demonstrated a reduction in GABA levels in the brains of patients with MDD (Sanacora et al., 1999; Hasler et al., 2007). GABA is synthesized from glutamate by glutamate decarboxylase (GAD). GAD exists in two isoforms, GAD67 and GAD65, which are independently encoded by the *GAD1* and *GAD2* genes, respectively (Soghomonian and Martin, 1998; Ji et al., 1999). Several studies have demonstrated decreased expressions of GAD67 but not GAD65 in the postmortem brains of patients with MDD (Karolewicz et al., 2010; Scifo et al., 2018), although these changes were not observed by others (Pehrson and Sanchez, 2015). Therefore, the emotional disabilities in patients with MDD may be associated with the dysfunction of GABAergic neurotransmission from SOM neurons, which disrupts an inhibitory control to neural excitability (Fee et al., 2017). Global GAD67 KO mice show cleft palate and omphalocele, and all of them die during the first day after birth (Asada et al., 1997; Kakizaki et al., 2015). We recently developed mice with conditional KO of GAD67 specifically in parvalbumin (PV)-expressing cells (PV-GAD67 mice) or SOM-expressing cells (SOM-GAD67 mice). The PV-GAD67 mice demonstrated oscillational disturbance across cortical layers and schizophrenia-like behavioral abnormalities (Fujihara et al., 2015; Kuki et al., 2015). However, we had yet to investigate the behavioral phenotypes of the SOM-GAD67 mice. Behavioral examination of SOM-GAD67 mice is important for clarifying whether the deficiency of GAD67-mediated GABA in SOM neurons contributes to MDD-related symptoms.

Akt and glycogen synthase kinase-3 β-isoform (GSK3β) are serine/threonine protein kinases that regulate multiple cellular functions including neuroplasticity and cell survival (Descorbeth et al., 2018; Wu et al., 2018). Akt/GSK3β signaling is an important signal that regulates emotional behaviors in rodents (Sui et al., 2008; Bali and Jaggi, 2016; Pan et al., 2016; Slouzkey and Maroun, 2016). Recently, the Akt/GSK3β pathway has attracted attention in the molecular biology of MDD and as a novel target of therapeutic agents (Kitagishi et al., 2012). Interestingly, GABA signaling affects Akt/GSK3β activities (Lu et al., 2012). Therefore, the functional alteration of SOM-expressing GABA neurons may affect Akt/GSK3β activities in the brain.

The aim of this study was to resolve the role of GAD67 in SOM neurons on emotional regulation using SOM-GAD67 mice. We also examined the plasma corticosterone levels and the expression levels of Akt and GSK3β proteins, which are relevant molecules to the pathophysiology of MDD.

MATERIALS AND METHODS

Ethics Statement

This study was performed in accordance with the Guidelines for Animal Experimentation at Gunma University Graduate School of Medicine and was approved by the Gunma University Ethics Committee (Permit number: 14-006). Every effort was made to minimize the number of animals used and their suffering.

Animals

We previously reported the generation of SOM-GAD67 mice (Kuki et al., 2015). Briefly, SOM-IRES-Cre mice (Taniguchi et al., 2011) were obtained from Jackson Laboratories (Bar Harbor, ME, USA; Stock No: 028864), and GAD67-floxed mice were previously described (Obata et al., 2008; Fujihara et al., 2015). $SOM^{IRES\text{-}Cre/+}$;$GAD67^{flox/flox}$ mice (SOM-GAD67 mice) were obtained by crossing female $GAD67^{flox/flox}$ mice and male $SOM^{IRES\text{-}Cre/+}$;$GAD67^{flox/+}$ mice. The littermate $GAD67^{flox/flox}$ mice were used as the control. We only used male mice from 8 weeks to 16 weeks of age for the behavioral tests, enzyme immunoassay and western blottings. The animals were housed with 2–3 mice per cage [16.5 × 27 × 12.5 (H) cm] and had free access to food and water. The animal rooms for breeding and experiments were maintained at 22 ± 3°C with a 12-h light-dark cycle (lights on at 6:00, lights off at 18:00). The animals were used only once.

Genotyping

Genotyping of the transgenic mice was performed by PCR using tail genomic DNA. The primer sequences were as follows: Cre allele, 5′-GTCTCTGGTGTAGCTGATGATCCGAA-3′ and 5′-CCCTGTTTCACTATCCAGGTTACGGA-3′; GAD67 allele, 5′-ACCTTGGCAGCTAACTAGGAGGA-3′ and 5′-ACAGAT CGGATGGGGAAGCATAA-3′. The lengths of the amplified DNA fragments were as follows: Cre allele, 321 bp; GAD67 allele, 155 bp; loxP-inserted GAD67 allele, 258 bp.

Open-Field Test

Each mouse was placed in the center of an open-field apparatus [50 cm × 50 cm × 40 (H) cm] that was illuminated by light-emitting diodes (30 lux at the center of the field) and allowed to move freely for 5 min. The time spent in the central area of the field (36% of the field) was recorded as the index of interest.

The data were collected and analyzed using ImageJ OF4 (O'Hara & Co., Ltd., Tokyo, Japan), which is a modified software that is also based on the public domain ImageJ program. The procedure was referenced to our previous report (Miyata et al., 2016).

Contextual Conditioned Fear Test

Training and testing took place in a chamber [10 × 10 × 12 (H) cm] equipped with a grid floor placed in an acoustic box. The grid floor was wired to an isolated shock generator (MSG-001, Toyo Sangyo Co. Ltd., Japan). The experiments were conducted over the course of two consecutive days. On day 1 (training session), mice were individually placed in the chamber and received scrambled foot-shocks (either 0.2 mA or 0.4 mA, 2 s) at pseudo-random times; 2.5, 5, 9 and 11.5 min, after the start of the session. Thirty seconds after the last foot shock, the mice were returned to the home cage. Twenty-four hours later, the mice were placed in the same chamber as on day 1 for 6 min without foot-shock exposure (test session). Background white-noise (55 dB) was presented during both the training and the test sessions. The protocol was based on the first two consecutive days of Lattal's method (Lattal et al., 2007) to test contextual fear conditioning. Mouse behavior was recorded and analyzed using Time FZ1 for Contextual and Cued Fear Conditioning Test software (O'Hara & Co., Ltd.). The percentage of duration of freezing behavior in the test session was calculated and compared between the genotypes.

Forced Swimming Test

Each mouse was placed in an acrylic cylinder (22 cm in height, 11.5 cm in diameter) containing 15 cm of water at room temperature (22 ± 3°C). The cylinder was placed in an isolation box. The behavior of each mouse was recorded for 6 min using a CCD camera connected to a personal computer and analyzed using ImageJ PS1 (O'Hara & Co., Ltd.), which is a modified software package that is based on the public domain ImageJ program (developed at the U.S. National Institutes of Health and available at: http://rsb.info.nih.gov/ij). The procedure was the same as that referenced in our previous report (Miyata et al., 2016). The percentage of time spent immobile during the 6-min period was calculated and compared between the genotypes.

Sucrose Preference Test

Sucrose preference test is a well-accepted behavioral test measuring an anhedonia-like state of mice and rats (Katz, 1982; Willner, 1997). Mice preferentially take sweet-taste solution compared with water. The sweet-taste preference disappears in model mice of depression, such as mice subjected to chronic mild stress. This behavioral phenotype disappears by sub-chronic treatment with antidepressant agents (Willner et al., 1987).

One week before the measurement, the mice were provided 2% sucrose solution in a drinking bottle for 24 h to habituate to sweet taste. Each mouse was subjected to water deprivation for 16 h before starting the measurement. Mice were transferred to an individual cage [16.5 × 27 × 12.5 (H) cm], and then two preweighted bottles (one containing tap water and another containing 2% sucrose solution) were presented to each mouse for 4 h. The bottles were weighed again, and the weight difference was considered to be the mouse intake from each bottle. The sum of water and sucrose intake was defined as the total intake, and sucrose preference was expressed as the percentage of sucrose intake from total intake.

Plasma Corticosterone

Blood samples were obtained from the tail vein by a small incision. Immediately after the initial sampling, the mice were restrained in 50-mL Falcon® tubes with air vents for 120 min. The blood samples were collected at 15 and 120 min during the restraint stress. After the cessation of restraint stress, the mice were returned to their home cage. Sixty minutes later, the final blood sampling was conducted. The blood samples were centrifuged at 1,000 *g* for 10 min at 4°C, and the plasma samples were collected and stored at −80°C until analysis. Blood sampling was conducted between 9:00 and 13:00 on the day of the experiment.

Plasma corticosterone concentrations were determined using a commercially available enzyme immunoassay kit (Enzo Life Sciences, Inc., Farmingdale, NY, USA) following the manufacturer's instructions.

Western Blot

The mice were killed by decapitation. The frontal cortex (FCx) was quickly dissected on an ice-cold stainless plate, immediately frozen in liquid nitrogen and stored at −80°C until use. The dissection was performed according to the Chiu's study (Chiu et al., 2007). The tissues were homogenized in ice-cold buffered sucrose (0.32 M) solution containing 20 mM Tris-HCl (pH 7.5), protease inhibitor cocktail (P8340, Sigma-Aldrich, Inc.) and phosphatase inhibitor cocktail (07575-51, Nacalai Tesque, Inc.). The homogenates were centrifuged at 1,000 *g* for 10 min at 4°C, and the supernatants were collected as the protein samples (S1 fraction). The protein concentrations were determined using a TaKaRa BCA Protein Assay Kit (T9300A, Takara Bio Inc., Japan).

The protein samples were diluted with electrophoresis sample buffer. Proteins (15 μg) were separated by SDS-polyacrylamide gels and transferred to a PVDF membrane. Blots were probed with antibodies to Akt (pan; 1:1,000, #4691, Cell Signaling Technology Japan, K.K.), phospho-Akt (Ser473; 1:2,000, #4060, Cell Signaling Technology, Danvers, MA, USA), phospho-Akt (Thr308; 1:1,000, #13038, Cell Signaling Technology, Danvers, MA, USA), GSK3β (1:1,000, #9832, Cell Signaling Technology, Danvers, MA, USA), phospho-GSK3β (Ser9; 1:1,000, #5558, Cell Signaling Technology, Danvers, MA, USA) and β-actin (1:4,000, M177-3, Medical and Biological Laboratories Co. Ltd., Japan). Immunoblots were developed using horseradish peroxidase-conjugated secondary antibodies (GE Healthcare) and then detected with chemiluminescence reagents (ECL prime, GE Healthcare) and visualized by an Light Capture AE-9672 (ATTO Co., Ltd.). The density of the bands was determined using ImageJ software.

The Akt and GSK3β activities were assessed by calculating the ratio of the band densities of phosphorylated/total proteins. The band densities of β-actin were used as the loading control.

Data Analysis

Statistical analyses were conducted using BellCurve for Excel ver. 2.12 (Social Survey Research Information Co., Ltd., Tokyo, Japan). Significant differences between two groups were evaluated by Student's *t*-test. Significant differences among the multiple groups were analyzed by one-way and two-way analysis of variance (ANOVA) with a Bonferroni multiple comparison test. Statistical significance was defined as a *p*-value less than 0.05. The data were expressed as means ± SE.

RESULTS

Behavioral Phenotypes of SOM-GAD67 Mice

To assess the anxiety-like state of mice, we performed the open-field test. The SOM-GAD67 mice exhibited significantly less time spent in the center field than the control mice (**Figures 1A,C**), but the total path length in the open-field test did not differ between the genotypes (**Figures 1B,C**).

Next, we evaluated the ability to form fear memory in mice in the contextual conditioned fear test. The duration of freezing behavior observed in the test session was not significantly different between the genotypes (**Figure 2**).

We further evaluated the depression-like state in mice in the forced swimming test and the sucrose preference test. In the forced swimming test, the duration of immobility was not significantly different between the genotypes (**Figure 3A**). In addition, there was also no difference in sucrose preference between the genotypes (**Figure 3B**).

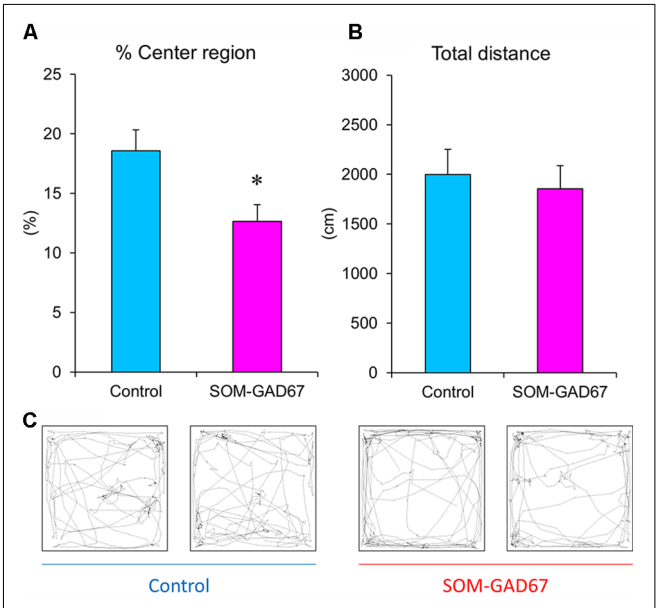

FIGURE 1 | Exploratory behaviors of the somatostatin (SOM)-glutamate decarboxylase 67 (GAD67) mice (n = 8) and control mice (n = 8) in the open-field test. The percent exploration of the center field **(A)** and total path length **(B)** for 5 min. **(C)** Illustrative examples of the travel pathway in two control and two SOM-GAD67 mice. Data represent the means + SE. *$p < 0.05$ vs. the control mice (Student's *t*-test).

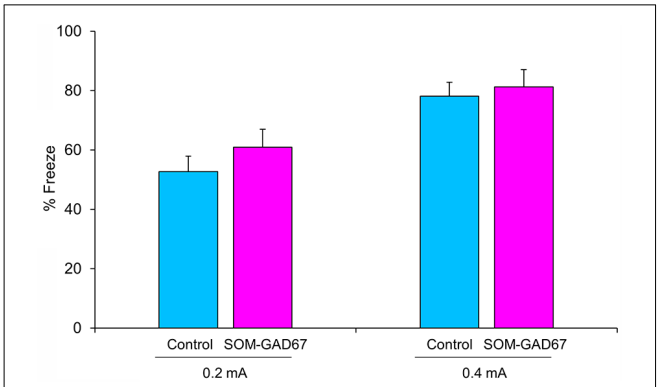

FIGURE 2 | Freezing behavior of the SOM-GAD67 mice and control mice in the contextual conditioned fear test. The mice were subjected to either 0.2 mA (SOM-GAD67; n = 7, control; n = 7) or 0.4 mA (SOM-GAD67; n = 6, control; n = 4) foot-shocks in the conditioning session. Twenty-four hours later, the mice were returned to the same chamber, and freezing behavior was measured for 6 min without foot-shock presentation. The percent duration of freezing is shown. Data represent the means + SE.

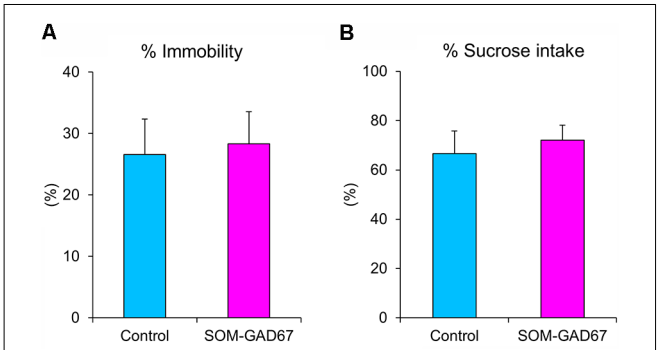

FIGURE 3 | Depression-like behaviors of the SOM-GAD67 mice and control mice in the forced swimming test and the sucrose preference test. **(A)** The percentage of time spent immobile in the forced swimming test is shown (SOM-GAD67; n = 9, control; n = 9). **(B)** The percent intake of sucrose in the sucrose preference test is shown (SOM-GAD67; n = 8, control; n = 7). Data represent the means + SE.

Stress Reactivity in SOM-GAD67 Mice

To assess the reactivity to stress, we measured the plasma corticosterone levels in mice under baseline conditions and during a stressful condition. Under baseline, there was no difference in the plasma corticosterone levels between the genotypes. Under conditions of restraint stress, the plasma corticosterone levels were increased in both genotypes, but the elevated plasma corticosterone levels were similar between the genotypes. One hour after cessation of the stress, the plasma corticosterone levels had decreased in both genotypes, but there were no differences in the plasma corticosterone levels between the genotypes (**Figure 4**).

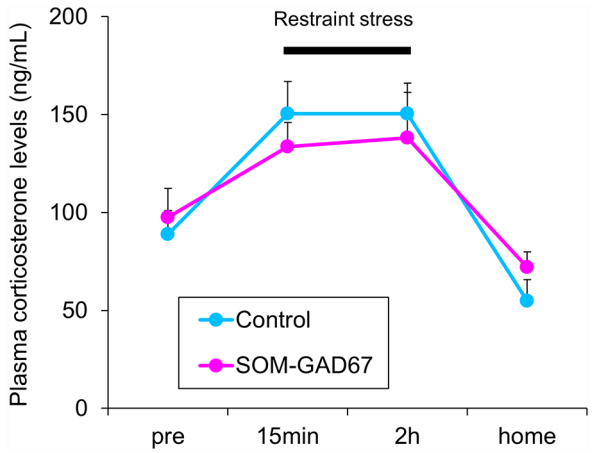

FIGURE 4 | Plasma corticosterone levels in the SOM-GAD67 mice (n = 7) and control mice (n = 7). After the first blood sample collection (pre), the mice were subjected to restraint stress for 120 min. The blood was collected 15 min and 120 min after the beginning of the stress exposure. After the cessation of the stress exposure, the mice were returned to their home cage, and 60 min later, the final blood sample was collected. The plasma corticosterone levels were determined by the enzyme immunoassay kit. Data represent the means + SE.

Cortical Akt/GSK3β Signaling in SOM-GAD67 Mice

To assess the link between Akt/GSK3β signaling and anxiety-like behavior in SOM-GAD67 mice, we examined the expression levels of Akt and GSK3β by Western blotting and calculated the expression ratio of phosphorylated forms/total proteins. The expression ratio of the p-Akt^{Ser473}/Akt protein was significantly lower in the FCx of the SOM-GAD67 mice than in that of the control mice (**Figure 5**). On the other hand, the expression ratio of the p-Akt^{Thr308}/Akt protein was not different between the genotypes. The expression ratio of p-GSK3β^{Ser9}/GSK-3β protein was significantly lower in the SOM-GAD67 mice than in the control mice (**Figure 5**).

DISCUSSION

In the current study, SOM-GAD67 mice exhibited behavioral abnormalities in the open-field test but no effects on locomotor activity. The reduction in exploration of the center region of the open field is accepted as anxiety-like behavior in rodents (Parks et al., 1998). Therefore, the deletion of GAD67 from SOM-expressing GABA neurons induced an anxiogenic-like effect in mice. In the contextual conditioned fear test, the duration of freezing was not different between the genotypes, indicating that the ability to form contextual fear memory is normal in SOM-GAD67 mice. Unexpectedly, the SOM-GAD67 mice showed depression-like behavior in neither the forced swimming test nor the sucrose preference test. The forced swimming test and the sucrose (or saccharine) preference test are accepted as animal models of depression and screening methods for antidepressant agents (Porsolt et al., 1977; Katz, 1982). Therefore, the deletion of GAD67 from SOM-expressing GABA neurons had no effect on the depression-like state in mice. Based on the current behavioral studies, we suggest that GAD67 in SOM neurons mainly regulates the anxiety-like state in mice.

In clinical studies, elevated concentrations of cortisol, the end product of the hypothalamic-pituitary-adrenal axis, are observed in the blood of patients with MDD (Schlesser et al., 1980). In addition, the blood concentrations of corticosterone, the major glucocorticoid in rodents, are increased in animal models of depression (Marcilhac et al., 1999; Miyata et al., 2004; Kubera et al., 2013; Iñiguez et al., 2014). We measured the plasma levels of corticosterone in the SOM-GAD67 mice before, during and after the restraint stress. Both genotypes demonstrated a stress-elicited increase in plasma corticosterone levels, but there was no difference between the genotypes at any time period measured. The results indicate that deletion of GAD67 from SOM neurons is not sufficient to affect the reactivity of the hypothalamic-pituitary-adrenal axis. SOM KO mice have been reported to exhibit an enhanced response to stress in plasma corticosterone levels (Zeyda et al., 2001; Lin and Sibille, 2015; Viollet et al., 2017). The hormonal reaction in the current SOM-GAD67 mice was different from that in SOM KO mice. SOM is coreleased with GABA to inhibit excitatory synaptic transmission (Martel et al., 2012). These findings indicate that the effects of SOM and GABA released from SOM neurons on the reactivity of the hypothalamic-pituitary-adrenal axis may be different.

Akt and GSK3β are serine/threonine protein kinases that regulate multiple cellular functions, including neuroplasticity and cell survival (Descorbeth et al., 2018; Wu et al., 2018). The phosphorylation of Akt at the Thr308 and Ser473 sites is needed for its full activation (Bellacosa et al., 1998). Akt at Thr308 is phosphorylated by phosphoinositide-dependent protein kinase-1 (Song et al., 2005). Akt at Ser473 is autophosphorylated or phosphorylated by mechanistic target of rapamycin complex-2 (Toker and Newton, 2000; Jacinto et al., 2006). Akt phosphorylates GSK3β at Ser9 and inhibits its kinase activity (Sutherland et al., 1993; Cross et al., 1995). Decreased activity of Akt and increased activity of GSK3β have been found in the prefrontal and occipital cortex of suicide victims with depressive disorder (Hsiung et al., 2003; Karege et al., 2007, 2011). In addition, Akt/GSK3β signaling is associated with the treatment responses of therapeutic agents of mental illness (Beaulieu et al., 2009; Kim et al., 2009; Zhang et al., 2010; Kitagishi et al., 2012; Costemale-Lacoste et al., 2016). In animal studies, mice lacking Akt2, an isoform of Akt, exhibited anxiety-like and depression-like behaviors (Leibrock et al., 2013). The expression levels of p-Akt^{Ser473} and the p-Akt^{Ser473}/Akt ratio were decreased in the hippocampus in animal models of depression (Xia et al., 2016; Wu et al., 2017). In addition, the expression level of p-GSK3β^{Ser9} in the frontal cortex was decreased in an animal model of depression (Szymańska et al., 2009). Treatments with antidepressant agents normalized these alterations in p-Akt^{Ser473} and p-GSK3β^{Ser9} expression in the prefrontal cortex and the hippocampus of those models (Xia et al., 2016; Szymańska et al., 2009; Wu et al., 2017). Furthermore, treatment with

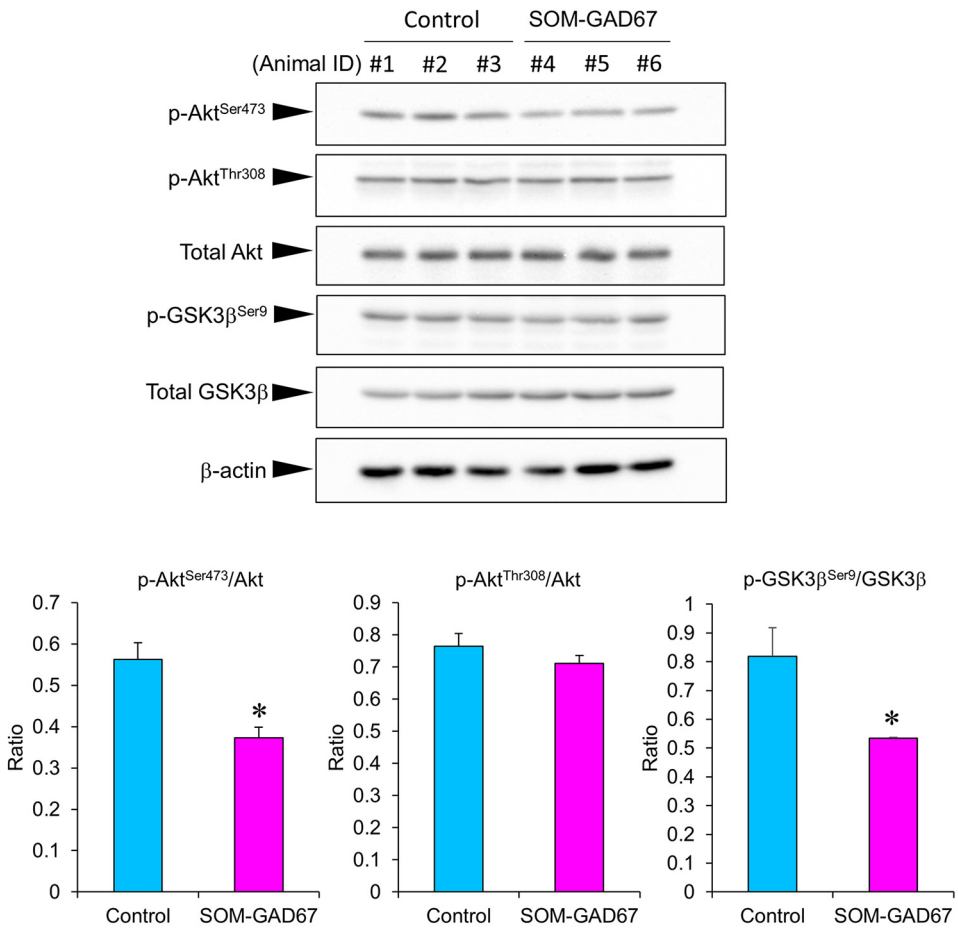

FIGURE 5 | Protein levels of Akt and glycogen synthase kinase-3 β (GSK3β) in the frontal cortex of the SOM-GAD67 mice (n = 3) and control mice (n = 3). The band densities were determined using ImageJ software. The expression ratio of phosphorylated/total proteins was compared between the genotypes. Data represent the means + SE. *$p < 0.05$ vs. the control mice (Student's t-test).

a GSK3β inhibitor ameliorated stress-elicited anxiety-like behavior in mice (Bali and Jaggi, 2017). In contrast, treatment with an Akt inhibitor interfered with the neuroprotective and anxiolytic-like effects of therapeutic agents (Pei et al., 2016). These findings indicate that the decreased activity of Akt and the increased activity of GSK3β contribute to the development of anxiety-like and depression-like states in rodents. In the current study, SOM-GAD67 mice demonstrated reductions in the p-Akt^{Ser473}/Akt ratio and p-GSK3β^{Ser9}/GSK3β ratios in the FCx, indicating that Akt kinase activity is decreased and GSK3β kinase activity is increased in the FCx of SOM-GAD67 mice, which are similar to the findings in the postmortem brain of depressive patients. The details of the mechanisms by which GAD67 in SOM neurons regulates Akt/GSK3β activity are still unclear, but impairment of Akt/GSK3β signaling may be associated with the development of an anxiety-like state in SOM-GAD67 mice. Further studies are needed to resolve this relationship.

In this study, SOM-GAD67 mice demonstrated anxiety-like behavior but not depression-like behavior. In psychiatric examinations, subsyndromal anxiety is often comorbid in patients with MDD (Zimmerman et al., 2000; Zbozinek et al., 2012; Steenkamp et al., 2017). Therefore, dysfunction of GAD67 in SOM neurons might be associated with subsyndromal anxiety but not depressive symptoms in patients with MDD.

CONCLUSION

GAD67 in SOM neurons regulates the anxiety-like state in mice mediated by the modification of cortical Akt/GSK3β activity.

DATA AVAILABILITY

All datasets generated for this study are included in the manuscript.

ETHICS STATEMENT

This study was performed in accordance with the Guidelines for Animal Experimentation at Gunma University Graduate School

of Medicine and was approved by the Gunma University Ethics Committee (Permit number: 14-006).

AUTHOR CONTRIBUTIONS

YY supervised the research. SM designed the experimental protocol, conducted the data analysis, interpretation and wrote the first draft of the manuscript. SM, RK and TK carried out animal studies including animal care. KF and KW provided critical suggestions for the research. All authors contributed to and approved the final manuscript.

FUNDING

This work was supported by Japan Society for the Promotion of Science (JSPS) KAKENHI Grant Number 26290002, 15H05872, 17H05550 and 17K17628 and Takeda Science Foundation.

ACKNOWLEDGMENTS

We thank Dr. Kunihiko Obata for providing GAD67-floxed mice and his encouragement. We also thank the staff at Bioresource Center, Gunma University Graduate School of Medicine for technical support.

REFERENCES

Asada, H., Kawamura, Y., Maruyama, K., Kume, H., Ding, R. G., Kanbara, N., et al. (1997). Cleft palate and decreased brain γ-aminobutyric acid in mice lacking the 67-kDa isoform of glutamic acid decarboxylase. *Proc. Natl. Acad. Sci. U S A* 94, 6496–6499. doi: 10.1073/pnas.94.12.6496

Bali, A., and Jaggi, A. S. (2016). Investigations on GSK-3β/NF-kB signaling in stress and stress adaptive behavior in electric foot shock subjected mice. *Behav. Brain Res.* 302, 1–10. doi: 10.1016/j.bbr.2016.01.014

Bali, A., and Jaggi, A. S. (2017). Anti-stress effects of a GSK-3β inhibitor, AR-A014418, in immobilization stress of variable duration in mice. *J. Basic Clin. Physiol. Pharmacol.* 28, 315–325. doi: 10.1515/jbcpp-2016-0157

Banasr, M., Lepack, A., Fee, C., Duric, V., Maldonado-Aviles, J., DiLeone, R., et al. (2017). Characterization of GABAergic marker expression in the chronic unpredictable stress model of depression. *Chronic Stress* 1, 1–13. doi: 10.1177/2470547017720459

Beaulieu, J.-M., Gainetdinov, R. R., and Caron, M. G. (2009). Akt/GSK3 signaling in the action of psychotropic drugs. *Annu. Rev. Pharmacol. Toxicol.* 49, 327–347. doi: 10.1146/annurev.pharmtox.011008.145634

Bellacosa, A., Chan, T. O., Ahmed, N. N., Datta, K., Malstrom, S., Stokoe, D., et al. (1998). Akt activation by growth factors is a multiple-step process: the role of the PH domain. *Oncogene* 17, 313–325. doi: 10.1038/sj.onc.1201947

Chiu, K., Lau, W. M., Lau, H. T., So, K.-F., and Chang, R. C.-C. (2007). Micro-dissection of rat brain for RNA or protein extraction from specific brain region. *J. Vis. Exp.* 7:269. doi: 10.3791/269

Costemale-Lacoste, J. F., Guilloux, J. P., and Gaillard, R. (2016). The role of GSK-3 in treatment-resistant depression and links with the pharmacological effects of lithium and ketamine: a review of the literature. *Encephale* 42, 156–164. doi: 10.1016/j.encep.2016.02.003

Cross, D. A. E., Alessi, D. R., Cohen, P., Andjelkovich, M., and Hemmings, B. A. (1995). Inhibition of glycogen synthase kinase-3 by insulin mediated by protein kinase B. *Nature* 378, 785–789. doi: 10.1038/378785a0

Descorbeth, M., Figueroa, K., Serrano-Illán, M., and De León, M. (2018). Protective effect of docosahexaenoic acid on lipotoxicity-mediated cell death in Schwann cells: implication of PI3K/AKT and mTORC2 pathways. *Brain Behav.* 8:e01123. doi: 10.1002/brb3.1123

Esclapez, M., and Houser, C. R. (1995). Somatostatin neurons are a subpopulation of GABA neurons in the rat dentate gyrus: evidence from colocalization of pre-prosomatostatin and glutamate decarboxylase messenger RNAs. *Neuroscience* 64, 339–355. doi: 10.1016/0306-4522(94)00406-u

Fee, C., Banasr, M., and Sibille, E. (2017). Somatostatin-positive gamma-aminobutyric acid interneuron deficits in depression: cortical microcircuit and therapeutic perspectives. *Biol. Psychiatry* 82, 549–559. doi: 10.1016/j.biopsych.2017.05.024

Fekadu, A., Wooderson, S. C., Markopoulo, K., Donaldson, C., Papadopoulos, A., and Cleare, A. J. (2009). What happens to patients with treatment-resistant depression? A systematic review of medium to long term outcome studies. *J. Affect. Disord.* 116, 4–11. doi: 10.1016/j.jad.2008.10.014

Fuchs, T., Jefferson, S. J., Hooper, A., Yee, P.-H., Maguire, J., and Luscher, B. (2017). Disinhibition of somatostatin-positive GABAergic interneurons results in an anxiolytic and antidepressant-like brain state. *Mol. Psychiatry* 22, 920–930. doi: 10.1038/mp.2016.188

Fujihara, K., Miwa, H., Kakizaki, T., Kaneko, R., Mikuni, M., Tanahira, C., et al. (2015). Glutamate decarboxylase 67 deficiency in a subset of GABAergic neurons induces schizophrenia-related phenotypes. *Neuropsychopharmacology* 40, 2475–2486. doi: 10.1038/npp.2015.117

Gonchar, Y., and Burkhalter, A. (1997). Three distinct families of GABAergic neurons in rat visual cortex. *Cereb. Cortex* 7, 347–358. doi: 10.1093/cercor/7.4.347

Guilloux, J.-P., Douillard-Guilloux, G., Kota, R., Wang, X., Gardier, A. M., Martinowich, K., et al. (2012). Molecular evidence for BDNF- and GABA-related dysfunctions in the amygdala of female subjects with major depression. *Mol. Psychiatry* 17, 1130–1142. doi: 10.1038/mp.2011.113

Hasler, G., van der Veen, J. W., Tumonis, T., Meyers, N., Shen, J., and Drevets, W. C. (2007). Reduced prefrontal glutamate/glutamine and γ-aminobutyric acid levels in major depression determined using proton magnetic resonance spectroscopy. *Arch. Gen. Psychiatry* 64, 193–200. doi: 10.1001/archpsyc.64.2.193

Hsiung, S. C., Adlersberg, M., Arango, V., Mann, J. J., Tamir, H., and Liu, K. P. (2003). Attenuated 5-HT1A receptor signaling in brains of suicide victims: involvement of adenylyl cyclase, phosphatidylinositol 3-kinase, Akt and mitogen-activated protein kinase. *J. Neurochem.* 87, 182–194. doi: 10.1046/j.1471-4159.2003.01987.x

Iñiguez, S. D., Riggs, L. M., Nieto, S. J., Dayrit, G., Zamora, N. N., Shawhan, K. L., et al. (2014). Social defeat stress induces a depression-like phenotype in adolescent male c57BL/6 mice. *Stress* 17, 247–255. doi: 10.3109/10253890.2014.910650

Jacinto, E., Facchinetti, V., Liu, D., Soto, N., Wei, S., Jung, S. Y., et al. (2006). SIN1/MIP1 maintains rictor-mTOR complex integrity and regulates Akt phosphorylation and substrate specificity. *Cell* 127, 125–137. doi: 10.1016/j.cell.2006.08.033

Ji, F., Kanbara, N., and Obata, K. (1999). GABA and histogenesis in fetal and neonatal mouse brain lacking both the isoforms of glutamic acid decarboxylase. *Neurosci. Res.* 33, 187–194. doi: 10.1016/s0168-0102(99)00011-5

Kakizaki, T., Oriuchi, N., and Yanagawa, Y. (2015). GAD65/GAD67 double knockout mice exhibit intermediate severity in both cleft palate and omphalocele compared with GAD67 knockout and VGAT knockout mice. *Neuroscience* 288, 86–93. doi: 10.1016/j.neuroscience.2014.12.030

Karege, F., Perroud, N., Burkhardt, S., Fernandez, R., Ballmann, E., La Harpe, R., et al. (2011). Alterations in phosphatidylinositol 3-kinase activity and PTEN phosphatase in the prefrontal cortex of depressed suicide victims. *Neuropsychobiology* 63, 224–231. doi: 10.1159/000322145

Karege, F., Perroud, N., Burkhardt, S., Schwald, M., Ballmann, E., La Harpe, R., et al. (2007). Alteration in kinase activity but not in protein levels of protein kinase B and glycogen synthase kinase-3β in ventral prefrontal cortex of depressed suicide victims. *Biol. Psychiatry* 61, 240–245. doi: 10.1016/j.biopsych.2006.04.036

Karolewicz, B., Maciag, D., O'Dwyer, G., Stockmeier, C. A., Feyissa, A. M., and Rajkowska, G. (2010). Reduced level of glutamic acid decarboxylase-67 kDa in

the prefrontal cortex in major depression. *Int. J. Neuropsychopharmacol.* 13, 411–420. doi: 10.1017/s1461145709990587

Katz, R. J. (1982). Animal model of depression: pharmacological sensitivity of a hedonic deficit. *Pharmacol. Biochem. Behav.* 16, 965–968. doi: 10.1016/0091-3057(82)90053-3

Kim, J. Y., Duan, X., Liu, C. Y., Jang, M.-H., Guo, J. U., Pow-anpongkul, N., et al. (2009). DISC1 regulates new neuron development in the adult brain *via* modulation of AKT-mTOR signaling through KIAA1212. *Neuron* 63, 761–773. doi: 10.1016/j.neuron.2009.08.008

Kitagishi, Y., Kobayashi, M., Kikuta, K., and Matsuda, S. (2012). Roles of PI3K/AKT/GSK3/mTOR pathway in cell signaling of mental illnesses. *Depress. Res. Treat.* 2012:752563. doi: 10.1155/2012/752563

Kosaka, T., Wu, J. Y., and Benoit, R. (1988). GABAergic neurons containing somatostatin-like immunoreactivity in the rat hippocampus and dentate gyrus. *Exp. Brain Res.* 71, 388–398. doi: 10.1007/bf00247498

Kubera, M., Curzytek, K., Duda, W., Leskiewicz, M., Basta-Kaim, A., Budziszewska, B., et al. (2013). A new animal model of (chronic) depression induced by repeated and intermittent lipopolysaccharide administration for 4 months. *Brain. Behav. Immun.* 31, 96–104. doi: 10.1016/j.bbi.2013.01.001

Kubota, Y., Hattori, R., and Yui, Y. (1994). Three distinct subpopulations of GABAergic neurons in rat frontal agranular cortex. *Brain Res.* 649, 159–173. doi: 10.1016/0006-8993(94)91060-x

Kuki, T., Fujihara, K., Miwa, H., Tamamaki, N., Yanagawa, Y., and Mushiake, H. (2015). Contribution of parvalbumin and somatostatin-expressing GABAergic neurons to slow oscillations and the balance in beta-gamma oscillations across cortical layers. *Front. Neural Circuits* 9:6. doi: 10.3389/fncir.2015.00006

Kupfer, D. J., Frank, E., and Phillips, M. L. (2012). Major depressive disorder: new clinical, neurobiological, and treatment perspectives. *Lancet* 379, 1045–1055. doi: 10.1016/S0140-6736(11)60602-8

Lattal, K. M., Barrett, R. M., and Wood, M. A. (2007). Systemic or intrahippocampal delivery of histone deacetylase inhibitors facilitates fear extinction. *Behav. Neurosci.* 121, 1125–1131. doi: 10.1037/0735-7044.121.5.1125

Leibrock, C., Ackermann, T. F., Hierlmeier, M., Lang, F., Borgwardt, S., and Lang, U. E. (2013). Akt2 deficiency is associated with anxiety and depressive behavior in mice. *Cell. Physiol. Biochem.* 32, 766–777. doi: 10.1159/000354478

Lin, L. C., and Sibille, E. (2015). Somatostatin, neuronal vulnerability and behavioral emotionality. *Mol. Psychiatry* 20, 377–387. doi: 10.1038/mp.2014.184

Lu, F. F., Su, P., Liu, F., and Daskalakis, Z. J. (2012). Activation of GABAB receptors inhibits protein kinase B/glycogen synthase kinase 3 signaling. *Mol. Brain* 5:41. doi: 10.1186/1756-6606-5-41

Marcilhac, A., Faudon, M., Anglade, G., Hery, F., and Siaud, P. (1999). An investigation of serotonergic involvement in the regulation of ACTH and corticosterone in the olfactory bulbectomized rat. *Pharmacol. Biochem. Behav.* 63, 599–605. doi: 10.1016/s0091-3057(99)00024-6

Martel, G., Dutar, P., Epelbaum, J., and Viollet, C. (2012). Somatostatinergic systems: an update on brain functions in normal and pathological aging. *Front. Endocrinol.* 3:154. doi: 10.3389/fendo.2012.00154

Miyata, S., Hirano, S., and Kamei, J. (2004). Diabetes attenuates the antidepressant-like effect mediated by the activation of 5-HT1A receptor in the mouse tail suspension test. *Neuropsychopharmacology* 29, 461–469. doi: 10.1038/sj.npp.1300354

Miyata, S., Kurachi, M., Okano, Y., Sakurai, N., Kobayashi, A., Harada, K., et al. (2016). Blood transcriptomic markers in patients with late-onset major depressive disorder. *PLoS One* 11:e0150262. doi: 10.1371/journal.pone.0150262

Obata, K., Hirono, M., Kume, N., Kawaguchi, Y., Itohara, S., and Yanagawa, Y. (2008). GABA and synaptic inhibition of mouse cerebellum lacking glutamate decarboxylase 67. *Biochem. Biophys. Res. Commun.* 370, 429–433. doi: 10.1016/j.bbrc.2008.03.110

Pan, B., Huang, X.-F., and Deng, C. (2016). Chronic administration of aripiprazole activates GSK3β-dependent signalling pathways and up-regulates GABAA receptor expression and CREB1 activity in rats. *Sci. Rep.* 6:30040. doi: 10.1038/srep30040

Parks, C. L., Robinson, P. S., Sibille, E., Shenk, T., and Toth, M. (1998). Increased anxiety of mice lacking the serotonin1A receptor. *Proc. Natl. Acad. Sci. U S A* 95, 10734–10739. doi: 10.1073/pnas.95.18.10734

Pehrson, A. L., and Sanchez, C. (2015). Altered γ-aminobutyric acid neurotransmission in major depressive disorder: a critical review of the supporting evidence and the influence of serotonergic antidepressants. *Drug Des. Devel. Ther.* 9, 603–624. doi: 10.2147/DDDT.S62912

Pei, B., Yang, M., Qi, X., Shen, X., Chen, X., and Zhang, F. (2016). Quercetin ameliorates ischemia/reperfusion-induced cognitive deficits by inhibiting ASK1/JNK3/caspase-3 by enhancing the Akt signaling pathway. *Biochem. Biophys. Res. Commun.* 478, 199–205. doi: 10.1016/j.bbrc.2016.07.068

Penninx, B. W. J. H., Milaneschi, Y., Lamers, F., and Vogelzangs, N. (2013). Understanding the somatic consequences of depression: biological mechanisms and the role of depression symptom profile. *BMC Med.* 11:129. doi: 10.1186/1741-7015-11-129

Porsolt, R. D., Bertin, A., and Jalfre, M. (1977). Behavioral despair in mice: a primary screening test for antidepressants. *Arch. Int. Pharmacodyn. Ther.* 229, 327–336.

Sanacora, G., Mason, G. F., Rothman, D. L., Behar, K. L., Hyder, F., Petroff, O. A., et al. (1999). Reduced cortical γ-aminobutyric acid levels in depressed patients determined by proton magnetic resonance spectroscopy. *Arch. Gen. Psychiatry* 56, 1043–1047. doi: 10.1001/archpsyc.56.11.1043

Sato, S., and Yeh, T. L. (2013). Challenges in treating patients with major depressive disorder: the impact of biological and social factors. *CNS Drugs* 27, S5–S10. doi: 10.1007/s40263-012-0028-8

Schlesser, M. A., Winokur, G., and Sherman, B. M. (1980). Hypothalamic-pituitary-adrenal axis activity in depressive illness. Its relationship to classification. *Arch. Gen. Psychiatry* 37, 737–743. doi: 10.1001/archpsyc.1980.01780200015001

Scifo, E., Pabba, M., Kapadia, F., Ma, T., Lewis, D. A., Tseng, G. C., et al. (2018). Sustained molecular pathology across episodes and remission in major depressive disorder. *Biol. Psychiatry* 83, 81–89. doi: 10.1016/j.biopsych.2017.08.008

Sibille, E., Morris, H. M., Kota, R. S., and Lewis, D. A. (2011). GABA-related transcripts in the dorsolateral prefrontal cortex in mood disorders. *Int. J. Neuropsychopharmacol.* 14, 721–734. doi: 10.1017/s1461145710001616

Slouzkey, I., and Maroun, M. (2016). PI3-kinase cascade has a differential role in acquisition and extinction of conditioned fear memory in juvenile and adult rats. *Learn. Mem.* 23, 723–731. doi: 10.1101/lm.041806.116

Soghomonian, J. J., and Martin, D. L. (1998). Two isoforms of glutamate decarboxylase: why? *Trends Pharmacol. Sci.* 19, 500–505. doi: 10.1016/s0165-6147(98)01270-x

Song, G., Ouyang, G., and Bao, S. (2005). The activation of Akt/PKB signaling pathway and cell survival. *J. Cell. Mol. Med.* 9, 59–71. doi: 10.1111/j.1582-4934.2005.tb00337.x

Steenkamp, L. R., Hough, C. M., Reus, V. I., Jain, F. A., Epel, E. S., James, S. J., et al. (2017). Severity of anxiety- but not depression- is associated with oxidative stress in major depressive disorder. *J. Affect. Disord.* 219, 193–200. doi: 10.1016/j.jad.2017.04.042

Sui, L., Wang, J., and Li, B.-M. (2008). Role of the phosphoinositide 3-kinase-Akt-mammalian target of the rapamycin signaling pathway in long-term potentiation and trace fear conditioning memory in rat medial prefrontal cortex. *Learn. Mem.* 15, 762–776. doi: 10.1101/lm.1067808

Sutherland, C., Leighton, I. A., and Cohen, P. (1993). Inactivation of glycogen synthase kinase-3β by phosphorylation: new kinase connections in insulin and growth-factor signalling. *Biochem. J.* 296, 15–19. doi: 10.1042/bj2960015

Szymańska, M., Suska, A., Budziszewska, B., Jaworska-Feil, L., Basta-Kaim, A., Leśkiewicz, M., et al. (2009). Prenatal stress decreases glycogen synthase kinase-3 phosphorylation in the rat frontal cortex. *Pharmacol. Rep.* 61, 612–620. doi: 10.1016/s1734-1140(09)70113-6

Taniguchi, H., He, M., Wu, P., Kim, S., Paik, R., Sugino, K., et al. (2011). A resource of Cre driver lines for genetic targeting of GABAergic neurons in cerebral cortex. *Neuron* 71, 995–1013. doi: 10.1016/j.neuron.2011.07.026

Toker, A., and Newton, A. C. (2000). Akt/protein kinase B is regulated by autophosphorylation at the hypothetical PDK-2 site. *J. Biol. Chem.* 275, 8271–8274. doi: 10.1074/jbc.275.12.8271

Tripp, A., Kota, R. S., Lewis, D. A., and Sibille, E. (2011). Reduced somatostatin in subgenual anterior cingulate cortex in major depression. *Neurobiol. Dis.* 42, 116–124. doi: 10.1016/j.nbd.2011.01.014

Uematsu, M., Hirai, Y., Karube, F., Ebihara, S., Kato, M., Abe, K., et al. (2008). Quantitative chemical composition of cortical GABAergic neurons revealed in transgenic venus-expressing rats. *Cereb. Cortex* 18, 315–330. doi: 10.1093/cercor/bhm056

Viollet, C., Simon, A., Tolle, V., Labarthe, A., Grouselle, D., Loe-Mie, Y., et al. (2017). Somatostatin-IRES-Cre mice: between knockout and wild-type? *Front. Endocrinol.* 8:131. doi: 10.3389/fendo.2017.00131

Willner, P. (1997). Validity, reliability and utility of the chronic mild stress model of depression: a 10-year review and evaluation. *Psychopharmacology* 134, 319–329. doi: 10.1007/s002130050456

Willner, P., Towell, A., Sampson, D., Sophokleous, S., and Muscat, R. (1987). Reduction of sucrose preference by chronic unpredictable mild stress and its restoration by a tricyclic antidepressant. *Psychopharmacology* 93, 358–364. doi: 10.1007/bf00187257

Wu, Z., Wang, G., Wei, Y., Xiao, L., and Wang, H. (2018). PI3K/AKT/GSK3β/CRMP-2-mediated neuroplasticity in depression induced by stress. *Neuroreport* 29, 1256–1263. doi: 10.1097/WNR.0000000000001096

Wu, R., Zhang, H., Xue, W., Zou, Z., Lu, C., Xia, B., et al. (2017). Transgenerational impairment of hippocampal Akt-mTOR signaling and behavioral deficits in the offspring of mice that experience postpartum depression-like illness. *Prog. Neuropsychopharmacol. Biol. Psychiatry* 73, 11–18. doi: 10.1016/j.pnpbp.2016.09.008

Xia, B., Chen, C., Zhang, H., Xue, W., Tang, J., Tao, W., et al. (2016). Chronic stress prior to pregnancy potentiated long-lasting postpartum depressive-like behavior, regulated by Akt-mTOR signaling in the hippocampus. *Sci. Rep.* 6:35042. doi: 10.1038/srep35042

Zbozinek, T. D., Rose, R. D., Wolitzky-Taylor, K. B., Sherbourne, C., Sullivan, G., Stein, M. B., et al. (2012). Diagnostic overlap of generalized anxiety disorder and major depressive disorder in a primary care sample. *Depress. Anxiety* 29, 1065–1071. doi: 10.1002/da.22026

Zeyda, T., Diehl, N., Paylor, R., Brennan, M. B., and Hochgeschwender, U. (2001). Impairment in motor learning of somatostatin null mutant mice. *Brain Res.* 906, 107–114. doi: 10.1016/s0006-8993(01)02563-x

Zhang, K., Yang, C., Xu, Y., Sun, N., Yang, H., Liu, J., et al. (2010). Genetic association of the interaction between the BDNF and GSK3B genes and major depressive disorder in a Chinese population. *J. Neural Transm.* 117, 393–401. doi: 10.1007/s00702-009-0360-4

Zimmerman, M., McDermut, W., and Mattia, J. I. (2000). Frequency of anxiety disorders in psychiatric outpatients with major depressive disorder. *Am. J. Psychiatry* 157, 1337–1340. doi: 10.1176/appi.ajp.157.8.1337

Conflict of Interest Statement: The authors declare that the research was conducted in the absence of any commercial or financial relationships that could be construed as a potential conflict of interest.

frontiers in Behavioral Neuroscience

BRIEF RESEARCH REPORT
published: 02 July 2019
doi: 10.3389/fnbeh.2019.00146

The Comparison of a New Ultrasound-Induced Depression Model to the Chronic Mild Stress Paradigm

Yana A. Zorkina[1]†, Eugene A. Zubkov[1†], Anna Yu. Morozova[1†], Valeriya M. Ushakova[1] and Vladimir P. Chekhonin[1,2]*

[1]*Department of Basic and Applied Neurobiology, V.P. Serbsky National Medical Research Center for Psychiatry and Narcology, Moscow, Russia,* [2]*Department of Medical Nanobiotechnology, Pirogov Russian National Research Medical University, Moscow, Russia*

Willner's "chronic mild stress" (CMS) model is a globally recognized and most commonly used depression model. A depression model induced by ultrasonic exposure of variable frequencies has been created in our laboratory. This article compares two models of the depressive-like state according to three validity criteria. *Face validity* has been demonstrated in sucrose preference test, Porsolt test, social interest, open field and the Morris water maze. Rats after ultrasound impact have more pronounced anhedonia and social isolation. *The construct validity* has been proven due to increased levels of corticosterone, epinephrine and norepinephrine and reduced levels of dopamine and some of its metabolites in rat plasma after ultrasound exposure. *Predictive validity* has been described previously, where the therapeutic effects of various classes of antidepressants have been shown. Our study has demonstrated that the ultrasound-induced depression model is suitable, such as the generally accepted CMS protocol, and meets all required validity criteria. The model presented in this article might help to study pathogenetic mechanisms of depressive disorders, as well as to test promising methods of depression treatment.

Keywords: depression, stress, rats, ultrasonic, chronic mild stress, animal model

OPEN ACCESS

Edited by:
Fuat Balcı,
Koç University, Turkey

Reviewed by:
Stefan Brudzynski,
Brock University, Canada
Ayse Karson,
Kocaeli University, Turkey

****Correspondence:***
Yana A. Zorkina
zorkina.ya@serbsky.ru

†These authors have contributed equally to this work

Received: *12 April 2019*
Accepted: *18 June 2019*
Published: *02 July 2019*

Citation:
Zorkina YA, Zubkov EA, Morozova AY, Ushakova VM and Chekhonin VP (2019) The Comparison of a New Ultrasound-Induced Depression Model to the Chronic Mild Stress Paradigm. Front. Behav. Neurosci. 13:146. doi: 10.3389/fnbeh.2019.00146

INTRODUCTION

At a global level, over 4.4% of the world's population is estimated to suffer from depression (WHO, 2017). The creation of models in psychiatry has its limitations due to the exceptional specificity of the human psychology including the presence of highly differentiated structures of the neocortex that form a functional unit responsible for consciousness and thinking, as well as for speech as a second signal system (Vocate, 1987). Depressions are divided into reactive (stress-induced) and endogenous conditionally induced (Malki et al., 2014). Stress-induced models include: deprivation models, models created by pain shock, placement in extreme conditions, immobilization, forced swimming, social isolation, and mice social defeat model. Sixty-six percentage of all articles published during the year 2018 about stress-induced depression are based on Willner's protocol. In this model, rats are exposed to stressors that change unpredictably resulting in depressive-like conditions in animals (Willner et al., 1987). The recently published meta-analysis shows that

chronic mild stress (CMS) protocol is strongly associated with anhedonic behavior in rodents. The authors point out the heterogeneity in the animals' responses, even in individual subgroups, because of the many variations of this protocol (Antoniuk et al., 2019). However, there is still no adequate and well-reproducible model describing a depressive-like state corresponding to that in humans.

The listed above protocols do not cause psychological trauma, without physical impact on the animal. Social isolation or separation from the mother may be partially considered models of psychological stress. But it is impossible to extrapolate these results to humans, because early social isolation does not always lead to depression in adulthood, and in adults, it causes other mental disorders (Tan et al., 2017).

Models of psychological trauma in animals are few; besides, protocols used to create such models contain, for the most part, stress stimuli that differ greatly from the negative factors affecting humans in the society in developed countries, namely, they do not focus on the chronic informational uncertainty. Therefore, there are no available animal models of depression-like behavior, where informational uncertainty, concerning for example terrorist acts, wars, catastrophes, as well as economic and social instability uncertainty would be the stress factor, being the main factor causing depression in humans (Neumann et al., 2011).

Informational uncertainty in rodents with subsequent induction of depressive-like behavior can be caused by exposure to ultrasound (US) of variable frequency. Exposure to US with a frequency of 20 kHz to 45 kHz simulates the information flow carrying a negative emotional load (Takahashi et al., 2011) and forms a state of learned helplessness, which is interpreted as a depressive-like state in animals. The first article about the new depression model was published in 2013 (Morozova et al., 2013a). At the beginning of the development of our US paradigm, we conducted the study that evaluated the impact of "white noise" on rats' behavior. According to previous work (Morozova et al., 2016), a comparison of a 3-week exposure to 50 dB-ultrasound of mixed frequencies ("white noise") at the range of 16–20 kHz did not result in a depressive-like state. The exposure of single frequency US-wave, 22 kHz, leads to anxiety in the first 5 min after exposure (Demaestri et al., 2019), but continuous action of 22 kHz does not lead to behavioral changes, because of an adaptation to the unchangeable stress impact (da Oliveira et al., 2015).

The aim of this article is to compare the CMS model with the ultrasound-induced depression model which has been developed in our laboratory.

MATERIALS AND METHODS

Animals

Experiments were performed on male Wistar rats (n = 60) that were 2.5 months old. The animals were provided by Pushchino, RAS, Moscow region. Experimental animals (US and CMS group) were housed individually in polycarbonate transparent cages (42 × 26 × 15 cm) during stress protocols. Control group were housed in groups of five animals in polycarbonate cages (55 × 35 × 20 cm). After the stress protocol rats from CMS and US group were placed in cages in groups. There was no group of experimental animals which was housed individually because our previous study showed that 3-week isolation does not lead to depressive-like behavior (Gorlova et al., 2018). They were maintained on a 12-h light/dark cycle under controllable laboratory conditions; food and water were available *ad libitum*. Housing conditions and all experimental procedures were set up and maintained in accordance with Directive 2010/63/EU of 22 September 2010 and approved by the local ethical committee of V.P. Serbsky National Medical Research Center for Psychiatry and Narcology.

Study Design

The animals were divided into the following experimental groups: control animals (n = 20); rats exposed to ultrasonic radiation for 3 weeks (n = 20); and rats exposed to CMS protocol (n = 20). On the next day after CMS and US exposure, the sucrose preference test was performed. The tests were conducted with a delay of 1 day between them in the following order: social interest test, open field, forced swim and Morris water maze.

Ultrasonic Exposure

The US exposure was performed for 24 h each day during 3 weeks and consists of periods between following range: low frequencies (20–25 kHz), middle range frequencies (25 < × < 40 kHz) and frequencies of high range (40–45 kHz). The ultrasound frequencies changed every 10 min. Low and middle frequency ultrasound constituted 35% of emission each, high frequencies constituted 30% of emission time. The loudness of the sound was fluctuating at the range ±10% of the averaged value, i.e., 50 ± 5 dB. Rats communicate with intensity up to 86 dB, so 50 dB is normal volume of sound (Smith, 1979). The ultrasonic device (Weitech, Belgium) was suspended from the ceiling, and the loudspeaker was oriented downwards, where there were cages with rats at a distance of 2 m (**Figure 1**). The position of the cages was changed every 3 days. The rats exposed to US were kept in the separate room in equal conditions with control and CMS groups.

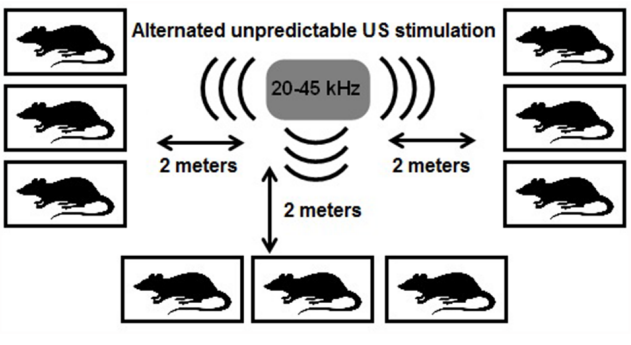

FIGURE 1 | Scheme of ultrasound (US) impact. All rats were placed in individual cages in equal distance (2 m) from US generator. It generates US waves of variable frequencies from 20 to 45 kHz. US exposure was performed 24-h per day during 3 weeks.

CMS Protocol

The CMS was performed for 3 weeks during following protocol: Monday 10 a.m.–6 p.m. food deprivation, Monday 6 p.m.–Tuesday 10 a.m. intermittent lighting (off/on every 2 h), Tuesday 10 a.m.–6 p.m. 45° cage tilt, Tuesday 6 p.m.–Wednesday 10 a.m. water deprivation, Wednesday 10 a.m.–6 p.m. stroboscopic illumination in the dark, Wednesday 6 p.m.–Thursday 10 a.m. light in the night; Thursday 10 a.m.–6 p.m. Food deprivation in soiled cage (water in sawdust; 250 ml of water in each cage), Thursday 6 p.m.–Friday 10 a.m. mouse cage, Friday 10 a.m.–6 p.m. intermittent lighting (off/on every 2 h), Friday 6 p.m.–Sunday 10 a.m. paired housing (new partner 6 month old), Sunday 10 a.m.–6 p.m. stroboscopic illumination in the dark, Sunday 6 p.m.–Monday 10 a.m. light in the night.

Behavior Tests

Social Interest Test

Social interaction test was performed as described previously (Morozova et al., 2016). The duration of social interaction was defined as any pro-active contacts that the rat has shown towards the juvenile male, which typically comprised of approaches, body contacts, following, sniffing and exploration, and was scored using RealTimer software (OpenScience, Russia).

Sucrose Test

During this test, rats were given a free choice between two bottles for 24 h, one with a 1% sucrose solution and another with tap water (Morozova et al., 2016). No previous food or water deprivation was applied before the test.

Open Field Test

The open field test was carried out in a round arena (d = 120 cm, h = 50 cm) made from gray plastic and illuminated with white light (25 lx). The animal was placed near the wall and its movements were tracked for a 5 min period with a digital camera which was placed above the arena. The number of crossed squares (horizontal locomotor activity) and the number of rearings (vertical activity) were evaluated using RealTimer software (OpenScience, Russia).

Forced Swim Test

A transparent cylindrical pool made of glass (diameter 15 cm, height 40 cm) was filled with water (24°C) to a level that prevented a rat from touching the bottom. Animals were put in the pool for 8 min. The absence of any directed movements of an animal's head and body was considered as immobility and was kept track of during the last 6 min of the test. We used the following protocol with some modification (Bourin et al., 2004).

Morris Test

Morris water maze was performed following standard procedures (Morris, 1984). The Morris water maze was represented by a round pool (diameter 150 cm) with gray walls. The pool was filled up with clear water (depth 40 cm, water temperature 24°C). The round plastic transparent platform (diameter 8 cm) was placed to the center of one of the pool quadrants and 2 cm under the surface. Training consisted of eight sessions. Each animal was placed into the water in different places. Swimming time was recorded until the animal reached the platform. Rats that were unable to find the platform for 60 s were then directed to the platform by a hand. Upon reaching the platform, the rats were left on it for 15 s. The interval between training sessions was 1 min. 48 h after training, the latency to find the platform was measured in one 60 s session. The orienting points were located around the maze on the walls.

Plasma Corticosterone and Catecholamine Levels

The plasma was collected from tail vein at the last day of US exposure at 11 a.m. in the tubes with heparin at the end of ultrasound exposure. The plasma corticosterone level was determined using a commercial ELISA assay kit (Cat. No: AC-14F1) supplied by Immunodiagnostic Systems Holdings PLC, United Kingdom according to the manufacturer's protocol.

Plasma catecholamine level was performed using HPLC. A chromatographic system with a pump PM-80 (BAS, USA) and an LC-4B electrochemical detector (BAS, USA) was used. Analytical column: Hypersil BDS-C18, 3 μm, 4.0 × 100 mm (Phenomenex, USA).

Statistical Analysis

Analysis was performed using STATICTICA software version 10.0. All groups in all tests were tested for normal distribution by Shapiro-Wilk test. The data in Social interest, Sucrose test, Open field (squares and rearings), FST, level of corticosterone, catecholamine and its metabolites have normal distribution (data are expressed as Mean ± SD). Then one-way ANOVA followed by Fisher's *post hoc* LSD test was applied to compare these groups. Kruskal-Wallis test with Newman-Keuls *post hoc* test was used to compare groups in Morris test, the data in this test did not have normal distribution (data are expressed as median ± quartile). The alpha level was set as $p < 0.05$.

RESULTS

The plasma level of corticosterone, epinephrine, norepinephrine was increased twice as high compared to control. The level of dopamine and its metabolites were decreased (see **Table 1**).

TABLE 1 | Level of corticosterone, catecholamine and it metabolites (nmol/l).

	Epinephrine	Norepinephrine	Dopamine	DOPA	DOPAC	Corticosterone
Control	3.03 ± 1.79	2.3 ± 1.26	11.17 ± 2.58	8.83 ± 3.17	10.27 ± 2.3	302.24 ± 144.15
US	5.78 ± 1.9**	7.6 ± 1.16**	5.77 ± 2.4**	4.05 ± 1.78**	5.38 ± 1.98**	602.65 ± 115.35**

*All substances were measured by HPLS, except for corticosterone (ELISA). Data presented as Mean ± SD. **$p < 0.01$ compared to control. $F_{(1,38)} = 8.75; 82.5; 12.9; 14.15; 23.3; 15.89$, respectively.*

Overall we observed the disturbance in catecholamine's concentration in blood that agrees with the conception of developed depressive-like behavior.

A decrease in sucrose preference index in CMS (62.7 ± 29) and US (62 ± 13%) groups compared to control (85 ± 8.7%; $F_{(2,57)}$ = 11.57; $p < 0.01$) revealed the development of anhedonia. Although no statistically significant difference was found between the CMS and US groups, SDs in CMS group were bigger (**Figure 2A**). The large SD in CMS group can be explained because 30% of animals did not show anhedonia. Total liquid intake did not differ between all experimental groups ($F_{(2,57)}$ = 0.124; p = 0.88).

Impact of US led to a marked reduction of social activity in the social interaction test in the US group (94.6 ± 30.5) and CMS group (159.1 ± 72.6), compared to the control group (213.5 ± 54.3; $F_{(2,57)}$ = 17.86; $p < 0.01$; **Figure 2B**). Social interaction in the CMS group was higher than the control group (p = 0.04). Contrary to that, the US group has much more pronounced differences to the control group ($p < 0.01$). Experimental animals after US exposure avoided contact with the juvenile male in every way, and in some cases showed freezing behavior when infant rat came into contact with them.

The number of squares and rearings in open field test has significant difference between experimental groups and control ($F_{(2,57)}$ = 17.16 and $F_{(2,57)}$ = 17.26 accordantly, $p < 0.01$). There was no difference between CMS and US group (**Figures 2C,D**). Thus, the stressed rats expressed marked decrease in exploration behavior.

In the forced swimming test US and CMS groups showed a significantly longer immobility time: US (215 ± 37.7) and CMS (159 ± 27.8) compared to the control group (91 ± 36.7; $F_{(2,57)}$ = 79.42; $p < 0.01$). The time of immobility was the highest in US group ($p < 0.01$ compared to CMS and control), the rats after CMS were less immobile than rats

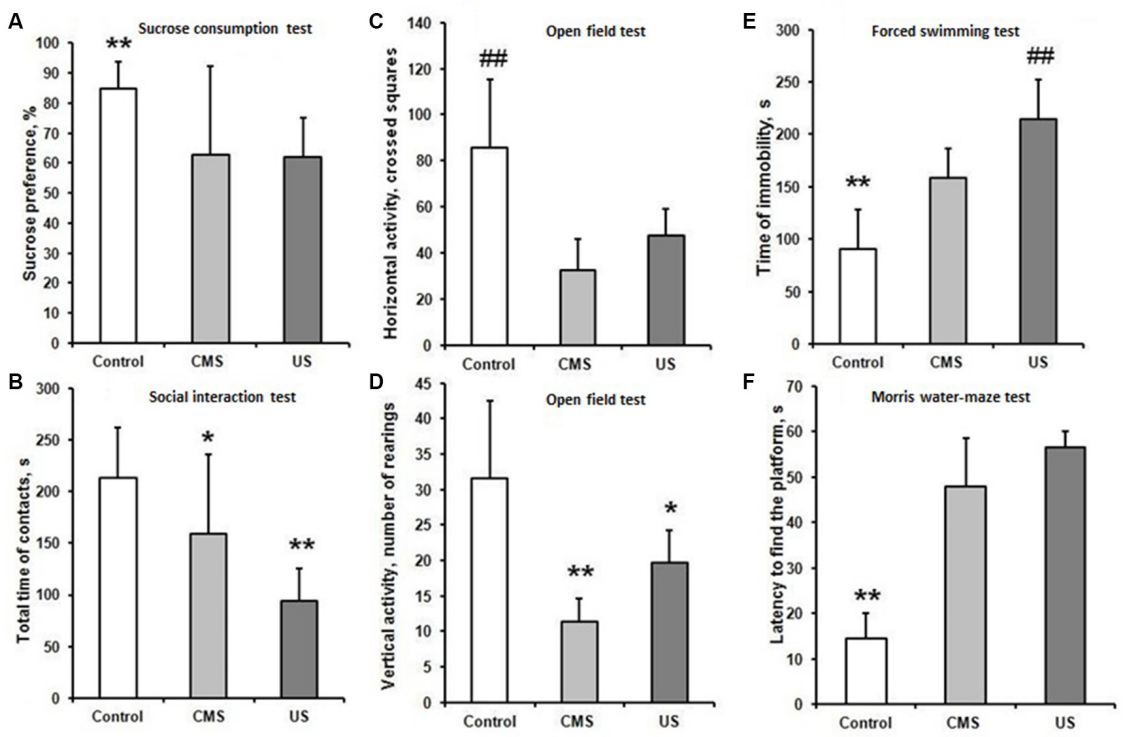

FIGURE 2 | Behavior tests. CMS—rats exposed to chronic mild stress, US—rats after 21-days ultrasound exposure. **(A)** Sucrose preference test. Preference index was calculated according to the formula: $(V_s + V_w)^*100\%$, where V_w is volume of consumed water, V_s is volume of consumed sweet water. Data presented as Mean ± SD. Data compared using one-way ANOVA with *post hoc* Fisher's LSD test. The sucrose preference index in CMS and US groups did not differ from each other and was significantly lower compared to control (**$p < 0.01$ compared to US and CMS groups). **(B)** Social interest test. Time of social contacts between the experimental animal and the juvenile male. Data presented as Mean ± SD. Data compared using one-way ANOVA with *post hoc* Fisher's LSD test. Time of social contacts was reduced in CMS group compared to control (*$p < 0.05$). In US group it was decreased more significantly (**$p < 0.01$ compared to control and CMS). **(C,D)** Open field test. Comparison of horizontal activity (number of crossed squares, **C**) and vertical activity (number of rearings, **D**) between control, US and to CMS groups. Data presented as Mean ± SD. Data compared using one-way ANOVA with *post hoc* Fisher's LSD test. The number of crossed squares was less in CMS and US group compared to control ($^{\#\#}p < 0.01$). The experimental groups were not differing from each other. The number of rearings was less in CMS and US group compared to control (**$p < 0.01$ and *$p < 0.05$, respectively). **(E)** Forced swimming test (Porsolt test). Comparison of immobility time during the last 6 min of an 8 min swim session between control, US and CMS groups. Data presented as Mean ± SD. Data compared using one-way ANOVA with *post hoc* Fisher's LSD test. Time of immobility was increased in CMS and US group compared to control (**$p < 0.01$). In US group it was increased more significantly ($^{\#\#}p < 0.01$ compared to CMS). **(F)** Morris water maze test. Test session 48 h after learning. Data presented as Median ± quartile. Data compared using one-way ANOVA with *post hoc* Fisher's LSD test. Time finding the platform was increased in CMS and US group, stressed groups did not differ from each other (**$p < 0.01$).

after US exposure ($p < 0.01$ CMS compared to control; **Figure 2E**). Although all experimental groups showed despair behavior, rats after US exposure struggled less than those in the CMS group.

In the Morris water maze the time of finding platform had significant difference from control–14.5 (7.8;5.5; $H_{(2,60)} = 12.84$; $p < 0.01$ for CMS and US group), but did not differ between the CMS–48 (13;10.5) and US–56.5 (25.3;3.5) group (**Figure 2F**). Therefore, mild stress altered long term spatial memory in the same manner as ultrasound protocol.

DISCUSSION

As it was emphasized by Willner, "Animal models of psychiatric states may be defined as procedures applied to laboratory animals that engender behavioral changes, which are intended to be homologous to aspects of psychiatric disorders, and can, therefore, be used as experimental tools to further the understanding of human psychopathology" (Willner, 2013). Most animal models of depression are based on the induction of a depressive-like behavior by stress. Among them, the CMS model is the most widely tested one (Antoniuk et al., 2019).

To evaluate the model as the one that is appropriate and adequately reproduces mental disorders, Willner proposed the following validity criteria: face validity, predictive validity, construct validity.

Face Validity

This criterion implies compliance of the model based on its behavioral manifestations. Sucrose preference, social interest and forced swim test are used to determine the depressive-like state in animals since there is a decrease in social interaction and sings of anhedonia in depression in both animals and human. In our study, in both models, the level of sucrose preference decreased and did not differ in the experimental groups. However, in 30% of rats subjected to CMS, the sucrose preference index was more than 90%, as in reference group animals, which suggests that rats after CMS consumed the same amount of sweet water as healthy animals. At the same time, in the ultrasound-induced depression model, such findings were not observed. The maximum preference index in US group was 75%. The fact that many of the CMS rats did not reduce sucrose intake in the sucrose preference test is actually not that surprising. On this basis, some researchers divide rats into susceptible and resistant to stress effects (Wiborg, 2013). Apparently, US exposure makes the threatened group more homogeneous and has a stronger effect on animals, although has no physical impact.

The forced swim test is used for the evaluation of depression (Kraeuter et al., 2019). In this test, rats after ultrasound exposure showed significantly higher immobility time than rats after CMS, about twice as much as in the control group.

In the social interest test, the group of animals after the CMS showed the decrease in time of social contact, but the difference between US group and control was much more remarkable, compared to the difference between CMS and control group. It is related to the fact that 40% of animals showed no decrease in social activity below 200 s; and three of these animals did not demonstrate anhedonia, either. The US group showed greater homogeneity with a lower standard deviation; the average of social contacts did not exceed 150 s. Therefore, according to three tests demonstrating a depressive-like state we found no signs of anhedonia and reduced social interaction in six animals; although the immobility time of these animals has been raised and did not exceed the minimum time of immobility in the US group. Therefore, if we take into account the development of depressive-like state by behavioral parameters of rats in all experimental tests, we can conclude that 30% of animals with the CMS model have not shown depressive-like state simultaneously in all three tests. Not only results of this study, but also already published data confirm this (Willner, 2017b). Immobility time, sucrose preference index, time of social contacts in US-induced depression model gave similar results in all experimental series. CMS protocol is often criticized for the non-reproducibility of behavioral test results. Willner himself confirms it having analyzed hundreds of publications made based on his model (Willner, 2017b). The meta-analysis of Willner's model also indicated this fact, except for anhedonia (Antoniuk et al., 2019). It should be noted that the test results of the failed CMS model are not likely to be published. However, we were able to find articles that discuss the failed test of this model (Krupina et al., 2012). The low reproducibility is primarily due to the ambiguity of the protocol used. Willner's model has been known since 1987. There are 230 publications from 180 labs in more than 30 countries (Willner, 2017a), and in the majority of these publications, the protocols are different. Even if types of stress stimuli are the same as in original Willner's articles, they do not have the same order, and the duration of CMS also differs. The variability of stressors and the human factor also contribute to the ambiguity: the variability of new partners (weight and age) and the ambiguity of the term "small and wet cage."

Willner's model involves the impact on the senses of animals (light) or physical discomfort (placement in wet sawdust, small cage), reversal of the day/night cycle, deprivation of water and food, and a new partner. Only some of these stress factors are present in the daily life of a human. As Willner says, animal models of psychiatric conditions can be defined as procedures applied to laboratory animals that produce behavioral changes; these are designed to be homologous to aspects of mental disorders and can, therefore, be used as experimental tools for further understanding human psychopathology (Willner, 2013). Physical discomfort and stress associated with the lack of water and food is not the main type of stress in developed countries, where depression is diagnosed with an incidence of up to 45% (Roohafza et al., 2011). Therefore, chronic information stress may be the stress which is similar to humans; in our animal experiments, it is caused by exposure to ultrasound of variable frequency. Therefore the US-induced depression model has some advantages due to the type of stress stimulus which is closer to the aspects of real-life situation observed in the human population.

Depression is also often accompanied by cognitive and motivational disorders. Long-term spatial memory, learning ability, locomotor activity in open field test and Morris water maze were also tested after two stress protocols. The search time for the platform in the Morris water maze in CMS and

US experimental groups of animals exposed to different types of stress did not differ, but it was longer than that in the control group. This suggests impairment of long-term spatial memory in rats, which is consistent with symptoms that occur in depression. According to this aspect of validity, both depression modeling protocols are equally good.

In the open field test, the parameters of locomotor and exploratory activities were investigated. The number of crossed squares and rearing did not differ in the experimental groups; it was significantly lower in CMS and US group compared to control.

The Construct Validity

This criterion suggests that the modeled depression features should be unambiguously interpreted and regarded as homologous, and should be related to depression both empirically and theoretically. The most powerful trigger for the development of depression is stress, which causes the depression symptoms. Under normal conditions, the response to stress is an integral part of adaptation. However, repeated stress affects the adaptation system. This potentiates the central nervous system vulnerability to depression and other disorders (McIsaac and Young, 2009). It is known that negative psychological factors lead to activate hypothalamic-adrenal axis in human (Dallé and Mabandla, 2018). Stress in rats leads to an increase in the plasma level of glucocorticoids, such as corticosterone, and catecholamine, such as epinephrine and norepinephrine (Smith and Vale, 2017). CMS also increases the normal steroid concentration in experimental animals (Azpiroz et al., 1999). Besides, basic and clinical studies demonstrate deficits and dysregulation of the dopaminergic system in depression (Belujon and Grace, 2017). In CMS models of depression, the normal dopamine concentration in blood serum and brain tissue is disturbed (Bekris et al., 2005). According to our data, the concentration of corticosterone, epinephrine and norepinephrine in the blood increased twice as high on the 21st day of ultrasound exposure, at the same time the concentration of dopamine and its metabolites was decreased. According to literature, anhedonia is induced by dopamine system dysregulation. This dysregulation is caused by failure of stress compensatory mechanisms (Belujon and Grace, 2017). Consequently, our US protocol meets the criteria of construct validity.

Predictive Validity

For the model of depressive-like behavior in animals, it primarily means a response to antidepressant therapy. Several classes of antidepressants were tested in our US-induced depression model: fluoxetine (a selective serotonin reuptake inhibitor), tianeptine (monoamine reuptake modulator), bupropion (a selective norepinephrine–dopamine reuptake inhibitor), which restored the behavioral test parameters to the level of untreated animals (**Table 2**; Morozova et al., 2013b). Moreover, the antidepressant effect of electroconvulsive therapy has also been demonstrated in our laboratory (Morozova et al., 2015), without negative effects on memory (Ushakova et al., 2017). According to the predictive validity, the US-induced depression model has all the necessary characteristics. Extensive use of the Willner's model for testing different types of antidepressants shows the predictive validity in this model, too.

In Willner's model, depressive-like behavior persists for up to 3 months (Willner, 1997) and at least 2 months in our model (Morozova et al., 2016).

It should be noted that labor usage, a parameter that is also very important in the reproduction and modeling of psychopathology, is very low in the US-induced depression model. At the same time, Willner's model implies daily procedures to be performed with the animal by the experimenter.

The ultrasonic model of depression is better than the CMS model from the point of view of animal's injury and ethics (Nuno, 2013).

Although the Willner's model has some drawbacks, it is most widely used in the world, therefore, using this model, researchers approached the understanding of the molecular mechanisms of depression and the study of its therapy.

In this study, modeling of the depressive-like state in animals was performed using two different protocols: Willner's model, the most commonly used model of depression and a new model developed in our laboratory, which involves a 3-week exposure to chronic information stress caused by exposure to US of variable frequency. This ultrasonic exposure is considered a chronic stress due to the fact that these signals carry a negative information load, to which the animal cannot adapt. In both models, there are cognitive symptoms and locomotor and exploratory activity impairment which are also typical for the depressive-like state;

TABLE 2 | Antidepressant's action in ultrasound-induced depression (US) model.

	Social interaction test	Porsolt test	Sucrose preference test
Control	216 ± 50 s**	83 ± 19 s##	78 ± 6%$$
US	107 ± 33 s	211 ± 48 s	56 ± 15%
US + Fluoxetine	228 ± 41 s	128 ± 56 s	69 ± 10%
US + Bupropion	143 ± 30 s	70 ± 16 s	78 ± 21%
US + Tianeptine	236 ± 40 s	106 ± 24 s	71 ± 8%

*Antidepressants were given during 21-days of US protocol. Data presented as Mean ± SD. In social interaction test, we evaluated time of contacts between experimental animal and juvenile rat (s). Time of social contacts was decreased in US group and corrected after antidepressant's treatment, except for bupropion. **$p < 0.01$ compared to US group and US + Bupropion. In Porsolt (forced swim) test, we compared immobility time (s). Time of immobility was increased in US group and corrected after antidepressant's treatment. ##$p < 0.01$ compared to US group. In sucrose preference test index was calculated according to the formula: $(V_s + V_w)*100\%$, where V_w is volume of consumed water, V_s is volume of consumed sweet water. The index was decreased in US group and corrected after antidepressant's treatment. $$$p < 0.01$ compared to all groups. Data included in the table was taken from our previous study (Morozova et al., 2013b) to emphasize the predictive validity of US-induced depression model.*

and they are equivalent in both depression models. According to the face validity criteria, the US-induced depression model in some tests shows more pronounced depressive-like behavior over Willner's protocol; and according to the construct and predictive validity criterion, these models are similar. However, we believe that the uniqueness of the protocol applied and the large homology of the type of stressor used in the US-induced depression model are its main advantages. Therefore, we can conclude that the model developed in our laboratory is not only equal to the most frequently used CMS model, but it is better in some aspects such as labor usage, ethical restrictions, easy and uniform protocol without physical impact. We hope the global scientific community will make use of the US-induced depression model in the future to obtain further data to study pathogenetic mechanisms of the depressive-like disorders caused by stressors, which are the closest ones to those present in everyday human life, as well as to test promising depression treatment options.

DATA AVAILABILITY

All datasets generated for this study are included in the manuscript.

ETHICS STATEMENT

Housing conditions and all experimental procedures were set up and maintained in accordance with Directive 2010/63/EU of 22 September 2010 and carried out under approval of the local veterinary committee.

AUTHOR CONTRIBUTIONS

YZ, EZ and AM planned, carried out the experiments and wrote the manuscript. VU took part in the experiments and VC revised the manuscript.

REFERENCES

Antoniuk, S., Bijata, M., Ponimaskin, E., and Wlodarczyk, J. (2019). Chronic unpredictable mild stress for modeling depression in rodents: meta-analysis of model reliability. *Neurosci. Biobehav. Rev.* 99, 101–116. doi: 10.1016/j.neubiorev.2018.12.002

Azpiroz, A., Fano, E., Garmendia, L., Arregi, A., Cacho, R., Beitia, G., et al. (1999). Effects of chronic mild stress (CMS) and imipramine administration, on spleen mononuclear cell proliferative response, serum corticosterone level and brain norepinephrine content in male mice. *Psychoneuroendocrinology* 24, 345–361. doi: 10.1016/s0306-4530(98)00084-5

Bekris, S., Antoniou, K., Daskas, S., and Papadopoulou-Daifoti, Z. (2005). Behavioural and neurochemical effects induced by chronic mild stress applied to two different rat strains. *Behav. Brain Res.* 161, 45–59. doi: 10.1016/j.bbr.2005.01.005

Belujon, P., and Grace, A. (2017). Dopamine system dysregulation in major depressive disorders. *Int. J. Neuropsychopharmacol.* 20, 1036–1046. doi: 10.1093/ijnp/pyx056

Bourin, M., Mocaër, E., and Porsolt, R. (2004). Antidepressant-like activity of S 20098 (agomelatine) in the forced swimming test in rodents: involvement of melatonin and serotonin receptors. *J. Psychiatry Neurosci.* 29, 126–133.

Dallé, E., and Mabandla, M. V. (2018). Early life stress, depression and Parkinson's disease: a new approach. *Mol. Brain* 11:18. doi: 10.1186/s13041-018-0356-9

Demaestri, C., Brenhouse, H. C., and Honeycutt, J. A. (2019). 22 kHz and 55 kHz ultrasonic vocalizations differentially influence neural and behavioral outcomes: implications for modeling anxiety via auditory stimuli in the rat. *Behav. Brain Res.* 360, 134–145. doi: 10.1016/j.bbr.2018.12.005

da Oliveira, S., Daniel, A. N., Nunes, P. T., Costa, K. A., Yehia, H. C., and Ribeiro, A. M. (2015). Intrauterine exposure to chronic 22 khz sound affects inhibitory avoidance and serotonergic parameters in forebrain areas of dams and rat offspring. *J. Behav. Brain Sci.* 5, 25–39. doi: 10.4236/jbbs.2015.52003

Gorlova, A. V., Pavlov, D. A., Zubkov, E. A., Morozova, A. Y., Inozemtsev, A. N., and Chekhonin, V. P. (2018). Three-week isolation does not lead to depressive-like disorders in rats. *Bull. Exp. Biol. Med.* 165, 181–183. doi: 10.1007/s10517-018-4125-7

Kraeuter, A. K., Guest, P. C., and Sarnyai, Z. (2019). The forced swim test for depression-like behavior in rodents. *Methods Mol. Biol.* 1916, 75–80. doi: 10.1007/978-1-4939-8994-2_5

Krupina, N. A., Khlebnikova, N. N., Orlova, I. N., Popkova, E. V., Rodina, V. I., and Kryzhanovsky, G. N. (2012). Effects of chronic mild stress in Wistar and August rats: behavior and mon amine content in the striatum. *Pathogenesis* 10, 50–58.

Malki, K., Keers, R., Tosto, M. G., Lourdusamy, A., Carboni, L., Domenici, E., et al. (2014). The endogenous and reactive depression subtypes revisited: integrative animal and human studies implicate multiple distinct molecular mechanisms underlying major depressive disorder. *BMC Med.* 12:73. doi: 10.1186/1741-7015-12-73

McIsaac, S. A., and Young, A. H. (2009). The role of hypothalamic pituitary-adrenal axis dysfunction in the etiology of depressive disorders. *Drugs Today* 45, 127–133. doi: 10.1358/dot.2009.45.2.1336104

Morozova, A., Zubkov, E., Gubskiy, I., and Chekhonin, V. (2015). Efficacy of ECT in ultrasound induced depression in rats. *Eur. Neuropsychopharmacol.* 25, S563–S564. doi: 10.1016/s0924-977x(15)30787-2

Morozova, A. Y., Zubkov, E. A., Storozheva, Z. I., Kekelidze, Z. I., and Chekhonin, V. P. (2013a). Effect of ultrasonic irradiation on the development of symptoms of depression and anxiety in rats. *Bull. Exp. Biol. Med.* 154, 740–743. doi: 10.1007/s10517-013-2044-1

Morozova, A. Y., Zubkov, E. A., Storozheva, Z. I., Koshkin, P. A., Shepeleva, I. I., Kekelidze, Z. I., et al. (2013b). Behavioral patterns and expression of genes coding serotonin receptors in rats with ultrasound induced depression. *Br. J. Med. Med. Res.* 3, 2107–2118. doi: 10.9734/bjmmr/2013/4994

Morozova, A., Zubkov, E., Strekalova, T., Kekelidze, Z., Storozeva, Z., Schroeter, C. A., et al. (2016). Ultrasound of alternating frequencies and variable emotional impact evokes depressive syndrome in mice and rats. *Prog. Neuropsychopharmacol. Biol. Psychiatry* 68, 52–63. doi: 10.1016/j.pnpbp.2016.03.003

Morris, R. (1984). Developments of water-maze procedure for studying spatial learning in the rat. *J. Neurosci.* 11, 47–60. doi: 10.1016/0165-0270(84)90007-4

Neumann, I. D., Wegener, G., Homberg, J. R., Cohen, H., Slattery, D. A., Zohar, J., et al. (2011). Animal models of depression and anxiety: what do they tell us about human condition? *Prog. Neuropsychopharmacol. Biol. Psychiatry* 35, 1357–1375. doi: 10.1016/j.pnpbp.2010.11.028

Nuno, H. F. (2013). Animal experiments in biomedical research: a historical perspective. *Animals* 3, 238–273. doi: 10.3390/ani3010238

Roohafza, H., Ramezani, M., Sadeghi, M., Shahnam, M., Zolfagari, B., and Sarafzadegan, N. (2011). Development and validation of the stressful life event questionnaire. *Int. J. Public Health* 56, 441–448. doi: 10.1007/s00038-011-0232-1

Smith, J. C. (1979). Factors affecting the transmission of rodent ultrasounds in natural environments. *Am. Zool.* 19, 432–442. doi: 10.1093/icb/19.2.432

Smith, S. M., and Vale, W. W. (2017). The role of the hypothalamic-pituitary-adrenal axis in neuroendocrine responses to stress. *Dialogues Clin. Neurosci.* 8, 383–395.

Takahashi, N., Kashino, M., and Hironaka, N. (2011). Structure of rat ultrasonic vocalizations and its relevance to behavior. *PLoS One* 5:e14115. doi: 10.1371/journal.pone.0014115

Tan, S., Ho, H. S., Song, A. Y., Low, J., and Je, H. S. (2017). Maternal separation does not produce a significant behavioral change in mice. *Exp. Neurobiol.* 26, 390–398. doi: 10.5607/en.2017.26.6.390

Ushakova, V. M., Zubkov, E. A., Morozova, A. Y., Gorlova, A. V., Pavlov, D. A., Inozemtsev, A. N., et al. (2017). Effect of electroconvulsive therapy on cognitive functions of rats with depression-like disorders induced by ultrasound exposure. *Bull. Exp. Biol. Med.* 163, 599–601. doi: 10.1007/s10517-017-3857-0

Vocate, D. R. (1987). *The Theory of A.R. Luria: Functions of Spoken Language in the Development of Higher Mental Processes.* Hillsdale, NJ: Lawrence Erlbaum associates Inc.

WHO. (2017). Depression and other common mental disorders. Available online at: http://apps.who.int/iris/bitstream/handle/10665/254610/WHO-MSD-MER-2017.2-eng.pdf. Accessed February 23, 2019.

Wiborg, O. (2013). Chronic mild stress for modeling anhedonia. *Cell Tissue Res.* 354, 155–169. doi: 10.1007/s00441-013-1664-0

Willner, P. (1997). Validity, reliability and utility of the chronic mild stress model of depression: a 10-year review and evaluation. *Psychopharmacology* 134, 319–329. doi: 10.1007/s002130050456

Willner, P. (2013). "Animal models for psychiatric states," in *Encyclopedia of Psychopharmacology*, eds I. Stolerman and L. Price (Heidelberg: Springer), 84.

Willner, P. (2017a). The chronic mild stress (CMS) model of depression: history, evaluation and usage. *Neurobiol. Stress* 6, 78–93. doi: 10.1016/j.ynstr.2016.08.002

Willner, P. (2017b). Reliability of the chronic mild stress model of depression: a user survey. *Neurobiol. Stress* 6, 68–77. doi: 10.1016/j.ynstr.2016.08.001

Willner, P., Towell, A., Sampson, D., Sophokleous, S., and Muscat, R. (1987). Reduction of sucrose preference by chronic unpredictable mild stress and its restoration by a tricyclic antidepressant. *Psychopharmacology* 93, 358–364. doi: 10.1007/bf00187257

Conflict of Interest Statement: The authors declare that the research was conducted in the absence of any commercial or financial relationships that could be construed as a potential conflict of interest.

frontiers in Behavioral Neuroscience

ORIGINAL RESEARCH
published: 10 July 2019
doi: 10.3389/fnbeh.2019.00151

Impact of Stress on Gamma Oscillations in the Rat Nucleus Accumbens During Spontaneous Social Interaction

*Ann Mary Iturra-Mena[1], Marcelo Aguilar-Rivera[2], Marcia Arriagada-Solimano[1], Catherine Pérez-Valenzuela[1], Pablo Fuentealba[3] and Alexies Dagnino-Subiabre[1]**

[1] *Laboratory of Stress Neurobiology, Center for Integrative Neurobiology and Pathophysiology, Institute of Physiology, Faculty of Sciences, Universidad de Valparaíso, Valparaíso, Chile,* [2] *Department of Bioengineering, University of California, San Diego, La Jolla, CA, United States,* [3] *Department of Psychiatry, Integrative Center for Neurosciences, Pontificia Universidad Católica de Chile, Santiago, Chile*

Alteration in social behavior is one of the most debilitating symptoms of major depression, a stress related mental illness. Social behavior is modulated by the reward system, and gamma oscillations in the nucleus accumbens (NAc) seem to be associated with reward processing. In this scenario, the role of gamma oscillations in depression remains unknown. We hypothesized that gamma oscillations in the rat NAc are sensitive to the effects of social distress. One group of male *Sprague-Dawley* rats were exposed to chronic social defeat stress (CSDS) while the other group was left undisturbed (control group). Afterward, a microelectrode array was implanted in the NAc of all animals. Local field potential (LFP) activity was acquired using a wireless recording system. Each implanted rat was placed in an open field chamber for a non-social interaction condition, followed by introducing another unfamiliar rat, creating a social interaction condition, where the implanted rat interacted freely and continuously with the unfamiliar conspecific in a natural-like manner (see **Supplementary Videos**). We found that the high-gamma band power in the NAc of non-stressed rats was higher during the social interaction compared to a non-social interaction condition. Conversely, we did not find significant differences at this level in the stressed rats when comparing the social interaction- and non-social interaction condition. These findings suggest that high-gamma oscillations in the NAc are involved in social behavior. Furthermore, alterations at this level could be an electrophysiological signature of the effect of chronic social stress on reward processing.

Keywords: gamma oscillations, nucleus accumbens, stress, depression, social behavior

OPEN ACCESS

Edited by:
Nadine Ravel,
INSERM U1028 Centre de Recherche en Neurosciences de Lyon, France

Reviewed by:
Dan Christoffel,
Stanford University, United States
David Dietz,
University at Buffalo, United States
Andre Der-Avakian,
University of California, San Diego, United States

****Correspondence:***
Alexies Dagnino-Subiabre
alexies.dagnino@uv.cl

Received: *05 April 2019*
Accepted: *21 June 2019*
Published: *10 July 2019*

Citation:
Iturra-Mena AM, Aguilar-Rivera M, Arriagada-Solimano M, Pérez-Valenzuela C, Fuentealba P and Dagnino-Subiabre A (2019) Impact of Stress on Gamma Oscillations in the Rat Nucleus Accumbens During Spontaneous Social Interaction. Front. Behav. Neurosci. 13:151. doi: 10.3389/fnbeh.2019.00151

INTRODUCTION

Humans as well as many other mammalian species exhibit social behaviors which imply several evolutionary advantages (Alexander, 1974). Moreover, social reward is crucial for emotional well-being; therefore, and impairment in this domain, is a key symptom in mood disorders (American Psychiatric Association, 2013). One of these conditions is depression; this disorder is characterized

Abbreviations: CSDS, chronic social defeat stress; dB, decibels; EEG, electroencephalography; GABA, gamma aminobutyric acid; Hz, Hertz; LFP, local field potential; MSNs, medium spiny neurons; NAc, nucleus accumbens; PV+ FSI, fast spiking interneurons expressing parvalbumin; SSR, sequential stopping rule; VTA, ventral tegmental area.

by "anhedonia" –the decreased reactivity to pleasurable stimuli – as well as by a deficiency in reward processing (Admon and Pizzagalli, 2015).

It has been shown that the NAc, that is part of the ventral striatum, is involved in motivation to carry out social interactions (Dolen et al., 2013). Additionally, reward conditioning for both drug and social interaction, leads to an increase of the electrical network activity in the NAc (Kummer et al., 2015). Likewise, clinical studies suggest that the NAc reward responsivity is altered in depressive patients (Pizzagalli et al., 2009; Misaki et al., 2016), and there is also evidence about the antidepressive effect of targeting the NAc with deep brain stimulation in patients suffering treatment-resistant depression (Schlaepfer et al., 2008; Nauczyciel et al., 2013).

Neural oscillations at the EEG or LFP levels, have been correlated to the activity of several cognitive functions in cortical and sub-cortical structures (Bosman et al., 2014), and they have also been linked to the symptomatology of neuropsychiatric disorders (Herrmann and Demiralp, 2005; Uhlhaas and Singer, 2010). Studies carried out in humans show that alterations among gamma oscillations, in EGG (30–100 Hz), represent an element of major depression (Herrmann and Demiralp, 2005; Uhlhaas and Singer, 2010). In line with this, gamma oscillations in the NAc of humans (Cohen et al., 2009; Lega et al., 2011) and rats (Berke, 2009; van der Meer and Redish, 2009) are evoked during reward processing. However, the role of gamma oscillations in the NAc during social interaction in healthy and depressive subjects remains unknown.

Negative stress or distress is a key environmental risk factor for mood disorders, such as major depression (Monroe et al., 2014; Pizzagalli, 2014). Distress can give way to depressive symptoms in healthy individuals (Berenbaum and Connelly, 1993; Charney and Manji, 2004), as well as deficit in brain reward system functions in laboratory animals (Der-Avakian et al., 2014; Donahue et al., 2014). Distress has also been shown to disrupt reward learning in humans (Bogdan and Pizzagalli, 2006; Pizzagalli et al., 2007; Bogdan et al., 2010, 2011) and rats (Der-Avakian et al., 2017). In line with this, CSDS experiment is carried out with an animal model which is commonly used to study susceptibility to depressive-like behaviors (Hammels et al., 2015). CSDS strongly decreases the reward system activity resulting in an long lasting anhedonic response in stressed rats (Der-Avakian et al., 2014), an element which can be reverted by an antidepressant treatment in mice (Berton et al., 2006; Tsankova et al., 2006; Krishnan et al., 2007). Several functional alterations in the NAc are induced by CSDS, not only at a molecular level, but also in neural-morphology and synaptic plasticity in rodents (Christoffel et al., 2011; Francis et al., 2015). Alterations in the metabolic profile and MSNs activity have been discovered in awake mice (Larrieu et al., 2017; Hamilton et al., 2018; Muir et al., 2018). The aforementioned evidence raises the question of what effects CSDS has on neural oscillations in the NAc when animals interact with a conspecific. In line with this, we hypothesized that CSDS disrupts gamma oscillations in the rat NAc during social interaction. In order to test this hypothesis, we performed *in vivo* electrophysiological recording in the NAc of stressed and non-stressed rats during social interaction with a conspecific. We found that gamma-band power in the NAc was higher in non-stressed rats during social interaction compared with the non-social interaction condition. Interestingly, gamma oscillations in stressed rats did not vary between the social and the non-social interaction conditions. These findings suggest that gamma oscillations are involved in social behavior, and that alterations at this level could be an electrophysiological signature of the effect of chronic social stress in reward processing.

MATERIALS AND METHODS

Animals

Male *Sprague-Dawley* rats (380–420 g, 80–85 days old at the start of the experiment), commercially procured (Charles River Laboratories, Wilmington, United States), were used for the electrophysiological experiments and adult male Long Evans rats (700–850 g) commercially procured (Charles River Laboratories, Senneville, QC, Canada) were used as aggressors in the CSDS paradigm. All rats were maintained under a 12-h light–dark cycle (lights on at 8:00 am) and provided with food (Prolab RMH 3000, LabDiet®, MO, United States) and water *ad libitum*. Experiments were performed during the light phase. Animals were maintained in a temperature and humidity-controlled room (21 ± 1°C, 55%), and housed in groups of three before the electrode's implantation. After surgery, and for the rest of the experiments, they were housed individually. Animals under the stress protocol were separated from non-stressed rats and kept in a different room specially designated for them. Body weights were monitored three times per week. All animal maintenance and experimentation procedures were approved by the Institutional Animal Ethics Committee of the Faculty of Sciences of the Universidad de Valparaíso (Chile) and were in strict accordance with animal care standards outlined in National Institutes of Health (United States) guidelines. Efforts were made to minimize the number of animals used and their suffering.

Experimental Design

Figure 1A shows the timeline of the experimental design. Body weight gain, social interaction, and sucrose preference were determined in both non-stressed rats and animals that were exposed to CSDS. Rats that were susceptible to CSDS had less social interaction as well as a decrease in sucrose preference in comparison with non-stressed rats. Three rats that were resilient to social stress were excluded from this study and used in another research. In the *in vivo* electrophysiological experiments, non-stressed rats (n = 6) were only compared with stress susceptible rats (n = 6; stressed group).

CSDS Protocol

The CSDS protocol used in this study was modified from the resident-intruder model (Miczek, 1979). Animals from the stressed group were subjected to CSDS for seven consecutive days. During each episode of social stress, a *Sprague-Dawley* rat (intruder) was placed into the home cage of an unfamiliar

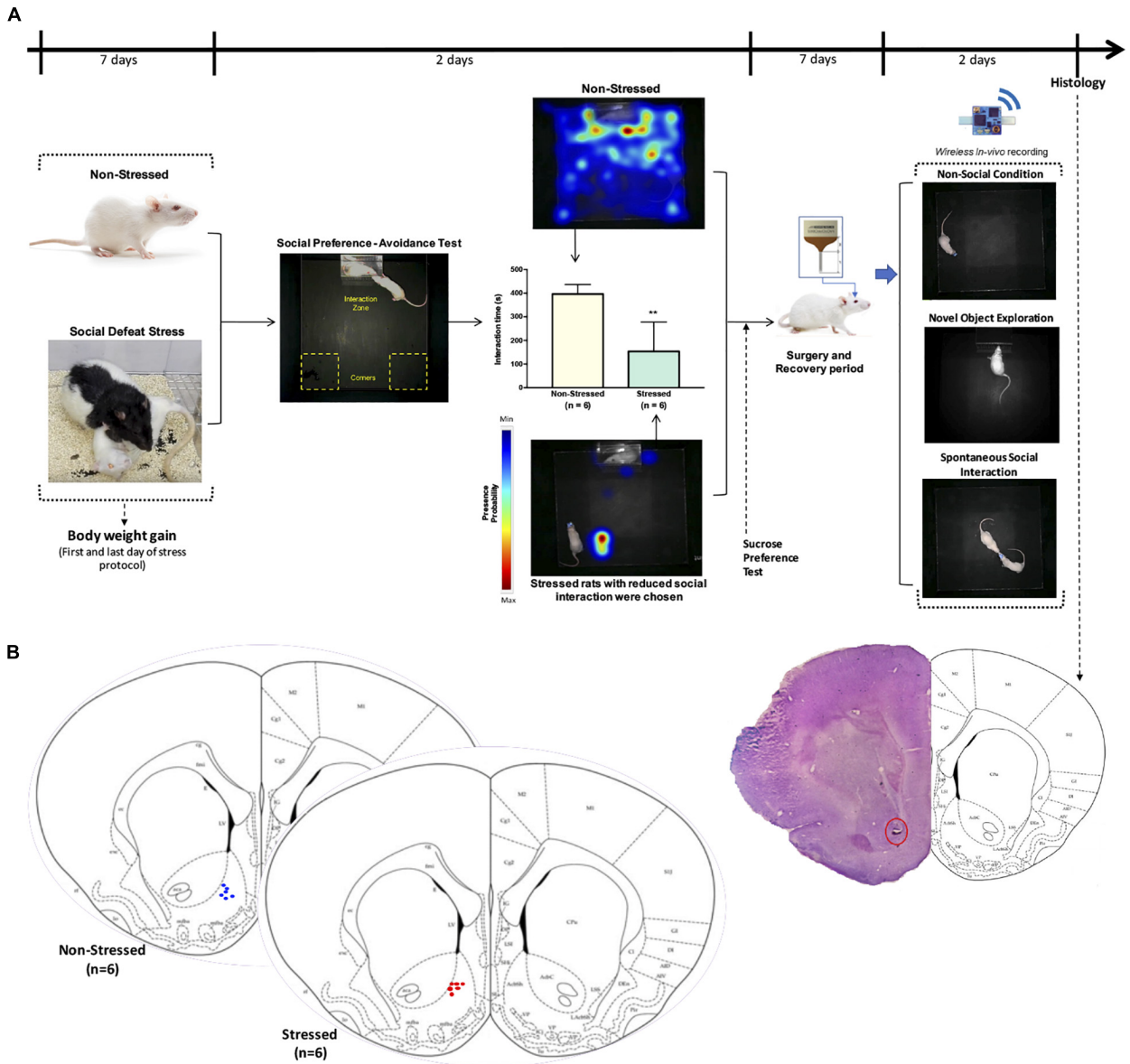

FIGURE 1 | (A) Timeline of the experimental design. Male *Sprague-Dawley* rats were exposed to CSDS and a non-stressed group (n = 6) was left undisturbed. Afterward, non-stressed and defeated rats were subjected to open field test, social preference-avoidance test, and sucrose preference test. Stressed animals that had interaction times two standard deviation below the mean of non-stressed rats were chosen for stressed group (n = 6). Representative heat maps are shown for non-stressed and stressed rat's tracking. A microelectrode array was implanted in the nucleus accumbens of all rats and local field potential activity was acquired using a wireless recording system in a non-social condition (open field), during exploration of a novel object, as well as when the implanted rats interacted freely and continuously with an unfamiliar conspecific in a natural-like manner. **(B)** Verification of electrode location. Schematic of final electrode locations in all rats. Each dot represents the electrode tips of one rat (n = 6 non-stressed and n = 6 stressed). Top right: example of a stained brain section with electrolytic lesions at the electrode tips (red circle).

male *Long-Evans* rat (resident). To classify the level of aggression before applying the CSDS protocol, the *Long-Evans* rats (resident) were previously exposed to five other adult male *Sprague-Dawley* rats (intruders) using the same resident-intruder paradigm described here. The resident rats who attacked at least 80% of the intruder rats in the first 60 s of the test were classified as highly aggressive. A typical agonistic encounter resulted in intruder subordination or defeat, signaled by the intruder assuming a supine position for approximately 3 s. After defeat, a wire mesh enclosure was placed into the cage to prevent physical contact between the resident and intruder, but allowing visual, auditory, and olfactory contact for the remainder of the 30-min defeat session. Rats were returned to their home cage after each session, and body weight gain was monitored daily to be used as a stress marker.

Open Field Test

Locomotor activity and anxiety like-behavior were evaluated using the open field test. All animals were naive to the test. Rats were placed individually in the center of a black Plexiglass cage (70 × 70 × 40 cm) for 5 min.

Total distance travelled, speed mean, and the time that rats spent in the perimeter and center (anxiety-like behavior marker) were automatically analyzed from video recordings using EthoVision® XT (Noldus, Wageningen, Netherlands).

Social Preference-Avoidance Test

Rats were tested for social behavior using a social interaction paradigm (Francis et al., 2015; Zoicas and Neumann, 2016). The rats were placed in an open field (85 cm × 35 cm × 50 cm) of which contained a transparent perforated chamber (25 cm × 15 cm) containing an empty enclosure and located in a designated interaction zone; the aforementioned transparent perforated chamber, they explored for 2.5 min. Time spent in the interaction zone for the experimental rat was measured using EthoVision® XT (Noldus, Wageningen, Netherlands). Afterward, the experimental rat explored the same perforated chamber for an additional 15 min after the introduction of a novel rat (male *Sprague-Dawley* of similar age) into the perforated chamber. The interactions were measured by the amount of time the experimental rat spent interacting with the other rat (considered as a stimulus). Representative heatmap for each experimental group were made using EthoVision® XT. The experimenter was blind to experimental group conditions. Stressed rats that had interaction times two standard deviations below the mean of non-stressed rat group were chosen for our study.

Sucrose Preference Test

As an efficacy measure for the CSDS protocol, depressive like-behavior was evaluated using the Sucrose Preference Test which evaluates the inability to experience pleasure in animals. The rats were first trained for 3 days to consume sweet liquid (5% sucrose), and water deprived for 12 h before the test. During the test, the rats were allowed to choose between two bottles for 1 h, one containing only water and the other containing a 5% sucrose solution. The amount of liquid consumed by the rats was measured, and the percentage of preference of sweet liquid in relation to the neutral liquid was calculated.

Surgery

The pre-operatory protocol consisted of 10 mg/kg of doxycycline applied orally a day before the surgery, as well as acepromazine 2.5 mg/kg and atropine 0.1 ml (both intramuscular) 30 min before the surgery. Through the surgery, 5 mg/kg of subcutaneous ketoprofen, 10 mg/kg of subcutaneous doxycycline, and 10 mg/kg of intraperitoneal tramadol were administered. For the post-operatory period, 2.5 mg/kg of ketoprofen and 10 mg/kg of oral doxycycline were applied orally for 3 days.

Rats were anaesthetized with isoflurane (induction 3%, maintenance 2%) in O_2. Body temperature was maintained at 37°C with a temperature controller system (RWD, Cat. No. 69001, Shenzhen, China). Rats were secured in a stereotaxic frame and unilaterally implanted in the left NAc with a microelectrode array aimed at the following coordinates: 1.8 mm anterior to the bregma, 1.0 mm lateral to the midline and 7.5 ventral from the skull (Paxinos and Watson, 2007). All implants were secured using dental cement. Rats were chronically implanted with a microelectrode array (Microprobes for Life Sciences, Gaithersburg, MD, United States) consisting of four individually insulated platinum/iridium wires (75 μm diameter, 3 MΩ, 250 μm distance between electrodes and rows) and attached to an 18-pin connector (Omnetics Connector Corp., Minneapolis, MN, United States). A local reference of the same metal, but lower impedance (10 KΩ) than the recording electrodes, was used. The ground consisted of a stainless-steel wire connected to the skull via a screw positioned on the cerebellum area.

After surgery, rats were allowed to recover for 7 days. They were habituated daily, including handling and head manipulation to avoid any possible stress that could be generated by the head-stage connection during the recordings.

In vivo Electrophysiology

The data were acquired with a wireless system (W2100, Multichannel Systems MCS GmbH, Harvard Bioscience, Inc., Reutlingen, Germany) using a 16-channels headstage with an amplifier bandwidth at 1 Hz to 5 kHz and a sampling rate at 25 kHz (gain at 101, input impedance at 1 GΩ, resolution of 16 bit, input voltage range of ±12.4 mV, input noise of <1.9 μVRMS and the distance for wireless link of 5 m). The acquisition software was the Multichannel Suite (Multi Channel Systems MCS GmbH, Harvard Bioscience, Inc., Reutlingen, Germany).

The signals were down-sampled offline to 1 kHz and bandpass filtered between 30 and 100 Hz. Electrodes with poor signal quality and movement artifacts were visually rejected by two researchers using EEGLab (Delorme and Makeig, 2004), based on spectral and time-domain characteristics, and confirmed by automated movement analysis of the recorded videos.

Spectral analysis was performed with the multitaper method using the Chronux toolbox (Bokil et al., 2010). Not all recordings had the same length because the headstage in some rats was disconnected before ending the testing procedure. So to guarantee comparability between animals, only the first 150 s of signal were extracted at each condition and multitaper parameters were set using window lengths of T = 2 s with 1.9 s overlap; time-bandwidth product TW = 2, and number of tapers K = 3. The median power at the 30–60 Hz and 61–90 Hz frequency range was calculated for each condition, and the linear scale changed to dB for the spectra plotting and statistical analysis.

Sample Size for *in vivo* Recording Experiments

The number of implanted rats that were used in our study was comparable with previously published studies on stressed rats (Jacinto et al., 2013, 2016). Thus, fifteen rats were implanted in the NAc (non-stressed, n = 8; stressed group, n = 7), three

rats were discarded from the experiments, because one rat did not undergo the recording procedure due to a premature detachment of the implant, and two rats were discarded because of microelectrode failure. Finally, twelve implanted rats were used in the electrophysiology experiments (non-stressed, $n = 6$; stressed group, $n = 6$).

Behavioral Testing

Prior to the behavioral testing, rats were habituated to the testing room for 30 min, 3 days consecutively. Non-stressed and stressed rats were subjected to a test consisting of three phases: in the first one, they were introduced for 5 min in an open field consisting of a square Plexiglass cage (70 × 70 × 40 cm), in which animals could freely explore (non-social condition). Then, a novel object consisting of a small cube of transparent acrylic was introduced into the box, allowing them to freely explore it for 5 min, followed by the removal of the novel object. Finally, another *Sprague-Dawley* rat of the same sex, with similar weight and previously evaluated as "non-aggressive" was introduced into the open field, allowing the animals to freely interact in a natural-like manner (social condition) for 5 min (see **Supplementary Videos S1, S2**). For the subsequent analysis of the behaviors, all tests were recorded with a video system, integrated, and synchronized with the electrophysiological recording (W2100-Video-System, Multichannel Systems MCS GmbH, Harvard Bioscience, Inc., Reutlingen, Germany). In addition, LFP acquisition was also synchronized with video recordings of the animal tracking and automatized analysis with EthoVision® XT (Noldus, Wageningen, Netherlands) to measure the speed and space-coordinates of the animals when they were performing the tasks.

Histology

After data collection was complete, a 25 μA current was passed through the electrodes for 20 s each. Three days following gliosis, rats were anesthetized with isoflurane and perfused intracardially with 4% paraformaldehyde in PBS. Brains were extracted and stored in 4% paraformaldehyde with 30% sucrose before being cut in 50-μm sections using a cryostat microtome (Kedee KD-2950, Zhejiang Jinhua Kedi Instrumental Equipment Co., Ltd., Zhejiang, China). Sections were mounted on gelatin-coated slides and stained using the Nissl method for localization of recording locations. Only data from electrodes with confirmed recording locations in the NAc were analyzed (**Figure 1B**).

Statistical Analyses

Data was analyzed using Prism 7 (GraphPad Software Inc., La Jolla, CA, United States), IBM SPSS® (IBM Corp, New York, NY, United States), or MATLAB (MathWorks, Natick, MA, United States). All variables that met the normal distribution test, using the Shapiro–Wilk test, and homoscedasticity, using the Levene test, were analyzed with parametric statistics. When the criteria for normality and homoscedasticity were not met, the data were analyzed with nonparametric statistics (Mann Whitney test or Wilcoxon test).

We used a two-tailed unpaired *t* test to compare the non-stressed and stressed groups in the behavioral parameters of the open field test, social interaction test, the sucrose preference test, and for body weight gain.

For the analysis of locomotor activity, we identified the events when the animal showed a speed, two standard deviations above ("fast movement") vs. below ("slow movement") the mean of locomotion, followed by the use of a two-tailed paired *t* test to compare the mean power for fast and slow movement events across the low and high-gamma frequency bands.

The Wilcoxon test was used for within a group of animals for comparison in regards to the power of low- and high-gamma oscillations in the non-social, novel object exploration, and social condition. Mann Whitney test was used to determine how significant was the percentage of change was between the non-social and social condition for the non-stressed and stressed groups in low (30–60 Hz) and high-gamma bands (61–90 Hz).

A probability level of 0.05 or less was accepted as significant. Results were expressed as the median, the 95% confidence interval of the spectral power (spectral plots) and as the median percentage of change in gamma-power during social interaction with respect to the non-social condition (open field exploration, considered as basal) with its minimum and maximum values (whiskers) in the box-and-whiskers plots.

RESULTS

Effects of CSDS on Weight Gain, Social Interaction, and Depressive-Like Behavior

Figure 1A shows that social interaction in the social preference-avoidance test was impaired in the rats that were exposed to CSDS (stressed group = 153.3 ± 124.5 s; non-stressed group = 395.8 ± 40.5 s, $P = 0.0011$). Maximum value of social interaction time (309.8 s) for stressed rats was two standard deviations below the mean of the non-stressed group (395.8 ± 40.5 s). In addition, stressed rats gained less weight than non-stressed rats ($t = 3.917$, df = 10; $P = 0.0014$) (**Figure 2A**). Along with this, the locomotor activity and anxiety-like behaviors of the animals were evaluated in the open field test (**Figures 2B–E**). Distance traveled and average speed were similar in all groups ($t = 1.141$, df = 10; $P = 0.2804$ and $t = 0.8302$, df = 10; $P = 0.4258$, respectively). Regarding anxiety-like behaviors, no significant differences were observed in the time that animals spent in the center ($t = 0.6661$, df = 10; $P = 0.5204$) or in the perimeter ($t = 0.6661$, df = 10; $P = 0.5204$) of the open field. Additionally, the *t* test showed differences between the groups in depressive-like behaviors based on the sucrose preference test ($t = 4.277$, df = 10; $P = 0.0016$), which allows obtaining an indicator of anhedonia in the stressed rats (**Figure 2F**).

Neural Oscillations in the NAc and Sociability of the Rats

Our first electrophysiology experiment investigated a possible relationship between LFP oscillations in the NAc and social interaction. With this purpose in mind, we implanted 4-channels microelectrode arrays into the NAc of the six non-stressed

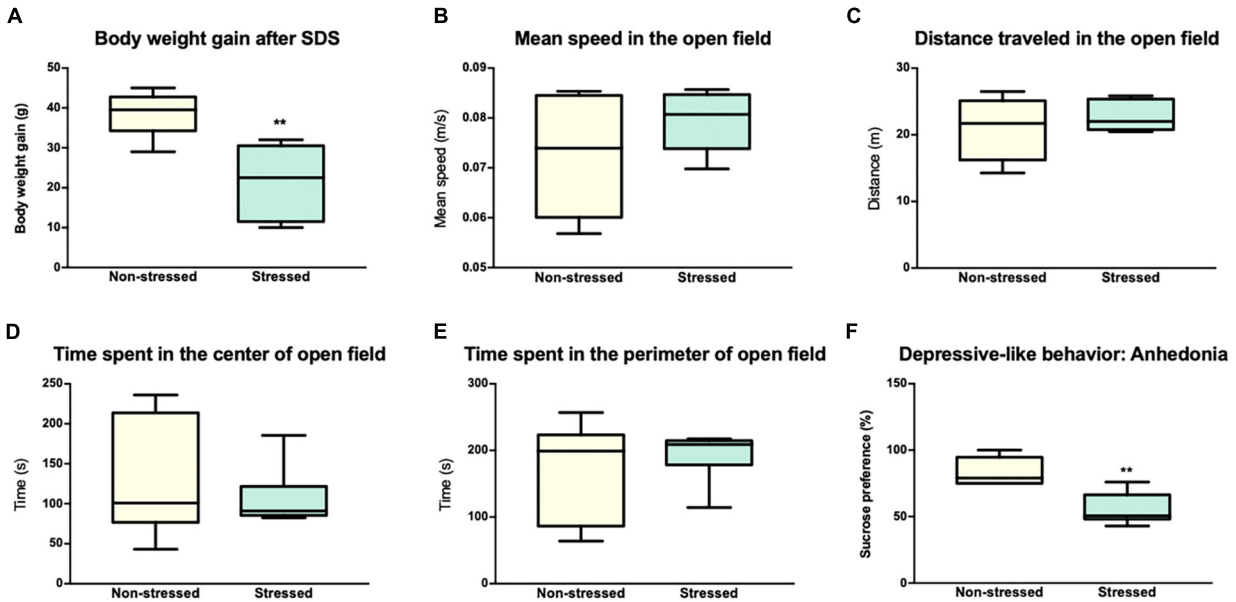

FIGURE 2 | Socially defeated rats showed an alteration in body weight gain, depressive like-behavior, and a normal performance in the open field. **(A)** Animals subjected to chronic social defeat stress (CSDS) showed a decrease in body weight gain compared to animals in the non-stressed group. The graph shows the body weight gain (grams) of the rats after 7 days of stress or 7 days without treatment in the case of non-stressed. **(B,C)** Locomotor activity in the open field. Distance traveled and average speed of the animals in the open field were similar in both groups. **(D,E)** Evaluation of anxiety-like behavior in the Open Field Test (time in the center and time in the perimeter). No statistically significant differences were observed between the groups in any of the parameters studied in the Open Field. **(F)** Evaluation of depressive-like behavior in the sucrose preference test. The animals of the stress group showed a significant decrease in the preference of sucrose compared to non-stressed rats. The values are presented as the median with its minimum and maximum. $^{**}p < 0.001$.

rats from the previous behavioral measures (**Figure 1A**). Then, we recorded *in vivo* LFP activity in the NAc when implanted rats performed spontaneous social interactions with a novel conspecific, using a wireless recording system. In this test, the rats were continuously interacting for 5 min (**Figure 1A**, see section "Materials and Methods"). For the analysis, the first 150 s of signal was extracted at each condition. We found that when rats experienced social interactions, gamma-band power in the NAc was higher in the high-gamma frequency band (61–90 Hz) compared to the non-social condition ($P = 0.010$) (see **Supplementary Figure S1**). In low-gamma, on the other hand, no significant differences were observed between both conditions ($P = 0.094$) (**Figures 3**, **6A**,**C**).

To exclude the effect of novelty as a confounding factor, the animals were subjected to a second non-social condition, which consisted of exploring a novel object. A significant difference was found in gamma oscillations between the social interaction and the exploration of the new object in the 61–90 Hz frequency band ($P = 0.031$) (**Figure 4A**), and not in the 30–60 Hz band ($P = 0.313$). The animals in both non-social conditions showed similar gamma-power at frequencies 30–60 Hz ($P = 0.563$) and 61–90 Hz ($P = 0.063$) (**Figure 4B**).

Subsequently, to evaluate whether this increase in high-gamma power was the mere consequence of motor related behavior, we analyzed those events offline when the animal increased the level of movement during social interaction ("fast movement") vs. those events when the animal moved slowly ("slow movement") using synchronized video recordings of the animal tracking and an automatized analysis with EthoVision® XT (Noldus, Wageningen, Netherlands) to measure the speed and space-coordinates of the animals when they were performing the tasks. We observed that the power of gamma oscillations was independent of the locomotor activity during social interaction both in the 30–60 Hz band ($t = 1.007$, df = 5; $P = 0.3602$) and in the 61–90 Hz ($t = 0.0268$, df = 5; $P = 0.9791$) (**Figure 5**).

Effects of CSDS on High-Gamma Oscillations in the NAc

The electrophysiology study involved the six stressed rats from the previous behavioral measures, which were implanted in the NAc (**Figure 1A**). No significant differences were observed for non-social and social condition in the high-gamma ($P = 0.438$) or low-gamma ($P = 0.438$) frequency band for rats that were exposed to CSDS (**Figures 6B,D**).

The unpaired t test showed that the percentage of power change between the social and non-social condition was lower for the implanted rats of the stressed group in the high-gamma band in comparison to non-stressed rats ($P = 0.041$) while no differences were found in the low-gamma band ($P = 0.738$) (**Figures 6E,F**).

DISCUSSION

The innovative aspect of our research considered the use of technology that allowed us to integrate an assessment of social

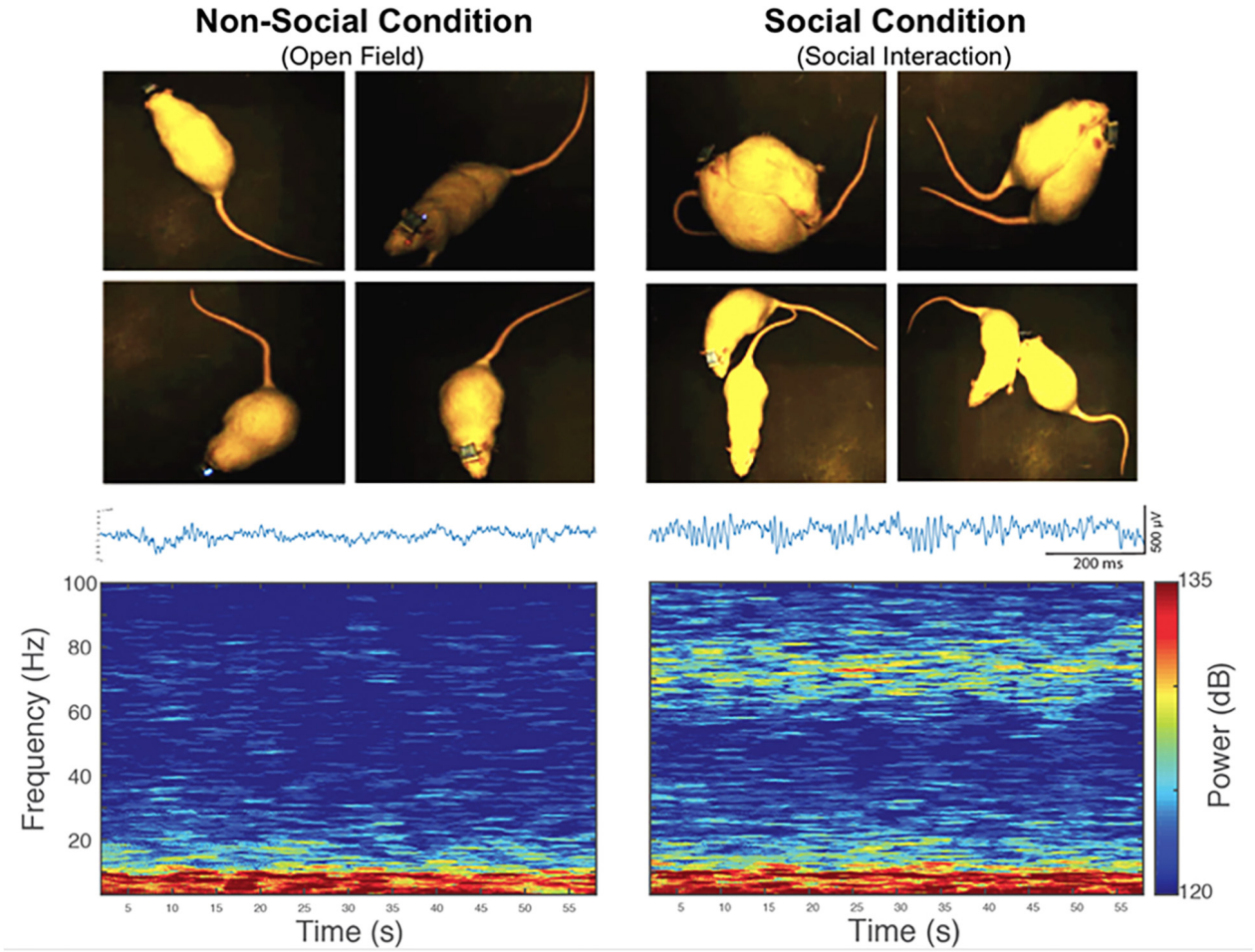

FIGURE 3 | An increase in the power of high-gamma oscillations in the rat nucleus accumbens during spontaneous social interaction in comparison to a non-social condition. Left: Representative picture of a rat exploring an open field (non-social condition) and then interacting socially with a conspecific (right). Bottom left: representative traces of LFP signal and spectrogram of the LFP registered in the NAc of a rat during 60 s of exploratory behavior in an open field (non-social condition). Bottom right: representative traces of LFP signal and 60-s spectrogram of spontaneous social interaction recorded in the same rat. Gamma oscillatory activity is prominent during spontaneous social interaction compared to the non-social condition.

interaction based on a natural-like interaction with the *in vivo* recordings of LFP oscillations in the NAc of stressed rats. The main objective of this study was to find the electrophysiological correlate of social interaction in an essential area for reward processing such as the NAc. Although there was already some evidence about the participation of the NAc in social behaviors (Alkire et al., 2018; Warnell et al., 2018) to date, it was unknown that social interaction correlated with the increase in high-gamma power (61–90 Hz, in the present study) in the NAc, which points to a possible brain oscillatory modulation based on social interaction, in that specific region, in high-gamma (**Figure 6**). In contrast, high-gamma power in the NAc of stressed rats was independent of social interaction (**Figure 6**).

It should be noted that the origin of gamma oscillations in the NAc could theoretically be attributed to different factors, including synaptic inputs that come from afferent areas such as the prefrontal cortex, the hippocampus, the amygdala, the VTA, and the thalamus (Colgin et al., 2009; Popescu et al., 2009; Muir et al., 2018). Also, they may be attributed to intrinsic local membrane potentials and multiunit activity of spikes (van der Meer et al., 2010), or to the synaptic currents resulting from local projections within the NAc. Some authors refer to the NAc as a "switchboard" (Redgrave et al., 1999; Goto and Grace, 2008; Gruber et al., 2009). This proposal implies that NAc is more than a simple passive receiver of incoming signals from afferents; rather, the NAc has a mechanism for the exchange between signals. In such an exchange scenario, the NAc would be able to "select" a dominant input. This suggests, for example, that during high-gamma oscillatory activity in the NAc, other areas that also exhibit such activity, as the prefrontal cortex, could be functionally synchronized with the NAc in non-stressed rats, having an influence on their behavior; on the other hand, while during low-gamma the piriform cortex or the amygdala – which also exhibit oscillations in this frequency band – would be controlling the output of the

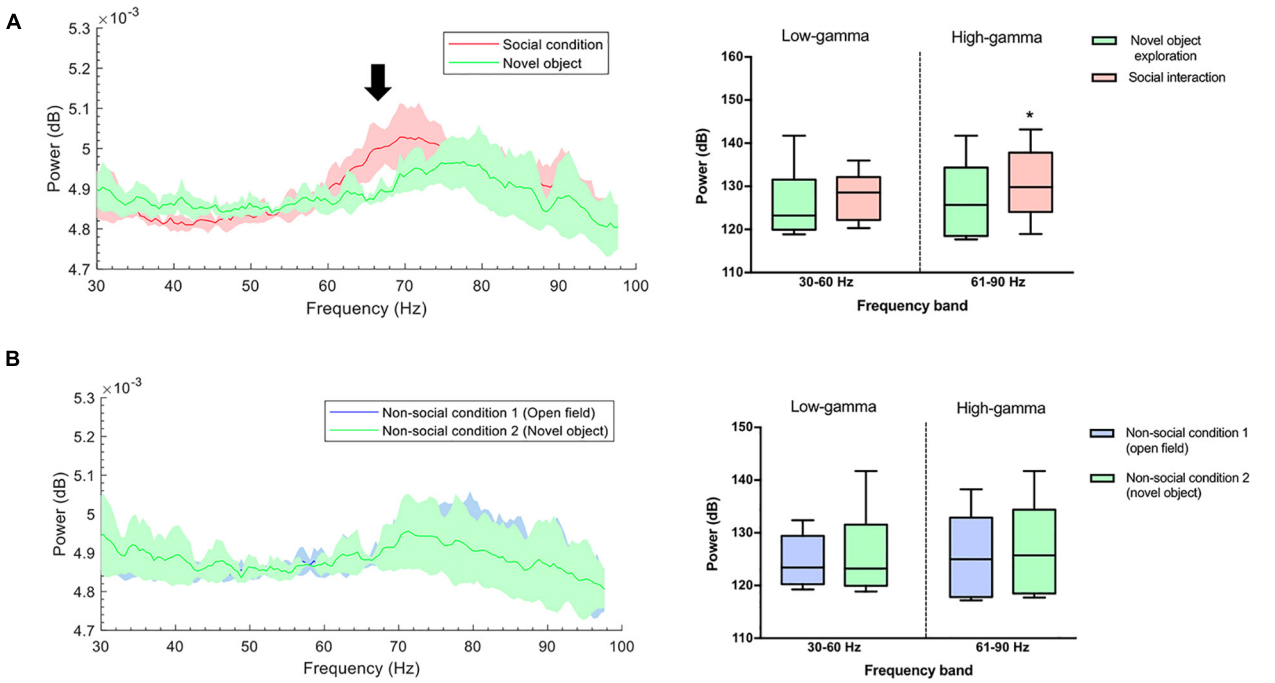

FIGURE 4 | (A) Gamma-band power during novel object recognition was lower compared with a social condition. Left: Group-median power spectra (solid line, median; shaded area, 25th–75th percentile) across the 30–100 frequency band showing increased power of the high-gamma frequency band (black arrow) during spontaneous social interaction (red) in comparison to the non-social condition/novel object (green). Right: Mean power (dB) for both conditions across two gamma frequency bands (low-gamma: 30–60 Hz and high-gamma: 61–90 Hz). The whiskers indicate the minimum and maximum values. $^*p < 0.05$. **(B)** The power of gamma oscillations between two non-social conditions was similar. Left: Group-median power spectra (solid line, median; shaded area, 25th–75th percentile) across the 30–100 frequency showing no differences between non-social condition 1 (open field) and non-social condition 2 (novel object) (green and blue line, respectively). Right: Mean power (dB) for both conditions across two gamma frequency bands (low-gamma: 30–60 Hz and high-gamma: 61–90 Hz). The whiskers indicate the minimum and maximum values.

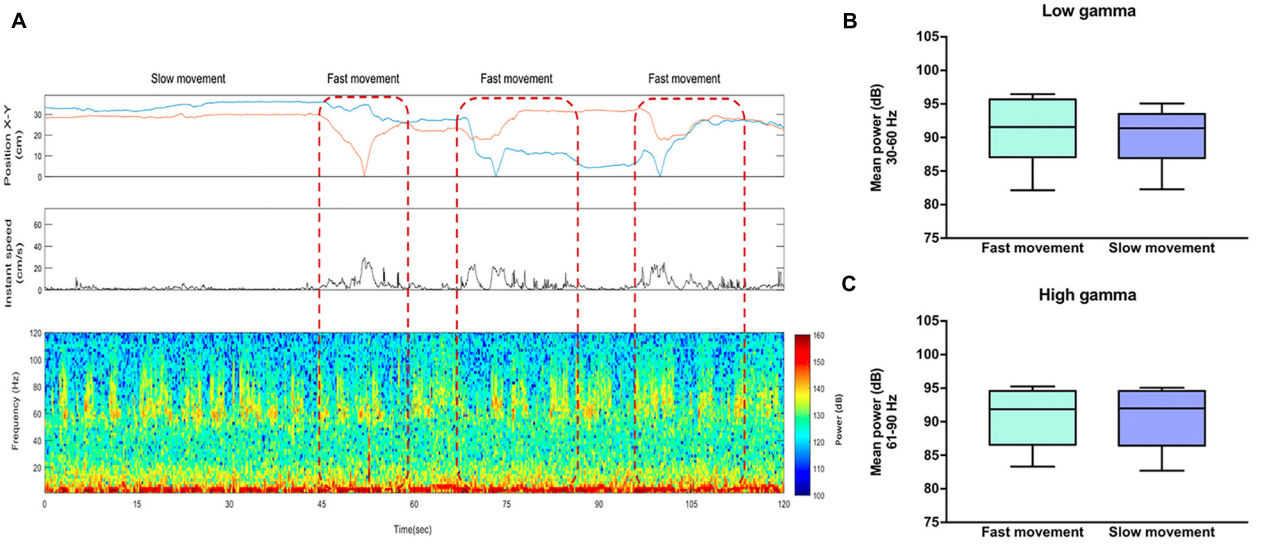

FIGURE 5 | High-gamma oscillations in the rat nucleus accumbens are independent of locomotor activity. **(A)** Top: The first box represents the position of the rat in a square arena and the second box represents the instant speed. Bottom: Representative LFP spectrogram from the NAc of a rat socially interacting. Red dotted lines indicate the events when the animal showed a speed two standard deviations above ("fast movement") vs. below ("slow movement") the mean of locomotion. **(B)** Mean power (dB) for fast and slow movement events across the low-gamma (30–60 Hz) and **(C)** high-gamma (61–90) frequency bands. The whiskers indicate the minimum and maximum values. The *t*-test shows no significant difference in low and high-gamma power between fast and slow movement.

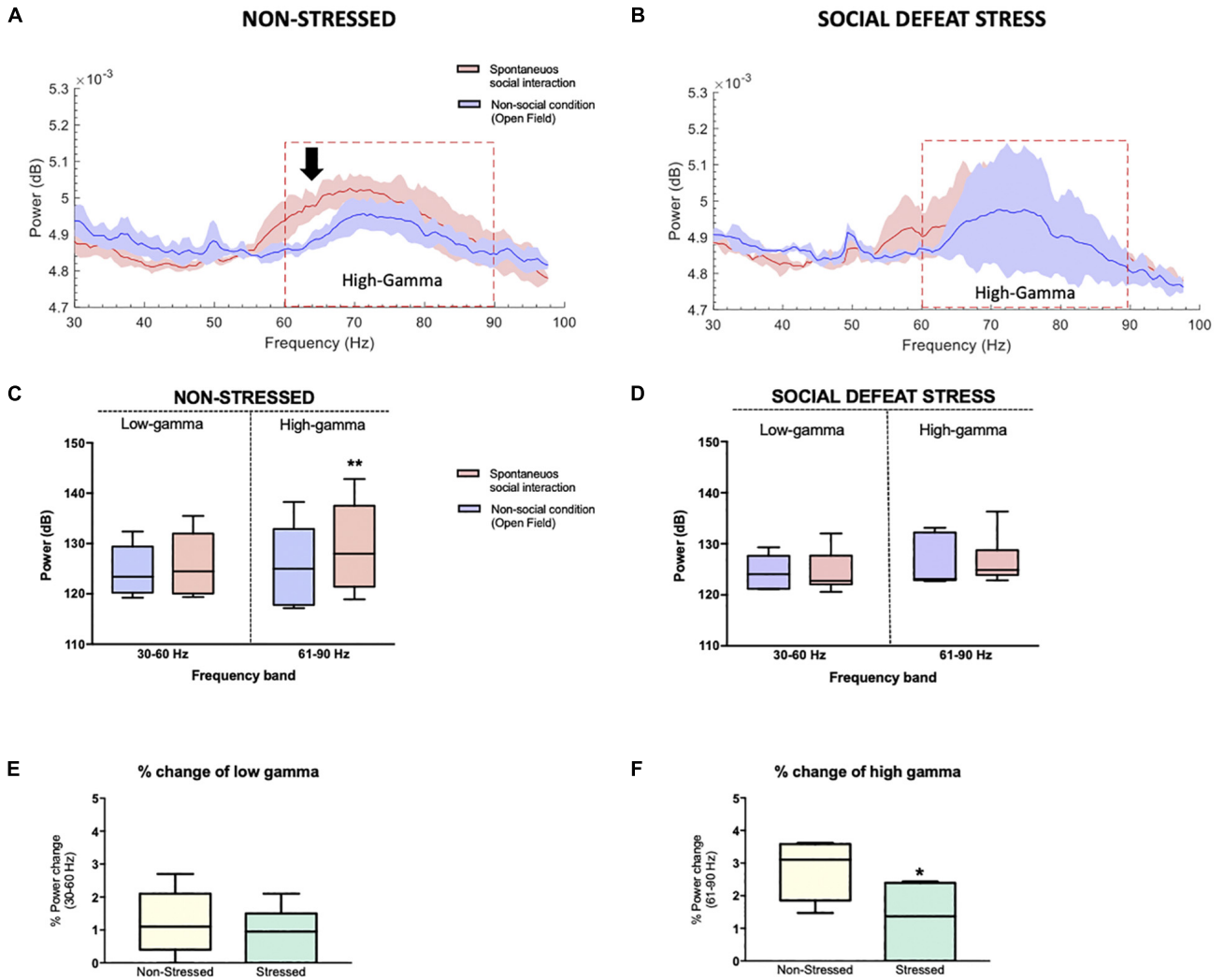

FIGURE 6 | Stressed rats did not show differences in the power of high-gamma oscillations in the NAc between the social and non-social condition: **(A)** Non-stressed group-median power spectra (solid line, median; shaded area, 25th–75th percentile) across the 30–100 frequency band showing increased power of the high-gamma frequency band (black arrow, red dotted line) during the spontaneous social interaction (red) in comparison to the non-social condition (blue). **(B)** Stressed group-median power spectra (solid line, median; shaded area, 25th–75th percentile) across the 30–100 frequency band showing no differences in the power of high-gamma (red dotted line) during spontaneous social interaction (red) in comparison to the non-social condition (blue). **(C,D)** Mean power (dB) for both conditions in two gamma frequency bands (30–60 Hz or "low-gamma," 61–90 Hz or "high-gamma") for non-stressed and stressed implanted rats. The whiskers indicate the minimum and maximum values. A significant difference was observed between the two conditions for the high-gamma frequency band. $^{**}p < 0.01$. Median percentage of change in low **(E)** and high-gamma **(F)** power during spontaneous social interaction compared with the non-social condition (open field exploration, considered as basal) with its minimum and maximum values. Rats that were exposed to CSDS had a decrease of % power change in high-gamma band. $^{*}P < 0.05$.

NAc (van der Meer et al., 2010). However, it might be that the NAc has the role of signal discrimination, allowing the selection and exchange of certain signals, passing them from one source to the next. In this regard, it has been reported that distress is related to alterations in synaptic transmission and volume atrophy in cortical and limbic regions, such as the prefrontal cortex (Holmes and Wellman, 2009; Negron-Oyarzo et al., 2014) and the hippocampus (McEwen, 2016; Perez et al., 2018). The aforementioned could affect the functional connectivity between the cortex and NAc in stressed animals, inducing the decrease of gamma power that we found in the stressed rats (**Figures 6B,D**). This could lead to a failure in the integration of cortical information in the NAc (Mallet et al., 2005), possibly from prefrontal cortex inputs, a brain region involved in social behavior, according to recent evidence (Alkire et al., 2018).

Regarding the possible origin of the gamma oscillations within the NAc, a reciprocally connected inhibitory network at NAc could generate gamma activity, as was proposed by Buzsaki and Wang, 2012, with parvalbumin positive fast spiking interneurons (PV+ FSI) which inhibit the MSNs (Mallet et al., 2005). The NAc is a subdivision of the ventral striatum. Furthermore, the

coupling to gamma rhythms has been described as being selective for the PV+ FSI in the stratium (Berke, 2009), which has been theoretically linked to the generation of oscillations in this frequency band (Popescu et al., 2009).

It is known that PV+ FSI strongly inhibit projection neurons in the NAc, which do not seem to inhibit each other significantly (Jaeger et al., 1994). Therefore, PV+ FSI are probably the main neurons responsible for the GABAergic inhibition of the striatum; this strongly limits the striatal output (Nisenbaum and Berger, 1992). Although PV+ FSI constitute only 1–2% of the neurons in the NAc, they provide a powerful feedforward inhibition that controls the firing of the MSNs (Warren and Whitaker, 2018). It becomes evident then that by exciting PV+ FSI and by reducing their synaptic inhibition, dopaminergic afferents can exert an important inhibitory influence in the striatum. Particularly, dopamine (DA) can critically regulate feedforward inhibition, which is a major feature of cortico-striatal communication (Koos and Tepper, 1999).

According to previous evidences, a possible explanation would be that under normal conditions, the increase of the neurotransmitter DA in the NAc during social interaction would excite the PV+ FSI directly through depolarization mediated by D1-type receptors, or indirectly, reducing its synaptic inhibition through presynaptic D2-type receptors (Bracci et al., 2002). This would increase the inhibitory activity of the PV+ FSI on the MSN, which would generate oscillations in gamma frequency. Therefore, in the case of stressed rats when interacting socially with another unfamiliar conspecific, it is proposed that there would be (1) a decrease in the levels of DA in the NAc compared to non-stressed rats in the same behavioral event, which leads to (2) a decrease in the activity of the PV+ FSI that generates (3) the alteration of the local inhibitory circuit between the PV+ FSI and the MSN and leads to (4) the decrease of gamma oscillations in the NAc (Buzsaki and Wang, 2012) during social interaction. Analyzing each aspect of this idea, the first element is the possible decrease in DA levels in the NAc of rats that were exposed to CSDS. Although this was not measured in the present study, there is previous evidences that supporting this idea and additional evidence that is contrary to the aforementioned. For example, an increase of activity of VTA DA neurons projecting to NAc and activation of D1-MSN is needed to initiate the social behavior (Gunaydin et al., 2014). In this regard, the study of Muir et al. (2018) is close to our findings because they measured D1-MSN activity specifically when implanted mice were carrying out social interaction. Authors found that social interaction evokes low levels of D1-MSN activity in pro-susceptible mice compared with pro-resilient mice (Muir et al., 2018). This evidence suggests that social interaction did not stimulate much DA release toward the NAc in susceptible mice, compared with resilient or non-stressed animals. In line with this, optostimulation of VTA DA in mice exposed to chronic mild stress decreases depressive-like behaviors (Tye et al., 2013), as well as chronic stress which leads to a decrease in dopamine levels in the NAc (Lehner et al., 2018). Conversely, phasic optostimulation of VTA DA neurons produce the susceptible behavioral phenotype in mice (Chaudhury et al., 2013) and susceptible mice show an increase in the firing rate of VTA DA neurons and D1-MSN hyperexcitability (Cao et al., 2010; Francis et al., 2019). This evidence suggests that the effects of stress on the VTA-NAc pathway depend on the type of stressor and its intensity. In this scenario, a fundamental piece in this puzzle is missing. DA concentration in the NAc has not yet been determined during social interaction in stressed rodents. It is possible that chronic exposure to CSDS could increase phasic firing rate of VTA DA neurons, which in turn desensitizes the D1-MSNs in the NAc and impairs social interaction.

At a clinical level, it has been shown that a rapid antidepressant effect of ketamine, an NMDA receptor antagonist, depends partly on the mesolimbic dopaminergic system (Belujon and Grace, 2014; Duman, 2018). In line with this, ketamine restores reduced VTA DA neuron activity of mice exposed to chronic mild stress (Rincón-Cortés and Grace, 2017). This evidence suggests that an antidepressant effect of ketamine could be induced by an increase of the VTA-NAc activity, which could be related with an increase in high gamma oscillations in the NAc during social behavior.

In conclusion, similar to previous studies that showed that gamma oscillations in the NAc are associated with the processing of natural rewards (e.g., food intake) or synthetic rewards such as drug use (Berke, 2009; Cohen et al., 2009; van der Meer and Redish, 2009; Lega et al., 2011), these results suggest, specifically, that high-gamma oscillations could also be involved in the rewarding effect generated by the presence of a conspecific, as well as socially interacting with it, and that chronic social stress disrupts these oscillations. Alterations in this domain seem to be involved in the etiology of neuropsychiatric disorders related to stress, such as major depression and anxiety disorders.

DATA AVAILABILITY

The datasets for this manuscript are not publicly available because they have not been published yet. Requests to access the datasets should be directed to alexies.dagnino@uv.cl.

ETHICS STATEMENT

All animal maintenance and experimentation procedures were approved by the Institutional Animal Ethics Committee of the Faculty of Sciences of the Universidad de Valparaíso (Chile) and were in strict accordance with animal care standards outlined in the National Institutes of Health (United States) guidelines. Efforts were made to minimize the number of animals used and their suffering.

AUTHOR CONTRIBUTIONS

AI-M and AD-S designed the research, analyzed the data, and wrote the manuscript. AI-M, MA-R, MA-S, CP-V, and PF performed the research. All authors contributed to the final version of the manuscript for submission.

FUNDING

In this work, AD-S was supported by FONDECYT (Grant Number 1141276) and Anillo de Ciencia y Tecnología, Programa PIA of CONICYT (Grant Number ACT1403).

SUPPLEMENTARY MATERIAL

The Supplementary Material for this article can be found online at: https://www.frontiersin.org/articles/10.3389/fnbeh.2019.00151/full#supplementary-material

REFERENCES

Admon, R., and Pizzagalli, D. A. (2015). Dysfunctional reward processing in depression. *Curr. Opin. Psychol.* 4, 114–118. doi: 10.1016/j.copsyc.2014.12.011

Alexander, R. D. (1974). The evolution of social behavior. *Annu. Rev. Ecol. Syst.* 5, 325–383. doi: 10.1146/annurev.es.05.110174.001545

Alkire, D., Levitas, D., Warnell, K. R., and Redcay, E. (2018). Social interaction recruits mentalizing and reward systems in middle childhood. *Hum. Brain Mapp.* 39, 3928–3942. doi: 10.1002/hbm.24221

American Psychiatric Association (2013). *Diagnostic and Statistical Manual of Mental Disorders*. Washington, DC: American Psychiatric Association.

Belujon, P., and Grace, A. A. (2014). Restoring mood balance in depression: ketamine reverses deficit in dopamine-dependent synaptic plasticity. *Biol. Psychiatry* 76, 927–936. doi: 10.1016/j.biopsych.2014.04.014

Berenbaum, H., and Connelly, J. (1993). The effect of stress on hedonic capacity. *J. Abnorm. Psychol.* 102, 474–481. doi: 10.1037//0021-843x.102.3.474

Berke, J. D. (2009). Fast oscillations in cortical-striatal networks switch frequency following rewarding events and stimulant drugs. *Eur. J. Neurosci.* 30, 848–859. doi: 10.1111/j.1460-9568.2009.06843.x

Berton, O., McClung, C. A., Dileone, R. J., Krishnan, V., Renthal, W., Russo, S. J., et al. (2006). Essential role of BDNF in the mesolimbic dopamine pathway in social defeat stress. *Science* 311, 864–868. doi: 10.1126/science.1120972

Bogdan, R., Perlis, R. H., Fagerness, J., and Pizzagalli, D. A. (2010). The impact of mineralocorticoid receptor ISO/VAL genotype (rs5522) and stress on reward learning. *Genes Brain Behav.* 9, 658–667. doi: 10.1111/j.1601-183X.2010.00600.x

Bogdan, R., and Pizzagalli, D. A. (2006). Acute stress reduces reward responsiveness: implications for depression. *Biol. Psychiatry* 60, 1147–1154. doi: 10.1016/j.biopsych.2006.03.037

Bogdan, R., Santesso, D. L., Fagerness, J., Perlis, R. H., and Pizzagalli, D. A. (2011). Corticotropin-releasing hormone receptor type 1 (CRHR1) genetic variation and stress interact to influence reward learning. *J. Neurosci.* 31, 13246–13254. doi: 10.1523/JNEUROSCI.2661-11.2011

Bokil, H., Andrews, P., Kulkarni, J. E., Mehta, S., and Mitra, P. P. (2010). Chronux: a platform for analyzing neural signals. *J. Neurosci. Methods* 192, 146–151. doi: 10.1016/j.jneumeth.2010.06.020

Bosman, C. A., Lansink, C. S., and Pennartz, C. M. (2014). Functions of gamma-band synchronization in cognition: from single circuits to functional diversity across cortical and subcortical systems. *Eur. J. Neurosci.* 39, 1982–1999. doi: 10.1111/ejn.12606

Bracci, E., Centonze, D., Bernardi, G., and Calabresi, P. (2002). Dopamine excites fast-spiking interneurons in the striatum. *J. Neurophysiol.* 87, 2190–2194. doi: 10.1152/jn.00754.2001

Buzsaki, G., and Wang, X. J. (2012). Mechanisms of gamma oscillations. *Annu. Rev. Neurosci.* 35, 203–225. doi: 10.1146/annurev-neuro-062111-150444

Cao, J. L., Covington, H. E. III, Friedman, A. K., Wilkinson, M. B., Walsh, J. J., Cooper, D. C., et al. (2010). Mesolimbic dopamine neurons in the brain reward circuit mediate susceptibility to social defeat and antidepressant action. *J. Neurosci.* 230, 16453–16458. doi: 10.1523/JNEUROSCI.3177-10.2010

Charney, D. S., and Manji, H. K. (2004). Life stress, genes, and depression: multiple pathways lead to increased risk and new opportunities for intervention. *Sci. STKE* 2004, re5. doi: 10.1126/stke.2252004re5

Chaudhury, D., Walsh, J. J., Friedman, A. K., Juarez, B., Ku, S. M., Koo, J. W., et al. (2013). Rapid regulation of depression-related behaviours by control of midbrain dopamine neurons. *Nature* 493, 532–536. doi: 10.1038/nature11713

Christoffel, D. J., Golden, S. A., Dumitriu, D., Robison, A. J., Janssen, W. G., Ahn, H. F., et al. (2011). IkappaB kinase regulates social defeat stress-induced synaptic and behavioral plasticity. *J. Neurosci.* 31, 314–321. doi: 10.1523/JNEUROSCI.4763-10.2011

Cohen, M. X., Axmacher, N., Lenartz, D., Elger, C. E., Sturm, V., and Schlaepfer, T. E. (2009). Good vibrations: cross-frequency coupling in the human nucleus accumbens during reward processing. *J. Cogn. Neurosci.* 21, 875–889. doi: 10.1162/jocn.2009.21062

Colgin, L. L., Denninger, T., Fyhn, M., Hafting, T., Bonnevie, T., Jensen, O., et al. (2009). Frequency of gamma oscillations routes flow of information in the hippocampus. *Nature* 462, 353–357. doi: 10.1038/nature08573

Delorme, A., and Makeig, S. (2004). EEGLAB: an open source toolbox for analysis of single-trial EEG dynamics including independent component analysis. *J. Neurosci. Methods* 134, 9–21. doi: 10.1016/j.jneumeth.2003.10.009

Der-Avakian, A., D'Souza, M. S., Potter, D. N., Chartoff, E. H., Carlezon, W. A. Jr., Pizzagalli, D. A., et al. (2017). Social defeat disrupts reward learning and potentiates striatal nociceptin/orphanin FQ mRNA in rats. *Psychopharmacology* 234, 1603–1614. doi: 10.1007/s00213-017-4584-y

Der-Avakian, A., Mazei-Robison, M. S., Kesby, J. P., Nestler, E. J., and Markou, A. (2014). Enduring deficits in brain reward function after chronic social defeat in rats: susceptibility, resilience, and antidepressant response. *Biol. Psychiatry* 76, 542–549. doi: 10.1016/j.biopsych.2014.01.013

Dolen, G., Darvishzadeh, A., Huang, K. W., and Malenka, R. C. (2013). Social reward requires coordinated activity of nucleus accumbens oxytocin and serotonin. *Nature* 501, 179–184. doi: 10.1038/nature12518

Donahue, R. J., Muschamp, J. W., Russo, S. J., Nestler, E. J., and Carlezon, W. A. Jr. (2014). Effects of striatal DeltaFosB overexpression and ketamine on social defeat stress-induced anhedonia in mice. *Biol. Psychiatry* 76, 550–558. doi: 10.1016/j.biopsych.2013.12.014

Duman, R. S. (2018). Ketamine and rapid-acting antidepressants: a new era in the battle against depression and suicide. *F1000Res.* 7:F1000FacultyRev–659. doi: 10.12688/f1000research.14344.1

Francis, T. C., Chandra, R., Friend, D. M., Finkel, E., Dayrit, G., Miranda, J., et al. (2015). Nucleus accumbens medium spiny neuron subtypes mediate depression-related outcomes to social defeat stress. *Biol. Psychiatry* 77, 212–222. doi: 10.1016/j.biopsych.2014.07.021

Francis, T. C., Gaynor, A., Chandra, R., Fox, M. E., and Lobo, M. K. (2019). The selective RhoA inhibitor rhosin promotes stress resiliency through enhancing D1-medium spiny neuron plasticity and reducing hyperexcitability. *Biol. Psychiatry* 85, 1001–1010. doi: 10.1016/j.biopsych.2019.02.007

Goto, Y., and Grace, A. A. (2008). Limbic and cortical information processing in the nucleus accumbens. *Trends Neurosci.* 31, 552–558. doi: 10.1016/j.tins.2008.08.002

Gruber, A. J., Hussain, R. J., and O'Donnell, P. (2009). The nucleus accumbens: a switchboard for goal-directed behaviors. *PLoS One* 4:e5062. doi: 10.1371/journal.pone.0005062

Gunaydin, L. A., Grosenick, L., Finkelstein, J. C., Kauvar, I. V., Fenno, L. E., Adhikari, A., et al. (2014). Natural neural projection dynamics underlying social behavior. *Cell* 157, 1535–1551. doi: 10.1016/j.cell.2014.05.017

Hamilton, P. J., Burek, D. J., Lombroso, S. I., Neve, R. L., Robison, A. J., Nestler, E. J., et al. (2018). Cell-type-specific epigenetic editing at the Fosb gene controls susceptibility to social defeat stress. *Neuropsychopharmacology* 43, 272–284. doi: 10.1038/npp.2017.88

Hammels, C., Pishva, E., De Vry, J., van den Hove, D. L., Prickaerts, J., van Winkel, R., et al. (2015). Defeat stress in rodents: from behavior to molecules. *Neurosci. Biobehav. Rev.* 59, 111–140. doi: 10.1016/j.neubiorev.2015.10.006

Herrmann, C. S., and Demiralp, T. (2005). Human EEG gamma oscillations in neuropsychiatric disorders. *Clin. Neurophysiol.* 116, 2719–2733. doi: 10.1016/j.clinph.2005.07.007

Holmes, A., and Wellman, C. L. (2009). Stress-induced prefrontal reorganization and executive dysfunction in rodents. *Neurosci. Biobehav. Rev.* 33, 773–783. doi: 10.1016/j.neubiorev.2008.11.005

Jacinto, L. R., Cerqueira, J. J., and Sousa, N. (2016). Patterns of theta activity in limbic anxiety circuit preceding exploratory behavior in approach-avoidance conflict. *Front. Behav. Neurosci.* 10:171. doi: 10.3389/fnbeh.2016.00171

Jacinto, L. R., Reis, J. S., Dias, N. S., Cerqueira, J. J., Correia, J. H., and Sousa, N. (2013). Stress affects theta activity in limbic networks and impairs novelty-induced exploration and familiarization. *Front. Behav. Neurosci.* 7:127. doi: 10.3389/fnbeh.2013.00127

Jaeger, D., Kita, H., and Wilson, C. J. (1994). Surround inhibition among projection neurons is weak or nonexistent in the rat neostriatum. *J. Neurophysiol.* 72, 2555–2558. doi: 10.1152/jn.1994.72.5.2555

Koos, T., and Tepper, J. M. (1999). Inhibitory non-stressed of neostriatal projection neurons by GABAergic interneurons. *Nat. Neurosci.* 2, 467–472. doi: 10.1038/8138

Krishnan, V., Han, M. H., Graham, D. L., Berton, O., Renthal, W., Russo, S. J., et al. (2007). Molecular adaptations underlying susceptibility and resistance to social defeat in brain reward regions. *Cell* 131, 391–404. doi: 10.1016/j.cell.2007.09.018

Kummer, K. K., El Rawas, R., Kress, M., Saria, A., and Zernig, G. (2015). Social interaction and cocaine conditioning in mice increase spontaneous spike frequency in the nucleus accumbens or septal nuclei as revealed by multielectrode array recordings. *Pharmacology* 95, 42–49. doi: 10.1159/000370314

Larrieu, T., Cherix, A., Duque, A., Rodrigues, J., Lei, H., Gruetter, R., et al. (2017). Hierarchical status predicts behavioral vulnerability and nucleus accumbens metabolic profile following chronic social defeat stress. *Curr. Biol.* 27, 2202–2210.e4. doi: 10.1016/j.cub.2017.06.027

Lega, B. C., Kahana, M. J., Jaggi, J., Baltuch, G. H., and Zaghloul, K. (2011). Neuronal and oscillatory activity during reward processing in the human ventral striatum. *Neuroreport* 22, 795–800. doi: 10.1097/WNR.0b013e32834b2975

Lehner, M. H., Karas-Ruszczyk, K., Zakrzewska, A., Gryz, M., Wislowska-Stanek, A., Kolosowska, K., et al. (2018). Chronic stress changes prepulse inhibition after amphetamine challenge: the role of the dopaminergic system. *J. Physiol. Pharmacol.* 69, 3475–3487. doi: 10.26402/jpp.2018.3.15

Mallet, N., Le Moine, C., Charpier, S., and Gonon, F. (2005). Feedforward inhibition of projection neurons by fast-spiking GABA interneurons in the rat striatum in vivo. *J. Neurosci.* 25, 3857–3869. doi: 10.1523/JNEUROSCI.5027-04.2005

McEwen, B. S. (2016). Stress-induced remodeling of hippocampal CA3 pyramidal neurons. *Brain Res.* 1645, 50–54. doi: 10.1016/j.brainres.2015.12.043

Miczek, K. A. (1979). Chronic delta9-tetrahydrocannabinol in rats: effect on social interactions, mouse killing, motor activity, consummatory behavior, and body temperature. *Psychopharmacology* 60, 137–146. doi: 10.1007/bf00432284

Misaki, M., Suzuki, H., Savitz, J., Drevets, W. C., and Bodurka, J. (2016). Individual variations in nucleus accumbens responses associated with major depressive disorder symptoms. *Sci. Rep.* 6:21227. doi: 10.1038/srep21227

Monroe, S. M., Slavich, G. M., and Georgiades, K. (2014). "The social environment and depression: the roles of life stress," in *Handbook of Depression*, ed. H. G. C. L. Hammen (New York, NY: Guilford Press), 296–314.

Muir, J., Lorsch, Z. S., Ramakrishnan, C., Deisseroth, K., Nestler, E. J., Calipari, E. S., et al. (2018). *In Vivo* fiber photometry reveals signature of future stress susceptibility in nucleus accumbens. *Neuropsychopharmacology* 43, 255–263. doi: 10.1038/npp.2017.122

Nauczyciel, C., Robic, S., Dondaine, T., Verin, M., Robert, G., Drapier, D., et al. (2013). The nucleus accumbens: a target for deep brain stimulation in resistant major depressive disorder. *J. Mol. Psychiatry* 1:17. doi: 10.1186/2049-9256-1-17

Negron-Oyarzo, I., Perez, M. A., Terreros, G., Munoz, P., and Dagnino-Subiabre, A. (2014). Effects of chronic stress in adolescence on learned fear, anxiety, and synaptic transmission in the rat prelimbic cortex. *Behav. Brain Res.* 259, 342–353. doi: 10.1016/j.bbr.2013.11.001

Nisenbaum, E. S., and Berger, T. W. (1992). Functionally distinct subpopulations of striatal neurons are differentially regulated by GABAergic and dopaminergic inputs–I. In vivo analysis. *Neuroscience* 48, 561–578. doi: 10.1016/0306-4522(92)90402-n

Paxinos, C., and Watson, G. (2007). *The Rat Brain in Stereotaxic Coordinates*, 6th Edn. Cambridge: Academic Press, Elsevier.

Perez, M. A., Penaloza-Sancho, V., Ahumada, J., Fuenzalida, M., and Dagnino-Subiabre, A. (2018). n-3 Polyunsaturated fatty acid supplementation restored impaired memory and GABAergic synaptic efficacy in the hippocampus of stressed rats. *Nutr. Neurosci.* 21, 556–569. doi: 10.1080/1028415X.2017.1323609

Pizzagalli, D. A. (2014). Depression, stress, and anhedonia: toward a synthesis and integrated model. *Annu. Rev. Clin. Psychol.* 10, 393–423. doi: 10.1146/annurev-clinpsy-050212-185606

Pizzagalli, D. A., Bogdan, R., Ratner, K. G., and Jahn, A. L. (2007). Increased perceived stress is associated with blunted hedonic capacity: potential implications for depression research. *Behav. Res. Ther.* 45, 2742–2753. doi: 10.1016/j.brat.2007.07.013

Pizzagalli, D. A., Holmes, A. J., Dillon, D. G., Goetz, E. L., Birk, J. L., Bogdan, R., et al. (2009). Reduced caudate and nucleus accumbens response to rewards in unmedicated individuals with major depressive disorder. *Am. J. Psychiatry* 166, 702–710. doi: 10.1176/appi.ajp.2008.08081201

Popescu, A. T., Popa, D., and Pare, D. (2009). Coherent gamma oscillations couple the amygdala and striatum during learning. *Nat. Neurosci.* 12, 801–807. doi: 10.1038/nn.2305

Redgrave, P., Prescott, T. J., and Gurney, K. (1999). The basal ganglia: a vertebrate solution to the selection problem? *Neuroscience* 89, 1009–1023. doi: 10.1016/s0306-4522(98)00319-4

Rincón-Cortés, M., and Grace, A. A. (2017). Sex-dependent effects of stress on immobility behavior and VTA dopamine neuron activity: modulation by ketamine. *Int. J. Neuropsychopharmacol.* 20, 823–832. doi: 10.1093/ijnp/pyx048

Schlaepfer, T. E., Cohen, M. X., Frick, C., Kosel, M., Brodesser, D., Axmacher, N., et al. (2008). Deep brain stimulation to reward circuitry alleviates anhedonia in refractory major depression. *Neuropsychopharmacology* 33, 368–377. doi: 10.1038/sj.npp.1301408

Tsankova, N. M., Berton, O., Renthal, W., Kumar, A., Neve, R. L., and Nestler, E. J. (2006). Sustained hippocampal chromatin regulation in a mouse model of depression and antidepressant action. *Nat. Neurosci.* 9, 519–525. doi: 10.1038/nn1659

Tye, K. M., Mirzabekov, J. J., Warden, M. R., Ferenczi, E. A., Tsai, H. C., Finkelstein, J., et al. (2013). Dopamine neurons modulate neural encoding and expression of depression-related behaviour. *Nature* 493, 537–541. doi: 10.1038/nature11740

Uhlhaas, P. J., and Singer, W. (2010). Abnormal neural oscillations and synchrony in schizophrenia. *Nat. Rev. Neurosci.* 11, 100–113. doi: 10.1038/nrn2774

van der Meer, M. A., Kalenscher, T., Lansink, C. S., Pennartz, C. M., Berke, J. D., and Redish, A. D. (2010). Integrating early results on ventral striatal gamma oscillations in the rat. *Front. Neurosci.* 4:300. doi: 10.3389/fnins.2010.00300

van der Meer, M. A., and Redish, A. D. (2009). Low and high gamma oscillations in rat ventral striatum have distinct relationships to behavior, reward, and spiking activity on a learned spatial decision task. *Front. Integr. Neurosci.* 3:9. doi: 10.3389/neuro.07.009.2009

Warnell, K. R., Sadikova, E., and Redcay, E. (2018). Let's chat: developmental neural bases of social motivation during real-time peer interaction. *Dev. Sci.* 21:e12581. doi: 10.1111/desc.12581

Warren, B. L., and Whitaker, L. R. (2018). Parvalbumin-expressing neurons in the nucleus accumbens: a new player in amphetamine sensitization and reward. *Neuropsychopharmacology* 43, 929–930. doi: 10.1038/npp.2017.256

Zoicas, I., and Neumann, I. D. (2016). Maternal separation facilitates extinction of social fear in adult male mice. *Behav. Brain Res.* 297, 323–328. doi: 10.1016/j.bbr.2015.10.034

Conflict of Interest Statement: The authors declare that the research was conducted in the absence of any commercial or financial relationships that could be construed as a potential conflict of interest.

The reviewer AD-A, declared a shared affiliation, with no collaboration, with one of the authors, MA-R, to the handling Editor at the time the of review.

frontiers in Behavioral Neuroscience

ORIGINAL RESEARCH
published: 08 August 2019
doi: 10.3389/fnbeh.2019.00180

An Automated Assay System to Study Novel Tank Induced Anxiety

Sara Haghani[1†], Maharshee Karia[2†], Ruey-Kuang Cheng[3] and Ajay S. Mathuru[1,4,5]*

[1]Yale-NUS College, Science Division, Singapore, Singapore, [2]Faculty of Science, McGill University, Montreal, QC, Canada, [3]Lee Kong Chian School of Medicine, Nanyang Technological University, Singapore, Singapore, [4]Institute of Molecular and Cell Biology (IMCB), Singapore, Singapore, [5]Department of Physiology, Yong Loo Lin School of Medicine, National University of Singapore, Singapore, Singapore

New environments are known to be anxiogenic initially for many animals including the zebrafish. In the zebrafish, a novel tank diving (NTD) assay for solitary fish has been used extensively to model anxiety and the effect of anxiolytics. However, studies can differ in the conditions used to perform this assay. Here, we report the development of an efficient, automated toolset and optimal conditions for effective use of this assay. Applying these tools, we found that two important variables in previous studies, the direction of illumination of the novel tank and the age of the subject fish, both influence endpoints commonly measured to assess anxiety. When tanks are illuminated from underneath, several parameters such as the time spent at the bottom of the tank, or the transitions to the top half of the tank become poor measures of acclimation to the novel environment. Older fish acclimate faster to the same settings. The size of the novel tank and the intensity of the illuminating light can also influence acclimation. Among the parameters measured, reduction in the frequency of erratic swimming (darting) is the most reliable indicator of anxiolysis. Open source pipeline for automated data acquisition and systematic analysis generated here and available to other researchers will improve accessibility and uniformity in measurements. They can also be directly applied to study other fish. As this assay is commonly used to model anxiety phenotype of neuropsychiatric ailments in zebrafish, we expect our tools will further aid comparative and meta-analyses.

Keywords: zebrafish, anxiety, novel tank diving test, automation, open source (OS)

OPEN ACCESS

Edited by:
Nuno Sousa,
University of Minho, Portugal

Reviewed by:
Roger P. Croll,
Dalhousie University, Canada
Chen-Min Yeh,
Salk Institute for Biological Studies, United States
Carla Denise Bonan,
Pontifical Catholic University of Rio Grande do Sul, Brazil

***Correspondence:**
Ajay S. Mathuru
ajay.mathuru@yale-nus.edu.sg

†These authors have contributed equally to this work

***Received:** 31 March 2019*
***Accepted:** 18 July 2019*
***Published:** 08 August 2019*

Citation:
Haghani S, Karia M, Cheng R-K and Mathuru AS (2019) An Automated Assay System to Study Novel Tank Induced Anxiety. Front. Behav. Neurosci. 13:180. doi: 10.3389/fnbeh.2019.00180

INTRODUCTION

Unfamiliar surroundings elicit a response of cautious exploration among animals. Among these, the open field test, originally introduced in 1934, Hall (1934) examines the motivational drive. The open field is often coupled with novel environment response test. In rodents, increased wall following and avoidance of the center, or thigmotaxis, has been used as a measure of anxiety in response to novel environments (Simon et al., 1994). The time taken or the latency to enter an operationally defined central area, or the total duration in that area has been used as an indicator of anxiolysis as animals acclimate to the novel environment (Prut and Belzung, 2003). Assays of similar nature have been used in birds and primates to model isolation-induced anxiety in novel environments (Simon et al., 1994; Moriarty, 1995).

An assay based on the concept of a novel environment, or a novel open tank as the equivalent of the commonly used open field test in rodents and its amenability for quantitative analysis in zebrafish was also described over a decade ago (Gerlai et al., 2000; Gerlai, 2003; Blaser and Gerlai, 2006). In the initial experiments, tanks were illuminated from the top to emulate an ethological context. The response of adult zebrafish in such a setup, that is, to stay at the bottom initially and slowly habituate to the rest of the tank, was interpreted as a precautionary antipredatory response followed by alleviation of anxiety, respectively. This interpretation was made on the basis of the observation that zebrafish swim at the surface of the tank for the most part of the day in the laboratory holding facilities (Gerlai et al., 2000). This type of behavior may be related to laboratory rearing conditions as field studies examining the vertical distribution of zebrafish and their gut content in the wild, in the floodplains of the Indian subcontinent, suggest that zebrafish likely occupy and feed uniformly throughout the depth of the water column in the day (Spence et al., 2006, 2007). It is nonetheless reasonable to interpret extended time spent at the bottom of a novel tank initially as an expression of anxiety, or a predator avoidance behavior. The vertical position changes rapidly and solitary zebrafish spend most of the time at the bottom of the tank when expressing innate fear after exposure to an alarm substance (Speedie and Gerlai, 2008; Parra et al., 2009; Wisenden, 2010; Mathuru et al., 2012; Gerlai, 2013). Innate fear and anxiety are dissociable, but are related phenomena that share circuits, physiological players, and behavioral expression in most animals examined (Adolphs and Anderson, 2018). Zebrafish are unlikely to be exceptions in this matter and bottom-dwelling may be a defensive strategy shared between the two phenomena.

Among the earliest studies that modeled isolation-induced anxiety in a novel tank and the effect of drugs in reducing this anxiety, was one using this assay to study the effects of nicotine (Levin et al., 2007). Subsequently, several others have used a version of this assay to examine the effect of substances known to be either anxiolytic, or anxiogenic in mammals, including humans, and established its use in zebrafish to study stress and anxiety (Bencan et al., 2009; Egan et al., 2009; Grossman et al., 2010). The main endpoint in these assays has been a quantification of the time spent in the bottom third of the tank or the diving response. Other parameters such as latency to transit to the top half and, the number of such transitions have also been used, but these are correlated with the initial diving phenomenon (Blaser and Gerlai, 2006). Erratic swimming or darting and immobility episodes are two other endpoints unrelated to diving that have been used as well. Treatment with many anxiolytics attenuates the measure of all these parameters, consistent with the interpretation that these anxiolytic compounds reduce anxiety in fish as they do in other animals by acting on common molecular targets (Bencan et al., 2009; Egan et al., 2009; Grossman et al., 2010). As a consequence, the novel tank diving (NTD) test has been used extensively and has become one of the two standard tests for anxiety in zebrafish (the other being scototaxis). A few among over a hundred studies that used this assay include (Bencan and Levin, 2008; Bencan et al., 2009; Egan et al., 2009; Cachat et al., 2010, 2013; Grossman et al., 2010; Sackerman et al., 2010; Khor et al., 2011; Maximino et al., 2011, 2013a,b; Parker et al., 2013; Pittman and Ichikawa, 2013; Vignet et al., 2013; Kulkarni et al., 2014; Mezzomo et al., 2016; Kalueff, 2017) and are reviewed in a meta-analysis (Kysil et al., 2017).

Surprisingly, however, in spite of such widespread use, the exact conditions used to perform the assay are still variable and not standardized between studies. Apart from the minor differences in the shape and size of the tank used as a novel environment, or the duration of the assay, a major difference is the manner in which the tank is illuminated. Tanks can be backlit while observing or video recording from the front (Bencan and Levin, 2008; Bencan et al., 2009; Pittman and Ichikawa, 2013), or lit from the top in a darkened room (Maximino et al., 2011, 2013a,b), or may be placed in ambient light (Egan et al., 2009; Cachat et al., 2010, 2013; Sackerman et al., 2010) with a light reflective surface at the bottom or at the tank's back wall, or left undescribed (Grossman et al., 2010; Wong et al., 2010; Khor et al., 2011; Parker et al., 2013, 2014; Kulkarni et al., 2014; Mezzomo et al., 2016). Whether these differences influence the endpoints measured has not been systematically evaluated. We were specifically interested in the variable of illumination because adult zebrafish avoid lit areas in a scototaxis assay (Maximino et al., 2010; Lau et al., 2011), and groups (including our own), interested in observing the locomotion of zebrafish in 3D may consider illuminating the tank from underneath, or use a highly reflective surface at the bottom of the observation tank to improve contrast (Stewart et al., 2015; Audira et al., 2018).

Here, we tested if the direction of illumination, from the bottom or the top of the tank, influences the behavior of adult zebrafish in the NTD test. We find that illumination direction changes time spent and distance traversed in the bottom of the tank and the frequency of transitions to the top—that is, it affects most measures used to ascertain the level of anxiety in zebrafish. As previous studies used fish over a range of age (between 3–12 months old) in such experiments, we also examined responses of two age groups of fish, 3–5 months old adults and 7–9 months or older adults. Older fish responses are notably different in many parameters measured as they appear to be less sensitive to the illumination conditions, and acclimate faster. In effect, this means studies adopting one of the two illumination conditions, or something in between, and/or differing in the age group of fish studied can reach different conclusions.

To aid future studies, we also explored the impact of common variables such as the size of the arena used as a novel tank, the intensity of light illuminating the novel tank, and the total duration of assay. We find that each of these variables also impacts the conclusion. Another potential source of variation is the method of quantification and definitions used. For instance, darting or erratic swimming can be subjectively coded differently among different studies or differently among different observers. One way to improve reproducibility is to automate quantitation and to use clearly defined criteria that

can be quantified. To this end, we also provide new open source tools with this manuscript that can be used to automate both the acquisition and the analysis of NTD behavior at a minimal cost. We expect these will allow more reliable and consistent phenotyping in studies using innate anxiety tests to investigate the genetics of comorbid mental disorders (Blaser and Rosemberg, 2012; Stewart et al., 2012; Kim et al., 2014; Meshalkina et al., 2018).

MATERIALS AND METHODS

Experimental Method

Experiments were performed in accordance with the guidelines recommended by the Institutional Animal Care and Use Committee (IACUC) of the Biological Resource Center at A*STAR. Approved experimental protocols (IACUC 161110) were followed.

Animals

One-hundred and forty AB wild type fish from two age groups (3–5 months old and 7–9 months old) with an equal number of males and females were used in the study. The fish were bred and grown in the laboratory fish facility (Institute of Molecular and Cell Biology, A*STAR) and housed in groups of 20–25 in 3-l tanks in standard conditions of the facility.

Procedure

Prior to the experiments described, the entire procedure of the experiment including netting, transport to the behavioral observation room, and transfer into observation tanks was standardized as moving fish from their home tanks in stressful for the fish (Mathuru et al., 2017). All experiments were then conducted in the following manner (**Figure 1**). Fish were netted from home tanks in pairs and transferred to the behavior examination room. The netting was done using standard aquaria nets that had stitches on the sides such that the middle part of the net had no folds or obstructions. In the behavior room, fish were transferred into two separate beakers (100 ml) with ∼25–30 ml of tank water immediately using the same net and were gently released into two observational glass tanks simultaneously. The transfer into beakers and release into the observation tanks were completed within 30 s. Standard observation tanks for all conditions tested were novel tanks that subject fish had not experienced. The dimensions were 20 cm × 12 cm × 5 cm; L × H × W. For the large tank condition, larger tanks of 14 cm × 12 cm × 14 cm; L × H × W were used. Tanks were filled with system water collected from the system housing the test subjects, filled up to the 10 cm mark and placed against a black background. Tank water was changed after testing four subjects.

Illumination Method and Conditions

Tanks were uniformly illuminated in different light conditions. For low-intensity top light, a natural light LED light bar (IKEA, model LEDBERG) placed approximately 15 cm above the tanks was used to deliver a uniform illumination of 1.5 $\mu W/mm^2$ of light when measured using a digital handheld optical power and energy meter in the 500–540 nm range (Thor Labs, PM100D). High-intensity light from the top, or the bottom was delivered using a lightbox (Artograph, LightPad 930 lx) that delivered 3 $\mu W/mm^2$ uniform illumination in the same wavelength. The measurements made at multiple points of the observation tank showed no measurable difference in intensity. Videos were recorded using a Basler Ace (acA1300–200 μm; 1,280 × 1,024) camera placed in front of the tanks at ∼40 cm distance. Videos were recorded at 10 frames per second for 600 s (10 min), except in the long duration condition where videos were recorded for 1,080 s (18 min). Subject fish could not view other fish during observation and the experimentalist were obscured by a curtain in the setup.

Video Acquisition and Analysis

The following pipeline for data acquisition and analysis were generated for this study (Supplementary Video S1) and are provided with this article as open source Python scripts. Videos and trajectories of fish locomotion were acquired online and stored as videos, tracked videos, and an Excel file.

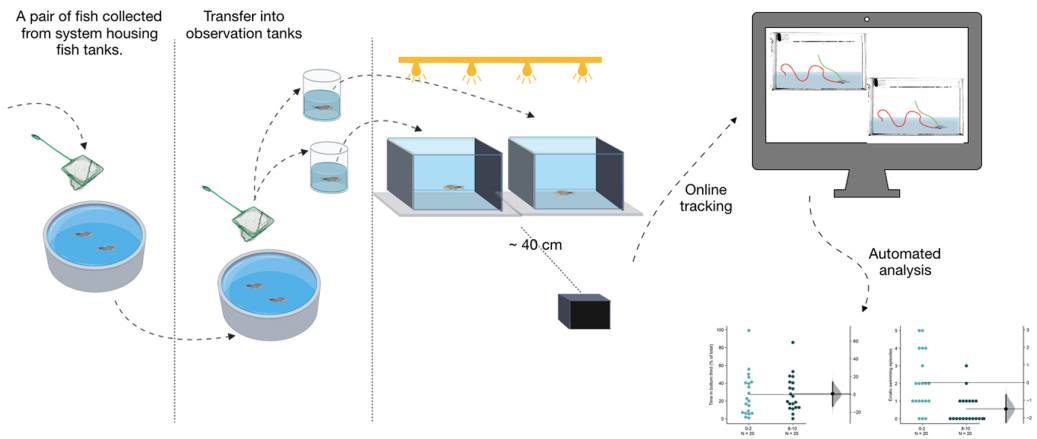

FIGURE 1 | Schematic. Graphical illustration of the study method and procedure.

Automated Tracking

The program we developed is versatile and can be adapted to any conditions, with minor modifications to the code. A detailed description is in the "Readme" file that accompanies the software at our website. In essence, the program utilizes the combination of Python and OpenCV machine vision libraries, both open source. We recommend using PyCharm community edition (also an open-source Python editor) version 5.0.2 or higher for optimal performance. The location of the fish in each image is determined by custom-written background subtraction algorithm. The background image is established by a moving average of about 10 (changeable) successive images after the fish is put into the tank. The moving average will cancel out any moving object in the image (i.e., the fish) thus resulting in a static background image. When detecting the location of the fish against the background image, a bounding rectangle of the fish is determined by using OpenCV library cv2.findContours. The center x-y coordinate of this rectangle is denoted as the center of the fish mass.

Automated Analysis Scripts

To analyze the data generated from the automated tracker, we also developed a set of analysis scripts written in Python. These scripts are also available at our website with detailed instructions on its use described in a Readme file. These analysis scripts generate graphics as well as spreadsheets with the data, listing both absolute values and relative percentages where appropriate (for example, percentage time of total in the center of the tank, vs. along the walls). Among the parameters analyzed include, total time (in seconds), percentage of total time, average velocity, and total distance swam in the—center, along the walls, in the bottom 1/4, in the bottom 1/2, in the bottom 1/3, of the tank. Latency to make the first and second transition to the top $\frac{1}{2}$ of the tanks and the number of such transitions are also calculated. The total duration of time spent freezing (displacement of ≤ 3 mm/s) and the number of freezing episodes (at least 1 s of immobility) are also calculated by the script. Finally, the number of erratic swimming or darting episodes are also calculated. As described previously (Schirmer et al., 2013) an episode of erratic swimming was quantified as a change in instantaneous velocity that exceeded the mean swimming velocity in the period of measurement by 8 standard deviations (8 SD) or more. Importantly, though we recommend keeping all the parameters described here fixed, users can change these settings when analyzing locomotion behavior of other animals. In the context of previous experiments of NTD, our analysis scripts take into account the differences in the settings, such as the duration that a researcher may want to perform the

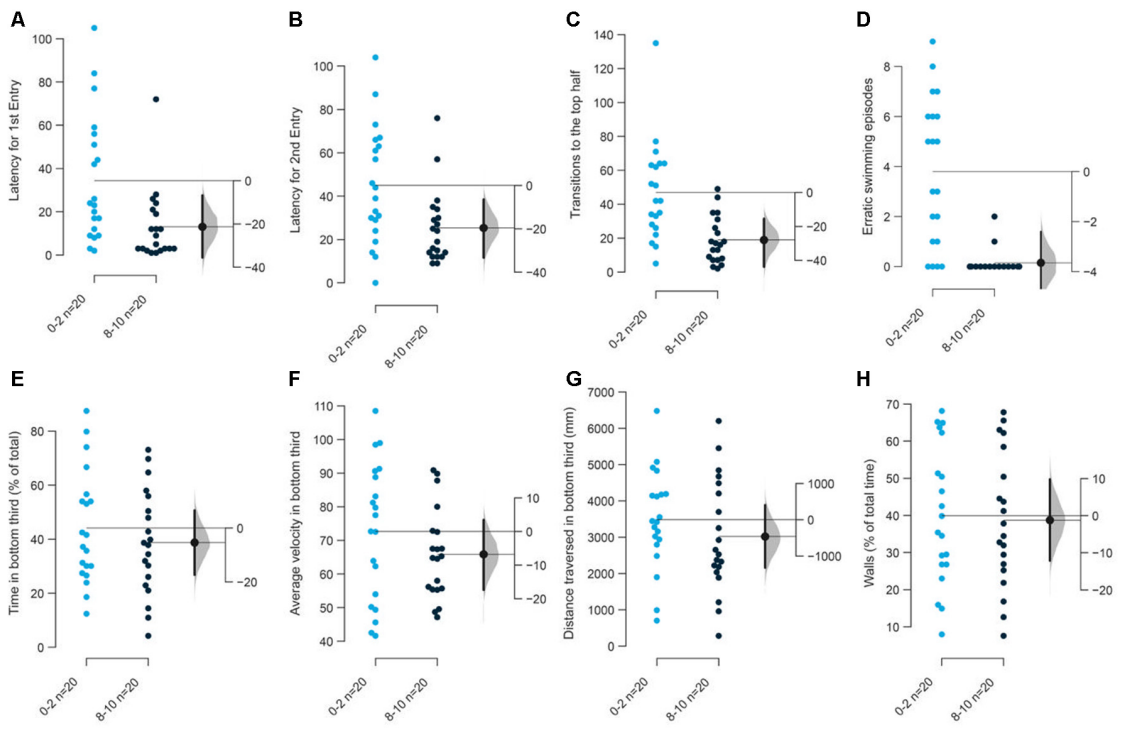

FIGURE 2 | Response of 3–5 months old adult zebrafish in top lit novel tank.The first set of experiments examined the response of 3–5 months old fish in top lit tanks. The mean difference between the first 2 (0–2) and the last 2-min (8–10) of 10 min are shown in Gardner-Altman estimation plots. The latency to make the **(A)** first entry, **(B)** second entry, to the top half of the tank, the frequency of **(C)** such transitions and **(D)** of the erratic swimming episodes. The **(E)** total percentage of time, **(F)** average velocity (in mm/s), **(G)** average distance traversed (in mm) in the bottom third of the tank. **(H)** Percentage of time of the total spent swimming along the edge (thigmotaxis). Each dot in the group represents the response of one individual. *N* = 20 per group. Groups are plotted on the left axis, while the mean difference between the groups is depicted as a black dot and is plotted on a floating axis on the right. Ends of the bar around the mean shows 95% confidence interval. The shaded region in gray is 5,000 bootstrap sampling distribution.

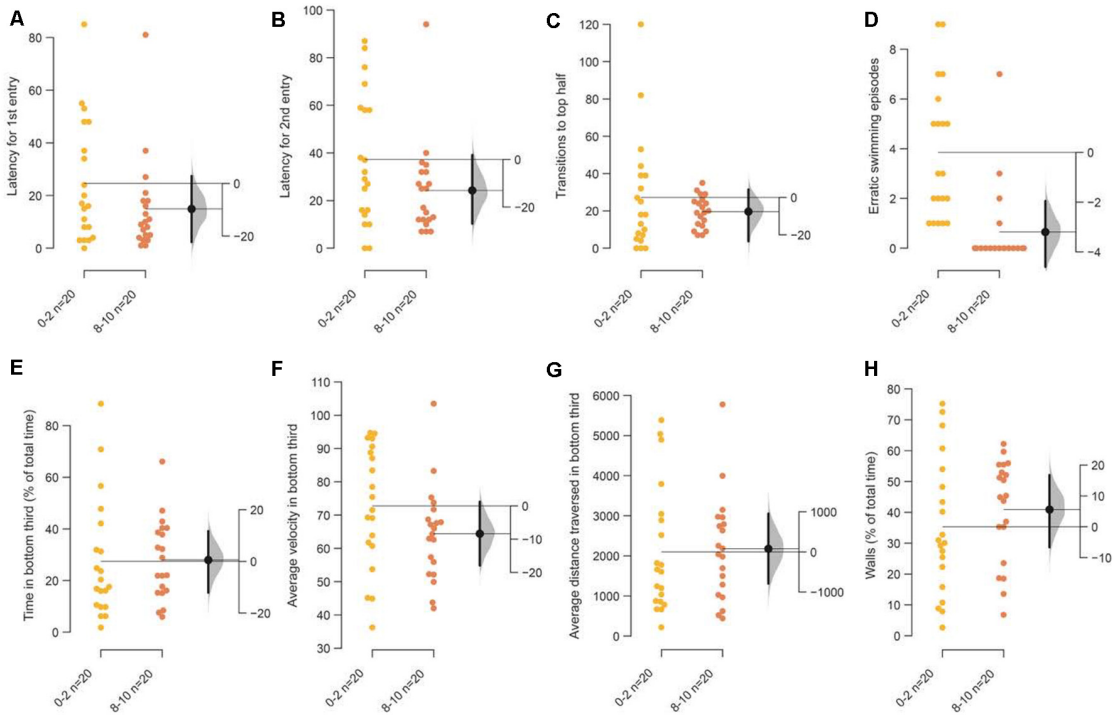

FIGURE 3 | Response of 3–5 months old adult zebrafish in bottom lit novel tank. The second set of experiments examined the response of 3–5 months old fish in bottom lit tanks. The mean difference between the first 2 (0–2) and the last 2-min (8–10) of 10 min are shown in Gardner-Altman estimation plots. The latency to make the **(A)** first entry, **(B)** second entry, to the top half of the tank, the frequency of **(C)** such transitions and **(D)** of the erratic swimming episodes. The **(E)** total percentage of time, **(F)** average velocity (in mm/s), **(G)** average distance traversed (in mm) in the bottom third of the tank. **(H)** Percentage of time of the total spent swimming along the edge (thigmotaxis). Each dot in the group represents the response of one individual. *N* = 20 per group. Groups are plotted on the left axis, while the mean difference between the groups is depicted as a black dot and is plotted on a floating axis on the right. Ends of the bar around the mean shows 95% confidence interval. The shaded region in gray is 5,000 bootstrap sampling distribution.

experiment for. We recommend performing the experiment for 10 min. However, 6 min experiments performed in the past by other researchers can also be directly analyzed with our scripts. Among the two analysis scripts, one generates an output for the entire duration of the experiment and the second allows users to specify the time window of analysis (0–2 min, 5–10 min, etc.). To allow for maximum flexibility, users define inputs including the dimensions of the observation tank and the duration of the experiment during analysis. Finally, the output generated also includes 95% confidence calculations for ease of making plots and graphics independent of those generated by the script.

Statistical Analysis

Null hypothesis significance testing and an overreliance on *p*-value based dichotomous interpretation of acceptance or rejection of a hypothesis have been criticized when studying behavior (du Prel et al., 2009; Halsey et al., 2015; Ho et al., 2019). In this manuscript, we adopted estimation statistics and Gardner-Altman plots to quantify effect sizes and to assess its precision (Ho et al., 2019). Briefly, in the figures, the primary axis (on the left) is used to represent the parameter being measured and all individual measurements are shown as a swarmplot to display the underlying distribution. Separate but aligned axes are used to show the effect size on the right, next to the groups being compared. The mean of the delta is shown by a black filled circle and the 95% bootstrap confidence intervals calculated from a nonparametric sampling of the observed data are shown by the shaded curve and whiskers. An open source website[1] was used to generate the figures and statistical analysis presented in this manuscript. *P*-values from paired or unpaired *t*-tests as suitable were also calculated and are reported alongside confidence intervals in the following format where necessary to aid readers unfamiliar with examining effect sizes [mean difference = xyz (95% confidence intervals—upper limit, lower limit), p = 0.0 xyz]. The *p*-values for all the comparisons made are tabulated and plots with traditional *p*-value reporting are described in **Supplementary Table S1**.

RESULTS

Parameters That Show an Acclimation Related Change in a Novel Tank

We used 3–5 months old adult male and female AB wild-type fish and examined their response in a novel tank when illuminated from the top, mimicking their natural habitats. Most tests

[1]http://www.estimationstats.com/#/

of anxiety and anxiolytics consider 6-min of assay time and measure the average response over the entire duration of the experiment (Levin et al., 2007; Egan et al., 2009). We matched the conditions of the experiment described by Levin et al. (2007), who introduced the test in the form used most commonly and examined the subjects for 10-min with the expectation that fish acclimate to the novel environment over this time. We then asked which among the commonly measured parameters change consistently as a consequence of acclimation. For this purpose, we generated new open source, stand-alone, automated online tracking and analysis tools in Python to acquire the behavioral data of fish in the observation tanks (see "Materials and Methods" section).

We first tested the condition where tanks were illuminated from above uniformly at 1.5 $\mu W/mm^2$. We found a decrease in the latency to enter the top half of the tank the first time [mean difference = −21.4 s (95 CI −35.5, −7.9), $p = 0.006$], the second time [mean difference = −19.6 s (95 CI −32.9, −4.7), $p = 0.022$], and a reduction in the number of such transitions [mean difference = −28.0 (95 CI −46.1, −15.7), $p = 0.001$], that is, factors dependent on the initial diving phenomenon are statistically significant between the first 2 vs. the last 2-min in the assay (**Figures 2A–C**). Fish also show fewer episodes of erratic swimming or darting [**Figure 2D**; mean difference = −3.65 (95 CI −4.9, −2.5), $p = 0.0004$; see "Materials and Methods" section for definition of erratic swimming episode]. On the other hand, parameters such as percentage time spent (**Figure 2E**), or their velocity (**Figure 2F**), or the distance traversed at the bottom third of the tank (**Figure 2G**), percentage of time following walls (**Figure 2H**)—other parameters measured in a novel tank assay, showed a trend but only a slight decrease only marginally. The total duration of immobility did not change in the first experiment but showed a decrease in repetition (see **Figure 9**).

Males and females showed a similar initial response to the novel tank for most measures, except average velocity (**Supplementary Figure S1**). A comparison between males and females during the first 2-min of the assay shows that the only notable difference is that males swim at a higher velocity than females [mean difference = 27.5 mm/s (95 CI 38.8, 12.3), $p = 0.0008$]. This difference persisted throughout the duration of the assay (data not shown).

Acclimation Is Difficult to Observe When Tanks Are Illuminated From the Bottom

Next, we examined age-matched adult siblings of the fish used in the assay above in the same novel tank, but this time the tanks were illuminated from beneath. Among the parameters that showed an acclimation related change above, only a reduction in erratic swimming or darting in the last 2-min compared to the first 2-min was notable [**Figure 3D**; mean difference = −3.3 (95 CI −4.5, −1.85), $p = 0.0001$]. All the other parameters directly dependent on the initial diving response—time in the bottom third of the tank, latency to enter the top half of the tank, the number of such transitions—show a trend similar to tanks illuminated from the top, but the decrease was marginal and the effects small (**Figures 3A–C,E–H**).

The main reason for marginal decrease appears to be a stunted diving response initially when tanks are illuminated from the bottom rather than an inability to acclimate. This is evidenced by the observation that in the first 2-min (**Figures 4A,B**) fish spend less time at the bottom of the tank and consequently have fewer transitions to the top half of the tank ($p = 0.02$ and 0.04, respectively), when tanks are illuminated from the bottom compared to from the top. This marginal initial effect becomes more pronounced over 10 min as fish in bottom lit tanks continue to swim in the top two-thirds of the tank (**Figures 4C,D**; $p = 0.003$ and 0.007, respectively). Therefore, though the endpoints used to measure anxiety and anxiolytic effects change in the expected direction when tanks are illuminated from beneath, the magnitude of the change

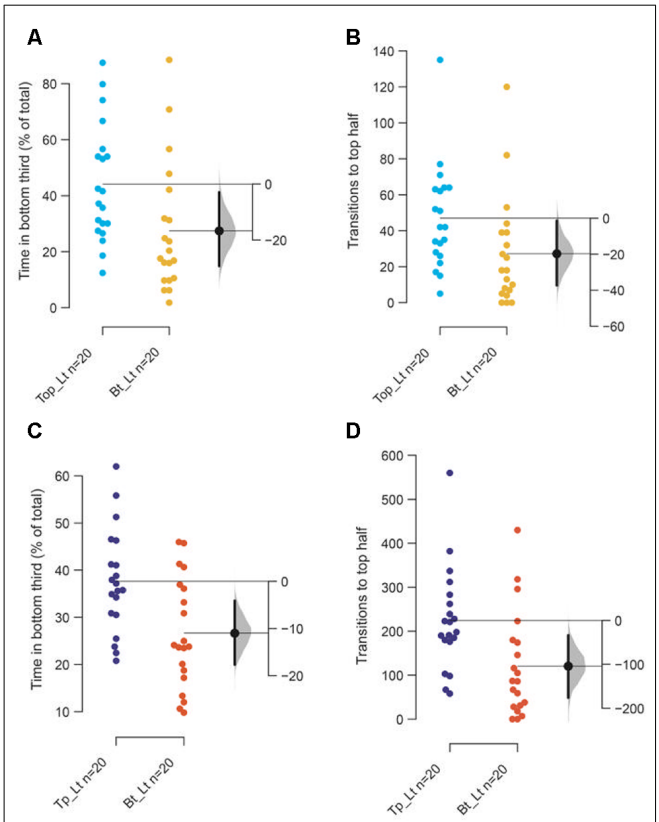

FIGURE 4 | Reasons for attenuated response. The mean difference between top lit and bottom lit groups are shown in Gardner-Altman estimation plots. The **(A)** total percentage of time in the bottom third of the tank and **(B)** the frequency of transitions to the top of the tank among 3–5-month-old adults. The **(C)** total percentage of time in the bottom third of the tank and **(D)** the frequency of transitions to the top of the tank among 7–9 months or older adults. Each dot in the group represents the response of one individual. $N = 20$ per group. Groups are plotted on the left axes, while the mean difference between the groups is depicted as a black dot and is plotted on a floating axis on the right. Ends of the bar around the mean shows 95% confidence interval. The shaded region in gray is the 5,000 bootstrap sampling distribution.

is smaller due to a stunted diving response at the start of the assay.

Older Adults Acclimate Faster and Are Less Anxious in Novel Tanks

In the next experiment, we examined if the response of the fish is consistent across age. We examined 7–9 months fish as many experiments have previously reported using fish between 3–12 months old, which is quite a wide range. One set of fish was examined in each of the two conditions of illumination described above.

Older fish are less sensitive to the illumination from the bottom. They dive initially and recover by the end of the assay duration (**Figures 5A–D**). This is apparent due to the decrease in latency to enter the top the first time [mean difference = −29.2 s (95 CI −41.2, −10.6), p = 0.003], the second time [mean difference = −29.9 s (95 CI −41.6, −12.1), p = 0.002], and the total number of such transitions [mean difference = −19.6 (95 CI −36.5, −7.25), p = 0.017]. Additionally, erratic swimming episodes decreased significantly in the last 2-min compared to the initial 2-min [**Figure 5D**; mean difference = −5.15 (95 CI −6.35, −4.05), $p < 0.0001$].

As seen for younger fish in the first experiment, when the tanks are illuminated from the top transitions [mean difference = −20.1 (95 CI −30.6; −10.2), p = 0.003] and erratic swimming [mean difference = −4.15 (95 CI −5.47; −3.15), p = 0.0002] showed a change in the same manner in older adults. Latency for the first [**Figure 5E**; mean difference = −5.6 s (95 CI −16.3, 2.5), p = 0.2] and second entry [mean difference = −15.5 s (95 CI −31.3, −1.75), p = 0.05] to the top half also change in the same direction as experiment 1, but these effects are marginal, once again suggesting faster recovery among older adults.

A major change in the swimming behavior with the age appears to be that older fish prefer to swim along the walls and make fewer transitions through the center of the tank (thigmotaxis), compared to younger fish as they acclimate irrespective of the illumination conditions (top lit **Figures 6A,B**; bottom lit **Figures 6C,D**). Unexpectedly therefore, thigmotaxis appears to increase in older fish towards the last 2-min (**Figures 6B,D**) compared to the first 2-min in the assay (**Figures 6A,C**).

Having established that the two most important parameters that vary across studies influence the results obtained from a novel tank assay, we next performed three more exploratory experiments.

Fish Acclimate Faster in Wider Tanks

The dimensions of our novel tank were based on the size of the tank used in previous studies which were narrow and range between 5–7 cm in width (for example, in Levin et al.,

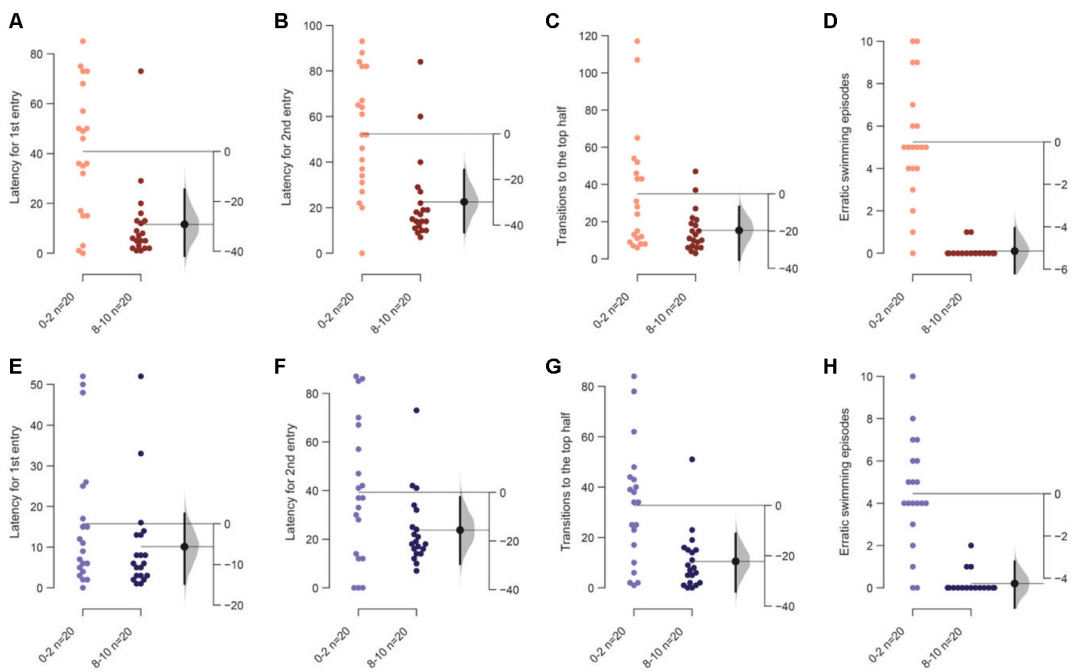

FIGURE 5 | Response of 7–9 months or older adult zebrafish in a novel tank. The mean difference between the first 2 (0–2) and the last 2-min (8–10) when tanks are bottom lit or top lit are shown in Gardner-Altman estimation plots. The latency to make the **(A)** first entry, **(B)** second entry, to the top half of the tank, the frequency of **(C)** such transitions and **(D)** of the erratic swimming episodes in bottom lit condition. The mean difference between the first 2 and the last 2-min when tanks are top lit are shown in Gardner-Altman estimation plots. The latency to make the **(E)** first entry, **(F)** second entry, to the top half of the tank, the frequency of **(G)** such transitions and **(H)** of the erratic swimming episodes. Each dot in the group represents the response of one individual. N = 20 per group. Groups are plotted on the left axis, while the mean difference between the groups is depicted as a black dot and is plotted on a floating axis on the right. Ends of the bar around the mean shows 95% confidence interval. The shaded region in gray is 5,000 bootstrap sampling distribution.

2007; Egan et al., 2009). As only two-dimensional videos are required, the standard aquaria tanks used in these studies are adequately suited for the need. In the next experiment, we asked if fish acclimate better or worse in novel tanks that were twice as wide (width = 14 cm). We found that several parameters that show a trend in the first experiment (**Figures 2E–G**) now showed statistically significant differences when the first 2-min were compared to the last 2-min in the 10-min assay. Fish spent less time [**Figure 7E**; mean difference = −23.4 s (95 CI −42.8, −2.2), p = 0.004], swam slower [**Figure 7F**; mean difference = −13.6 mm/s (95 CI −30.5, −0.65), p = 0.03], and traversed less distance [**Figure 7G**; mean difference = −1087.4 mm (95 CI −1667.9, −549.55), p = 0.0002] in the bottom third of the tank. Erratic swimming episodes (**Figure 7D**) also changed in the same manner as observed in experiment 1 (**Figure 2D**). However, latency for first, second entry, and the number of transition to the top half of the tank show only a marginal difference (**Figures 7A–C**). Further examination reveals that this is likely explained again by a faster rate of acclimation in the wider tank. Compared to the mean value of 34.4 s for the latency to enter the top half the first time in the initial 2-min (**Figure 2A**), the mean value for the same when the tank is wider is only 27.2 s. Therefore, fish acclimate faster in wider novel tanks.

Acclimation Is Difficult to Observe in Brightly Lit Novel Tanks

In the experiments described untill until now, the top illumination settings delivered a uniform illumination of 1.5 μW/mm^2. In the next exploratory experiment, we doubled the intensity of this illumination to 3 μW/mm^2. Similar to the second experiment (**Figure 3**) with bottom illumination, it was not possible to detect an acclimation dependent change across most parameters (**Figures 8A–H**), except for a reduction in erratic swimming or darting in the last 2-min compared to the first 2-min [**Figure 8D**, mean difference = −1.5 (95 CI −2.35, −0.8), p = 0.0008]. Once again, the lack of significant changes in other parameters (**Figures 8A–C,E–H**) at the end of the assay compared to the beginning can be explained by a stunted initial diving response (**Supplementary Figure S2**). Compared to the fish in the lower intensity top light in the first experiment, fish in the high intensity lighted tanks spend less time initially [mean difference = −16.8 s (95 CI −29.7, −1.8), p = 0.02] in the bottom third. As subjects in this condition are mostly swimming in the middle of the tank, they also make fewer transitions to the top half in the first 2-min [mean difference = −37.7 s (95 CI −53.35, −27.65), p = 1.786 e-6 or 0.000001]. Therefore, high-intensity top illumination makes an examination of the novel tank induced anxiety and recovery difficult to quantify.

Longer Duration for Acclimation

Finally, as the last exploratory experiment, we asked if the measures that showed a trend of decrease in the first experiment (**Figures 2E–G**) reach statistical significance if acclimated for a longer duration. To address this question, we repeated

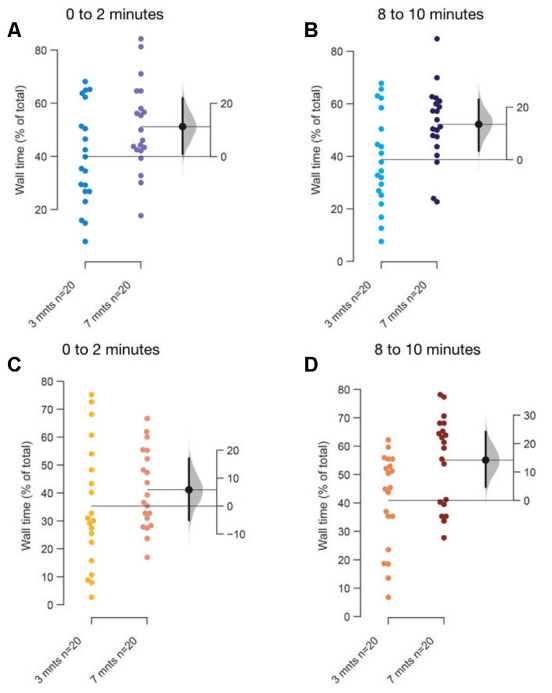

FIGURE 6 | Age-dependent differences in thigmotaxis. The mean difference between 3–5 months and 7–9 months fish when tanks are top lit **(A,B)**, or bottom lit **(C,D)** are shown in Gardner-Altman estimation plots. The percentage of total time along the edges of the tank in **(A)** first 2-min, and in **(B)** last 2-min when tanks are lit from the top. The percentage of total time along the edges of the tank in **(C)** first 2-min, and in the **(D)** last 2-min when tanks are bottom lit. Each dot in the group represents the response of one individual. N = 20 per group. Groups are plotted on the left axis, while the mean difference between the groups is depicted as a black dot and is plotted on a floating axis on the right. Ends of the bar around the mean shows 95% confidence interval. The shaded region in gray is 5,000 bootstrap sampling distribution.

the first experiment with the same lighting conditions (low intensity of 1.5 μW/mm^2 from the top) but observed the subjects for 18 min instead of 10 min. This duration is thrice as long as the duration normally used (Levin et al., 2007; Egan et al., 2009). We also analyzed the time in the bottom half rather than a third of the tank as a few studies report this instead. We found that indeed fish show changes suggestive of improved acclimation as they spend less time in the bottom third [mean difference = −21.1 (95 CI −37.3, −3.6), p = 0.020] or in the bottom half [mean difference = −19.2 (95 CI −33.2, −2.9), p = 0.018] when their behavior between 0–2 min is compared with their behavior between 16–18 min (**Figures 9A,B**). Apart from a reduction in the erratic swimming episodes like the first experiment (**Figure 9C**), we also observed a reduction in immobility episodes in this repetition [**Figure 9D**; mean difference = −9.8 s (95 CI −18.5, −4.3), p = 0.010]. Further analysis comparing fish in experiment 1 with this dataset showed that fish in the repetition displayed more episodes of immobility [**Figure 9E**, mean difference = −10.05 episodes (95 CI 4.6, 18.8), p = 0.0007] and fewer erratic swimming episodes in the first

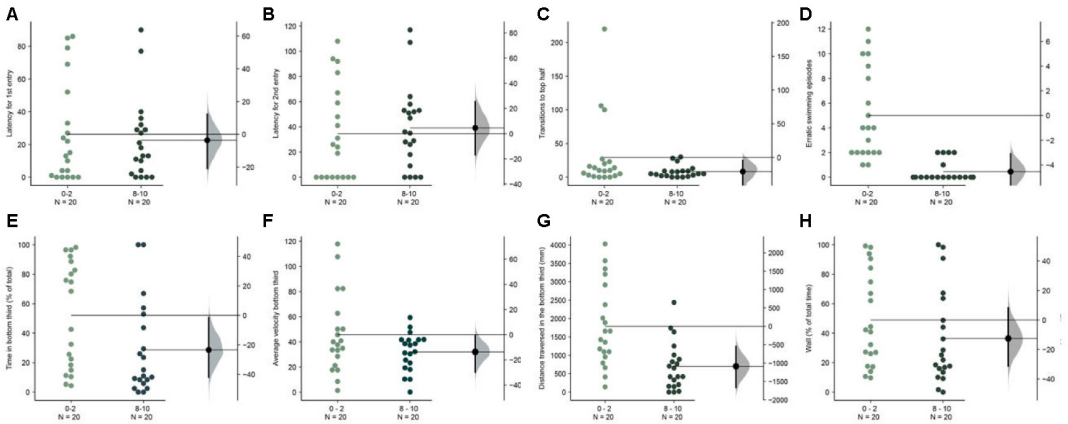

FIGURE 7 | Faster acclimation in wider tank. The mean difference between the first 2 (0–2) and the last 2-min (8–10) are shown in Gardner-Altman estimation plots. The latency to make the **(A)** first entry, **(B)** second entry, to the top half of the tank, the frequency of **(C)** such transitions and **(D)** of the erratic swimming episodes. The **(E)** total percentage of the time, **(F)** average velocity (in mm/s), **(G)** average distance traversed (in mm) in the bottom third of the tank. **(H)** Percentage of time of the total spent swimming along the edge (thigmotaxis). Each dot in the group represents the response of one individual. *N* = 20 per group. Groups are plotted on the left axis, while the mean difference between the groups is depicted as a black dot and is plotted on a floating axis on the right. Ends of the bar around the mean shows 95% confidence interval. The shaded region in gray is 5,000 bootstrap sampling distribution.

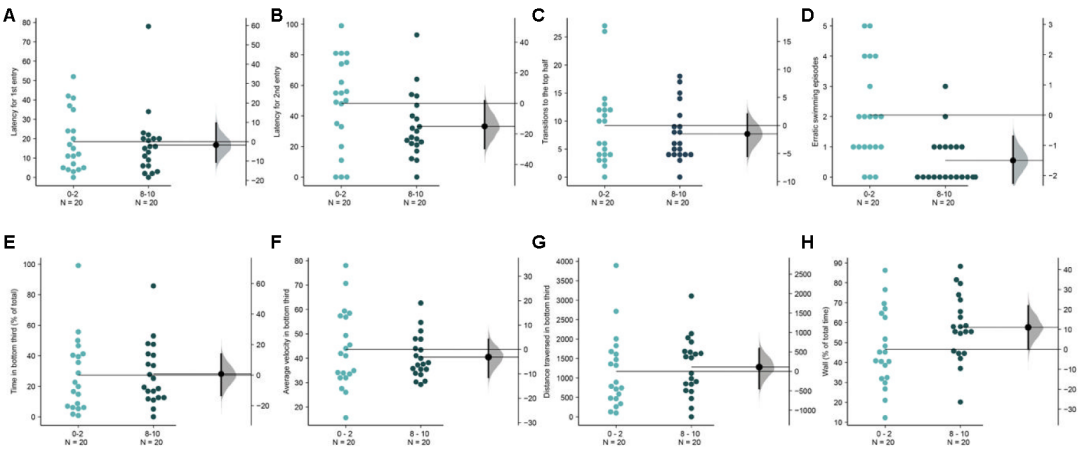

FIGURE 8 | Acclimation in brightly lit novel tanks. The mean difference between the first 2 (0–2) and the last 2-min (8–10) are shown in Gardner-Altman estimation plots. The latency to make the **(A)** first entry, **(B)** second entry, to the top half of the tank, the frequency of **(C)** such transitions and **(D)** of the erratic swimming episodes. The **(E)** total percentage of time, **(F)** average velocity (in mm/s), **(G)** average distance traversed (in mm) in the bottom third of the tank. **(H)** Percentage of time of the total spent swimming along the edge (thigmotaxis). Each dot in the group represents the response of one individual. *N* = 20 per group. Groups are plotted on the left axis, while the mean difference between the groups is depicted as a black dot and is plotted on a floating axis on the right. Ends of the bar around the mean shows 95% confidence interval. The shaded region in gray is 5,000 bootstrap sampling distribution.

2-min [**Figure 9F**, mean difference = −1.6 episodes (95 CI −0.1, −3), p = 0.04]. Therefore, zebrafish acclimate better to novel tanks in approximately 15 min, and express anxiety in the novel tank initially either by becoming immobile, or by swimming erratically.

DISCUSSION

Modeling phenotypes associated with human neuropsychiatric disorders in animals is essential to gain a mechanistic understanding of the molecular and genetic players that influence the phenomenon and to devise intervention strategies (Lim and Mathuru, 2017). Zebrafish are used extensively in both cellular and molecular modeling of diseases (Bourque and Houvras, 2011; Santoriello and Zon, 2012; Ablain and Zon, 2013) as well as in pharmacological studies relying on behavioral assays (Cachat et al., 2010; Stewart et al., 2012, 2015; Norton, 2013; Kalueff, 2017; Bao et al., 2019; Fontana et al., 2019).

Among the multitude of assays used to study anxiety, novel tank assays are easy to perform, informative, and are now validated through a large number of studies (Bencan and Levin, 2008; Bencan et al., 2009; Egan et al., 2009; Cachat et al., 2010,

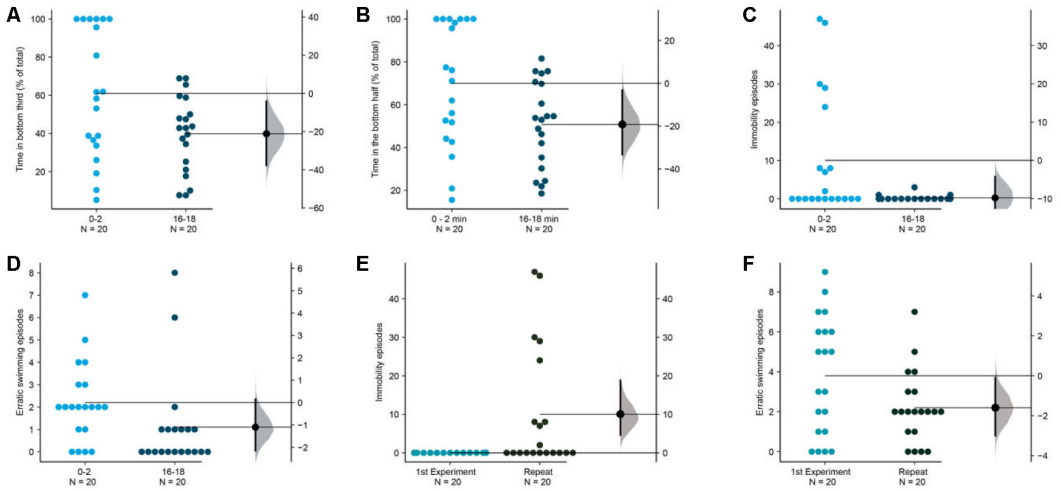

FIGURE 9 | Longer duration improves measures of acclimation. The mean difference between the first 2 (0–2) and the last 2-min (16–18) are shown in Gardner-Altman estimation plots. The percentage of total time in the **(A)** bottom third and **(B)** bottom half, the frequency of **(C)** immobility episodes and **(D)** erratic swimming episodes are reduced in the last 2-min. Fish in this repetition show more **(E)** immobility episodes and fewer **(F)** erratic swimming episodes in the first 2-min compared to the fish in the first experiment shown in **Figure 1**. Each dot in the group represents the response of one individual. *N* = 20 per group. Groups are plotted on the left axis, while the mean difference between the groups is depicted as a black dot and is plotted on a floating axis on the right. Ends of the bar around the mean shows 95% confidence interval. The shaded region in gray is 5,000 bootstrap sampling distribution.

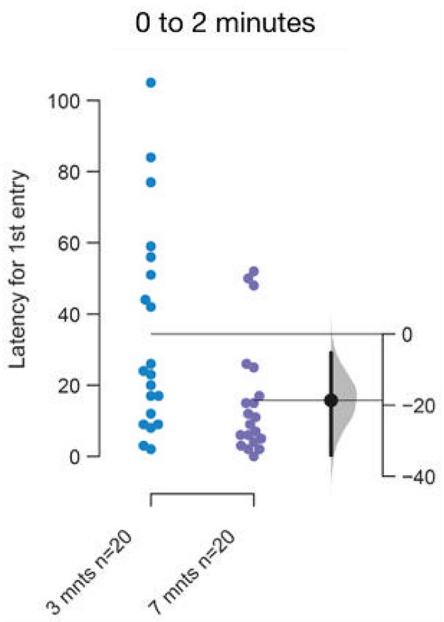

FIGURE 10 | Faster acclimation to novel talk in 7–9 months or older fish. The mean difference between top and bottom lit groups are shown in Gardner-Altman estimation plot. The latency to make the first entry into the top half of the tank is reduced in older fish. Each dot in the group represents the response of one individual. *N* = 20 per group. Groups are plotted on the left axes, while the mean difference between the groups is depicted as a black dot and is plotted on a floating axes on the right. Ends of the bar around the mean shows 95% confidence interval. The shaded region in gray is 5,000 bootstrap sampling distribution.

2013; Grossman et al., 2010; Sackerman et al., 2010; Khor et al., 2011; Maximino et al., 2011, 2013a,b; Parker et al., 2013; Pittman and Ichikawa, 2013; Vignet et al., 2013; Kulkarni et al., 2014; Mezzomo et al., 2016; Kalueff, 2017). In this study, we developed a simple pipeline from acquisition to analysis and explored conditions to perform this assay reliably. We expect this will reduce subjective bias in assaying the phenotype, inter-laboratory differences, potential miscommunication about effects observed, and expedite the experimental analysis.

The pipeline used here allows for online tracking of pairs of fish at a time (**Figure 1**). Using these tools we find that fish acclimate to a novel tank at different rates depending on the conditions of the setup. Among the optimal conditions for this assay is a uniform illumination from above the tank at approximately 1.5 $\mu W/mm^2$. Fish acclimate faster in a wider tank (up to 14 cm), however, a narrow tank (approximately 5–6 cm) used in previous studies to perform this assay is adequate to observe both anxiety and recovery within 10 min. In bottom lit tanks, or when tanks are brightly lit (at 3 $\mu W/mm^2$), the endpoints used to infer anxious behavior in the novel tank, or acclimation to it, show a smaller effect and therefore need to be interpreted with caution. A stunted diving response initially in the first 2-min is the main contributing factor for the smaller effect. Increased brightness in case of high-intensity illumination also increased reflected light from the floor of the tank, likely contributing to the stunted diving. This is consistent with the response of zebrafish in a light/dark novel chamber also used to assess anxiety behavior. In this assay, called scototaxis, given a choice between a white background and a dark one, adult zebrafish prefer spending more time in darker areas and display avoidance of brightly lit lighted areas (Stewart

et al., 2011). Taken together with our results, it suggests that adult zebrafish display a negatively phototactic behavior when anxious. The neural circuit mediating such behavior requires further research. Apart from the regular mode of photoreception through the pineal and the eyes, photoreceptivity can occur deep within the brain through photosensitive neurons that express melanopsin (*opn4*) in larval zebrafish that can impact locomotion (Fernandes et al., 2012, 2013). Though this system is also proposed to have a role in fight/flight or freezing behavior (Tay et al., 2011), whether the same is applicable to adult zebrafish is unknown.

Behavioral differences between the sexes have been described in guppies in the past for some exploratory behaviors (Lucon-Xiccato and Dadda, 2016). In each of our experiments, we examined approximately equal number of males and females. We noted some sex differences between male and female swimming patterns consistent with other studies (Tran and Gerlai, 2013; Porseryd et al., 2017), however, we did not observe a reliable or a systematic difference in their rate of acclimation (**Supplementary Figure S1**).

Finally, our results (**Figure 6**) suggest that older zebrafish also show increased levels of thigmotaxis regardless of the light conditions when compared to the younger fish over the 10-min recording period. The magnitude of this difference increases over time. This suggests that an increase in thigmotaxis in zebrafish in such settings might be an indicator of anxiolysis. This is counterintuitive in comparison to expectation from rodent studies. One caveat in our experiments was the position of video recording from the front rather than from the top and therefore needs further experimentation before reliable conclusions can be drawn.

The difference between the rate of acclimation between young adults, 3–5 months old and 7–9 months or older fish in the ethologically relevant illumination condition was also unanticipated by us [**Figure 10**; mean difference = −18.65 s (95 CI −34.05, −5.3), p = 0.01]. This faster acclimation rate could explain the smaller marginal effect for one out of the four parameters seen in **Figure 5**. The change in the rate of acclimation is small, yet this result again highlights the need to use age-matched subjects when testing differences between any two conditions.

Several commercial software packages are available to perform these experiments, however, the tools provided with this study require no additional costs or investments, other than the installation of an open source software to execute the Python scripts. They allow the use of any standard web camera to acquire data. Automation also allowed us to streamline the experimental method (please see "Materials and Methods" section) and make efficient use of experimental time. Online tracking avoids the additional time required to track videos after acquisition and the automated analysis of tracked data to quantify the behavioral data reduces dependence on human behavior coders. A complete set of experiments, for example, experiments that require comparing two conditions (a mutant, and a wild type) with n = 18–24 per condition, will require a maximum of 4 days of daily experimentation at 3 h/day. These tools are available to the reader as open-source, stand-alone Python scripts. As minimal training in computation is required to use them, researchers with limited experience in coding will be able to utilize them with relative ease. Further, researchers with limited expertise in performing behavioral studies such as those focused on examining developmental defects in genetic mutants in zebrafish, but interested in performing such experiments will also be able to adapt them rapidly.

Based on the results presented above and comparing previous literature (**Supplementary Table S1**), we recommend that researchers use top light illumination at low intensity (∼1.5 $\mu W/mm^2$) and select subjects from a smaller age range (1–2 months). This is particularly relevant when comparing the response of two conditions, such as treated and untreated or mutants and wild type. We expect adopting these recommendations will reduce the noise and increase the "dynamic range" in the study of anxiety and anxiolysis using the zebrafish.

DATA AVAILABILITY

Publicly available datasets were generated and analyzed in this study. This data can be found here: https://drive.google.com/open?id=1euoh2dVesnXRUQzaFWru54_ENrXOlfzQ.

ETHICS STATEMENT

This study was carried out in accordance with the guidelines recommended by the Institutional Animal Care and Use Committee (IACUC) of the Biological Resource Center at A*STAR. Approved experimental protocols (IACUC 161110) were followed.

AUTHOR CONTRIBUTIONS

SH performed experiments and analyzed the data. MK and R-KC developed software and analysis tools. AM conceived and supervised the project, performed experiments and analyzed the data, and wrote the manuscript with assistance from SH.

FUNDING

This work was supported by Yale-NUS College through grants R-607-265-225-121 and IG16-LR003.

ACKNOWLEDGMENTS

We acknowledge the zebrafish facility staff for fish husbandry.

SUPPLEMENTARY MATERIAL

The Supplementary Material for this article can be found online at: https://www.frontiersin.org/articles/10.3389/fnbeh.2019.00180/full#supplementary-material

FIGURE S1 | The first set of experiments examined the response of 3-5 month old fish in top lit tanks. The mean difference between males and females in the

first 2 min are shown in Gardner-Altman estimation plots. The latency to make the **(A)** first entry, **(B)** second entry, to the top half of the tank, the frequency of **(C)** such transitions and **(D)** of the erratic swimming episodes. The **(E)** total percentage of time, **(F)** average velocity (in mm/s), **(G)** average distance traversed (in mm) in the bottom third of the tank. **(H)** Percentage of time of the total spent swimming along the edge (thigmotaxis). Each dot in the group represents the response of one individual. N is given under the figure. Groups are plotted on the left axis, while the mean difference between the groups is depicted as a black dot and is plotted on a floating axis on the right. Ends of the bar around the mean shows 95% confidence interval. The shaded region in grey is 5,000 bootstrap sampling distribution. Only notable difference is that males swim at a higher velocity than females [**Supplementary Figure S1**; mean difference = 27.5 mm/s (95 CI 38.8, 12.3), $p = 0.0008$]. Only notable difference is that males swim at a higher velocity than females [**Supplementary Figure S1** F; mean difference = 27.5 mm/s (95 CI 38.8, 12.3), $p = 0.0008$].

FIGURE S2 | The mean difference between fish in novel tanks with normal or bright illumination in first 2 min are shown in Gardner-Altman estimation plots. **(A)** Percentage of total time in the bottom third and **(B)** The number of transitions to the top half are plotted show that high-intensity top illumination causes stunted diving response. Each dot in the group represents the response of one individual. $N = 20$. Groups are plotted on the left axis, while the mean difference between the groups is depicted as a black dot and is plotted on a floating axis on the right. Ends of the bar around the mean shows 95% confidence interval. The shaded region in grey is 5,000 bootstrap sampling distribution.

TABLE S1 | Results presented here are compared with previous literature.

REFERENCES

Ablain, J., and Zon, L. I. (2013). Of fish and men: using zebrafish to fight human diseases. *Trends Cell Biol.* 23, 584–586. doi: 10.1016/j.tcb.2013.09.009

Adolphs, R., and Anderson, D. J. (2018). *The Neuroscience of Emotion: A New Synthesis.* Princeton University Press. Available online at: https://market.android.com/details?id=book-0xtFDwAAQBAJ.

Audira, G., Sampurna, B., Juniardi, S., Liang, S.-T., Lai, Y.-H., and Hsiao, C.-D. (2018). A simple setup to perform 3D locomotion tracking in zebrafish by using a single camera. *Inventions* 3:11. doi: 10.3390/inventions3010011

Bao, W., Volgin, A. D., Alpyshov, E. T., Friend, A. J., Strekalova, T. V., de Abreu, M. S., et al. (2019). Opioid neurobiology, neurogenetics and neuropharmacology in zebrafish. *Neuroscience* 404, 218–232. doi: 10.1016/j.neuroscience.2019.01.045

Bencan, Z., and Levin, E. D. (2008). The role of α7 and α4β2 nicotinic receptors in the nicotine-induced anxiolytic effect in zebrafish. *Physiol. Behav.* 95, 408–412. doi: 10.1016/j.physbeh.2008.07.009

Bencan, Z., Sledge, D., and Levin, E. D. (2009). Buspirone, chlordiazepoxide and diazepam effects in a zebrafish model of anxiety. *Pharmacol. Biochem. Behav.* 94, 75–80. doi: 10.1016/j.pbb.2009.07.009

Blaser, R., and Gerlai, R. (2006). Behavioral phenotyping in zebrafish: comparison of three behavioral quantification methods. *Behav. Res. Methods* 38, 456–469. doi: 10.3758/bf03192800

Blaser, R. E., and Rosemberg, D. B. (2012). Measures of anxiety in zebrafish (*Danio rerio*): dissociation of black/white preference and novel tank test. *PLoS One* 7:e36931. doi: 10.1371/journal.pone.0036931

Bourque, C., and Houvras, Y. (2011). Hooked on zebrafish: insights into development and cancer of endocrine tissues. *Endocr. Relat. Cancer* 18, R149–R164. doi: 10.1530/ERC-11-0099

Cachat, J., Canavello, P., Elegante, M., Bartels, B., Hart, P., Bergner, C., et al. (2010). Modeling withdrawal syndrome in zebrafish. *Behav. Brain Res.* 208, 371–376. doi: 10.1016/j.bbr.2009.12.004

Cachat, J., Kyzar, E. J., Collins, C., Gaikwad, S., Green, J., Roth, A., et al. (2013). Unique and potent effects of acute ibogaine on zebrafish: the developing utility of novel aquatic models for hallucinogenic drug research. *Behav. Brain Res.* 236, 258–269. doi: 10.1016/j.bbr.2012.08.041

du Prel, J.-B., Hommel, G., Röhrig, B., and Blettner, M. (2009). Confidence interval or P-value? part 4 of a series on evaluation of scientific publications. *Dtsch. Arztebl. Int.* 106, 335–339. doi: 10.3238/arztebl.2009.0335

Egan, R. J., Bergner, C. L., Hart, P. C., Cachat, J. M., Canavello, P. R., Elegante, M. F., et al. (2009). Understanding behavioral and physiological phenotypes of stress and anxiety in zebrafish. *Behav. Brain Res.* 205, 38–44. doi: 10.1016/j.bbr.2009.06.022

Fernandes, A. M., Fero, K., Arrenberg, A. B., Bergeron, S. A., Driever, W., and Burgess, H. A. (2012). Deep brain photoreceptors control light-seeking behavior in zebrafish larvae. *Curr. Biol.* 22, 2042–2047. doi: 10.1016/j.cub.2012.08.016

Fernandes, A. M., Fero, K., Driever, W., and Burgess, H. A. (2013). Enlightening the brain: linking deep brain photoreception with behavior and physiology. *Bioessays* 35, 775–779. doi: 10.1002/bies.201300034

Fontana, B. D., Franscescon, F., Rosemberg, D. B., Norton, W. H. J., Kalueff, A. V., and Parker, M. O. (2019). Zebrafish models for attention deficit hyperactivity disorder (ADHD). *Neurosci. Biobehav. Rev.* 100, 9–18. doi: 10.1016/j.neubiorev.2019.02.009

Gerlai, R. (2003). Zebra fish: an uncharted behavior genetic model. *Behav. Genet.* 33, 461–468. doi: 10.1023/A:1025762314250

Gerlai, R. (2013). Antipredatory behavior of zebrafish: adaptive function and a tool for translational research. *Evol. Psychol.* 11, 591–605. doi: 10.1177/147470491301100308

Gerlai, R., Lahav, M., Guo, S., and Rosenthal, A. (2000). Drinks like a fish: zebra fish (*Danio rerio*) as a behavior genetic model to study alcohol effects. *Pharmacol. Biochem. Behav.* 67:147470491301100. doi: 10.1016/s0091-3057(00)00422-6

Grossman, L., Utterback, E., Stewart, A., Gaikwad, S., Chung, K. M., Suciu, C., et al. (2010). Characterization of behavioral and endocrine effects of LSD on zebrafish. *Behav. Brain Res.* 214, 277–284. doi: 10.1016/j.bbr.2010.05.039

Hall, C. S. (1934). Drive and emotionality: factors associated with adjustment in the rat. *J. Comp. Psychol.* 17, 89–108. doi: 10.1037/h0073676

Halsey, L. G., Curran-Everett, D., Vowler, S. L., and Drummond, G. B. (2015). The fickle *P* value generates irreproducible results. *Nat. Methods* 12, 179–185. doi: 10.1038/nmeth.3288

Ho, J., Tumkaya, T., Aryal, S., Choi, H., and Claridge-Chang, A. (2019). Moving beyond *P* values: data analysis with estimation graphics. *Nat. Methods* 16, 565–566. doi: 10.1038/s41592-019-0470-3

Kalueff, A. V. (2017). *The Rights and Wrongs of Zebrafish: Behavioral Phenotyping of Zebrafish.* Springer. Available online at: https://market.android.com/details?id=book-4WUSDgAAQBAJ.

Khor, B.-S., Jamil, M. F. A., Adenan, M. I., and Shu-Chien, A. C. (2011). Mitragynine attenuates withdrawal syndrome in morphine-withdrawn zebrafish. *PLoS One* 6:e28340. doi: 10.1371/journal.pone.0028340

Kim, L., He, L., Maaswinkel, H., Zhu, L., Sirotkin, H., and Weng, W. (2014). Anxiety, hyperactivity and stereotypy in a zebrafish model of fragile X syndrome and autism spectrum disorder. *Prog. Neuropsychopharmacol. Biol. Psychiatry* 55, 40–49. doi: 10.1016/j.pnpbp.2014.03.007

Kulkarni, P., Chaudhari, G. H., Sripuram, V., Banote, R. K., Kirla, K. T., Sultana, R., et al. (2014). Oral dosing in adult zebrafish: proof-of-concept using pharmacokinetics and pharmacological evaluation of carbamazepine. *Pharmacol. Rep.* 66, 179–183. doi: 10.1016/j.pharep.2013.06.012

Kysil, E. V., Meshalkina, D. A., Frick, E. E., Echevarria, D. J., Rosemberg, D. B., Maximino, C., et al. (2017). Comparative analyses of zebrafish anxiety-like behavior using conflict-based novelty tests. *Zebrafish* 14, 197–208. doi: 10.1089/zeb.2016.1415

Lau, B. Y. B., Mathur, P., Gould, G. G., and Guo, S. (2011). Identification of a brain center whose activity discriminates a choice behavior in zebrafish. *Proc. Natl. Acad. Sci. U S A* 108, 2581–2586. doi: 10.1073/pnas.1018275108

Levin, E. D., Bencan, Z., and Cerutti, D. T. (2007). Anxiolytic effects of nicotine in zebrafish. *Physiol. Behav.* 90, 54–58. doi: 10.1016/j.physbeh.2006.08.026

Lim, C. H., and Mathuru, A. S. (2017). Modeling Alzheimer's and other age related human diseases in embryonic systems. *J. Dev. Biol.* 6:1. doi: 10.3390/jdb6010001

Lucon-Xiccato, T., and Dadda, M. (2016). Guppies show behavioural but not cognitive sex differences in a novel object recognition test. *PLoS One* 11:e0156589. doi: 10.1371/journal.pone.0156589

Mathuru, A. S., Kibat, C., Cheong, W. F., Shui, G., Wenk, M. R., Friedrich, R. W., et al. (2012). Chondroitin fragments are odorants that trigger fear behavior in fish. *Curr. Biol.* 22, 538–544. doi: 10.1016/j.cub.2012.01.061

Mathuru, A. S., Schirmer, A., Tabitha, N. P. Y., Kibat, C., Cheng, R.-K., and Jesuthasan, S. (2017). Familiarity with companions aids recovery from fear in zebrafish. *BioRxiv* [Preprint]. doi: 10.1101/098509

Maximino, C., Araujo, J., Leão, L. K. R., Grisolia, A. B. A., Oliveira, K. R. M., Lima, M. G., et al. (2011). Possible role of serotoninergic system in the neurobehavioral impairment induced by acute methylmercury exposure in zebrafish (*Danio rerio*). *Neurotoxicol. Teratol.* 33, 727–734. doi: 10.1016/j.ntt.2011.08.006

Maximino, C., Marques de Brito, T., de Dias, C. A. G. M., Gouveia, A. Jr., and Morato, S. (2010). Scototaxis as anxiety-like behavior in fish. *Nat. Protoc.* 5, 209–216. doi: 10.1038/nprot.2009.225

Maximino, C., Puty, B., Benzecry, R., Araújo, J., Lima, M. G., de Jesus Oliveira Batista, E., et al. (2013a). Role of serotonin in zebrafish (*Danio rerio*) anxiety: relationship with serotonin levels and effect of buspirone, WAY 100635, SB 224289, fluoxetine and para-chlorophenylalanine (pCPA) in two behavioral models. *Neuropharmacology* 71, 83–97. doi: 10.1016/j.neuropharm.2013.03.006

Maximino, C., Puty, B., Matos Oliveira, K. R., and Herculano, A. M. (2013b). Behavioral and neurochemical changes in the zebrafish leopard strain. *Genes Brain Behav.* 12, 576–582. doi: 10.1111/gbb.12047

Meshalkina, D. A., N Kizlyk, M., V Kysil, E., Collier, A. D., Echevarria, D. J., Abreu, M. S., et al. (2018). Zebrafish models of autism spectrum disorder. *Exp. Neurol.* 299, 207–216. doi: 10.1016/j.expneurol.2017.02.004

Mezzomo, N. J., Silveira, A., Giuliani, G. S., Quadros, V. A., and Rosemberg, D. B. (2016). The role of taurine on anxiety-like behaviors in zebrafish: a comparative study using the novel tank and the light-dark tasks. *Neurosci. Lett.* 613, 19–24. doi: 10.1016/j.neulet.2015.12.037

Moriarty, D. D. (1995). Anxiogenic effects of a β-carboline on tonic immobility and open field behavior in chickens (*Gallus gallus*). *Pharmacol. Biochem. Behav.* 51, 795–798. doi: 10.1016/0091-3057(95)00036-v

Norton, W. H. J. (2013). Toward developmental models of psychiatric disorders in zebrafish. *Front. Neural Circuits* 7:79. doi: 10.3389/fncir.2013.00079

Parker, M. O., Brock, A. J., Millington, M. E., and Brennan, C. H. (2013). Behavioural phenotyping of casper mutant and 1-pheny-2-thiourea treated adult zebrafish. *Zebrafish* 10, 466–471. doi: 10.1089/zeb.2013.0878

Parker, M. O., Leonette, V., Annan, L. V., Kanellopoulos, A. H., Brock, A. J., Combe, F. J., et al. (2014). The utility of zebrafish to study the mechanisms by which ethanol affects social behavior and anxiety during early brain development. *Prog. Neuropsychopharmacol. Biol. Psychiatry* 55, 94–100. doi: 10.1016/j.pnpbp.2014.03.011

Parra, K. V., Adrian, J. C. Jr., and Gerlai, R. (2009). The synthetic substance hypoxanthine 3-N-oxide elicits alarm reactions in zebrafish (*Danio rerio*). *Behav. Brain Res.* 205, 336–341. doi: 10.1016/j.bbr.2009.06.037

Pittman, J. T., and Ichikawa, K. M. (2013). iPhone® applications as versatile video tracking tools to analyze behavior in zebrafish (*Danio rerio*). *Pharmacol. Biochem. Behav.* 106, 137–142. doi: 10.1016/j.pbb.2013.03.013

Porseryd, T., Volkova, K., Reyhanian Caspillo, N. R., Källman, T., Dinnetz, P., and Hällström, I. P. (2017). Persistent effects of developmental exposure to 17α-ethinylestradiol on the zebrafish (*Danio rerio*) brain transcriptome and behavior. *Front. Behav. Neurosci.* 11:69. doi: 10.3389/fnbeh.2017.00069

Prut, L., and Belzung, C. (2003). The open field as a paradigm to measure the effects of drugs on anxiety-like behaviors: a review. *Eur. J. Pharmacol.* 463, 3–33. doi: 10.1016/s0014-2999(03)01272-x

Sackerman, J., Donegan, J. J., Cunningham, C. S., Nguyen, N. N., Lawless, K., Long, A., et al. (2010). Zebrafish behavior in novel environments: effects of acute exposure to anxiolytic compounds and choice of *Danio rerio* line. *Int. J. Comp. Psychol.* 23, 43–61.

Santoriello, C., and Zon, L. I. (2012). Hooked! modeling human disease in zebrafish. *J. Clin. Invest.* 122, 2337–2343. doi: 10.1172/JCI60434

Schirmer, A., Jesuthasan, S., and Mathuru, A. S. (2013). Tactile stimulation reduces fear in fish. *Front. Behav. Neurosci.* 7:167. doi: 10.3389/fnbeh.2013.00167

Simon, P., Dupuis, R., and Costentin, J. (1994). Thigmotaxis as an index of anxiety in mice. Influence of dopaminergic transmissions. *Behav. Brain Res.* 61, 59–64. doi: 10.1016/0166-4328(94)90008-6

Speedie, N., and Gerlai, R. (2008). Alarm substance induced behavioral responses in zebrafish (*Danio rerio*). *Behav. Brain Res.* 188, 168–177. doi: 10.1016/j.bbr.2007.10.031

Spence, R., Fatema, M. K., Reichard, M., Huq, K. A., Wahab, M. A., Ahmed, Z. F., et al. (2006). The distribution and habitat preferences of the zebrafish in Bangladesh. *J. Fish Biol.* 69, 1435–1448. doi: 10.1111/j.1095-8649.2006.01206.x

Spence, R., Gerlach, G., Lawrence, C., and Smith, C. (2007). The behaviour and ecology of the zebrafish, *Danio rerio*. *Biol. Rev. Camb. Philos. Soc.* 83, 13–34. doi: 10.1111/j.1469-185x.2007.00030.x

Stewart, A., Gaikwad, S., Kyzar, E., Green, J., Roth, A., and Kalueff, A. V. (2012). Modeling anxiety using adult zebrafish: a conceptual review. *Neuropharmacology* 62, 135–143. doi: 10.1016/j.neuropharm.2011.07.037

Stewart, A. M., Grieco, F., Tegelenbosch, R. A. J., Kyzar, E. J., Nguyen, M., Kaluyeva, A., et al. (2015). A novel 3D method of locomotor analysis in adult zebrafish: implications for automated detection of CNS drug-evoked phenotypes. *J. Neurosci. Methods* 255, 66–74. doi: 10.1016/j.jneumeth.2015.07.023

Stewart, A., Maximino, C., Marques de Brito, T., Herculano, A. M., Gouveia, A., Morato, S., et al. (2011). Neurophenotyping of adult zebrafish using the light/dark box paradigm. *Zebrafish Neurobehav. Protoc.* 51, 157–167. doi: 10.1007/978-1-60761-953-6_13

Tay, T. L., Ronneberger, O., Ryu, S., Nitschke, R., and Driever, W. (2011). Comprehensive catecholaminergic projectome analysis reveals single-neuron integration of zebrafish ascending and descending dopaminergic systems. *Nat. Commun.* 2:171. doi: 10.1038/ncomms1171

Tran, S., and Gerlai, R. (2013). Individual differences in activity levels in zebrafish (*Danio rerio*). *Behav. Brain Res.* 257, 224–229. doi: 10.1016/j.bbr.2013.09.040

Vignet, C., Bégout, M.-L., Péan, S., Lyphout, L., Leguay, D., and Cousin, X. (2013). Systematic screening of behavioral responses in two zebrafish strains. *Zebrafish* 10, 365–375. doi: 10.1089/zeb.2013.0871

Wisenden, B. D. (2010). "Quantifying anti-predator responses to chemical alarm cues," in *Zebrafish Neurobehavioral Protocols* (Vol. 51), eds A. Kalueff, and J. Cachat (Switzerland: Springer Nature), 49–60.

Wong, K., Elegante, M., Bartels, B., Elkhayat, S., Tien, D., Roy, S., et al. (2010). Analyzing habituation responses to novelty in zebrafish (*Danio rerio*). *Behav. Brain Res.* 208, 450–457. doi: 10.1016/j.bbr.2009.12.023

Conflict of Interest Statement: The authors declare that the research was conducted in the absence of any commercial or financial relationships that could be construed as a potential conflict of interest.

frontiers in Behavioral Neuroscience

ORIGINAL RESEARCH
published: 29 October 2019
doi: 10.3389/fnbeh.2019.00249

Acute Chemogenetic Activation of CamKIIα-Positive Forebrain Excitatory Neurons Regulates Anxiety-Like Behaviour in Mice

*Sonali S. Salvi†, Sthitapranjya Pati†, Pratik R. Chaudhari, Praachi Tiwari, Toshali Banerjee and Vidita A. Vaidya**

Department of Biological Sciences, Tata Institute of Fundamental Research, Mumbai, India

Anxiety disorders are amongst the most prevalent mental health disorders. Several lines of evidence have implicated cortical regions such as the medial prefrontal cortex, orbitofrontal cortex, and insular cortex along with the hippocampus in the top–down modulation of anxiety-like behaviour in animal models. Both rodent models of anxiety, as well as treatment with anxiolytic drugs, result in the concomitant activation of multiple forebrain regions. Here, we sought to examine the effects of chemogenetic activation or inhibition of forebrain principal neurons on anxiety and despair-like behaviour. We acutely activated or inhibited Ca^{2+}/calmodulin-dependent protein kinase II α (CamKIIα)-positive forebrain excitatory neurons using the hM3Dq or the hM4Di Designer Receptor Exclusively Activated by Designer Drug (DREADD) respectively. Circuit activation was confirmed via an increase in expression of the immediate early gene, c-Fos, within both the hippocampus and the neocortex. We then examined the influence of DREADD-mediated activation of forebrain excitatory neurons on behavioural tests for anxiety and despair-like behaviour. Our results indicate that acute hM3Dq DREADD activation of forebrain excitatory neurons resulted in a significant decline in anxiety-like behaviour on the open field, light–dark avoidance, and the elevated plus maze test. In contrast, hM3Dq DREADD activation of forebrain excitatory neurons did not alter despair-like behaviour on either the tail suspension or forced swim tests. Acute hM4Di DREADD inhibition of CamKIIα-positive forebrain excitatory neurons did not modify either anxiety or despair-like behaviour. Taken together, our results demonstrate that chemogenetic activation of excitatory neurons in the forebrain decreases anxiety-like behaviour in mice.

Keywords: DREADD, hM3Dq, hM4Di, clozapine-*N*-oxide, anxiety, open field test, light–dark avoidance test, elevated plus maze

OPEN ACCESS

Edited by:
Gregg Stanwood, Florida State University, United States

Reviewed by:
Annelyn Torres-Reveron, University of Texas Rio Grande Valley Edinburg, United States
Devon L. Graham, Florida State University, United States

***Correspondence:**
Vidita A. Vaidya
vvaidya@tifr.res.in

†These authors have contributed equally to this work as first authors

Specialty section:
This article was submitted to Emotion Regulation and Processing, a section of the journal Frontiers in Behavioral Neuroscience

Received: *20 August 2019*
Accepted: *14 October 2019*
Published: *29 October 2019*

Citation:
Salvi SS, Pati S, Chaudhari PR, Tiwari P, Banerjee T and Vaidya VA (2019) Acute Chemogenetic Activation of CamKIIα-Positive Forebrain Excitatory Neurons Regulates Anxiety-Like Behaviour in Mice. Front. Behav. Neurosci. 13:249. doi: 10.3389/fnbeh.2019.00249

INTRODUCTION

Multiple cortical circuits including the medial prefrontal cortex (mPFC) (Davidson, 2002; Tovote et al., 2015), orbitofrontal cortex (Milad and Rauch, 2007), anterior insula (Paulus and Stein, 2006), primary motor cortex (Li et al., 2018), somatosensory cortices (Rauch, 1995), and the hippocampal subfields (Shin and Liberzon, 2010; Calhoon and Tye, 2015) are implicated in the modulation of anxiety-like behaviour. These circuits contribute to adaptive emotional control, via the top down-regulation of several components of limbic neurocircuitry that modulate anxiety-like behaviour,

such as the amygdala (Adhikari, 2014; Makovac et al., 2016), septum (Parfitt et al., 2017), bed nucleus of the stria terminalis (BNST) (Adhikari, 2014), and hypothalamus (Jimenez et al., 2018). While several previous studies using rodent models have dissected the contribution of individual cortical and subcortical circuits in the modulation of specific anxiety-like behavioural responses, it is likely that diverse brain regions, including multiple cortical circuits, would be concomitantly recruited in an ethological context. This is supported by studies in diverse rodent models associated with increased anxiety-like behaviour, such as immobilisation stress (Ons et al., 2004), air puff (Duncan et al., 1996), swim stress (Molteni et al., 2008), exposure to novel environments such as an open field (Santini et al., 2011), elevated plus maze (EPM) (Muigg et al., 2009), and exposure to cat odour (Úbeda-Contreras et al., 2018), as well as in response to pharmacological agents that modulate anxiety-like behaviour (Hoehn-Saric et al., 2004; Linden et al., 2004; Wise et al., 2007). Such altered neuronal activation patterns across multiple forebrain regions have been observed in these studies as inferred using immunoreactivity for the immediate early genes, c-Fos, egr2, and Arc. This is also supported by clinical observations in humans with high anxiety using both functional magnetic resonance imaging and positron emission tomography indicating the involvement of broad cortical regions, including the frontal cortex (Wang et al., 2016), cingulate cortex (Eser et al., 2009), orbitofrontal cortex (Breiter, 1996), insula (Paulus and Stein, 2006), and hippocampus (Cha et al., 2016).

Anxiolytics, which are pharmacological agents routinely used to treat patients with anxiety disorder, include anxiolytics that target the ion channels, as well as those that act via G-protein coupled receptors (GPCRs) (Griebel and Holmes, 2013). Systemic administration of these compounds also modulates activity in broad telencephalic regions such as the frontal cortex (Wise et al., 2007; Bechtholt et al., 2008), prefrontal cortex (Maslowsky et al., 2010), cingulate cortex (Beck and Fibiger, 1995), and the hippocampus (Beck and Fibiger, 1995; de Medeiros et al., 2005). Spatiotemporal modulation of specific neurocircuits using optogenetics (Tye and Deisseroth, 2012; Nieh et al., 2013) and chemogenetics (Burnett and Krashes, 2016; Whissell et al., 2016) has substantially advanced the understanding of the neurocircuitry that regulates mood-related behaviours. These studies capitalise on topographically restricted neuronal manipulation, and have been instrumental in characterising local microcircuits and neuronal pathways, along with contributions made by specific neuronal cell-types, to explain the regulation of different facets of mood-related behaviours across diverse behavioural paradigms (Tye and Deisseroth, 2012; Burnett and Krashes, 2016). Although these studies have contributed to providing a working understanding of the neurocircuitry of emotional behaviours, the effects of neuronal activity perturbations that recruit broader circuits concomitantly such as within the forebrain, are still not well-understood.

In this study, we sought to investigate the effects of altered activity within the broad forebrain circuits including the neocortex and hippocampus on anxiety and despair-like behaviour using chemogenetics. Excitatory neurons constitute a majority of the neuronal subpopulations within the forebrain (Megìas et al., 2001; Douglas and Martin, 2004). We used transgenic mouse lines expressing engineered human muscarinic receptors, i.e., the excitatory hM3Dq or the inhibitory hM4Di Designer Receptors Exclusively Activated by Designer Drugs (DREADDs) (Armbruster et al., 2007; Nawaratne et al., 2008), in Ca^{2+}/calmodulin-dependent protein kinase II α (CamKIIα)-positive excitatory neurons of the forebrain, to examine effects of forebrain principal neuron activation and inhibition on mood-related behaviours. Our results indicate that acute DREADD ligand [clozapine-*N*-oxide (CNO)] mediated hM3Dq activation of CamKIIα-positive forebrain excitatory neurons evokes anxiolysis in the open field test, light–dark avoidance test and EPM test, but does not influence despair-like behaviour. Acute CNO-mediated hM4Di DREADD inhibition of CamKIIα-positive forebrain excitatory neurons did not influence either anxiety or despair-like behaviour. These findings indicate that acute chemogenetic activation of forebrain excitatory neurons exerts anxiolytic effects across diverse anxiety-related behavioural tasks.

MATERIALS AND METHODS

Animals

Bigenic CamKIIα-tTA:TetO-hM3Dq, CamKIIα-tTA:TetO-hM4Di, and C57BL/6J mice were bred in the Tata Institute of Fundamental Research (TIFR) animal facility and were maintained on a 12-h light–dark cycle (lights on from 7:00 AM) with *ad libitum* access to food and water. CamKIIα-tTA transgenic mice were a kind gift from Dr. Christopher Pittenger, Yale School of Medicine. TetO-hM3Dq [Cat. No. 014093; Tg(tetO-CHRM3*)1Blr/J], TetO-hM4Di [Cat No. 024114; Tg(tetO-CHRM4*)2Blr/J] mouse lines, and C57BL/6J mice were purchased from Jackson Laboratories, United States. All bigenic mouse lines were maintained on a doxycycline–free diet from development onwards to facilitate transgene expression. Genotypes were determined using PCR based analysis. All experimental procedures were carried out following the guidelines of the Committee for the Purpose of Control and Supervision of Experiments on Animals (CPCSEA), Government of India and were approved by the TIFR institutional animal ethics committee.

Experimental Paradigm

Age-matched (3–5 months), adult male bigenic CamKIIα-tTA:TetO-hM3Dq (n = 9–10/group), CamKIIα-tTA:TetO-hM4Di (n = 9–10/group) mice, and C57BL/6J (n = 10–12/group) mice were intraperitoneally injected with either 0.5 mg/kg CNO (Cat no. 4936; Tocris, United Kingdom) or vehicle (0.9% NaCl). Behavioural analysis on the open field test (OFT), elevated plus maze test (EPM), light–dark (LD) avoidance test, tail suspension test (TST), and forced swim test (FST) were performed 30 min following CNO/vehicle injection. An interim washout period (7–10 days) was provided between all behavioural tests, with the tests for anxiety-like behaviours preceding the despair-like behaviour tests. A separate cohort of adult CamKIIα-tTA:TetO-hM3Dq (n = 4/group) and CamKIIα-tTA:TetO-hM4Di (n = 4/group)

male mice were sacrificed 2 h following 0.5 mg/kg CNO or vehicle administration for western blotting experiments. An additional cohort of CamKIIα-tTA:TetO-hM3Dq (n = 9–10/group) adult male mice (5 months) were injected with either 0.5 mg/kg CNO or vehicle, and sacrificed 2 h later by transcardial perfusion with 4% paraformaldehyde for immunohistochemical analysis.

Behavioural Assays

To assess anxiety-like behaviour, vehicle and CNO-treated CamKIIα-tTA:TetO-hM3Dq, vehicle and CNO-treated CamKIIα-tTA:TetO-hM4Di, and vehicle and CNO-treated C57BL/6J male mice were subjected to OFT, EPM test, and LD avoidance tests. Despair-like behaviour was assessed using the TST, followed by FST. Care was taken to clean and dry the behavioural arenas with ethanol between individual trials during each behavioural test. Behavioural tests on the same cohort of mice were set apart by an interim washout period of 7–10 days. Behavioural analysis on the OFT and EPM tests were performed using Ethovision XT 11 (Noldus, Netherlands). Behavioural analysis on the LD avoidance test, TST, and FST were carried out manually from video recordings, by an experimenter blind to the treatment groups.

Open Field Test

Mice were introduced at random into a corner of the OFT box (40 cm × 40 cm × 40 cm) and allowed to explore the arena for a duration of 5 min. Behaviour was recorded using an infrared overhead camera (Harvard Apparatus, United States) followed by analysing anxiety-like behaviour, using the measures of total distance travelled, percent distance travelled in centre and percent time spent in the centre of the arena (20 cm × 20 cm), as well as number of entries made to the centre of the arena.

Elevated Plus Maze Test

The EPM test consisted of an elevated platform raised 50 cm above the ground with opposing open and closed arms. Mice were introduced into the centre of the EPM, facing the open arms and allowed to explore for a total duration of 10 min. Ethovision analysis for anxiety-like behaviour was based on assessing measures of total distance travelled, percent distance travelled in the open arms, percent time spent in the open arms, and number of entries to the open arms of the EPM.

LD Avoidance Test

Mice were introduced into a box with a light and a dark chamber connected through an entrance and allowed to explore the arena for 10 min. Video recordings were then manually analysed for percent time spent, and number of entries into the light chamber to assess anxiety-like behaviour.

Tail Suspension Test

Tail suspension test was performed by suspending the mice by their tails 50 cm from the ground and behaviour was recorded for a duration of 6 min. Despair-like behaviour was assessed based on percent time spent immobile by the mice during the last 5 min of the TST.

Forced Swim Test

Forced swim test was performed by introducing mice into a cylindrical Plexiglas chamber filled with water (22°C) and behaviour was recorded for 6 min. Percent time spent immobile by the mice during the last 5 min of the behaviour was used as a measure to assess despair-like behaviour.

Immunohistochemistry

Vehicle or CNO-treated CamKIIα-tTA:TetO-hM3Dq adult male mice, naive for behavioural testing, were sacrificed by transcardial perfusion with 4% paraformaldehyde 2 h post-drug treatments, for c-Fos immunohistochemistry (IHC). Free-floating (40 μM) coronal sections cut on the vibratome (Leica, Germany) were incubated with the blocking solution (10% horse serum, 0.3% TritonX-100 in 0.1M Phosphate buffer) at room temperature for 2 h. Sections were then incubated with rabbit anti-c-Fos antibody (1:1000, Cat no. 2250, Cell Signalling Technology, United States) for 2 days at 4°C, followed by sequential washes, and incubation with the secondary antibody (biotinylated goat anti-rabbit, 1:500, Cat no. BA9400, Vector Labs, United States) for 2 h at room temperature. Signal amplification was performed using an Avidin-biotin complex based system (Vector lab, Vectastain ABC kit Elite PK1600, United States) and visualised using the substrate, Diaminobenzidine tetrahydrochloride (Cat no. D5905, Sigma-Aldrich, United States).

Cell Counting Analysis

Quantitative analysis of c-Fos immunopositive cells was performed in specific hippocampal subfields namely the CA1, CA3, and dentate gyrus (DG) using a brightfield microscope (Zeiss Axioskop 2 plus, Germany) at a magnification of 200X. Six sections of each region, spanning the rostrocaudal extent of the hippocampus at a periodicity of 200 μm, were selected per animal. Cell counting analysis was carried out by an experimenter blind to the treatment groups. Contours were drawn for each hippocampal subfield using Neurolucida explorer (MBF Biosciences, United States) and an average area in mm^2 for the CA1, CA3, and DG hippocampal subfields was calculated for both vehicle-treated controls and CNO treated animals. Results are expressed as the number of c-Fos-positive cells per mm^2 for each hippocampal subfield analysed.

Western Blotting

Western blotting analysis was performed on tissue samples that were snap-frozen in liquid nitrogen. Tissue homogenisation was carried out in Radioimmunoprecipitation assay (RIPA) buffer (10 mM Tris-Cl (pH 8.0), 1 mM EDTA, 0.5 mM EGTA, 1% Triton X-100, 0.1% sodium deoxycholate, 0.1% SDS, 140 mM NaCl) using a Dounce homogeniser. Protease and phosphatase inhibitors (Sigma-Aldrich, United States) were added to the buffer prior to lysis. Estimation of the protein concentration was performed using a Quantipro BCA assay kit (Sigma-Alrich,

United States). Protein lysates (50 μg) were resolved using a 10% sodium dodecyl sulphate polyacrylamide gel electrophoresis (SDS PAGE) system and transferred onto polyvinylidene fluoride membranes. Blots were then incubated with blocking solution (5% milk in TBST) and exposed to either rabbit anti-HA (1:1500, Cat no. H6908, Sigma-Aldrich, United States), rabbit anti-c-Fos (1:1000, Cat no. 2250, Cell Signalling Technology, United States), or rabbit anti-actin (1: 10,000, Cat no. AC026, Abclonal Technology, United States) primary antibodies made in 5% milk. Subsequent to sequential washes, blots were incubated with HRP conjugated goat anti-rabbit (1:6000, Cat no. AS014, Abclonal Technology, United States) secondary antibody and the signal was visualised with the GE Amersham Imager 600 (GE life sciences, United States) using a western blotting detection kit (WesternBright ECL, Advansta, United States). Densitometric analysis of the blots was performed using ImageJ software.

Statistical Analysis

Statistical analyses was performed using the two-tailed unpaired Student's *t*-test (Instat, GraphPad Software, Inc., United States) with significance determined at a p-value < 0.05. Results were subjected to the Kolmogorov–Smirnov test to determine normality prior to statistical analysis. Results are expressed as mean ± standard error of mean (SEM).

RESULTS

hM3Dq and hM4Di DREADD-Mediated Activation and Inhibition of CamKIIα-Positive Forebrain Excitatory Neurons

Bigenic CamKIIα-tTA:TetO-hM3Dq and CamKIIα-tTA:TetO-hM4Di mice were generated for the chemogenetic manipulation of CamKIIα-positive forebrain excitatory neurons (**Figure 1A**). Expression of the HA-tagged excitatory (hM3Dq) and inhibitory (hM4Di) DREADDs in the forebrain was confirmed using western blotting for the HA antigen in the cortex and hippocampus (**Figure 1B**). The excitatory and inhibitory DREADD expression was not observed within hindbrain regions such as the cerebellum (data not shown).

We investigated the hM3Dq DREADD-mediated activation of the cortex and hippocampus, 2 h following acute CNO (0.5 mg/kg) administration using western blotting and immunohistochemistry for the neuronal activity marker, c-Fos (**Figure 1C**). Western blotting analysis clearly indicated a significant increase in expression of c-Fos protein following acute CNO treatment in the hippocampi ($p = 0.004$) derived from bigenic CamKIIα-tTA:TetO-hM3Dq, as compared to their vehicle-treated controls (**Figure 1D**), and a trend ($p = 0.07$) toward a significant induction of c-Fos protein levels in the cortex (**Figure 1D**). Additionally, immunohistochemical analysis indicated a significant increase in c-Fos positive cell numbers within the dentate gyrus (DG), CA1, and CA3 hippocampal subfields of CNO treated CamKIIα-tTA:TetO-hM3Dq mice (**Figure 1E**, $p = 0.015$ DG, $p = 0.009$ CA1, $p = 0.03$ CA3). We next examined the influence of hM4Di DREADD-mediated inhibition of the cortex and hippocampus 2 h following acute CNO (0.5 mg/kg) administration using western blotting for the neuronal activity marker, c-Fos (**Figure 1F**). Western blotting analysis revealed a significant decline in the c-Fos protein in the hippocampus ($p = 0.01$) and no significant change noted for c-Fos protein levels in the cortex, following acute CNO-mediated hM4Di DREADD stimulation (**Figure 1G**).

Acute CNO-Mediated DREADD Activation of CamKIIα-Positive Forebrain Excitatory Neurons Reduces Anxiety-Like Behaviour on the OFT

We then examined the influence of acute CNO (0.5 mg/kg)-mediated hM3Dq DREADD activation of CamKIIα-positive forebrain excitatory neurons on a battery of anxiety and despair-like behavioural tasks. Behavioural testing on the OFT was performed 30 min following acute CNO administration (**Figure 2A**). Acute hM3Dq DREADD-mediated activation of forebrain excitatory neurons evoked a significant decline in anxiety-like behaviour on the OFT (**Figures 2B–F**). This was indicated by an increase in the total distance travelled (**Figure 2C**, $p = 0.006$), percent distance travelled within the centre (**Figure 2D**, $p = 0.006$) and percent time spent within the centre (**Figure 2E**, $p = 0.0003$) of the OFT arena by CNO-treated CamKIIα-tTA:TetO-hM3Dq mice as compared to their vehicle-treated controls. The number of entries made to the centre of the OFT arena (**Figure 2F**) did not differ across the groups. These results indicate an anxiolytic response in the OFT following acute CNO-mediated hM3Dq DREADD activation of the forebrain excitatory neurons.

Acute CNO-Mediated DREADD Activation of CamKIIα-Positive Forebrain Excitatory Neurons Reduces Anxiety-Like Behaviour on the Light–Dark Avoidance and Elevated Plus Maze Test

We then assessed the effect on anxiety-like behaviour following hM3Dq DREADD-mediated activation of CamKIIα-positive forebrain excitatory neurons using the LD avoidance and EPM test, with an interim washout period of 7–10 days between behavioural tasks (**Figure 3A**). Behavioural analysis on the LD avoidance test revealed a decline in anxiety-like behaviour (**Figures 3B,C**), as noted with a significant increase in both the percent time spent in the light chamber (**Figure 3B**, $p = 0.05$) and number of entries to the light chamber (**Figure 3C**, $p = 0.04$) by the CNO-treated cohort. We next assessed the influence of hM3Dq DREADD activation of forebrain excitatory neurons on anxiety-like behaviour on the EPM test (**Figures 3D–H**). We noted a significant increase in the number of entries made into the open arms (**Figure 3H**, $p = 0.02$) of the EPM. We did not observe any significant difference on other measures, namely the total distance travelled in the EPM arena (**Figure 3E**), percent

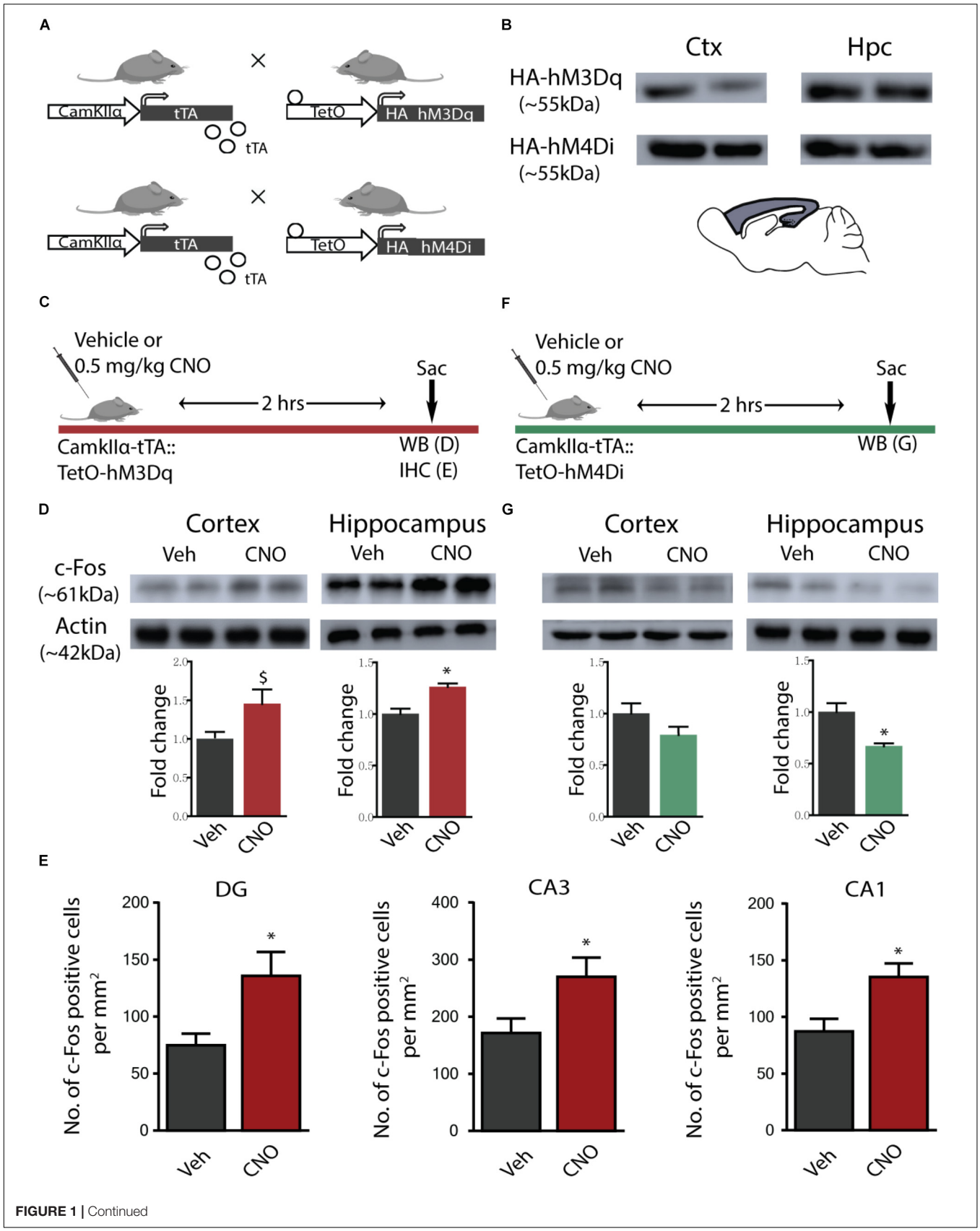

FIGURE 1 | Continued

FIGURE 1 | hM3Dq and hM4Di DREADD-mediated activation and inhibition of CamKIIα-positive forebrain excitatory neurons. **(A)** Shown is a schematic of the genetic strategy used to create bigenic CamKIIα-tTA:TetO-hM3Dq and CamKIIα-tTA:TetO-hM4Di mice to drive expression of the hM3Dq and hM4Di DREADD in forebrain CamKIIα-positive excitatory neurons respectively. **(B)** Shown is protein expression of the HA antigen in the forebrain circuits of the cortex (Ctx) and the hippocampus (Hpc) confirming expression of the HA-tagged hM3Dq (HA-hM3Dq) and hM4Di (HA-hM4Di) DREADD. **(C)** Shown is a schematic of the experimental paradigm used to confirm the activation of the hM3Dq DREADD in the forebrain. **(D)** Western blotting analysis revealed that adult bigenic CamKIIα-tTA:TetO-hM3Dq mice injected with CNO (0.5 mg/kg) showed significant induction in c-Fos protein expression in the hippocampus (n = 4/group), and a trend toward an increase in the cortex. **(E)** Immunohistochemical analysis indicated that acute CNO-mediated hM3Dq DREADD activation resulted in a significant increase in the number of c-Fos positive cells in the hippocampal subfields, namely the Dentate gyrus (DG), CA3, and CA1 (n = 9–10/group). **(F)** Shown is a schematic of the experimental paradigm used to confirm the activation of the hM4Di DREADD in the forebrain. **(G)** Western blotting analysis revealed that adult bigenic CamKIIα-tTA:TetO-hM4Di mice injected with CNO (0.5 mg/kg) showed a significant decline in c-Fos protein expression in the hippocampus (n = 4/group), and no change in c-Fos protein levels in the cortex. Results are expressed as the mean ± SEM, $^{*}p < 0.05$, $^{\$}p = 0.07$, as compared to vehicle-treated control mice using the two-tailed, unpaired Student's t-test.

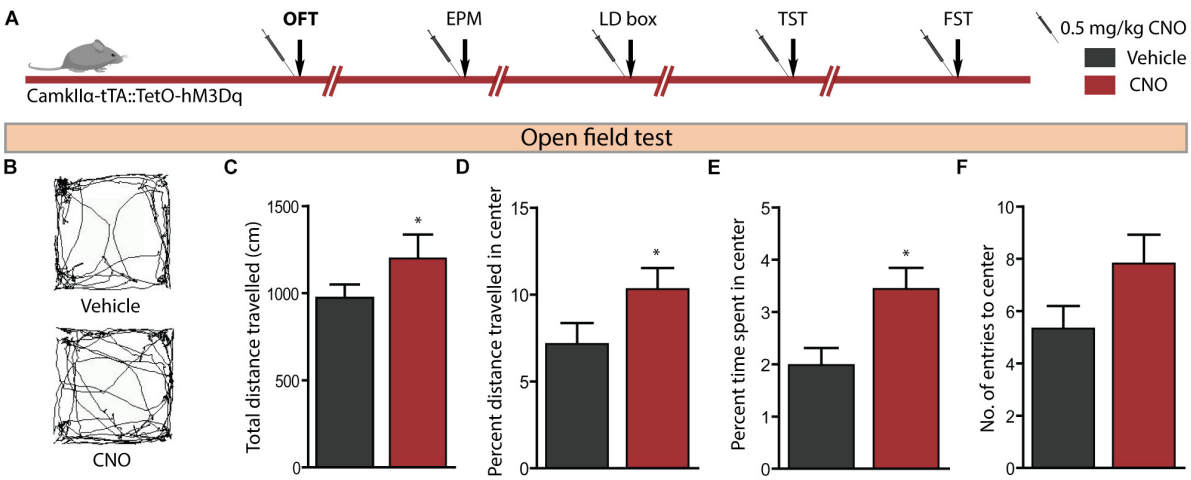

FIGURE 2 | Acute CNO-mediated DREADD activation of CamKIIα-positive forebrain excitatory neurons reduces anxiety-like behaviour on the open field test (OFT). **(A)** Shown is a schematic of the experimental paradigm used to determine the influence of acute CNO (0.5 mg/kg)-mediated hM3Dq activation of CamKIIα-positive forebrain excitatory neurons in adult male bigenic CamKIIα-tTA:TetO-hM3Dq mice on anxiety and despair-like behaviour. Treatment groups were subjected to a battery of anxiety and despair-like behavioural tasks, with an interim washout period of 7–10 days (n = 9–10/group). Shown in this figure is the anxiety-like behaviour on the OFT **(B–F)** following acute hM3Dq DREADD activation of forebrain excitatory neurons, commencing 30 min following CNO administration. **(B)** Shown are representative tracks from a vehicle and CNO treated CamKIIα-tTA:TetO-hM3Dq mouse in the OFT. CNO-mediated hM3Dq DREADD activation of CamKIIα-positive forebrain excitatory neurons resulted in decline in anxiety-like behaviour on the OFT as revealed by significant increases in the total distance travelled **(C)**, percent distance travelled in the centre **(D)**, and percent time spent in the centre **(E)** of the OFT arena as compared to the vehicle-treated group. No significant difference was observed in the number of entries made to the centre of the arena **(F)**. Results are expressed as the mean ± SEM (n = 9–10/group), $^{*}p < 0.05$, as compared to vehicle-treated CamKIIα-tTA:TetO-hM3Dq mice, two-tailed, unpaired Student's t-test. EPM, elevated plus maze test; LD, light–dark avoidance test; TST, tail suspension test; FST, forced swim test.

distance travelled in the open arms (**Figure 3F**), and percent time spent in the open arms (**Figure 3G**) following CNO-mediated hM3Dq DREADD activation. These results indicate that acute CNO-mediated hM3Dq DREADD activation in the forebrain excitatory neurons evokes a prominent anxiolytic response on the LD avoidance test and on specific measures of the EPM test.

Acute CNO-Mediated DREADD Activation of CamKIIα-Positive Forebrain Excitatory Neurons Does Not Influence Despair-Like Behaviour

Given we noted robust anxiolytic responses on multiple behavioural tests for anxiety-like behaviour following acute hM3Dq DREADD-mediated activation of forebrain excitatory neurons, we next assessed for effects on despair-like behaviour using the TST and FST (**Figure 4A**). hM3Dq DREADD-mediated activation of forebrain excitatory neurons did not influence despair-like behaviour on either the TST (**Figure 4B**) or the FST (**Figure 4C**) with no change noted in percent immobility time in both tasks. These results indicate that acute DREADD-mediated activation of the CamKIIα-positive forebrain excitatory neurons influences anxiety but not despair-like behaviour.

Acute hM4Di DREADD-Mediated Inhibition of CamKIIα-Positive Forebrain Excitatory Neurons Does Not Influence Anxiety or Despair-Like Behaviour

We then sought to examine the effects of acute CNO (0.5 mg/kg)-mediated hM4Di DREADD inhibition of CamKIIα-positive forebrain excitatory neurons on anxiety-like behaviour in the OFT, EPM, and LD avoidance test and on despair-like behaviour in the TST and FST paradigms (**Figure 5A**). Acute hM4Di

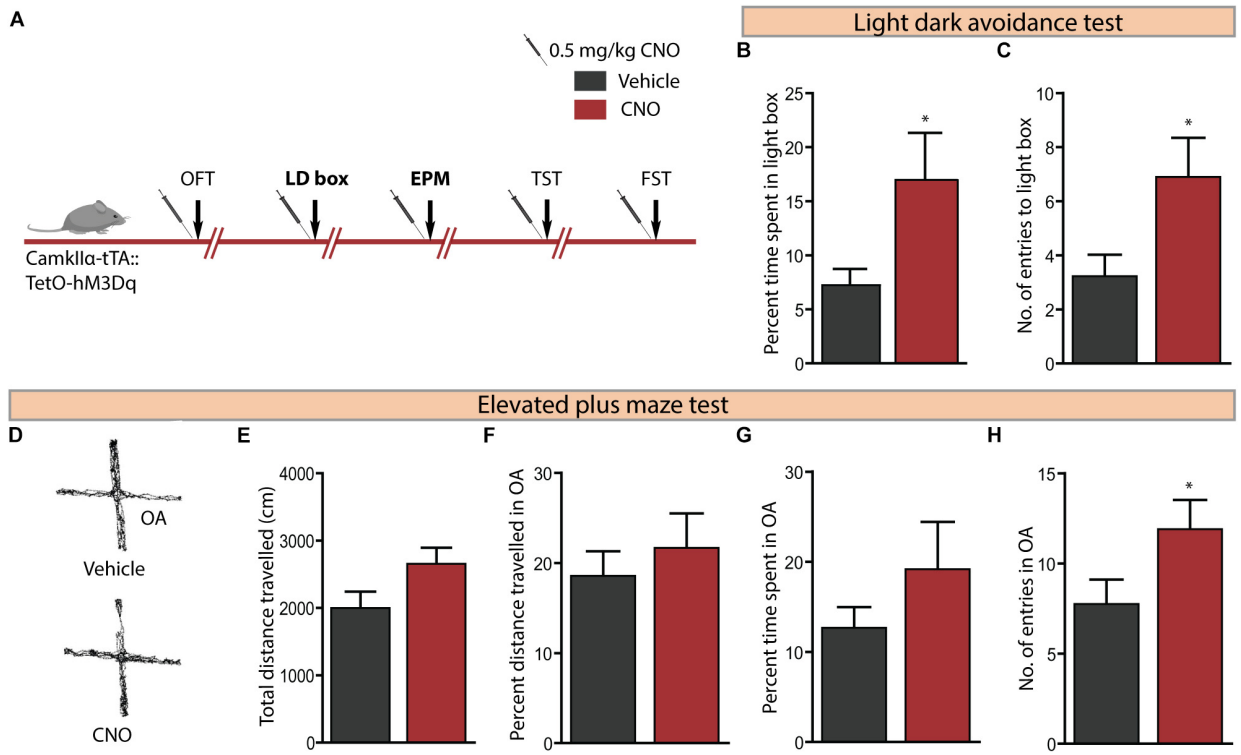

FIGURE 3 | Acute CNO-mediated DREADD activation of CamKIIα-positive forebrain excitatory neurons reduces anxiety-like behaviour on the light dark avoidance and EPM test. **(A)** Shown is a schematic of the experimental paradigm used to determine the influence of acute CNO (0.5 mg/kg)-mediated hM3Dq activation of CamKIIα-positive forebrain excitatory neurons in adult male bigenic CamKIIα-tTA:TetO-hM3Dq mice on anxiety and despair-like behaviour. Treatment groups were subjected to a battery of anxiety and despair-like behavioural tasks, with an interim washout period of 7–10 days (n = 9–10/group). Shown in this figure is the anxiety-like behaviour on the light–dark avoidance test (LD) **(B,C)** and EPM test **(D–H)** following acute hM3Dq DREADD activation of forebrain excitatory neurons, commencing 30 min following CNO administration. CNO-mediated hM3Dq DREADD activation of CamKIIα-positive forebrain excitatory neurons resulted in a decline in anxiety-like behaviour on the LD avoidance test as revealed by significant increases in percent time spent in the light chamber **(B)** and number of entries made to the light chamber **(C)** of the LD avoidance test arena. **(D)** Shown are representative tracks from a vehicle and CNO treated CamKIIα-tTA:TetO-hM3Dq mouse in the EPM test. CNO-mediated hM3Dq DREADD activation of CamKIIα-positive forebrain excitatory neurons resulted in no change in the total distance travelled **(E)**, percent distance travelled in the open arms (OA) **(F)**, and percent time spent in the open arms **(G)** of the EPM compared to the vehicle-treated group. A significant increase in the number of entries to the open arms of the EPM arena **(H)** was noted following hM3Dq DREADD activation of forebrain excitatory neurons. Results are expressed as the mean ± SEM (n = 9–10/group), $^*p < 0.05$, as compared to vehicle-treated CamKIIα-tTA:TetO-hM3Dq mice, two-tailed, unpaired Student's t-test. OFT, open field test; TST, tail suspension test; FST, forced swim test.

DREADD-mediated inhibition of forebrain excitatory neurons revealed no influence on anxiety-like behaviour in the OFT (**Figures 5B–F**). This was indicated by no difference on measures of the total distance travelled in the arena (**Figure 5C**), percent distance travelled in the centre (**Figure 5D**), percent time spent in the centre (**Figure 5E**), and number of entries made to the centre of the OFT arena (**Figure 5F**) between treatment groups. Acute hM4Di DREADD-mediated inhibition of forebrain excitatory neurons did not alter anxiety-like behaviour on the EPM test (**Figures 5G–K**). No significant differences were noted on measures of the total distance travelled (**Figure 5H**), percent distance travelled in the open arms (**Figure 5I**), percent time spent in the open arms (**Figure 5J**), and number of entries made to the open arms (**Figure 5K**) between the CNO and vehicle-treated groups. We also assessed anxiety-like behaviour on the light–dark avoidance test (**Figures 5L–N**), with no difference observed in either percent time spent in the light chamber (**Figure 5M**) or number of entries made to the light chamber (**Figure 5N**) following CNO-mediated hM4Di DREADD inhibition of forebrain excitatory neurons. Further, we examined despair-like behaviour on the TST and FST, and noted that percent immobility time was unchanged in both the TST (**Figure 5O**) and FST (**Figure 5P**) following hM4Di DREADD-mediated inhibition of forebrain excitatory neurons. Taken together, these results indicate that acute hM4Di DREADD-mediated inhibition of the forebrain excitatory neurons does not influence anxiety-like behaviour on the OFT, EPM, and LD avoidance test and despair-like behaviour on the TST and FST.

Acute Administration of CNO in C57BL/6J Mice Does Not Influence Anxiety-Like or Despair-Like Behaviour

Given concerns that CNO metabolism results in the formation of active metabolites, namely clozapine and *N*-desmethylclozapine (Manvich et al., 2018), which are known to bind to endogenous

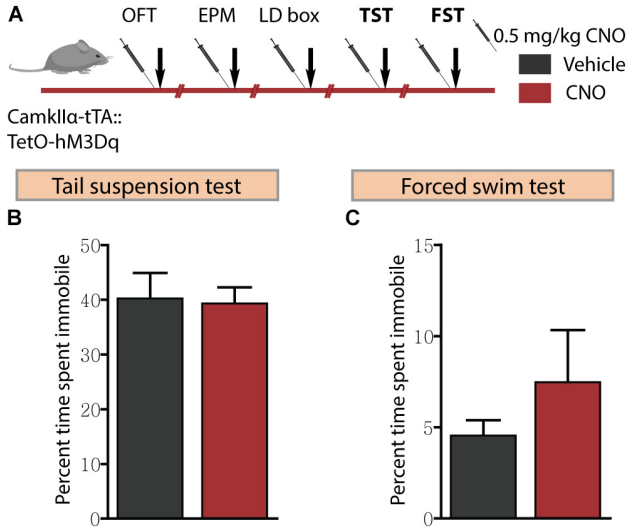

FIGURE 4 | Acute CNO-mediated DREADD activation of CamKIIα-positive forebrain excitatory neurons does not influence despair-like behaviour. **(A)** Shown is a schematic of the experimental paradigm used to determine the influence of acute CNO (0.5 mg/kg)-mediated hM3Dq activation of CamKIIα-positive forebrain excitatory neurons in adult male bigenic CamKIIα-tTA:TetO-hM3Dq mice on despair-like behaviour. Treatment groups were subjected to the TST and the FST to assess despair-like behaviour, with an interim washout period of 7–10 days (n = 9–10/group). CNO-mediated hM3Dq DREADD activation of CamKIIα-positive forebrain excitatory neurons did not alter despair-like behaviour on either the TST or FST, with no difference noted in percent time spent immobile in the TST **(B)** and the FST **(C)** tests, as compared to vehicle-treated CamKIIα-tTA:TetO-hM3Dq mice. Results are expressed as the mean ± SEM (n = 9–10/group), two-tailed, unpaired Student's t-test.

receptors (Meltzer, 1994; Lameh et al., 2007), it is important to control for potential off-target behavioural effects of CNO administration. We examined the influence of CNO (0.5 mg/kg) administration in C57BL/6J mice, the background strain for the bigenic CamKIIα-tTA:TetO-hM3Dq and CamKIIα-tTA:TetO-hM4Di mouse lines, on anxiety and despair-like behaviours (**Figure 6A**). Administration of CNO to C57BL/6J mice did not influence anxiety-like behaviour on the OFT (**Figures 6B–F**) as indicated by no change in the total distance travelled (**Figure 6C**), percent distance travelled in the centre (**Figure 6D**), percent time spent in the centre (**Figure 6E**), and number of entries made to the centre (**Figure 6F**) of the OFT arena. Similarly, CNO administration to C57BL/6J mice did not influence anxiety-like behaviour on either the EPM (**Figures 6G–K**) or the LD avoidance test (**Figures 6L–N**). Next, we assessed despair-like behaviour on the TST and FST. CNO-treated mice showed no significant difference in percent immobility time on either the TST (**Figure 6O**) or FST (**Figure 6P**). Taken together, these results provide an important control indicating that acute administration of CNO in C57BL/6J mice, or the generation of CNO metabolites at this dose (0.5 mg/kg, CNO) do not influence anxiety or despair-like behaviour. Thesed control experiments strengthen our observation that the anxiolytic behavioural responses following CNO-mediated hM3Dq DREADD activation of forebrain principal neurons do not involve any off-target actions of CNO, or its metabolites.

DISCUSSION

Our findings indicate that acute hM3Dq DREADD-mediated activation of CamKIIα-positive forebrain excitatory neurons evokes a significant decline in anxiety-like behaviour on multiple tasks, namely the OFT, LD avoidance, and the EPM test, with no change noted in despair-like behaviour. In contrast, acute hM4Di DREADD-mediated inhibition of CamKIIα-positive forebrain excitatory neurons does not influence anxiety or despair-like behaviour. These observations indicate that acute chemogenetic activation of forebrain excitatory neurons can elicit an anxiolytic behavioural response.

Acute hM3Dq DREADD-mediated activation of forebrain excitatory neurons significantly increased the expression of the immediate early gene, c-Fos, as characterised by western blotting and immunohistochemistry, in the cortex and hippocampus. This indicates that acute CNO administration to CamKIIα-tTA:TetO-hM3Dq mice results in broad circuit activation, within both cortical and hippocampal regions, as expected based on the genetic driver (CamKIIα-tTA) used (Mayford et al., 1996). The nature of c-Fos activation in our study is reflective of the pattern of CamKIIα-tTA driver expression, which has been previously characterised to drive the strongest transgene expression within the hippocampus, in particular the CA subfields, with strong expression also noted in cortical regions (Mayford et al., 1996; Alexander et al., 2009). Prior reports have carried out detailed electrophysiological investigation using the same bigenic mouse line, CamKIIα-tTA:TetO-hM3Dq, used in our study, indicating CNO-evoked depolarisation and enhanced firing rate, through a Gq-coupled GPCR signalling driven mechanism (Alexander et al., 2009). It is important to note that we cannot preclude the possibility that CNO-mediated hM3Dq DREADD stimulation may evoke a differential degree of activation across specific forebrain circuits (Alexander et al., 2009), which should be taken into account in the interpretation of our behavioural results. Nevertheless, such broad activation of multiple forebrain regions is common in diverse ethological contexts (Duncan et al., 1996; Ons et al., 2004; Park and Chung, 2019), as well as in response to therapeutic modalities (Linden et al., 2004; Wise et al., 2007; Bechtholt et al., 2008) used to target mood-related disorders.

To address the influence of acute hM3Dq DREADD-mediated activation of CamKIIα-positive forebrain excitatory neuron on mood-related behaviour, we subjected the mice to a battery of behavioural tasks including OFT, LD avoidance, EPM, TST, and FST. On tasks that assessed avoidance and defencive behaviour based responses namely the OFT, LD avoidance, and EPM, CNO-mediated activation of hM3Dq DREADD resulted in decreased anxiety-like behaviour that was most apparent on the OFT and LD avoidance test on multiple measures. The effects on anxiety-like behaviour in the EPM were restricted to only the measure of the number of entries made to the open arms. Taken together, acute chemogenetic activation of forebrain

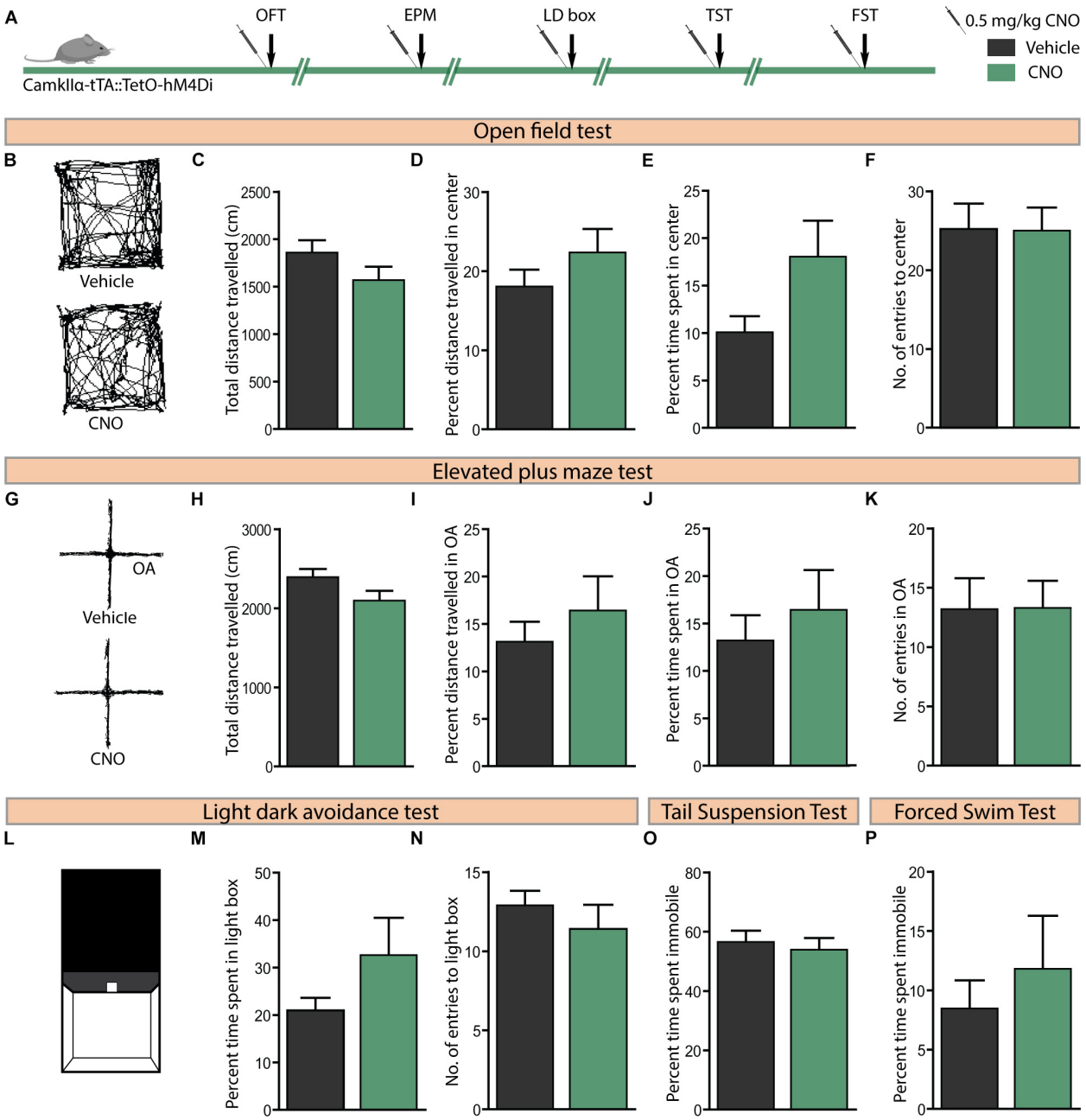

FIGURE 5 | Acute CNO-mediated DREADD inhibition of CamKIIα-positive forebrain excitatory neurons does not alter anxiety or despair-like behaviour. **(A)** Shown is a schematic of the experimental paradigm used to determine the influence of acute CNO (0.5 mg/kg)-mediated hM4Di DREADD inhibition of CamKIIα-positive forebrain excitatory neurons in adult male bigenic CamKIIα-tTA:TetO-hM4Di mice on anxiety and despair-like behaviour. Treatment groups were subjected to a battery of anxiety and despair-like behavioural tasks, with an interim washout period of 7–10 days (n = 9–10/group). **(B)** Shown are representative tracks from a vehicle and CNO-treated CamKIIα-tTA:TetO-hM4Di mouse in the OFT **(B–F)**. CNO-mediated hM4Di DREADD inhibition of CamKIIα-positive forebrain excitatory neurons did not influence anxiety-like behaviour in the OFT as indicated by no change observed in the total distance travelled **(C)**, percent distance travelled in the centre **(D)**, percent time spent in the centre **(E)**, and number of entries made to the centre **(F)** as compared to vehicle-treated controls. **(G)** Shown are representative tracks from a vehicle and CNO treated CamKIIα-tTA:TetO-hM4Di mouse in the EPM test **(G–K)**. CNO-mediated hM4Di DREADD inhibition of CamKIIα-positive forebrain excitatory neurons did not influence the total distance travelled **(H)**, percent distance travelled in the open arms (OA) **(I)**, percent time spent in the open arms **(J)**, and number of entries to the open arms **(K)** of the EPM. **(L)** Shown is an illustration of the chamber used in the light–dark (LD) avoidance test **(L–N)**. CNO-mediated hM4Di DREADD inhibition of CamKIIα-positive forebrain excitatory neurons did not influence percent time spent in the light chamber **(M)** and number of entries made to the light chamber **(N)**. CNO-mediated hM4Di DREADD inhibition of CamKIIα-positive forebrain excitatory neurons did not influence despair-like behaviour in the TST and FST, with no change noted in percent immobility time in both the TST **(O)** and the FST **(P)**, as compared to vehicle-treated CamKIIα-tTA:TetO-hM4Di mice. Results are expressed as the mean ± SEM (n = 9–10/group), two-tailed, unpaired Student's t-test.

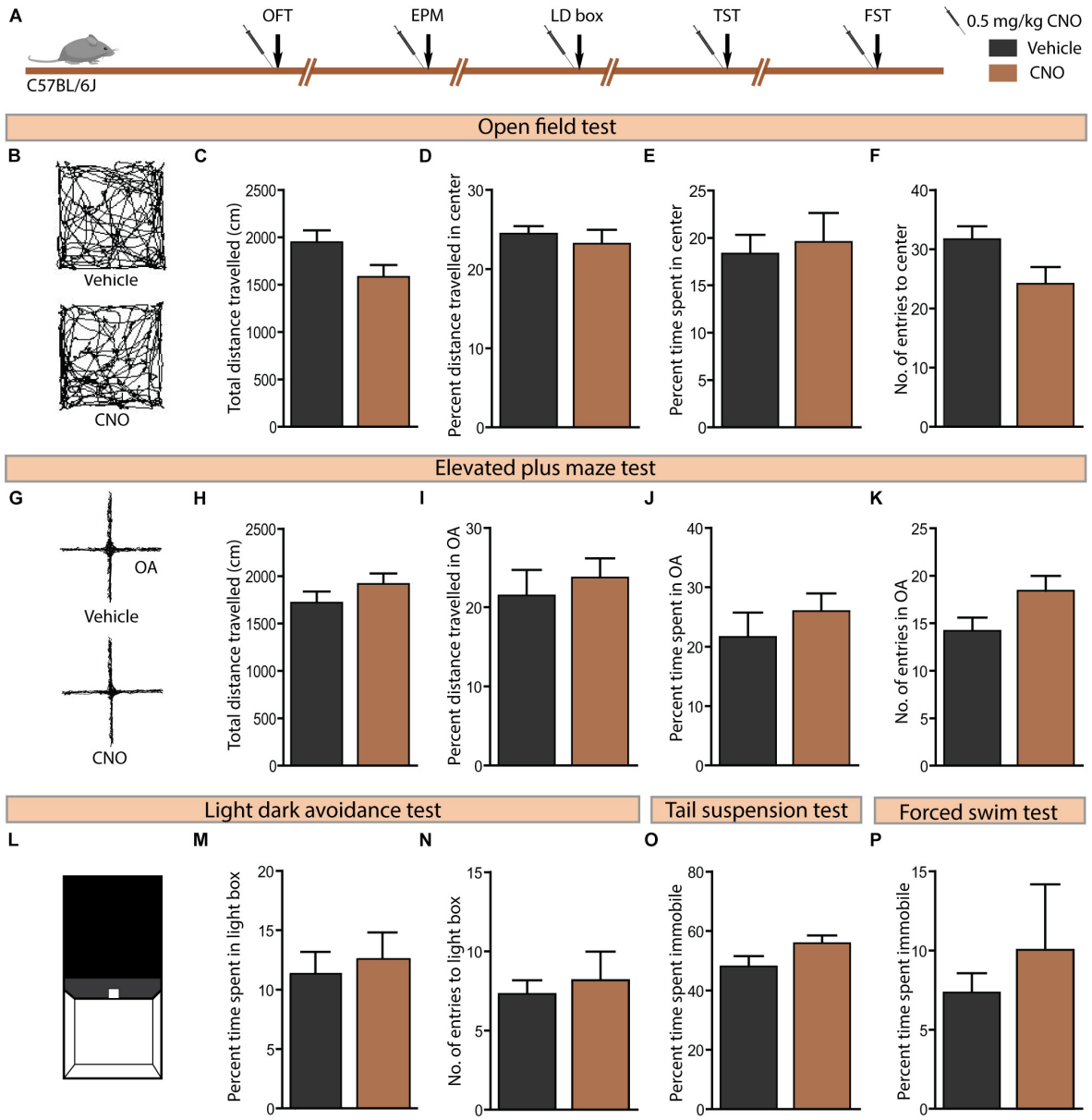

FIGURE 6 | Acute CNO administration in C57BL/6J mice does not influence anxiety or despair-like behaviour. **(A)** Shown is a schematic of the experimental paradigm used to determine the influence of acute CNO (0.5 mg/kg) administration in C57BL/6J mice, the background strain for the bigenic CamKIIα-tTA:TetO-hM3Dq and CamKIIα-tTA:TetO-hM4Di mouse lines, on anxiety and despair-like behaviours. Treatment groups were subjected to a battery of anxiety and despair-like behavioural tasks, with an interim washout period of 7–10 days (n = 10–12/group). **(B)** Shown are representative tracks from a vehicle and CNO treated C57BL/6J mouse in the OFT **(B–F)**. CNO administration to C57BL/6J mice did not influence anxiety-like behaviour in the OFT as indicated by no change observed in the total distance travelled **(C)**, percent distance travelled in the centre **(D)**, percent time spent in the centre **(E)**, and number of entries made to the centre **(F)** as compared to vehicle-treated controls. **(G)** Shown are representative tracks from a vehicle and CNO treated C57BL/6J mouse in the EPM test **(G–K)**. CNO administration to C57BL/6J mice did not influence the total distance travelled **(H)**, percent distance travelled in the open arms (OA) **(I)**, percent time spent in the open arms **(J)**, and number of entries to the open arms **(K)** of the EPM. **(L)** Shown is an illustration of the chamber used in the light–dark (LD) avoidance test **(L–N)**. CNO administration to C57BL/6J mice did not influence percent time spent in the light chamber **(M)** and number of entries made to the light chamber **(N)**. CNO administration to C57BL/6J mice did not influence despair-like behaviour in the TST and FST, with no change noted in percent time spent immobile in both the TST **(O)** and the FST **(P)**, as compared to vehicle-treated CamKIIα-tTA:TetO-hM4Di mice. Results are expressed as the mean ± SEM (n = 10–12/group), two-tailed, unpaired Student's t-test.

excitatory neurons clearly results in a reduction in anxiety-like behaviour, but to a different extent based on the behavioural test employed. These results suggest possible task-specific anxiolytic responses that vary in magnitude following hM3Dq DREADD-mediated forebrain excitatory neuron activation. CNO-treated CamKIIα-tTA:TetO-hM3Dq mice also exhibited increased total

movement in the OFT, which is in agreement with a prior report of enhanced ambulation following hM3Dq DREADD activation of the CamKIIα-positive excitatory neurons (Alexander et al., 2009). Though the CamKIIα-tTA:TetO-hM3Dq bigenic mouse line has been previously assessed for effects in the EPM, the authors did not report any effect on anxiety-like behaviour (Alexander et al., 2009). Our results also indicate that the most robust anxiolytic effects of DREADD activation in the CamKIIα-tTA:TetO-hM3Dq mouse line are noted in the OFT and LD avoidance test, with a subtle change noted in the EPM. Differential recruitment of specific forebrain circuits following CNO-mediated hM3Dq DREADD activation could contribute to the differences noted in the degree of behavioural responses across tasks such as the OFT, LD avoidance and EPM. While chemogenetic activation of forebrain excitatory neurons reduced anxiety-like behaviour, we did not observe any influence on despair-related behavioural measures in either the TST or FST. Overall, analysis across diverse mood-related behavioural tasks reveal that hM3Dq DREADD activation of CamKIIα-positive excitatory neurons enhances anxiolytic behaviours, with no influence on despair-like responses.

Our studies using bigenic CamKIIα-tTA:TetO-hM4Di mice indicated no effects of CNO treatment on anxiety or despair-like behaviours. Acute CNO administration to CamKIIα-tTA:TetO-hM4Di mice reduced c-Fos expression significantly within the hippocampus, but not in the cortex, with this decline in IEG expression interpreted as indicative of a decline in neuronal activity. This suggests that while the enhancement of Gq-coupled GPCR signalling via hM3Dq DREADD activation in forebrain excitatory neurons is capable of reducing anxiety-like behaviour, acute increases in Gi-coupled GPCR signalling via hM4Di DREADD activation within forebrain principal neurons did not alter anxiety-like responses. A point for consideration is that the dose of CNO (0.5 mg/kg) used in our study may not activate Gi signalling as effectively as it influences Gq signalling, given differences in affinity of CNO for hM4Di versus hM3Dq DREADDs (Gomez et al., 2017). However, it is important to keep in mind that doses of CNO as low as 0.3 mg/kg have been used to successfully inhibit specific neuronal populations expressing hM4Di (Krashes et al., 2011), and the decline noted in c-Fos within the hippocampus in our results indicates inhibition at the dose used in our study. However, further experiments across a wider dose range of CNO would be required prior to concluding that hM4Di-mediated DREADD inhibition of CamKIIα-positive forebrain excitatory neurons does not influence anxiety-like behaviour. We did note a difference in baseline total locomotion in CamKIIα-tTA:TetO-hM4Di bigenic mice as compared to the CamKIIα-tTA:TetO-hM3Dq bigenic cohort. While both the bigenic strains share a similar genetic background, they do appear to exhibit distinct baseline locomotor activity when placed in novel arenas, which could result from genetic changes at the level of quantitative trait loci across several generations of breeding these distinct bigenic mouse lines. Thus, a direct comparison of locomotor activity across these two bigenic lines needs to factor in these baseline differences, and we have restricted our statistical comparisons to the effect of acute CNO-treatment with corresponding vehicle-treated controls within the same bigenic line. The DREADD ligand CNO, used in our study, is known to metabolise into clozapine and *N*-desmethylclozapine (Manvich et al., 2018), that target endogenous receptors (Meltzer, 1994; Lameh et al., 2007). Studies have reported behavioural effects of CNO administration in the absence of DREADD expression (MacLaren et al., 2016), possibly via the metabolites of CNO (Manvich et al., 2018). Administering CNO to the C57BL/6J mice, the background strain, did not alter anxiety or despair-like behaviour, providing support to the evidence that the anxiolytic behavioural effects noted upon CNO administration to CamKIIα-tTA:TetO-hM3Dq mice are specific to hM3Dq DREADD-mediated activation of forebrain excitatory neurons.

Previous studies have capitalised on optogenetic and chemogenetic tools to delineate the contribution of specific circuits, including the ventral hippocampus (vHPC), mPFC, BNST, and amygdala (Nieh et al., 2013; Adhikari, 2014; Burnett and Krashes, 2016) in the regulation of anxiety-like behaviours in rodent models. Strategies that result in broader activation patterns likely encompassing multiple circuits simultaneously, and their impact on these anxiety-related behavioural assays have not been extensively explored. We have used a CamKIIα-driven transgene system, which successfully drives the expression of the relevant DREADD in the hippocampus and cortex, albeit with higher binding reported in the hippocampus (Alexander et al., 2009). The cortex and hippocampus are highly implicated in regulating emotional behaviour given their reciprocal connections with other limbic brain regions (Rajmohan and Mohandas, 2007), and control over the stress response pathways (Jankord and Herman, 2008). Although the circuits involved in the modulation of anxiety-like behaviour are distributed in a brain-wide network, the role of a few specific circuits is better delineated. The mPFC and vHPC along with the amygdala form the emotional triad that integrate sensory information, contextual information, and valence (Adhikari, 2014; Fastenrath et al., 2014; Reznikov et al., 2016; Hiser and Koenigs, 2018; Willinger et al., 2019); thereby play a key role in regulating various aspects of anxiety-like behaviour. vHPC-mPFC projections have been shown to be necessary for anxiety-related neuronal activity and behavioural outcomes (Adhikari et al., 2010, 2011). Single units in the mPFC preferentially fire in either the open or closed arm of the EPM and are influenced by activity in the vHPC (Adhikari et al., 2011). Both optogenetic and chemogenetic activation of CamKIIα-positive mPFC neurons using viral strategies has been shown to decrease anxiety-like behaviour (Wang et al., 2015; Pati et al., 2018), which is consistent with our result of decline in anxiety-like behaviour following broad activation of CamKIIα-positive forebrain excitatory neurons using the CamKIIα-tTA:TetO-hM3Dq bigenic mouse line. Interestingly, optogenetic activation of the granule cells in the DG reduces anxiety-like behavioural responses, and increases exploratory behaviour on approach-avoidance conflict based tasks (Kheirbek et al., 2013). The CamKIIα-tTA:TetO-hM3Dq bigenic mouse line used in our study, would likely recruit both the hippocampus and mPFC, and it is not possible to parse out the relative contribution of these individual forebrain circuits to the anxiolytic behaviours observed following CamKIIα-positive forebrain excitatory neuron activation. Rather, our results inform

us that such broad activation of forebrain principal neurons is associated with a robust decrease in anxiety-like behaviour, possibly through the recruitment of both the hippocampus and the mPFC, each of which have been individually shown to influence anxiety-like responses (Calhoon and Tye, 2015; Tovote et al., 2015). Further studies are required to address the hierarchy of contribution of individual forebrain circuits under ethological contexts, wherein more than one individual circuit that modulates anxiety-like behavioural responses is recruited simultaneously.

Recent clinical studies using deep brain stimulation (DBS) of specific limbic brain regions have demonstrated powerful symptomatic relief through an influence on the regulation of negative emotional states and affect, likely via the recruitment of multiple networks implicated in the neurocircuitry of psychopathology (Velasques et al., 2014). Preclinical studies serve to clarify the impact of DBS delivered to specific brain regions, factoring in the nature of frequency stimulation, recruitment of specific interconnected networks, and the associated consequences on a variety of mood-related behaviours (Reznikov et al., 2016). Interestingly, DBS stimulation to the infralimbic prefrontal cortex reduced anxiety-like behaviour in a preclinical post-traumatic stress disorder (PTSD) model (Reznikov et al., 2018). High frequency stimulation to the hippocampus is reported to enhance fear extinction learning and reduce fear recall (Farinelli et al., 2006; Deschaux et al., 2011). Optogenetic excitation of ventral DG granule cells evokes an anxiolytic response, whereas ventral DG granule cell inhibition has no effect on anxiety-like behaviour (Kheirbek et al., 2013). However, in the context of the hippocampus studies using both optogenetic and electrical stimulation indicate differing results on fear extinction/recall and anxiety-like behaviour, based on the temporal context, hippocampal subfield targetted, the nature of stimulation used and the behavioural paradigm (Garcia et al., 2008; Deschaux et al., 2011; Goshen et al., 2011; Lovett-Barron et al., 2014). Our results indicating that acute chemogenetic activation of forebrain principal neurons can elicit an anxiolytic state in diverse behavioural tasks, suggesting that these behavioural consequences may arise through recruitment of the hippocampus and interconnected neocortical circuits, thus influencing state-dependent anxiety in ethologically relevant behavioural paradigms.

DATA AVAILABILITY STATEMENT

The raw data supporting the conclusions of this manuscript will be made available by the authors, without undue reservation, to any qualified researcher.

ETHICS STATEMENT

All procedures involving animal handling and treatment were carried out in accordance with the guidelines of the Committee for the Purpose of Control and Supervision of Experiments on Animals (CPCSEA), Government of India and were approved by the TIFR Institutional Animal Ethics Committee.

AUTHOR CONTRIBUTIONS

SP, SS, and VV designed the experiments and wrote the manuscript. SS and PC performed the Western blotting experiments. SS, SP, PT, and TB performed the behavioural experiments and data analysis. SS performed the immunohistochemical analysis.

FUNDING

This work was supported by a TIFR intramural grant (VV), funded by the Department of Atomic Energy (DAE), Government of India.

ACKNOWLEDGMENTS

We would like to acknowledge Dr. Shital Suryavanshi for his assistance with genotyping and animal husbandry.

REFERENCES

Adhikari, A. (2014). Distributed circuits underlying anxiety. *Front. Behav. Neurosci.* 8:112. doi: 10.3389/fnbeh.2014.00112

Adhikari, A., Topiwala, M. A., and Gordon, J. A. (2010). Synchronized activity between the ventral hippocampus and the medial prefrontal cortex during anxiety. *Neuron* 65, 257–269. doi: 10.1016/j.neuron.2009.12.002

Adhikari, A., Topiwala, M. A., and Gordon, J. A. (2011). Single units in the medial prefrontal cortex with anxiety-related firing patterns are preferentially influenced by ventral hippocampal activity. *Neuron* 71, 898–910. doi: 10.1016/j.neuron.2011.07.027

Alexander, G. M., Rogan, S. C., Abbas, A. I., Armbruster, B. N., Pei, Y., Allen, J. A., et al. (2009). Remote control of neuronal activity in transgenic mice expressing evolved G protein-coupled receptors. *Neuron* 63, 27–39. doi: 10.1016/j.neuron.2009.06.014

Armbruster, B. N., Li, X., Pausch, M. H., Herlitze, S., and Roth, B. L. (2007). Evolving the lock to fit the key to create a family of G protein-coupled receptors potently activated by an inert ligand. *Proc. Natl. Acad. Sci. U.S.A.* 104, 5163–5168. doi: 10.1073/pnas.0700293104

Bechtholt, A. J., Valentino, R. J., and Lucki, I. (2008). Overlapping and distinct brain regions associated with the anxiolytic effects of chlordiazepoxide and chronic fluoxetine. *Neuropsychopharmacology* 33, 2117–2130. doi: 10.1038/sj.npp.1301616

Beck, C. H. M., and Fibiger, H. C. (1995). Conditioned fear-induced changes in behavior and in the expression of the immediate early gene c-Fos: with and without diazepam pretreatment. *J. Neurosci.* 15(1 Pt 2), 709–720. doi: 10.1523/jneurosci.15-01-00709.1995

Breiter, H. C. (1996). Functional magnetic resonance imaging of symptom provocation in obsessive-compulsive disorder. *Arch. Gen. Psychiatry* 53:595. doi: 10.1001/archpsyc.1996.01830070041008

Burnett, C. J., and Krashes, M. J. (2016). Resolving behavioral output via chemogenetic designer receptors exclusively activated by designer drugs. *J. Neurosci.* 36, 9268–9282. doi: 10.1523/JNEUROSCI.1333-16.2016

Calhoon, G. G., and Tye, K. M. (2015). Resolving the neural circuits of anxiety. *Nat. Neurosci.* 18, 1394–1404. doi: 10.1038/nn.4101

Cha, J., Greenberg, T., Song, I., Blair Simpson, H., Posner, J., and Mujica-Parodi, L. R. (2016). Abnormal hippocampal structure and function in clinical anxiety and comorbid depression. *Hippocampus* 26, 545–553. doi: 10.1002/hipo.22566

Davidson, R. J. (2002). Anxiety and affective style: role of prefrontal cortex and amygdala. *Biol. Psychiatry* 51, 68–80. doi: 10.1016/S0006-3223(01)01328-2

de Medeiros, M. A., Carlos Reis, L., and Eugênio Mello, L. (2005). Stress-induced c-Fos expression is differentially modulated by dexamethasone. *Neuropsychopharmacology* 30, 1246–1256. doi: 10.1038/sj.npp.1300694

Deschaux, O., Motanis, H., Spennato, G., Moreau, J.-L., and Garcia, R. (2011). Re-emergence of extinguished auditory-cued conditioned fear following a sub-conditioning procedure: effects of hippocampal and prefrontal tetanic stimulations. *Neurobiol. Learn. Mem.* 95, 510–518. doi: 10.1016/j.nlm.2011.03.002

Douglas, R. J., and Martin, K. A. C. (2004). Neuronal circuits of the neocortex. *Annu. Rev. Neurosci.* 27, 419–451. doi: 10.1146/annurev.neuro.27.070203.144152

Duncan, G. E., Knapp, D. J., and Breese, G. R. (1996). Neuroanatomical characterization of Fos induction in rat behavioral models of anxiety. *Brain Res.* 713, 79–91. doi: 10.1016/0006-8993(95)01486-1

Eser, D., Leicht, G., Lutz, J., Wenninger, S., Kirsch, V., Schüle, C., et al. (2009). Functional neuroanatomy of CCK-4-induced panic attacks in healthy volunteers. *Hum. Brain Mapp.* 30, 511–522. doi: 10.1002/hbm.20522

Farinelli, M., Deschaux, O., Hugues, S., Thevenet, A., and Garcia, R. (2006). Hippocampal train stimulation modulates recallof fear extinction independently of prefrontalcortex synaptic plasticity and lesions. *Learn. Mem.* 13, 329–334. doi: 10.1101/lm.204806

Fastenrath, M., Coynel, D., Spalek, K., Milnik, A., Gschwind, L., Roozendaal, B., et al. (2014). Dynamic modulation of amygdala-hippocampal connectivity by emotional arousal. *J. Neurosci.* 34, 13935–13947. doi: 10.1523/JNEUROSCI.0786-14.2014

Garcia, R., Spennato, G., Nilsson-Todd, L., Moreau, J.-L., and Deschaux, O. (2008). Hippocampal low-frequency stimulation and chronic mild stress similarly disrupt fear extinction memory in rats. *Neurobiol. Learn. Mem.* 89, 560–566. doi: 10.1016/j.nlm.2007.10.005

Gomez, J. L., Bonaventura, J., Lesniak, W., Mathews, W. B., Sysa-Shah, P., Rodriguez, L. A., et al. (2017). Chemogenetics revealed: DREADD occupancy and activation via converted clozapine. *Science* 357, 503–507. doi: 10.1126/science.aan2475

Goshen, I., Brodsky, M., Prakash, R., Wallace, J., Gradinaru, V., Ramakrishnan, C., et al. (2011). Dynamics of retrieval strategies for remote memories. *Cell* 147, 678–689. doi: 10.1016/j.cell.2011.09.033

Griebel, G., and Holmes, A. (2013). 50 years of hurdles and hope in anxiolytic drug discovery. *Nat. Rev. Drug Discov.* 12, 667–687. doi: 10.1038/nrd4075

Hiser, J., and Koenigs, M. (2018). The multifaceted role of the ventromedial prefrontal cortex in emotion. *Biol. Psychiatry* 83, 638–647. doi: 10.1016/j.biopsych.2017.10.030

Hoehn-Saric, R., Schlund, M. W., and Wong, S. H. (2004). Effects of citalopram on worry and brain activation in patients with generalized anxiety disorder. *Psychiatry Res. Neuroimaging* 131, 11–21. doi: 10.1016/j.pscychresns.2004.02.003

Jankord, R., and Herman, J. P. (2008). Limbic regulation of hypothalamo-pituitary-adrenocortical function during acute and chronic stress. *Ann. N. Y. Acad. Sci.* 1148, 64–73. doi: 10.1196/annals.1410.012

Jimenez, J. C., Su, K., Goldberg, A. R., Luna, V. M., Biane, J. S., Ordek, G., et al. (2018). Anxiety cells in a hippocampal-hypothalamic circuit. *Neuron* 97, 670–683.e6. doi: 10.1016/j.neuron.2018.01.016

Kheirbek, M. A., Drew, L. J., Burghardt, N. S., Costantini, D. O., Tannenholz, L., Ahmari, S. E., et al. (2013). Differential control of learning and anxiety along the dorsoventral axis of the dentate gyrus. *Neuron* 77, 955–968. doi: 10.1016/j.neuron.2012.12.038

Krashes, M. J., Koda, S., Ye, C., Rogan, S. C., Adams, A. C., Cusher, D. S., et al. (2011). Rapid, reversible activation of AgRP neurons drives feeding behavior in mice. *J. Clin. Invest.* 121, 1424–1428. doi: 10.1172/JCI46229

Lameh, J., Burstein, E. S., Taylor, E., Weiner, D. M., Vanover, K. E., and Bonhaus, D. W. (2007). Pharmacology of N-desmethylclozapine. *Pharmacol. Ther.* 115, 223–231. doi: 10.1016/J.PHARMTHERA.2007.05.004

Li, C., Lu, C., Wu, Y., Hui Lee, S., Wen Chu, R., and Su, T. (2018). Attenuated motor cortical responsiveness to motor and cognitive tasks in generalized anxiety disorder. *Neuropsychiatry* 08, 843–853. doi: 10.4172/Neuropsychiatry.1000411

Linden, A.-M., Greene, S. J., Bergeron, M., and Schoepp, D. D. (2004). Anxiolytic activity of the MGLU2/3 receptor agonist LY354740 on the elevated plus maze is associated with the suppression of stress-induced c-Fos in the hippocampus and increases in c-Fos induction in several other stress-sensitive brain regions. *Neuropsychopharmacology* 29, 502–513. doi: 10.1038/sj.npp.1300321

Lovett-Barron, M., Kaifosh, P., Kheirbek, M. A., Danielson, N., Zaremba, J. D., Reardon, T. R., et al. (2014). Dendritic inhibition in the hippocampus supports fear learning. *Science* 343, 857–863. doi: 10.1126/science.1247485

MacLaren, D. A. A., Browne, R. W., Shaw, J. K., Krishnan Radhakrishnan, S., Khare, P., Espana, R. A., et al. (2016). Clozapine N-Oxide administration produces behavioral effects in long-evans rats: implications for designing DREADD experiments. *eNeuro* 3:ENEURO.219-16.2016. doi: 10.1523/ENEURO.0219-16.2016

Makovac, E., Meeten, F., Watson, D. R., Herman, A., Garfinkel, S. N., Critchley, H. D., et al. (2016). Alterations in Amygdala-prefrontal functional connectivity account for excessive worry and autonomic dysregulation in generalized anxiety disorder. *Biol. Psychiatry* 80, 786–795. doi: 10.1016/j.biopsych.2015.10.013

Manvich, D. F., Webster, K. A., Foster, S. L., Farrell, M. S., Ritchie, J. C., Porter, J. H., et al. (2018). The DREADD agonist clozapine N-oxide (CNO) is reverse-metabolized to clozapine and produces clozapine-like interoceptive stimulus effects in rats and mice. *Sci. Rep.* 8:3840. doi: 10.1038/s41598-018-22116-z

Maslowsky, J., Mogg, K., Bradley, B. P., McClure-Tone, E., Ernst, M., Pine, D. S., et al. (2010). A preliminary investigation of neural correlates of treatment in adolescents with generalized anxiety disorder. *J. Child Adolesc. Psychopharmacol.* 20, 105–111. doi: 10.1089/cap.2009.0049

Mayford, M., Bach, M. E., Huang, Y.-Y., Wang, L., Hawkins, R. D., and Kandel, E. R. (1996). Control of memory formation through regulated expression of a CaMKII transgene. *Science* 274, 1678–1683. doi: 10.1126/science.274.5293.1678

Megìas, M., Emri, Z., Freund, T., and Gulyás, A. (2001). Total number and distribution of inhibitory and excitatory synapses on hippocampal CA1 pyramidal cells. *Neuroscience* 102, 527–540. doi: 10.1016/S0306-4522(00)00496-6

Meltzer, H. Y. (1994). An overview of the mechanism of action of clozapine. *J. Clin. Psychiatry* 55(Suppl. B), 47–52.

Milad, M. R., and Rauch, S. L. (2007). The role of the orbitofrontal cortex in anxiety disorders. *Ann. N. Y. Acad. Sci.* 1121, 546–561. doi: 10.1196/annals.1401.006

Molteni, R., Calabrese, F., Mancini, M., Racagni, G., and Riva, M. A. (2008). Basal and stress-induced modulation of activity-regulated cytoskeletal associated protein (Arc) in the rat brain following duloxetine treatment. *Psychopharmacology* 201, 285–292. doi: 10.1007/s00213-008-1276-7

Muigg, P., Scheiber, S., Salchner, P., Bunck, M., Landgraf, R., and Singewald, N. (2009). Differential stress-induced neuronal activation patterns in mouse lines selectively bred for high, normal or low anxiety. *PLoS One* 4:e5346. doi: 10.1371/journal.pone.0005346

Nawaratne, V., Leach, K., Suratman, N., Loiacono, R. E., Felder, C. C., Armbruster, B. N., et al. (2008). New insights into the function of M4 muscarinic acetylcholine receptors gained using a novel allosteric modulator and a DREADD (designer receptor exclusively activated by a designer drug). *Mol. Pharmacol.* 74, 1119–1131. doi: 10.1124/mol.108.049353

Nieh, E. H., Kim, S.-Y., Namburi, P., and Tye, K. M. (2013). Optogenetic dissection of neural circuits underlying emotional valence and motivated behaviors. *Brain Res.* 1511, 73–92. doi: 10.1016/j.brainres.2012.11.001

Ons, S., Marti, O., and Armario, A. (2004). Stress-induced activation of the immediate early gene Arc (activity-regulated cytoskeleton-associated protein) is restricted to telencephalic areas in the rat brain: relationship to c-Fos mRNA. *J. Neurochem.* 89, 1111–1118. doi: 10.1111/j.1471-4159.2004.02396.x

Parfitt, G. M., Nguyen, R., Bang, J. Y., Aqrabawi, A. J., Tran, M. M., Seo, D. K., et al. (2017). bidirectional control of anxiety-related behaviors in mice: role of inputs arising from the ventral hippocampus to the lateral septum and medial prefrontal cortex. *Neuropsychopharmacology* 42, 1715–1728. doi: 10.1038/npp.2017.56

Park, K., and Chung, C. (2019). Systemic cellular activation mapping of an extinction-impaired animal model. *Front. Cell. Neurosci.* 13:99. doi: 10.3389/fncel.2019.00099

Pati, S., Sood, A., Mukhopadhyay, S., and Vaidya, V. A. (2018). Acute pharmacogenetic activation of medial prefrontal cortex excitatory neurons regulates anxiety-like behaviour. *J. Biosci.* 43, 85–95. doi: 10.1007/s12038-018-9732-y

Paulus, M. P., and Stein, M. B. (2006). An insular view of anxiety. *Biol. Psychiatry* 60, 383–387. doi: 10.1016/j.biopsych.2006.03.042

Rajmohan, V., and Mohandas, E. (2007). The limbic system. *Indian J. Psychiatry* 49, 132–139. doi: 10.4103/0019-5545.33264

Rauch, S. L. (1995). A positron emission tomographic study of simple phobic symptom provocation. *Arch. Gen. Psychiatry* 52, 20–28. doi: 10.1001/archpsyc.1995.03950130020003

Reznikov, R., Bambico, F. R., Diwan, M., Raymond, R. J., Nashed, M. G., Nobrega, J. N., et al. (2018). Prefrontal cortex deep brain stimulation improves fear and anxiety-like behavior and reduces basolateral amygdala activity in a preclinical model of posttraumatic stress disorder. *Neuropsychopharmacology* 43, 1099–1106. doi: 10.1038/npp.2017.207

Reznikov, R., Binko, M., Nobrega, J. N., and Hamani, C. (2016). Deep brain stimulation in animal models of fear, anxiety, and posttraumatic stress disorder. *Neuropsychopharmacology* 41, 2810–2817. doi: 10.1038/npp.2016.34

Santini, M. A., Klein, A. B., El-Sayed, M., Ratner, C., Knudsen, G. M., Mikkelsen, J. D., et al. (2011). Novelty-induced activity-regulated cytoskeletal-associated protein (Arc) expression in frontal cortex requires serotonin 2A receptor activation. *Neuroscience* 190, 251–257. doi: 10.1016/j.neuroscience.2011.05.048

Shin, L. M., and Liberzon, I. (2010). The neurocircuitry of fear, stress, and anxiety disorders. *Neuropsychopharmacology* 35, 169–191. doi: 10.1038/npp.2009.83

Tovote, P., Fadok, J. P., and Luthi, A. (2015). Neuronal circuits for fear and anxiety. *Nat. Rev. Neurosci.* 16, 317–331. doi: 10.1038/nrn3945

Tye, K. M., and Deisseroth, K. (2012). Optogenetic investigation of neural circuits underlying brain disease in animal models. *Nat. Rev. Neurosci.* 13, 251–266. doi: 10.1038/nrn3171

Úbeda-Contreras, J., Marín-Blasco, I., Nadal, R., and Armario, A. (2018). Brain c-fos expression patterns induced by emotional stressors differing in nature and intensity. *Brain Struct. Funct.* 223, 2213–2227. doi: 10.1007/s00429-018-1624-2

Velasques, B., Diniz, C., Teixeira, S., Cartier, C., Peressutti, C., Silva, F., et al. (2014). Deep brain stimulation: a new treatment in mood and anxiety disorders. *CNS Neurol. Disord. Drug Targets* 13, 961–971. doi: 10.2174/1871527313666140612122929

Wang, G.-Q., Cen, C., Li, C., Cao, S., Wang, N., Zhou, Z., et al. (2015). Deactivation of excitatory neurons in the prelimbic cortex via Cdk5 promotes pain sensation and anxiety. *Nat. Commun.* 6:7660. doi: 10.1038/NCOMMS8660

Wang, Y., Chai, F., Zhang, H., Liu, X., Xie, P., Zheng, L., et al. (2016). Cortical functional activity in patients with generalized anxiety disorder. *BMC Psychiatry* 16:217. doi: 10.1186/s12888-016-0917-3

Whissell, P. D., Tohyama, S., and Martin, L. J. (2016). The use of DREADDs to deconstruct behavior. *Front. Genet.* 7:70. doi: 10.3389/fgene.2016.00070

Willinger, D., Karipidis, I. I., Beltrani, S., Di Pietro, S. V., Sladky, R., Walitza, S., et al. (2019). Valence-dependent coupling of prefrontal-amygdala effective connectivity during facial affect processing. *eNeuro* 6:ENEURO.0079-19.2019. doi: 10.1523/ENEURO.0079-19.2019

Wise, R. G., Lujan, B. J., Schweinhardt, P., Peskett, G. D., Rogers, R., and Tracey, I. (2007). The anxiolytic effects of midazolam during anticipation to pain revealed using fMRI. *Magn. Reson. Imaging* 25, 801–810. doi: 10.1016/J.MRI.2007.03.016

Conflict of Interest: The authors declare that the research was conducted in the absence of any commercial or financial relationships that could be construed as a potential conflict of interest.

frontiers in Behavioral Neuroscience

ORIGINAL RESEARCH
published: 06 November 2019
doi: 10.3389/fnbeh.2019.00240

LPS-Induced Systemic Neonatal Inflammation: Blockage of P2X7R by BBG Decreases Mortality on Rat Pups and Oxidative Stress in Hippocampus of Adult Rats

*Clivandir Severino da Silva[1], Michele Longoni Calió[2], Amanda Cristina Mosini[1], Jaime Moreira Pires[1], Débora da Silva Bandeira Rêgo[1], Luiz E. Mello[1,3] and Ana Teresa Figueiredo Stochero Leslie[4]**

[1]Departamento de Fisiologia, Universidade Federal de São Paulo—UNIFESP, São Paulo, Brazil, [2]Departamento de Bioquímica, Universidade Federal de São Paulo—UNIFESP, São Paulo, Brazil, [3]D'Or Institute for Research and Education (IDOR), Rio de Janeiro, Brazil, [4]Departamento de Pediatria, Universidade Federal de São Paulo—UNIFESP, São Paulo, Brazil

OPEN ACCESS

Edited by:
Jee Hyun Kim,
Florey Institute of Neuroscience and Mental Health, Australia

Reviewed by:
Rachel Anne Hill,
Monash University, Australia
Savina Apolloni,
Santa Lucia Foundation (IRCCS), Italy

***Correspondence:**
Ana Teresa F. S. Leslie
aterasass@gmail.com

Specialty section:
This article was submitted to Emotion Regulation and Processing, a section of the journal Frontiers in Behavioral Neuroscience

Received: 14 January 2019
Accepted: 24 September 2019
Published: 06 November 2019

Citation:
Silva CS, Calió ML, Mosini AC, Pires JM, Rêgo DSB, Mello LE and Leslie ATFS (2019) LPS-Induced Systemic Neonatal Inflammation: Blockage of P2X7R by BBG Decreases Mortality on Rat Pups and Oxidative Stress in Hippocampus of Adult Rats. Front. Behav. Neurosci. 13:240. doi: 10.3389/fnbeh.2019.00240

Neonatal lipopolysaccharide (LPS) exposure-induced brain inflammation has been associated to neuronal injury and facilitates the development of models of neurological disorders in adult rats. The P2X7 receptor (P2X7R) plays a fundamental role in the onset and maintenance of the inflammatory cascade. Brilliant blue G (BBG), a P2X7R antagonist, has been shown to effectively promote neuroinflammatory protection. Here, we have investigated the long-term effects of the neonatal systemic inflammation on hippocampal oxidative stress, anxiety behavior and pain sensitivity in adulthood. We hypothesized that P2X7R blockade is able to modulate the effects of inflammation on these variables. Male and female rat pups received LPS and/or BBG solution intraperitoneally on the 1st, 3rd, 5th and 7th postnatal days. The survival rate and body weight were evaluated during the experimental procedures. The animals were submitted to behavioral tests for anxiety (elevated plus maze, EPM) and nociception (hot-plate and tail-flick) and the oxidative stress was measured by superoxide production in the dentate gyrus of the hippocampus using dihydroethidium (DHE) probe. BBG increased the survival rate in LPS-treated rats. No significant differences were found regarding anxiety behavior and pain sensitivity between the experimental groups. Systemic neonatal inflammation leads to a higher production of superoxide anion in the dentate gyrus of the hippocampus in adulthood and BBG inhibited that effect. Our data suggest that blocking the activation of the P2X7R during neonatal systemic inflammation may have a potential neuroprotective effect in adulthood.

Keywords: P2X7 receptor, brilliant blue G, lipopolysaccharide, neonate, inflammation, nervous system

INTRODUCTION

Perinatal inflammation is a major contributor to brain injury in preterm infants. The immune system response induced by inflammation, in especial during the neonatal period, where the developing brain is vulnerable to adverse events, may play an important role in the brain function, leading to long-term neurological and psychiatric disorders, such as schizophrenia, autism, bipolar disorder and major depression (Peng et al., 2019).

Strong evidence has shown that systemic inflammation can activate microglia, leading to neuronal death and a significant increased extracellular adenosine triphosphate (ATP) concentration (Raetz and Whitfield, 2002; Fan et al., 2005, 2008, 2011; Ling et al., 2006). Activated microglia secretes high levels of inflammatory mediators, including tumor necrosis factor-α (TNF-α), interleukin-1β (IL-1β) and reactive oxygen species (ROS; Qian et al., 2010). These inflammatory mediators impair neurons and further activate microglia, which promotes further inflammation and neurodegeneration (Gao et al., 2002; Politis et al., 2012). The free radical production associated with the microglial cells activation, mainly superoxide radical, can trigger brain damage (Lambert and Brand, 2009).

Superoxide can be synthesized by the action of nicotinamide adenine dinucleotide phosphate (NADPH) oxidase 2 (NOX2). This enzyme is part of the family proteins constitute by seven members specialized in the synthesis of ROS, being a multicomponent enzyme system composed of membrane-bound (p22-phox and gp91-phox) and cytoplasmic subunits (p40-phox, p47-phox, and p67-phox; Bedard and Krause, 2007).

Gilles first documented in 1976 the vulnerability of the newborn brain to inflammation using the lipopolysaccharide (LPS; Gilles et al., 1976) and since then, several models have been published. Neonatal exposure to LPS, an endotoxin component of the cell wall of gram-negative bacteria (Raetz and Whitfield, 2002), has been considered a model of inflammation in which there is increased risk of neural disorders (Ling et al., 2006; Fan et al., 2011) as well as of functional disability, such as sensory, motor, emotional and cognitive impairment in juvenile rats (Fan et al., 2005, 2008). Also, LPS treatment causes a dose-dependent increase in pro-inflammatory cytokines (Peng et al., 2019). Recent data has demonstrated that the neonatal exposure to LPS may lead to persistent hippocampal injury (Wang et al., 2013).

The chemical composition of LPS varies according to the bacterial serotype, but its general structure consists of a hydrophilic polysaccharide domain linked to a hydrophobic lipid component, called lipid A (Raetz and Whitfield, 2002; Fan et al., 2011). LPS is not recognized by the host's immune system while anchored to the outer bacterial membrane. The proliferation and bacterial lysis, however, cause the release of LPS from the membrane and the exposure of lipid A, which is recognized by the immune system (Raetz and Whitfield, 2002; Fan et al., 2005, 2011; Ling et al., 2006).

P2X7 receptor (P2X7R), a purinergic ATP-binding receptor, has been identified as a key player in the neuroinflammatory cascade controlling the onset and progression of a wide range of neurological conditions (Parvathenani et al., 2003; Monif et al., 2009; Ulrich et al., 2012; Burnstock and Volonté, 2012; Sperlágh and Illes, 2014). The expression of P2X7R is enhanced in several types of brain diseases, in which the presence of activated microglia is a concurrent feature (Sperlágh and Illes, 2014). The outflow of ATP from damaged and dead cells leads to the proliferation and activation of microglia by P2X7R, which also stimulates the production of superoxide (Parvathenani et al., 2003; Monif et al., 2009).

Díaz-Hernández et al. (2009) demonstrated that administration of brilliant blue G (BBG), a P2X7R antagonist, in an animal model of Huntington's disease in mice, prevented neuronal apoptosis and attenuated body weight loss and motor-coordination deficits. In another study, BBG injection after spinal cord injury resulted in the recovery of motor function (Peng et al., 2009). The blockade of P2X7R-mediated activity by BBG also showed to be neuroprotective in an animal model of Alzheimer's disease (Ryu and McLarnon, 2008).

Here, we hypothesized that P2X7R blockade in the LPS model could reduce the hippocampal oxidative stress and also would attenuate anxiety and nociceptive responses in adulthood resulting in neonate inflammation.

MATERIALS AND METHODS

Animals

Rats (*Wistar norvegicus)* were obtained and maintained in the Center for the Development of Experimental Models in Medicine and Biology (CEDEME) of Universidade Federal de São Paulo (UNIFESP). A total of 121 Wistar rat pups were used in the present study. Twenty-one days after birth the animals were separated by sex. All animals were housed in polypropylene cages under standard pathogen-free conditions (light/dark cycle 12 h/12 h, under constant room temperature at 22 ± 2°C, food, and tap water *ad libitum*). All of the experimental procedures were conducted according to international regulations of the National Institutes of Health, Guide for the Care and Use of Laboratory Animals (NIH Publication No. 8023), revised 2011, and approved by the internal Ethics Committee on Animal Research of UNIFESP (approval n° 4591030915).

Drug Administration

On the 1st day after birth (post natal day, PND 1) the pups were randomly allocated into four groups as described below:

1. NAIVE = no drug administration;
2. SAL + SAL = two injections of sterile 0.9% saline solution 5 mL/Kg;
3. SAL + LPS = injection of sterile 0.9% saline solution 5 mL/Kg and injection of LPS, 1 mg/Kg dissolved in saline;
4. BBG + LPS = injection of BBG 50 mg/Kg (Feng et al., 2015) dissolved in water and injection of LPS 1 mg/Kg dissolved in saline.

Drugs: LPS (Sigma L-2630; *Escherichia coli*, 0111:B4); BBG (Sigma-Aldrich B0770). All of the drugs were administered

intraperitoneally (i.p.) on PND1, 3, 5 and 7 with a 30 min interval between injections. The animals were continuously monitored during handling, administration of the drugs and after the procedures and all events and observations from the pups were recorded. Body weight was assessed on PND1, 10, 21, 45 and 89. The NAIVE and SAL + SAL groups were initially compared using the Fisher's exact test or the *t*-Student test and the results of the two groups were pooled as no statistically significant differences existed between both. The resulting group is reported as CONTROL.

It is known that a single systemic injection of LPS is used to reproduce acute systemic inflammation, whereas multiple injections mimic a chronic inflammatory condition (Simons and Tibboel, 2006; Püntener et al., 2012; Rousset et al., 2013; Dinel et al., 2014; Ming et al., 2015). Although LPS penetration into the central nervous system (CNS) is low, a single systemic injection is sufficient to trigger acute neuroinflammation (Elmquist and Flier, 2004; Sachot et al., 2004; Spencer et al., 2006). However, repetitive systemic use of LPS supports the activated microglial phenotype and causes changes in *blood–brain barrier*, increasing the penetration of LPS into the CNS and mobilizing other elements involved in the inflammatory response, and neuronal death (Schwartz et al., 2000; Benatti et al., 2009; Cervetto et al., 2013). For these reasons, repeated injections of LPS in alternate days was used in our model, in order to mimic a process of persistent neonatal inflammation. We created a new protocol aiming to reproduce a persistent inflammatory process in the first week of life and the dose of LPS was chosen based on the study by Okuyama et al. (2013).

Behavioral and Nociceptive Tests

In all experiments, the animals were observed in a blind manner as to which group the animals belonged to, and the apparatus was cleaned with a 5% alcohol solution after each session. In order to verify the influence of estrous cycle on treatment, female rats were evaluated according to the stage of the estrous cycle (see **Supplementary Material**).

Elevated Plus-Maze

The elevated plus maze (EPM) test evaluates anxiety-like behavior and combines natural preferences of rodents for dark spaces and aversions to illuminated, open and or elevated areas (Lezak et al., 2017). The EPM test was performed on PND80. As described by Pellow et al. (1985), the EPM consists of an apparatus made of wood, with two open arms (50 × 10 × 1 cm), and two closed arms (50 × 10 × 50 cm) with an open roof and arranged such that the two arms are opposite and perpendicular to each other, elevated 50 cm above the floor. The animals were individually placed at the center of the maze, facing towards one of the open arms and observed for 5 min. The ratio of time spent in the open arms, the ratio of time spent in central platform, the ratio of entries into open arms, the total number of entries into the arms (enclosed plus open), and the traveled distance were calculated. The measures for EPM test were taken using a camera (Panasonic; model WV-CP504) and analyzed with the program EthoVision (Noldus, 7.0).

Hot-Plate

The hot plate test evaluates pain by the supra-spinal pathways (Woolfe and Macdonald, 1943; Eddy and Leimbach, 1953). Reaction latency to the hot-plate was measured at PND82. Rats were placed individually on a hot-plate metallic surface (Ugo Basile S.R.L, model 35100-001) maintained at 55° ± 0.2°C. The latency time was measured by the time between placement of the animal on the hot-plate and the occurrence of the first sign of nociception, paw licking, flinching or jump response to avoid the heat. Reaction time was recorded and the animal immediately removed from the hot plate. A cut-off period of 30 s was set to avoid tissue damage to the paws. The values were taken manually.

Tail-Flick

The tail-flick test evaluates spinal reflex that can be an indication of pain (D'Amour and Smith, 1941; Cartens and Wilson, 1993). The nociceptive response was also evaluated by recording the latency to withdrawal of the tail in response to heat on PND84. Rats were habituated to handling and to being inserted into plastic cylindrical tubes before the experimental procedures. The tails of the rats were immersed in heated water. The heat intensity was set by adjusting the temperature at 52° ± 1°C. When a withdrawal response occurred, the stimulus was terminated and the response latency was measured. A cut-off time of 30 s was used to avoid tissue damage. The values were taken manually.

Tissue Preparation

The animals were maintained until the PND89, when euthanasia was performed. Animals were deeply anesthetized with a lethal dose of ketamine cocktail 80 mg/Kg ketamine (100 mg/mL—Syntec), 15 mg/Kg xylazine (20 mg/mL—Syntec) and 1 mg/Kg acepromazine (2 mg/mL—Vetnil) and intracardially perfused (infusion pump Cole-Parmer/Masterflex; model 7518-00), through the ascending aorta with 0.9% saline solution and 4% cold paraformaldehyde. The brain tissues were fixed in 4% paraformaldehyde for 24 h followed by immersion in a 30% sucrose in 0.1 M phosphate buffer at 4°C for 72 h. Brain tissues were frozen in O.C.T. compound (A.O. Company, Milwaukee, WI, USA), and the organs were cut into 30 μm coronal sections on a cryostat (HYRAX C25 cryostat, Zeiss). The sections were stored in a cryoprotectant solution (30% sucrose, 30% ethylene glycol, 0.1 M phosphate buffer) at −80°C until processing for superoxide detection. We decided to select the dentate gyrus of the hippocampus because this is the most sensitive region to damage and neuronal death caused by oxidative stress.

Evaluation of ROS Production

Detection of Superoxide

Superoxide was detected with the oxidative fluorescent probe DHE (dihydroethidium; Molecular Probes, CA, USA), which was oxidized to 2-hydroxyethidium, which then produced red fluorescence. Double staining was performed to assess the presence of DHE in three types of brain cells that express neuronal nuclear protein

(NeuN) or glial fibrillary acid protein (GFAP) or ionized calcium binding adaptor molecule 1 (Iba1) as described below.

Tissue samples were washed three times with 0.1 M phosphate buffer for 5 min. Brain sections were incubated in a light-protected humidified chamber with 5 μM DHE. Cell nuclei were stained with nuclear tracer DAPI (4′,6-diamidino-2-phenylindole; 5 μM; Sigma-Aldrich). Stained slides were examined and imaged using a confocal microscope (Leica SP8 Lightning, Leica Microsystems with LAS × Lite software). Fluorescence was detected with 510–560 nm excitation and 590 nm emission filters. The results are expressed as the DHE/DAPI ratio. ImageJ was used for quantification of the red emission signal and pixilation analysis. The amount of red emission signal was normalized with DAPI. Pixilations were analyzed in four acquired non-overlapping images (10 stacks) per slice of each animal, being that six hippocampal slices per animal were analyzed.

gp91-phox/NOX 2 Expression

Immunofluorescence was used to detect gp91-phox subunit expression. Also, double immunofluorescence staining was performed to assess expression of gp91-phox in three types of brain cells, that express NeuN, GFAP and Iba1. The sections were incubated with 3% H_2O_2 and then incubated 2% normal blocking bovine serum. Next, the sections were incubated with primary antibody anti-gp91-phox (Novus Biologicals NBP2-13037; 1:200), anti-NeuN (Millipore MAB377; 1:500), anti-GFAP (Sigma-Aldrich G3893; 1:500) and/or anti-Iba1 (Abcam ab5076; 1:500) in room temperature. One day later, the sections were rinsed and incubated with secondary conjugated antibody Alexa Fluor 488 (Invitrogen A11034; Life Technologies A21202e A11055; 1:500), Alexa Fluor 546 (Invitrogen A11056; 1:500) and/or Alexa Fluor 594 (Invitrogen A21203; 1:500) and DAPI (5 μM; Sigma-Aldrich) for nuclear staining for 2 h. Stained slides were examined and imaged using a confocal microscope (Zeiss Axiovert 100 M; Carl Zeiss, Germany; connected to an LSM 810 Confocal Laser Scanning System or Leica SP8 Lightning, Leica Microsystems with LAS × Lite software). The results are expressed as the NOX2/DAPI ratio. ImageJ was used for quantification and pixilation analysis. The amount of green emission signal was normalized with DAPI. Pixilations were analyzed in two acquired non-overlapping images (five stacks) per slice of each animal, being that one hippocampal slice per animal was analyzed.

Statistical and Data Analysis

Pearson's Chi-squared and Fisher's exact tests were applied to analyze the mortality rates in the groups or to compare males/females. The results were expressed as a percentage. When pertinent, one or two-way analysis of variance (ANOVA) followed by the Tukey's correction *post hoc* test was used for multiple comparisons of groups vs. sex or groups (females only) vs. estrous cycle. The data were presented as mean ± SEM (standard error of the mean). A p-value < 0.05 was considered significant. Statistical analysis was performed using SPSS software (20.0.0), *Statistica* 13 software and GraphPad Prism 5.0.

RESULTS

Effects of Neonatal LPS and BBG-Treatment on Mortality

Survival rates were 97.7% in the control group, 49% in SAL+LPS-treated group and 85.2% in BBG+LPS-treated group, with rats dying between PND1 and 11. The significantly higher mortality rate after LPS ($p < 0.001$; control group vs. SAL+LPS group) was not seen when the BBG treatment was associated ($p = 0.002$; SAL + LPS group vs. BBG+LPS group; **Figure 1**). No significant difference was observed in the mortality rate between males and females ($p = 0.323$). The LPS-treated pups demonstrated a "sick" appearance when compared to the other experimental group, showing pallor due to peripheral vasoconstriction, poor growth, lethargy and less mobility (see **Supplementary Figure S1**).

Effects of Neonatal LPS and BBG-Treatment on the Body Weight Gain

There was no difference between the groups with respect to body weight on PND1 (males, $p = 0.346$; females, $p = 0.414$). However, significant differences were observed for males on PND10 ($p < 0.001$), SAL+LPS and BBG+LPS groups presented lower body weight when compared to control group; on PND21 ($p < 0.001$), SAL+LPS and BBG+LPS groups presented lower body weight when compared to control group; on PND45 ($p = 0.008$), SAL+LPS group presented lower body weight when compared to control group and on PND89 ($p = 0.048$), SAL + LPS group when compared to control group (**Figure 2A**).

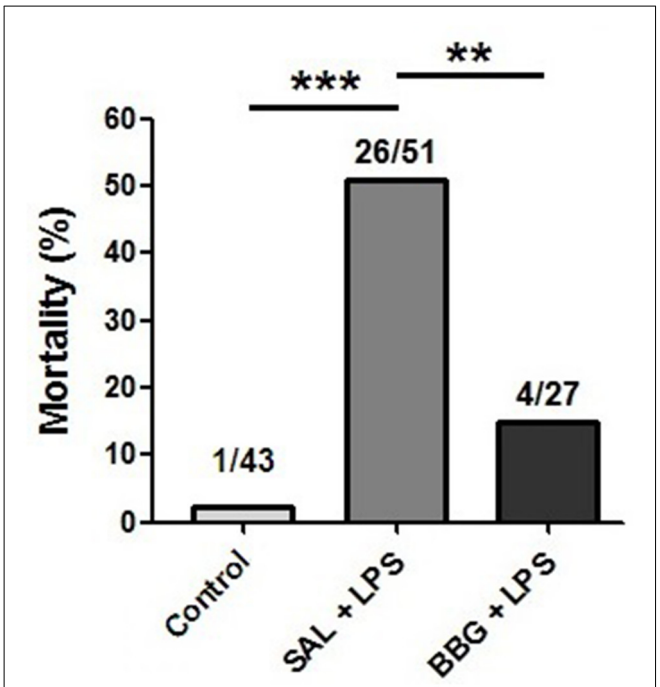

FIGURE 1 | Effects of neonatal lipopolysaccharide (LPS) and brilliant blue G (BBG)-treatment on the mortality. BBG increased survival rate in LPS-treated rats. Data on bars represent percentage of dead animals (numbers listed above bars). $^{**}p < 0.01$, $^{***}p < 0.001$.

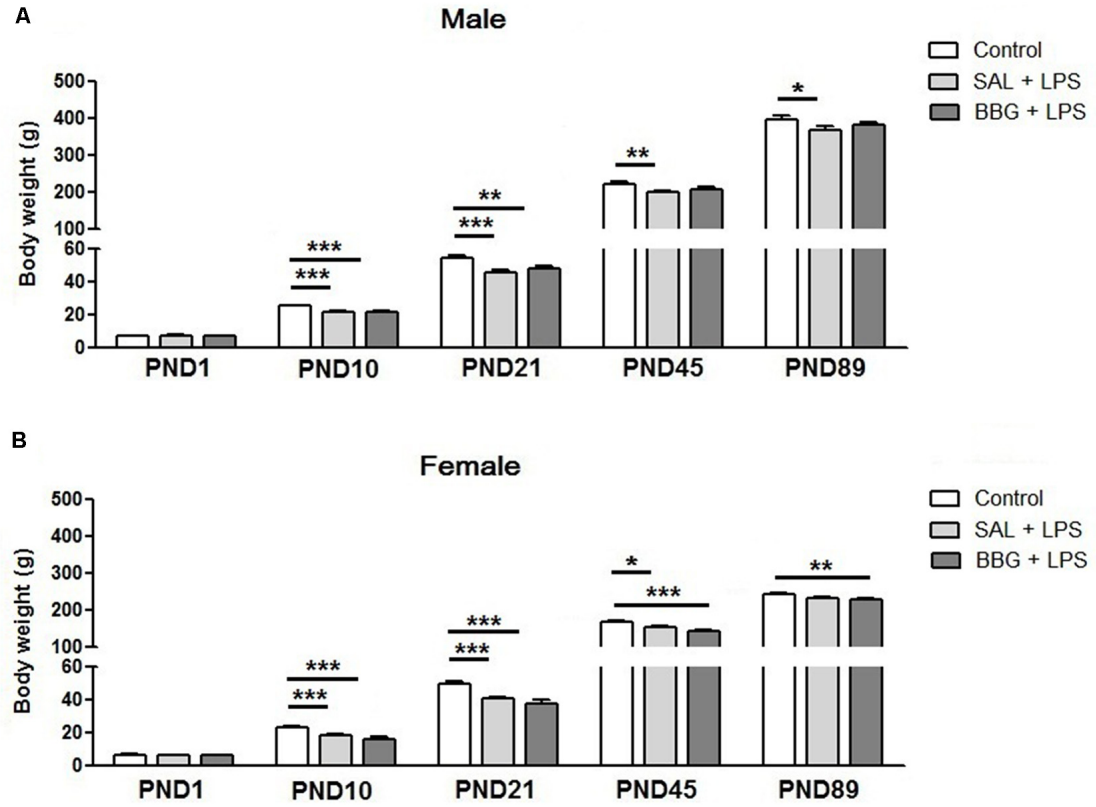

FIGURE 2 | Effects of neonatal LPS and BBG-treatment on the body weight gain. The development of body weight was measured on PND1, 10, 21, 45 and 89 for male **(A)** and female **(B)** animals. LPS induced a decrease in weight gain. On the other hand, BBG induces increase in weight gain in male and a decrease in female. Data are expressed as mean ± standard error of the mean (SEM). *$p < 0.05$, **$p < 0.01$, ***$p < 0.001$.

We also observed significant differences for females on PND10 ($p < 0.001$), SAL+LPS and BBG+LPS groups presented lower body weight when compared to control group; on PND21 ($p < 0.001$), SAL+LPS and BBG+LPS groups presented lower body weight when compared to control group; on PND45 ($p < 0.001$), SAL+LPS and BBG+LPS groups presented lower body weight when compared to control group and on PND89 ($p = 0.006$), BBG+LPS group presented lower body weight when compared to control group (**Figure 2B**).

Effects of Neonatal LPS and BBG-Treatment on the Behavioral and Nociceptive

Elevated Plus-Maze Test

There were no significant differences in the analyzed behavioral parameters between groups [ratio of time spent in the open arms: $p = 0.334$; ratio of time spent in central platform: $p = 0.053$; ratio of entries into open arms: $p = 0.076$; total number of arms entries (open and closed arms): $p = 0.910$; traveled distance: $p = 0.772$], as well as for the interaction of groups vs. sex ($p = 0.455$; $p = 0.522$; $p = 0.832$; $p = 0.150$; $p = 0.356$; respectively; **Figures 3A–E**). On the other hand, we observed differences with respect to the sex of the animals to the ratio of entries into open arms ($p = 0.023$; females presented more entries when compared to males), the ratio of time spent in central platform ($p = 0.002$; females spent more time when compared to males) and the traveled distance ($p < 0.001$; females traveled a longer distance as compared to males; see **Supplementary Figure S2**). There were significant changes in the analyzed behavioral parameters only between the estrous cycle phases, regardless of the experimental group (see **Supplementary Table S1** and **Supplementary Figure S3**).

Hot-Plate Test

There were no significant differences in reaction latency among groups ($p = 0.856$), even between males and females ($p = 0.310$), as well as for the interaction of groups vs. sex ($p = 0.369$; **Figure 4**). There were no significant changes regarding the estrous cycle (see **Supplementary Table S2**).

Tail-Flick Test

There were no significant differences in reaction latency between groups ($p = 0.299$), as well as for the interaction of groups vs. sex ($p = 0.807$; **Figure 5**). However, females showed a significantly lower response ($p < 0.001$) when compared to the males (see **Supplementary Figure S4**). There were no significant changes in reaction latency regarding estrous cycle (see **Supplementary Table S3**).

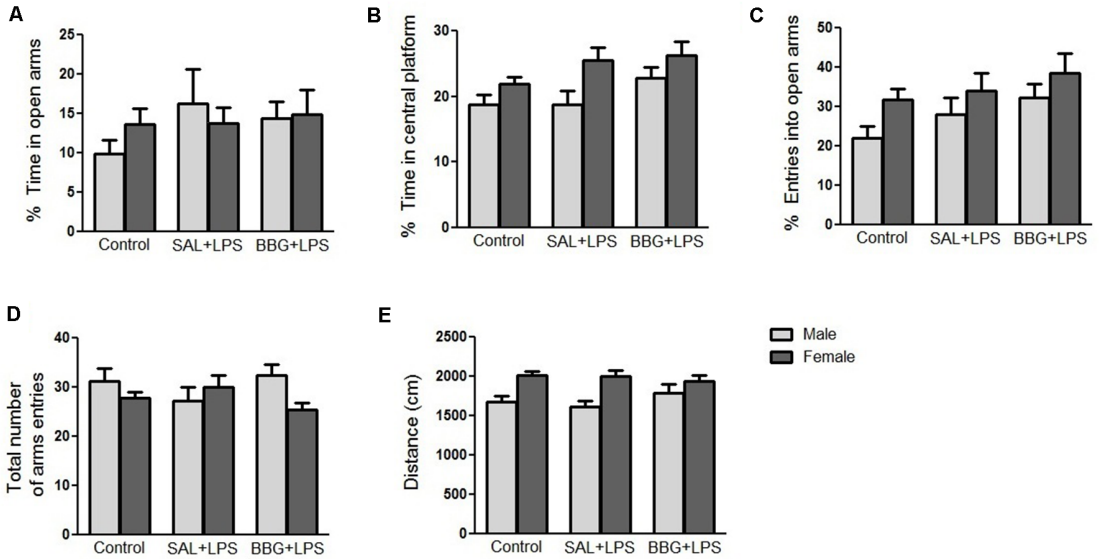

FIGURE 3 | Effects of neonatal LPS and BBG-treatment on the anxiety-like behavior analyzed by elevated plus maze (EPM) test. The treatment did not show significant changes on behavioral parameters between groups and there were no interaction of group/sex: percentage of time spent in the open arms **(A)**, percentage of time spent on the central platform **(B)**, percentage of entries into open arms **(C)**, total number of arms entries (open and closed arms; **D**) and distance travaled **(E)**. Data are expressed as mean ± SEM. $p > 0.05$.

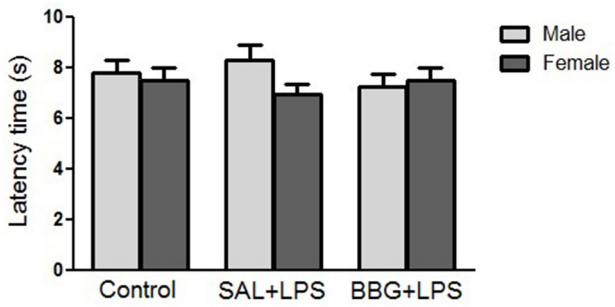

FIGURE 4 | Effects of neonatal LPS and BBG-treatment on the pain sensitivity analyzed by hot-plate test. The treatment did not show significant changes on latency time between groups and there were no interaction of group/sex. Data are expressed as mean ± SEM. $p > 0.05$.

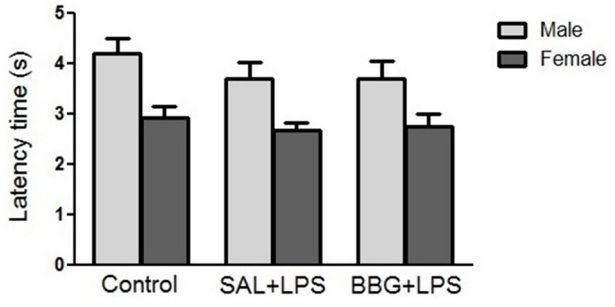

FIGURE 5 | Effects of neonatal LPS and BBG-treatment on the pain sensitivity analyzed by tail-flick test. The treatment did not show significant changes in latency time between groups and there was no interaction of group/sex. Data are expressed as mean ± SEM. $p > 0.05$.

Effects of Neonatal LPS and BBG-Treatment on Oxidative Stress

We observed significant differences in DHE intensity among groups ($p < 0.001$), although no difference was noted between males and females ($p = 0.734$), as well as for the interaction of groups vs. sex ($p = 0.815$). The **Figure 6A** shows the images of stained brain slices with DHE. The LPS-treated group exhibited higher level of DHE intensity when compared to control and BBG groups, as well as BBG group when compared to control group (**Figure 6B**).

Also, significant differences were found in the immunoreactivity for 91-phox/NOX2 between the groups ($p < 0.001$). The **Figure 7A** shows the images of stained brain with anti-gp91-phox/NOX2. The LPS-treated group exhibited higher levels of intensity for gp91-phox/NOX2 when compared to control and BBG groups, as well as BBG group when compared to control group (**Figure 7B**).

We used samples from LPS group to access the presence of superoxide by double staining. DHE probe showed an overlap only with NeuN staining (**Figure 8**) while gp91-phox/NOX2 overlaps with the astrocyte marker, GFAP (**Figure 9**).

DISCUSSION

Neonatal inflammation affects 11% of all live births and depending on the gestational age at birth (Vergnano et al., 2011),

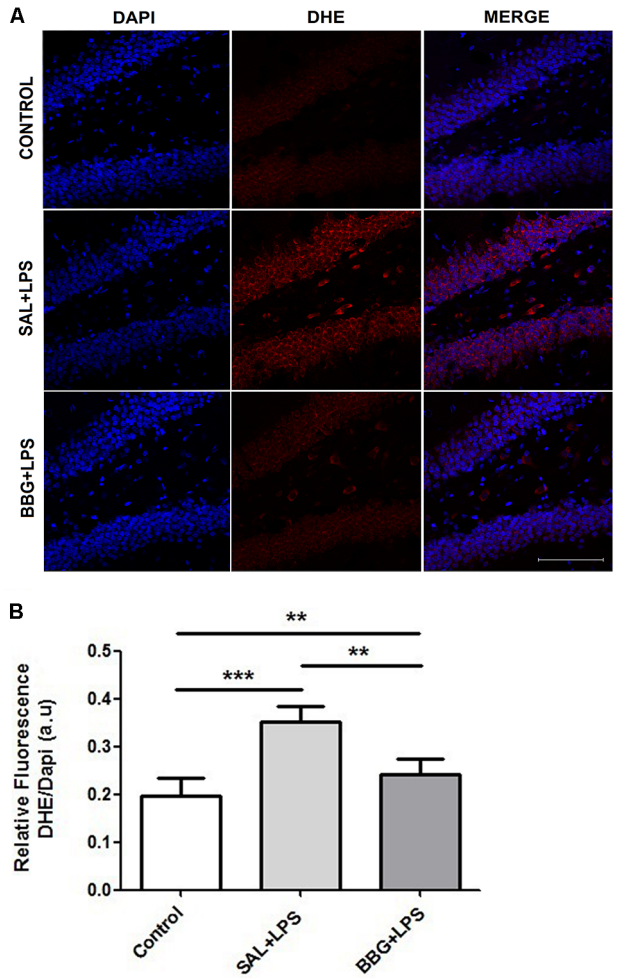

FIGURE 6 | Effects of neonatal LPS and BBG-treatment on the superoxide production. Superoxide anion were detected in hippocampus of animals by confocal microscope using DHE probe and ROS level was represented by fluorescence intensity. A decrease in BBG-treated animals was observed when compared to LPS-treated animals. Confocal microscopy of hippocampus of different groups **(A)**. Quantification of superoxide anion by the analysis of pixelationv Higher level of DHE intensity was observed in the LPS-treated group and it is opposite of the result showed in the BBG group **(B)**. DHE: red spots and DAPI: all blue nucleus. Scale bar represents 100 μm. Data are expressed as mean ± S.E.M. $^{**}p < 0.01$, $^{***}p < 0.001$. a.u: arbitrary units.

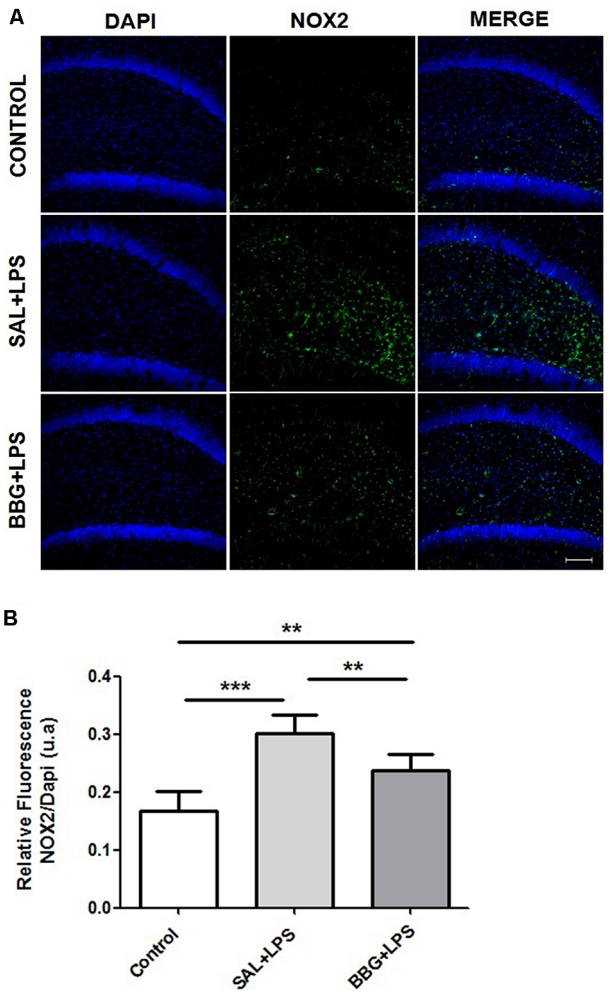

FIGURE 7 | Effects of neonatal LPS and BBG-treatment on the gp91-phox/NOX2 expression. NOX2 subunit were detected in the hippocampus of animals by immunofluorescence. A decrease in BBG-treated animals was observed when compared to LPS-treated animals. Confocal microscopy of hippocampus of different groups **(A)**. Quantification of gp91-phox by the analysis of pixilation. Higher level of gp91-phox intensity was observed in the LPS-treated group. On the other hand, a decreased level was found in the BBG group. **(B)**. gp91-phox: green spots and DAPI: all blue nucleus. Scale bar represents 100 μm. Data are expressed as mean ± SEM. $^{**}p < 0.01$, $^{***}p < 0.001$. a.u: arbitrary units.

25%–60% of the extremely preterm infants experience at least one episode of invasive bacterial infection during their entire staying in the neonatal intensive care unit (Stoll et al., 2010). A large amount of evidence has shown that the early life exposure to inflammation has been associated with long-term neurological impairment such as motor dysfunction in childhood and psychiatric disorders in adulthood. The first week of life is characterized by great plasticity and reorganization of the CNS (Bartlett et al., 2017) and represents a critical period in which inflammatory events can have significant neurological long-term consequences. The neonatal inflammation may induce long lasting changes in the CNS functioning, as the regulation of microglial and astrocyte activity, the synthesis and secretion of cytokines; the neurotransmission and the function of the adrenal pituitary hypothalamus axis (Ren et al., 2004; LaPrairie and Murphy, 2007).

In our study, the animals exposed to the inflammatory stimulus presented a significantly higher mortality rate when compared to the control group during the first week of life. This increased mortality may be related to a strong systemic inflammatory response syndrome (SIRS) induced by the LPS, resulting in multiple organ dysfunction (Mason, 1993; Zouikr et al., 2014). SIRS is characterized by excessive systemic cytokine synthesis, damage and cell death and tissue damage (Davies and Hagen, 1997; Cauwels et al., 2014). On the other hand,

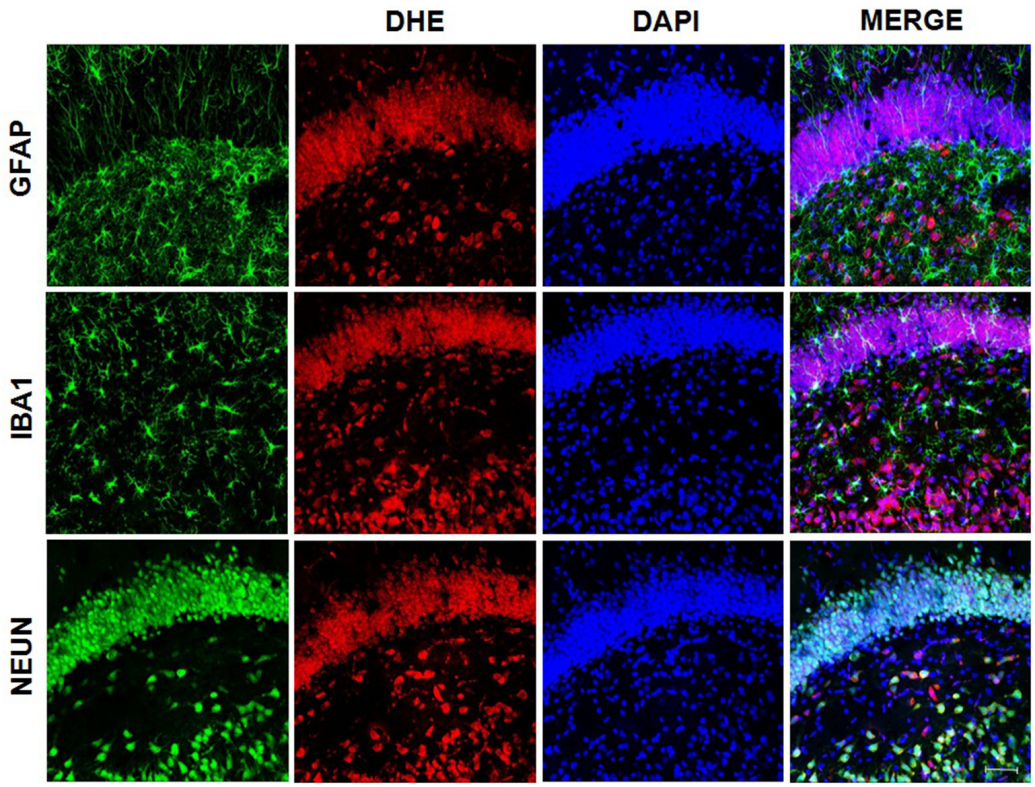

FIGURE 8 | Superoxide presence on neurons. Superoxide anion was detected using DHE probe. Confocal microscopy of hippocampus showed that DHE probe overlaps with NeuN, indicating the presence of superoxide in neurons.

animals exposed to neonatal inflammation treated with BBG had lower mortality rate. Cauwels et al. (2014) demonstrated that the removal of extracellular ATP using systemic apyrase prevented the increase of cytokines and also prevented necrosis, mitochondrial damage, apoptosis, and death of animals. Thus, systemic blockade of P2X7R with BBG may have played similar effects as the systemic apyrase in the cytokine secretion and therefore, reducing the mortality rate.

Body weight gain is also an indicator of the impact of inflammatory processes during the neonatal period. Spencer et al. (2006) demonstrated that animals exposed to an inflammatory stimulus on the PND7 had a significantly lower body weight in PND74 when compared to controls. Similar findings were observed by Hodgson et al. (2001), which demonstrated that repeated inflammatory stimuli in the neonatal period is associated to limited body weight gain in adulthood. Our results support this data, whereas LPS-treated animals showed decreased body weight compared to controls in all time points from PND10 for males and females. Here, LPS treatment clearly affected body weight gain and the association with BBG treatment was able to reverse this effect only in males from PND45, but not in females.

We believe that the decreased body weight gain in the LPS-treated rats could be related to the reduction in frequency of feeding during the first week of life when the LPS injections were administered to the pups. Also, inflammation may alter levels of leptin and neuropeptide Y, which play a critical control over satiety and body weight in the long term (Schwartz et al., 2000; Sachot et al., 2004). The neonatal period is crucial for the development of the neural circuits that control feeding, and satiety and inflammation can also change it (Elmquist and Flier, 2004; Spencer et al., 2006). The mechanisms involved in the effects of P2X7R blockade on body weight are still unclear, but sexual dimorphism, in this case, may be associated with genetic and hormonal differences (Cario-Toumaniantz et al., 1998; Heiman-Patterson et al., 2005; Novak et al., 2010).

Oxidative stress is triggered by increased production of different free radicals (Hsieh and Yang, 2013). In our study, the production of ROS was assessed by the measurement of superoxide anion in response to systemic inflammation. Considering the experimental groups, regardless of the sex of animals, we noted that the animals exposed to systemic inflammation in the neonatal period presented a significantly higher superoxide production in the dentate gyrus of hippocampus, when compared to control animals. Most importantly, our findings suggest that the blockade of P2X7R with BBG during the inflammatory process down regulated the superoxide anion production in the brain of adult animals when compared to the animals that received LPS. This finding corroborates the studies of Feng et al. (2015) and Munoz et al. (2017), which demonstrated the attenuation of free radical production by blocking the activation of P2X7R.

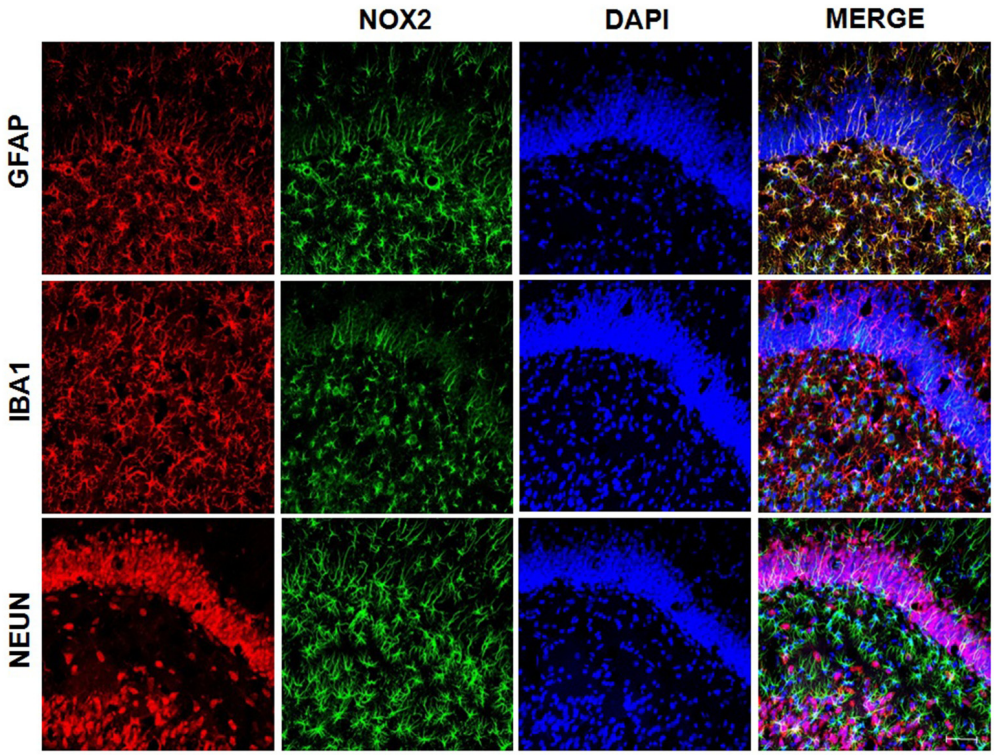

FIGURE 9 | gp91-phox/NOX2 expression on astrocytes. gp91-phox was detected using immunofluorescence. Confocal microscopy of hippocampus showed colocalization with glial fibrillary acid protein (GFAP), indicating its expression on astrocytes.

The relationship between oxidative stress in the CNS and systemic inflammation has been documented in the literature. Correa et al. (2013) demonstrated that 24 h after systemic administration of LPS in neonatal rats, there was an increased level of superoxide dismutase (SOD) and other proteins associated with antioxidant systems in the brain. It is known that NOX plays a significant role in the synthesis of ROS induced by the activation of P2X7R, which induces the increase of proinflammatory cytokines (Hewinson and MacKenzie, 2007; Mead et al., 2012; Jiang et al., 2015). Thus, activation of P2X7R contributes doubly to the increase of superoxide production and, consequently, may favor the maintenance of the vicious cycle of oxidative stress/inflammation/oxidative stress, which can be minimized by the use of antagonists of this receptor (Parvathenani et al., 2003; Pfeiffer et al., 2007).

In the present study, we demonstrated that the increased production of superoxide in the dentate gyrus of the hippocampus in adult rats exposed to neonatal inflammation was associated to an increased immunoreactivity for gp91-phox, the NOX2 catalytic subunit (Yu et al., 1998), which can be expressed by neuron, astrocyte and microglia (Park et al., 2007; Dohi et al., 2010; Li et al., 2014).

Each member of NOX family proteins reveals a distinct cellular and tissue distribution pattern with specific roles in the ROS production (Noguchi et al., 2008). These data corroborate with our findings, in which we observed that gp91-phox expression occurs particularly in astrocytes, although superoxide accumulation has been observed in neurons. It is known that superoxide, a diffusible messenger, can permeate cell membranes and acts as a neuron-glial transcellular signal (Atkins and Sweatt, 1999; Reyes et al., 2012; Spiers et al., 2015). On the other hand, the treatment with P2X7R antagonist leads to a decreased hippocampal production of superoxide and reduced immunoreactivity for gp91-phox. As the literature has demonstrated, this finding is consistent with the activation of the P2X7R, which is associated to an upregulation of NOX2, as suggested by Noguchi et al. (2008) and Deng et al. (2015), whereas C-terminal of P2X7R may regulate NOX2 activation.

Neonatal exposure to inflammatory process can lead to increased anxiety in adult animals, as cytokines modulate neurotransmitters turnover, hypothalamus-pituitary-adrenal axis, synaptic plasticity and neural circuits associated to emotional expression (Breivik et al., 2002; Salim et al., 2012). When comparing the different experimental groups, no significant difference was observed in the behavioral parameters evaluated in the EPM test for the LPS group as compared to the control group. This finding diverges from the study by Walker et al. (2004), who demonstrated that inflammatory stimuli on the 3rd and 5th days of life resulted in increased anxiety-associated behavior in the EPM test in PND80. However, the literature reveals controversial data. When using lower doses of LPS, where the neonatal exposure to 50 μg/Kg of LPS at PND3 and PND5, an increase in anxiety-like behavior was observed in male rats

(Walker et al., 2004). In contrast, Spencer et al. (2005) reported no significant changes in anxiety levels following administration of 100 μg/Kg of LPS at PND14 in male rats. In another report, with higher LPS dose, anxiety-like behavior was decreased in female rats given 1 mg/Kg at PND5 (Wang et al., 2013). Therefore, the effect of LPS injection on anxiety behavior in EPM test is highly dependent on the dose and time of LPS administration.

When assessing the effect of the sex of the animals on the anxiety behavior, females were less anxious than males, as they spent longer in the central platform and presented a greater number of entries in the open arms, and greater locomotor activity as compared to the males. These findings are in agreement with a previous report, which suggested that female rats show less anxious behavior when compared to male rats based on their performance in an EPM test (Johnston and File, 1991). However, there was no interaction between the treatments used and the sex of the animals in this study.

The exposure to an inflammatory insult such as LPS during the first week of life is likely to interfere with the normal developmental trajectory of the nociceptive system, leading to changes in the behavioral responses following re-exposure to noxious stimuli later in life (Zouikr et al., 2014). Our results suggested that neonatal LPS injections did not affect pain sensitivity assessed by hot-plate and tail-flick tests in adulthood. However, recent studies have shown the LPS injections induce hyperalgesia (Mason, 1993; Davies and Hagen, 1997; Zouikr et al., 2014). In another study, Yirmiya et al. (1994) demonstrated that LPS-induced analgesia began about 2 h after and disappeared 30 h after the administration of LPS. Considering these controversial results, further research is required to explain these findings.

It is known that females have lower levels of stress-induced analgesia, a consequence of differences in the endogenous opioid system (Kavaliers and Innes, 1987; Wiesenfeld-Hallin, 2005). Interestingly, considering only the sex independently of the experimental groups, there was no significant difference in latency between males and females in the hot-plate test. On the other hand, in the tail-flick test, females showed a significantly lower latency compared to males. However, we also did not observe interaction between the treatments used and the sex of the animals in both tests.

Although the primary function of the hippocampus is learning and memory (Eichenbaum et al., 1992), it is also associated with emotions and nociception (Ploghaus et al., 2001; McHugh et al., 2004; Liu and Chen, 2009; Vachon-Presseau et al., 2013). In this sense, evidence begins to appear that increased oxidative stress in the hippocampus may at least have relevance in triggering anxious behavior (de Oliveira et al., 2007). Considering the fact that the animals of the LPS group showed higher levels of oxidative stress than the animals of other experimental groups, it is interesting that they did not present alterations in behaviors associated with anxiety or in the sensitivity to pain once several studies suggest that oxidative stress has great relevance in triggering anxiety disorders and in altering nociception (de Oliveira et al., 2007; Bouayed et al., 2009; Raut and Ratka, 2009).

As already mentioned, our data diverges from the literature. We developed a chronic protocol, using several doses of LPS during an extended treatment time. On the other hand, previous reports usually refer to acute treatments, done with one or two doses of LPS injection, which interfered significantly in the results of anxiety and nociception presented, but even in literature, the results are paradoxical. Therefore, it is important to highlight that age and the LPS dose are critical in generating conflicting outcomes. These models have been designed for a clear understanding of the human condition, which leads to extensive variations in many studied parameters.

Our findings suggest critical functions of P2X7R-mediated oxidative stress and mortality. Importantly, inhibition of P2X7R by BBG has been found effective in reducing superoxide production that leads to inflammatory responses and mortality rate, conferring neuroprotection in adulthood. Furthermore, our study proposes that pharmacological modulation of P2X7R mediated by its antagonist may represent a potential therapeutic target in neurological diseases.

ETHICS STATEMENT

This study was carried out and approved in accordance with the recommendations of "Ethics Committee of UNIFESP."

AUTHOR CONTRIBUTIONS

CS conceived the study, carried out the laboratory experiments, behavioral tests, analyzed the data and performed the statistical analysis. JP and SR assisted drugs injection, behavioral tests, data collection and formatted the references. AM carried out the brain samples and helped to draft the article. MC performed immunofluorescence experiments, photographed, analyzed the images and helped to draft and critically revised the article. LM contributed with the study design and the article revision and interpreted the results. AL contributed with the study design, the data analysis, reagents, materials and critically revised the article. The work presented here was carried out in collaboration between all authors. All authors reviewed and approved the final manuscript.

FUNDING

This work was supported by Fundação de Amparo à Pesquisa do Estado de São Paulo (FAPESP) and Conselho Nacional de Desenvolvimento Científico e Tecnológico (CNPq; Brazil).

ACKNOWLEDGMENTS

We are grateful to the Center for the Development of Experimental Models in Medicine and Biology of the Universidade Federal de São Paulo (CEDEME—UNIFESP) for the animal supply and facilities. We would like to thank Professor Aparecida Emiko Hirata (Departmento de Fisiologia—UNIFESP); Francisco Rafael Martins Laurindo

(Faculdade de Medicina—USP); Ivarne Luis Dos Santos Tersariol (Departamento de Bioquímica—UNIFESP); Lucia Rossetti Lopes (Instituto de Ciências Biomédicas—USP) and Angelo Rafael Carpinelli (Instituto de Ciências Biomédicas—USP) for the *gp91-phox/NOX2* antibodies and technical assistance.

SUPPLEMENTARY MATERIAL

The Supplementary Material for this article can be found online at: https://www.frontiersin.org/articles/10.3389/fnbeh.2019.00240/full#supplementary-material.

REFERENCES

Atkins, C. M., and Sweatt, J. D. (1999). Reactive oxygen species mediate activity-dependent neuron-glia signaling in output fibers of the hippocampus. *J. Neurosci.* 19, 7241–7248. doi: 10.1523/JNEUROSCI.19-17-07241.1999

Bartlett, R., Sluyter, V., Watson, D., Sluyter, R., and Yerbury, J. J. (2017). P2X7 antagonism using Brilliant Blue G reduces body weight loss and prolongs survival in female SOD1G93A amyotrophic lateral sclerosis mice. *PeerJ* 5:e3064. doi: 10.7717/peerj.3064

Bedard, K., and Krause, K. H. (2007). The NOX family of ROS-generating NADPH oxidases: physiology and pathophysiology. *Physiol. Rev.* 87, 245–313. doi: 10.1152/physrev.00044.2005

Benatti, C., Alboni, S., Capone, G., Corsini, D., Caggia, F., Brunello, N., et al. (2009). Early neonatal inflammation affects adult pain reactivity and anxiety related traits in mice: genetic background counts. *Int. J. Dev. Neurosci.* 27, 661–668. doi: 10.1016/j.ijdevneu.2009.07.009

Bouayed, J., Rammal, H., and Soulimani, R. (2009). Oxidative stress and anxiety: relationship and cellular pathways. *Oxid. Med. Cell. Longev.* 2, 63–67. doi: 10.4161/oxim.2.2.7944

Breivik, T., Stephan, M., Brabant, G. E., Straub, R. H., Pabst, R., and von Hörsten, S. (2002). Postnatal lipopolysaccharide-induced illness predisposes to periodontal disease in adulthood. *Brain Behav. Immun.* 16, 421–438. doi: 10.1006/brbi.2001.0642

Burnstock, G., and Volonté, C. (2012). Editorial: pharmacology and therapeutic activity of purinergic drugs for disorders of the nervous system. *CNS Neurol Disord. Drug Targets* 11, 649–651. doi: 10.2174/187152712803581119

Cario-Toumaniantz, C., Loirand, G., Ferrier, L., and Pacaud, P. (1998). Non-genomic inhibition of human P2X7 purinoceptor by 17β-oestradiol. *J. Physiol.* 508, 659–666. doi: 10.1111/j.1469-7793.1998.659bp.x

Cartens, E., and Wilson, C. (1993). Rat tail flick reflex: magnitude measurement of stimulus response function, supression by morphine and habituation. *J. Neuropharmacol.* 70, 630–639. doi: 10.1152/jn.1993.70.2.630

Cauwels, A., Rogge, E., Vandendriessche, B., Shiva, S., and Brouckaert, P. (2014). Extracellular ATP drives systemic inflammation, tissue damage and mortality. *Cell Death Dis.* 5:e1102. doi: 10.1038/cddis.2014.70

Cervetto, C., Frattaroli, D., Maura, G., and Marcoli, M. (2013). Motor neuron dysfunction in a mouse model of ALS: gender-dependent effect of P2X7 antagonism. *Toxicology* 311, 69–77. doi: 10.1016/j.tox.2013.04.004

Correa, F., Ljunggren, E., Patil, J., Wang, X., Hagberg, H., Mallard, C., et al. (2013). Time-dependent effects of systemic lipopolysaccharide injection on regulators of antioxidant defence Nrf2 and PGC-1α in the neonatal rat brain. *Neuroimmunomodulation* 20, 185–193. doi: 10.1159/000347161

Díaz-Hernández, M., Díez-Zaera, M., Sánchez-Nogueiro, J., Gómez-Villafuertes, R., Canals, J. M., Alberch, J., et al. (2009). Altered P2X7-receptor level and function in mouse models of Huntington's disease and therapeutic efficacy of antagonist administration. *FASEB J.* 23, 1893–1906. doi: 10.1096/fj.08-122275

D'Amour, F. E., and Smith, D. L. (1941). A method for determining loss of pain sensation. *J. Pharmacal. Exp. Ther.* 72, 74–79.

Davies, M. G., and Hagen, P. O. (1997). Systemic inflammatory response syndrome. *Br. J. Surg.* 84, 920–935. doi: 10.1002/bjs.1800840707

de Oliveira, M. R., Silvestrin, R. B., Mello E Souza, T., and Moreira, J. C. (2007). Oxidative stress in the hippocampus, anxiety-like behavior and decreased locomotory and exploratory activity of adult rats: effects of subacute vitamin A supplementation at therapeutic doses. *Neurotoxicology* 28, 1191–1199. doi: 10.1016/j.neuro.2007.07.008

Deng, Y., Guo, X. L., Yuan, X., Shang, J., Zhu, D., and Liu, H. G. (2015). P2X7 receptor antagonism attenuates the intermittent hypoxia-induced spatial deficits in a murine model of sleep apnea *via* inhibiting neuroinflammation and oxidative stress. *Chin. Med. J.* 128, 2168–2175. doi: 10.4103/0366-6999.162495

Dinel, A.-L., Joffre, C., Trifilieff, P., Aubert, A., Foury, A., Le Ruyet, P., et al. (2014). Inflammation early in life is a vulnerability factor for emotional behavior at adolescence and for lipopolysaccharide-induced spatial memory and neurogenesis alteration at adulthood. *J. Neuroinflammation* 11:155. doi: 10.1186/s12974-014-0155-x

Dohi, K., Ohtaki, H., Nakamachi, T., Yofu, S., Satoh, K., Miyamoto, K., et al. (2010). Gp91 phox (NOX2) in classically activated microglia exacerbates traumatic brain injury. *J. Neuroinflammation* 7:41. doi: 10.1186/1742-2094-7-41

Eddy, N. B., and Leimbach, D. (1953). Synthetic analgesics: II. Dithienylbutenyl- and dithienylbutylamines. *J. Pharmacal. Exp. Ther.* 107, 385–393.

Eichenbaum, H., Otto, T., and Cohen, N. J. (1992). The hippocampus—what does it do? *Behav. Neural Biol.* 57, 2–36. doi: 10.1016/0163-1047(92)90724-i

Elmquist, J. K., and Flier, J. S. (2004). The fat-brain axis enters a new dimension. *Science* 304, 63–64. doi: 10.1126/science.1096746

Fan, L. W., Pang, Y., Lin, S., Tien, L. T., Ma, T., Rhodes, P. G., et al. (2005). Minocycline reduces lipopolysaccharide-induced neurological dysfunction and brain injury in the neonatal rat. *J. Neurosci. Res.* 82, 71–82. doi: 10.1002/jnr.20623

Fan, L. W., Tien, L. T., Lin, R. C., Simpson, K. L., Rhodes, P. G., and Cai, Z. (2011). Neonatal exposure to lipopolysaccharide enhances vulnerability of nigrostriatal dopaminergic neurons to rotenone neurotoxicity in later life. *Neurobiol. Dis.* 44, 304–316. doi: 10.1016/j.nbd.2011.07.011

Fan, L. W., Tien, L. T., Mitchell, H. J., Rhodes, P. G., and Cai, Z. (2008). α-Phenyl-n-tert-butyl-nitrone ameliorates hippocampal injury and improves learning and memory in juvenile rats following neonatal exposure to lipopolysaccharide. *Eur. J. Neurosci.* 27, 1475–1484. doi: 10.1111/j.1460-9568.2008.06121.x

Feng, L., Chen, Y., Ding, R., Fu, Z., Yang, S., Deng, X., et al. (2015). P2X7R blockade prevents NLRP3 inflammasome activation and brain injury in a rat model of intracerebral hemorrhage: involvement of peroxynitrite. *J. Neuroinflammation* 12:190. doi: 10.1186/s12974-016-0627-2

Gao, H. M., Jiang, J., Wilson, B., Zhang, W., Hong, J. S., and Liu, B. (2002). Microglial activation-mediated delayed and progressive degeneration of rat nigral dopaminergic neurons: relevance to Parkinson's disease. *J. Neurochem.* 81, 1285–1297. doi: 10.1046/j.1471-4159.2002.00928.x

Gilles, F. H., Leviton, A., and Kerr, C. S. (1976). Endotoxin leucoencephalopathy in the telencephalon of the newborn kitten. *J. Neurol. Sci.* 27, 183–191. doi: 10.1016/0022-510x(76)90060-5

Heiman-Patterson, T. D., Deitch, J. S., Blankenhorn, E. P., Erwin, K. L., Perreault, M. J., Alexander, B. K., et al. (2005). Background and gender effects on survival in the TgN(SOD1–G93A)1Gur mouse model of ALS. *J. Neurol. Sci.* 236, 1–7. doi: 10.1016/j.jns.2005.02.006

Hewinson, J., and MacKenzie, A. B. (2007). P2X7 receptor-mediated reactive oxygen and nitrogen species formation: from receptor to generators. *Biochem. Soc. Trans.* 35, 1168–1170. doi: 10.1042/bst0351168

Hodgson, D. M., Knott, B., and Walker, F. R. (2001). Neonatal endotoxin exposure influences hpa responsivity and impairs tumor immunity in fischer 344 rats in adulthood. *Pediatr. Res.* 50, 750–755. doi: 10.1203/00006450-200112000-00020

Hsieh, H. L., and Yang, C. M. (2013). Role of redox signaling in neuroinflammation and neurodegenerative diseases. *Biomed Res. Int.* 2013:484613. doi: 10.1155/2013/484613

Jiang, T., Hoekstra, J., Heng, X., Kang, W., Ding, J., Liu, J., et al. (2015). P2X7 receptor is critical in α-synuclein—mediated microglial NADPH oxidase activation. *Neurobiol. Aging* 36, 2304–2318. doi: 10.1016/j.neurobiolaging.2015.03.015

Johnston, A. L., and File, S. E. (1991). Sex differences in animal tests of anxiety. *Physiol. Behav.* 49, 245–250. doi: 10.1016/0031-9384(91)90039-q

Lambert, A. J., and Brand, M. D. (2009). Reactive oxygen species production by mitochondria. *Methods Mol. Biol.* 554, 165–181. doi: 10.1007/978-1-59745-521-3_11

LaPrairie, J. L., and Murphy, A. Z. (2007). Female rats are more vulnerable to the long-term consequences of neonatal inflammatory injury. *Pain* 132, S124–S133. doi: 10.1016/j.pain.2007.08.010

Lezak, K. R., Missig, G., and Carlezon, W. A. Jr. (2017). Behavioral methods to study anxiety in rodents. *Dialogues Clin. Neurosci.* 19, 181–191.

Li, H., Wang, Y., Feng, D., Liu, Y., Xu, M., Gao, A., et al. (2014). Alterations in the time course of expression of the Nox family in the brain in a rat experimental cerebral ischemia and reperfusion model: effects of melatonin. *J. Pineal Res.* 57, 110–119. doi: 10.1111/jpi.12148

Ling, Z., Zhu, Y., Tong, C., Snyder, J. A., Lipton, J. W., and Carvey, P. M. (2006). Progressive dopamine neuron loss following supra-nigral lipopolysaccharide (LPS) infusion into rats exposed to LPS prenatally. *Exp. Neurol.* 199, 499–512. doi: 10.1016/j.expneurol.2006.01.010

Liu, M. G., and Chen, J. (2009). Roles of the hippocampal formation in pain information processing. *Neurosci. Bull.* 25, 237–266. doi: 10.1007/s12264-009-0905-4

Kavaliers, M., and Innes, D. (1987). Stress-induced opioid analgesia and activity in deer mice: sex and population differences. *Brain Res.* 425, 49–56. doi: 10.1016/0006-8993(87)90482-3

Mason, P. (1993). Lipopolysaccharide induces fever and decreases tail flick latency in awake rats. *Neurosci. Lett.* 154, 134–136. doi: 10.1016/0304-3940(93)90189-r

McHugh, S. B., Deacon, R. M., Rawlins, J. N., and Bannerman, D. M. (2004). Amygdala and ventral hippocampus contribute differentially to mechanisms of fear and anxiety. *Behav. Neurosci.* 118, 63–78. doi: 10.1037/0735-7044.118.1.63

Mead, E. L., Mosley, A., Eaton, S., Dobson, L., Heales, S. J., and Pocock, J. M. (2012). Microglial neurotransmitter receptors trigger superoxide production in microglia; consequences for microglial-neuronal interactions. *J. Neurochem.* 121, 287–301. doi: 10.1111/j.1471-4159.2012.07659.x

Ming, Z., Sawicki, G., and Bekar, L. K. (2015). Acute systemic LPS-mediated inflammation induces lasting changes in mouse cortical neuromodulation and behavior. *Neurosci. Lett.* 590, 96–100. doi: 10.1016/j.neulet.2015.01.081

Monif, M., Reid, C. A., Powell, K. L., Smart, M. L., and Williams, D. A. (2009). The P2X7 receptor drives microglial activation and proliferation: a trophic role for P2X7R pore. *J. Neurosci.* 29, 3781–3791. doi: 10.1523/JNEUROSCI.5512-08.2009

Munoz, F. M., Gao, R., Tian, Y., Henstenburg, B. A., Barrett, J. E., and Hu, H. (2017). Neuronal P2X7 receptor-induced reactive oxygen species production contributes to nociceptive behavior in mice. *Sci. Rep.* 7:3539. doi: 10.1038/s41598-017-03813-7

Noguchi, T., Ishii, K., Fukutomi, H., Naguro, I., Matsuzawa, A., Takeda, K., et al. (2008). Requirement of reactive oxygen species-dependent activation of ASK1–p38 MAPK pathway for extracellular ATP-induced apoptosis in macrophage. *J. Biol. Chem.* 283, 7657–7665. doi: 10.1074/jbc.M708402200

Novak, I., Jans, I. M., and Wohlfahrt, L. (2010). Effect of $P2X_7$ receptor knockout on exocrine secretion of pancreas, salivary glands and lacrimal glands. *J. Physiol.* 588, 3615–3627. doi: 10.1113/jphysiol.2010.190017

Okuyama, S., Makihata, N., Yoshimura, M., Amakura, Y., Yoshida, T., Nakajima, M., et al. (2013). Oenothein B suppresses lipopolysaccharide (LPS)-induced inflammation in the mouse brain. *Int. J. Mol. Sci.* 14, 9767–9778. doi: 10.3390/ijms14059767

Püntener, U., Booth, S. G., Perry, V. H., and Teeling, J. L. (2012). Long-term impact of systemic bacterial infection on the cerebral vasculature and microglia. *J. Neuroinflammation* 9:146. doi: 10.1186/1742-2094-9-146

Park, L., Anrather, J., Girouard, H., Zhou, P., and Iadecola, C. (2007). Nox2-derived reactive oxygen species mediate neurovascular dysregulation in the aging mouse brain. *J. Cereb. Blood Flow Metab.* 27, 1908–1918. doi: 10.1038/sj.jcbfm.9600491

Parvathenani, L. K., Tertyshnikova, S., Greco, C. R., Roberts, S. B., Robertson, B., and Posmantur, R. (2003). $P2X_7$ mediates superoxide production in primary microglia and is up-regulated in a transgenic mouse model of Alzheimer's disease. *J. Biol. Chem.* 278, 13309–13317. doi: 10.1074/jbc.m209478200

Pellow, S., Chopin, P., File, S. E., and Briley, M. (1985). Validation of open:closed arm entries in an elevated plus-maze as a measure of anxiety in the rat. *J. Neurosci. Methods* 14, 149–167. doi: 10.1016/0165-0270(85)90031-7

Peng, W. M. L., Cotrina, X., Han, H., Yu, L., Bekar, L., Blum, T., et al. (2009). Systemic administration of an antagonist of the ATP-sensitive receptor P2X7 improves recovery after spinal cord injury. *Proc. Natl. Acad. Sci. U S A* 106, 12489–12493. doi: 10.1073/pnas.0902531106

Peng, L., Zhu, M., Yang, Y., Weng, Y., Zou, W., Zhu, X., et al. (2019). Neonatal lipopolysaccharide challenge induces long-lasting spatial cognitive impairment and dysregulation of hippocampal histone acetylation in mice. *Neuroscience* 398, 76–87. doi: 10.1016/j.neuroscience.2018.12.001

Pfeiffer, Z. A., Guerra, A. N., Hill, L. M., Gavala, M. L., Prabhu, U., Aga, M., et al. (2007). Nucleotide receptor signaling in murine macrophages is linked to reactive oxygen species generation. *Free Radic. Biol. Med.* 42, 1506–1516. doi: 10.1016/j.freeradbiomed.2007.02.010

Ploghaus, A., Narain, C., Beckmann, C. F., Clare, S., Bantick, S., Wise, R., et al. (2001). Exacerbation of pain by anxiety is associated with activity in a hippocampal network. *J. Neurosci.* 21, 9896–9903. doi: 10.1523/JNEUROSCI.21-24-09896.2001

Politis, M., Su, P., and Piccini, P. (2012). Imaging of microglia in patients with neurodegenerative disorders. *Front. Pharmacol.* 3:96. doi: 10.3389/fphar.2012.00096

Qian, L., Flood, P. M., and Hong, J. S. (2010). Neuroinflammation is a key player in Parkinson's disease and a prime target for therapy. *J. Neural Transm.* 117, 971–979. doi: 10.1007/s00702-010-0428-1

Raetz, C. R., and Whitfield, C. (2002). Lipopolysaccharide endotoxins. *Annu. Rev. Biochem.* 71, 635–700. doi: 10.1146/annurev.biochem.71.110601.135414

Raut, A., and Ratka, A. (2009). Oxidative damage and sensitivity to nociceptive stimulus and opioids in aging rats. *Neurobiol. Aging* 30, 910–919. doi: 10.1016/j.neurobiolaging.2007.09.010

Ren, K., Anseloni, V., Zou, S. P., Wade, E. B., Novikova, S. I., Ennis, M., et al. (2004). Characterization of basal and re-inflammation-associated long-term alteration in pain responsivity following short-lasting neonatal local inflammatory insult. *Pain* 110, 588–596. doi: 10.1016/s0304-3959(04)00196-4

Reyes, R. C., Brennan, A. M., Shen, Y., Baldwin, Y., and Swanson, R. A. (2012). Activation of neuronal NMDA receptors induces superoxide-mediated oxidative stress in neighboring neurons and astrocytes. *J. Neurosci.* 32, 12973–12978. doi: 10.1523/JNEUROSCI.1597-12.2012

Rousset, C. I., Kassem, J., Aubert, A., Planchenault, D., Gressens, P., Chalon, S., et al. (2013). Maternal exposure to lipopolysaccharide leads to transient motor dysfunction in neonatal rats. *Dev. Neurosci.* 35, 172–181. doi: 10.1159/000346579

Ryu, J. K., and McLarnon, J. G. (2008). Block of purinergic P2X7 receptor is neuroprotective in an animal model of Alzheimer's disease. *Neuroreport* 19, 1715–1719. doi: 10.1097/wnr.0b013e3283179333

Sachot, C., Poole, S., and Luheshi, G. N. (2004). Circulating leptin mediates lipopolysaccharide-induced anorexia and fever in rats. *J. Physiol.* 561, 263–272. doi: 10.1113/jphysiol.2004.074351

Salim, S., Chugh, G., and Asghar, M. (2012). Inflammation in anxiety. *Adv. Protein Chem. Struct. Biol.* 88, 1–25. doi: 10.1016/B978-0-12-398314-5.00001-5

Schwartz, M. W., Woods, S. C., Porte, D. Jr., Seeley, R. J., and Baskin, D. G. (2000). Central nervous system control of food intake. *Nat. Med.* 404, 661–671. doi: 10.1038/35007534

Simons, S. H., and Tibboel, D. (2006). Pain perception development and maturation. *Semin. Fetal Neonatal Med.* 11, 227–231. doi: 10.1016/j.siny.2006.02.010

Spencer, S. J., Heida, J. G., and Pittman, Q. J. (2005). Early life immune challenge-effects on behavioural indices of adult rat fear and anxiety. *Behav. Brain Res.* 164, 231–238. doi: 10.1016/j.bbr.2005.06.032

Spencer, S. J., Martin, S., Mouihate, A., and Pittman, Q. J. (2006). Early-life immune challenge: defining a critical window for effects on adult responses to immune challenge. *Neuropsychopharmacology* 31, 1910–1918. doi: 10.1038/sj.npp.1301004

Sperlágh, B., and Illes, P. (2014). P2X7 receptor: an emerging target in central nervous system diseases. *Trends Pharmacol. Sci.* 35, 537–547. doi: 10.1016/j.tips.2014.08.002

Spiers, J. G., Chen, H. J., Sernia, C., and Lavidis, N. A. (2015). Activation of the hypothalamic-pituitary-adrenal stress axis induces cellular oxidative stress. *Front. Neurosci.* 8:456. doi: 10.3389/fnins.2014.00456

Stoll, B. J., Hansen, N. I., Bell, E. F., Shankaran, S., Laptook, A. R., Walsh, M. C., et al. (2010). Neonatal outcomes of extremely preterm infants from the

NICHD neonatal research network. *Pediatrics* 126, 443–456. doi: 10.1542/peds.2009-2959

Ulrich, H., Abbracchio, M. P., and Burnstock, G. (2012). Extrinsic purinergic regulation of neural stem/progenitor cells: implications for CNS development and repair. *Stem Cell Rev. Rep.* 8, 755–767. doi: 10.1007/s12015-012-9372-9

Vachon-Presseau, E., Roy, M., Martel, M. O., Caron, E., Marin, M. F., Chen, J., et al. (2013). The stress model of chronic pain: evidence from basal cortisol and hippocampal structure and function in humans. *Brain* 136, 815–827. doi: 10.1093/brain/aws371

Vergnano, S., Menson, E., Kennea, N., Embleton, N., Russell, A. B., Watts, T., et al. (2011). Neonatal infections in England: the NeonIN surveillance network. *Arch. Dis. Child. Fetal Neonatal Ed.* 96, F9–F14. doi: 10.1136/adc.2009.178798

Walker, F. R., March, J., and Hodgson, D. M. (2004). Endotoxin exposure in early life alters the development of anxiety-like behaviour in the Fischer 344 rat. *Behav. Brain Res.* 154, 63–69. doi: 10.1016/j.bbr.2004.01.019

Wang, K. C., Fan, L. W., Kaizaki, A., Pang, Y., Cai, Z., and Tien, L. T. (2013). Neonatal lipopolysaccharide exposure induces long-lasting learning impairment, less anxiety-like response and hippocampal injury in adult rats. *Neuroscience* 234, 146–157. doi: 10.1016/j.neuroscience.2012.12.049

Wiesenfeld-Hallin, Z. (2005). Sex differences in pain perception. *Gend. Med.* 2, 137–145. doi: 10.1016/s1550-8579(05)80042-7

Woolfe, G., and Macdonald, A. D. (1943). The evaluation of the analgesic action of pethidine hydrochloride (demerol). *J. Pharmacal. Exp. Ther.* 80, 300–307.

Yirmiya, R., Rosen, H., Donchin, O., and Ovadia, H. (1994). Behavioral effects of lipopolysaccharide in rats: involvement of endogenous opioids. *Brain Res.* 648, 80–86. doi: 10.1016/0006-8993(94)91908-9

Yu, L., Quinn, M. T., Cross, A. R., and Dinauer, M. C. (1998). Gp91phox is the heme binding subunit of the superoxide-generating NADPH oxidase. *Proc. Natl. Acad. Sci. U S A* 95, 7993–7998. doi: 10.1073/pnas.95.14.7993

Zouikr, I., James, M. H., Campbell, E. J., Clifton, V. L., Beagley, K. W., Dayas, C. V., et al. (2014). Altered formalin-induced pain and Fos induction in the periaqueductal grey of preadolescent rats following neonatal LPS exposure. *PLoS One* 9:98382. doi: 10.1371/journal.pone.0098382

Conflict of Interest: The authors declare that the research was conducted in the absence of any commercial or financial relationships that could be construed as a potential conflict of interest.

frontiers in Behavioral Neuroscience

ORIGINAL RESEARCH
published: 24 January 2020
doi: 10.3389/fnbeh.2019.00284

Financial Stress Interacts With *CLOCK* Gene to Affect Migraine

*Daniel Baksa[1,2], Xenia Gonda[3,4,5], Nora Eszlari[2,3], Peter Petschner[2,5], Veronika Acs[6], Lajos Kalmar[6,7], J. F. William Deakin[8], Gyorgy Bagdy[2,3,5] and Gabriella Juhasz[1,2,5]**

[1]SE-NAP2 Genetic Brain Imaging Migraine Research Group, Hungarian Brain Research Program, Semmelweis University, Budapest, Hungary, [2]Department of Pharmacodynamics, Faculty of Pharmacy, Semmelweis University, Budapest, Hungary, [3]NAP-2-SE New Antidepressant Target Research Group, Hungarian Brain Research Program, Semmelweis University, Budapest, Hungary, [4]Department of Psychiatry and Psychotherapy, Semmelweis University, Budapest, Hungary, [5]MTA-SE Neuropsychopharmacology and Neurochemistry Research Group, Hungarian Academy of Sciences, Semmelweis University, Budapest, Hungary, [6]Research Centre for Natural Sciences, Institute of Enzymology, Budapest, Hungary, [7]Department of Veterinary Medicine, University of Cambridge, Cambridge, United Kingdom, [8]Neuroscience and Psychiatry Unit, The University of Manchester and Manchester Academic Health Sciences Centre, Manchester, United Kingdom

OPEN ACCESS

Edited by:
Graziano Pinna,
University of Illinois at Chicago, United States

Reviewed by:
Francisco J. Monje,
Medical University of Vienna, Austria
Anat Lan,
Ben-Gurion University of the Negev, Israel

***Correspondence:**
Gabriella Juhasz
juhasz.gabriella@pharma.semmelweis-univ.hu

Specialty section:
This article was submitted to Emotion Regulation and Processing, a section of the journal Frontiers in Behavioral Neuroscience

Received: *22 February 2019*
Accepted: *12 December 2019*
Published: *24 January 2020*

Citation:
Baksa D, Gonda X, Eszlari N, Petschner P, Acs V, Kalmar L, Deakin JFW, Bagdy G and Juhasz G (2020) Financial Stress Interacts With CLOCK Gene to Affect Migraine. Front. Behav. Neurosci. 13:284. doi: 10.3389/fnbeh.2019.00284

Previous studies suggested that both maladaptive stress response and circadian dysregulation might have a role in the background of migraine. However, effects of circadian genes on migraine have not been tested yet. In the present study, we investigated the main effect of rs10462028 of the circadian locomotor output cycles kaput (*CLOCK*) gene and its interaction with different stress factors on migraine. In our cross-sectional study 2,157 subjects recruited from Manchester and Budapest completed the ID-Migraine questionnaire to detect migraine type headaches (migraineID). Additional stress factors were assessed by a shortened version of the Childhood Trauma Questionnaire, the List of Threatening Experiences questionnaire, and a validated questionnaire to identify financial difficulties. Rs10462028 showed no main genetic effect on migraineID. However, chronic stress indexed by financial difficulties showed a significant interaction effect with rs10462028 (p = 0.006 in recessive model) on migraineID. This result remained significant after correction for lifetime bipolar and unipolar depression and was replicated in both subsamples, although only a trend effect was reached after Bonferroni-correction, which is the strictest correction not considering interdependences. Childhood adversity (CHA) and Recent negative life events (RLE) showed no significant gene × stress interaction with rs10462028. In addition, *in silico* analysis demonstrated that the genetic region tagged by rs10462028 alters the binding of several miRNAs. Our exploratory study suggests that variations in the *CLOCK* gene, with moderating effect on gene function through miRNA binding, in interaction with financial difficulties might influence the risk of migraine-type headaches. Thus, financial hardship as a chronic stress factor may affect migraine through altering circadian rhythms.

Keywords: migraine, circadian rhythms, circadian locomotor output cycles kaput, financial hardship, chronic stress, gene × environment interaction

INTRODUCTION

Migraine is a debilitating disorder affecting approximately one billion people worldwide (Gormley et al., 2016). Despite extensive research, its pathomechanism is still questionable. Migraine is heritable with estimated values of 0.34–0.57 (Chasman et al., 2016) reflecting an important role of environmental factors, also. A large number of genes of small effects appear to be involved in migraine (Anttila et al., 2013; Gormley et al., 2016), and their interactions with environmental factors have also been suggested (Sauro and Becker, 2009; Juhasz et al., 2017) but there is a significant lack of gene × environment interaction studies of migraine. As our knowledge about the pathogenesis of migraine accumulates, we may still overlook important contributing factors. One of these somewhat unacknowledged components might be circadian rhythmicity.

Circadian rhythms regulate several important physiological parameters (Johnston, 2014) enabling the organism to anticipate and adapt to environmental changes as a form of predictive homeostatis (Moore-Ede, 1986). Circadian dysregulation has been connected previously to various diseases (Hansen et al., 2011), including depression (Kishi et al., 2009) which shows a strong comorbidity with migraine (Breslau et al., 2003).

Several studies revealed circadian periodicity of migraine attack onset (van Oosterhout et al., 2018), but the underlying mechanism is not understood yet (Gori et al., 2012). Sleeping problems are also regular among migraineurs (Rains, 2018). Melatonin also might have a role in the pathophysiology of migraine, for example through the hypothalamic output of melatonin cycle influencing the trigeminal nucleus caudalis, a known component of migraine pathophysiology (Vogler et al., 2006). Related investigations mostly show lower levels of melatonin among migraineurs vs. controls (Vogler et al., 2006). A recent study (van Oosterhout et al., 2018) suggested a different setting of the circadian pacemaker among migraineurs: migraineurs compared to headache-free controls declared to be more affected by changes in circadian rhythm and more prone to have early or late chronotypes. This suggestion may be supported by genetic data: in two families with advanced sleep phase syndrome, migraine associated with a mutation in the casein kinase Iδ gene (*CK1*δ) showing phosphorylating effect on Per2 circadian protein (Brennan et al., 2013).

All these data together suggest a possible connection between circadian rhythms and migraine. However, the connection between (common) migraine headache and circadian genes has not been investigated yet.

The circadian pacemaker's (suprachiasmatic nucleus—SCN) 24-h time-keeping capacity arises from a transcriptional/post-translation feedback loop with rhythmic expression of circadian genes (Hansen et al., 2011). One of these primary genes is circadian locomotor output cycles kaput gene (*CLOCK*) working as a transcriptional activator in the circadian clock mechanism. For our investigation we selected rs10462028 of *CLOCK* (**Figure 1**), which has been used as a tagSNP of *CLOCK* in a previous study showing its association with bipolar disorder (Soria et al., 2010)—a comorbid disease of migraine with overlapping genetic factors (Oedegaard et al., 2010).

Recent meta-analyses of genome-wide association studies (GWASs) for migraine (Anttila et al., 2013; Gormley et al., 2016) have not identified *CLOCK* as a susceptibility gene for migraine. However, besides genetic factors, environmental factors are important elements to address in migraine research, especially stress: as the disease has been connected to several stressors, including various forms of childhood abuse (Tietjen, 2016), recent negative life events (RLE; Juhasz et al., 2017), and low socioeconomic status (Stewart et al., 2013). A recent review (Koch et al., 2017) also discusses the connection between circadian rhythms and stress which is based on the interaction of the hypothalamic-pituitary-adrenal axis and autonomic nervous system, both playing roles in stress-related regulation and having strong circadian inputs.

A review (Sauro and Becker, 2009) collected multiple roles of stress in migraine. Stress is the factor most often listed by migraineurs as a trigger of their attacks. It can amplify attack intensity and duration and might be a risk factor for migraine chronification. Stress may play an important role in migraine comorbidities: for example, a prospective longitudinal study confirmed the known bidirectional connection of migraine and depression, but this significant association disappeared after controlling for the measured stress factors (Swanson et al., 2013). This strong connection of migraine and stress can be explained by the concept of maladaptive stress response among migraineurs: repeated stress leads to allostatic load causing alterations in normal homeostatic processes, failure in habituation, and closing of the stress response (Borsook et al., 2012). The "migraine brain" shows an enhanced perception of environmental stimuli (for a review see Schwedt and Chong, 2015) and structural and functional alterations in many brain regions including the ones that are directly involved in stress response (for example: amygdala, hypothalamus, hippocampus, prefrontal cortex; Borsook et al., 2012). These data confirm the need to include stress factors in migraine studies.

To further investigate the role of circadian rhythm in migraine, we tested in our exploratory study the effect of rs10462028 on migraine in interaction with three forms of stress that has been previously connected to migraine: childhood adversity (CHA), RLE, and low socioeconomic status in the form of financial difficulties.

MATERIALS AND METHODS

Subjects

Two-thousand one-hundred and fifty-seven subjects were recruited through general practices and advertisements from Greater Manchester, UK (n = 1,277) and Budapest, Hungary (n = 880; aged between 18 and 60). The study was held under the aegis of NewMood (New Molecules in Mood Disorders, 2004-2009), an EU funded research program about pathomechanism of depression and related conditions. Our study was approved by the local Ethics Committees (Scientific and Research Ethics Committee of the Medical Research Council, Budapest, Hungary, ad.225/KO/2005; ad.323-60/2005-1018EKU

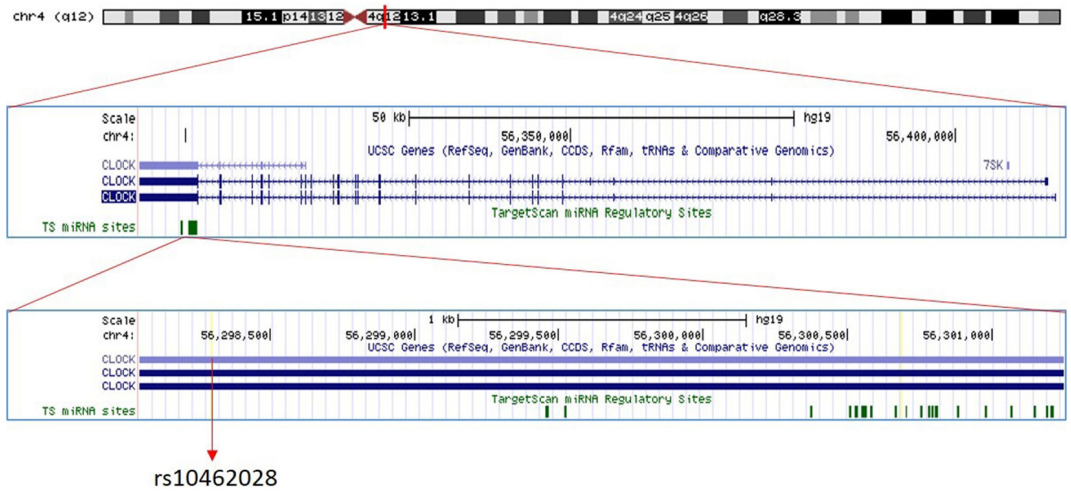

FIGURE 1 | The position of *circadian locomotor output cycles kaput (CLOCK)* rs10462028. The position of rs10462028 on *CLOCK* gene which is located on chromosome four is shown. Created with UCSC Genome Browser (https://genome.ucsc.edu/).

and ad.226/KO/2005; ad.323-61/2005-1018 EKU; North Manchester Local Research Ethics Committee, Manchester, UK REC reference number: 05/Q1406/26) and was carried out in accordance with the Declaration of Helsinki. All participants administered written informed consent to the study. In the present investigation, we selected participants who were of European white origin, completed the questionnaires, and consented to DNA analysis. In every analysis we included subjects showing all the necessary data for the investigated variables. The total subject number was reached after screening for the following data: ethnicity, gender, age, migraine status, and rs10462028 genotype. Further details of the recruitment strategies and response rates can be found in our earlier publications (Juhasz et al., 2009; Lazary et al., 2009).

Questionnaires

Brief standard questionnaires were administered for the study (English and Hungarian versions, respectively). The background questionnaire assembled information about socio-demographic data, personal and family psychiatric history. Gender, age, ethnicity, and reported lifetime bipolar disorder (MANIC) and lifetime depression (DEPR) data were derived from this validated questionnaire (Juhasz et al., 2011).

The ID-migraine questionnaire was used to measure migraine (migraineID). It is a validated screening tool for migraine (Lipton et al., 2003), which includes three items of the main migraine symptoms: nausea, photophobia, and disability (experienced in the past 3 months). In the present study, we defined migraineID as YES answers to two or three migraine symptom questions—this criterion has 0.93 positive predictive value of having migraine based on Lipton et al. (2003).

The following tools were applied to capture different stress factors. A shortened version of the Childhood Trauma Questionnaire (Bernstein et al., 1997) was our previously validated (Juhasz et al., 2011) tool to measure CHA. The four items of the questionnaire relate to emotional or physical abuse and neglect. It was completed with an additional question about potential loss of parents during childhood. RLE were measured with the validated List of Threatening Experiences questionnaire (Brugha et al., 1985). Financial hardship (FINANC) was derived from the background questionnaire and was previously used to test gene × environmental interaction effect in a study of ours (Sarginson et al., 2014). It captures a personal feeling of financial status (instead of a direct question about income). The original FINANC variable contained five categories, but three categories of FINANC were used for the primary analysis (combining the first two and the last two categories) to gain more appropriate sample sizes: (1) "*living very/quite comfortably*"; (2) "*just getting by*"; and (3) "*finding it difficult to make ends meet/not able to make ends meet.*"

Genotyping

Genomic DNA was derived from buccal mucosa cells (Juhasz et al., 2009). After extraction of DNA the Sequenom® MassARRAY technology (Sequenom®, San Diego, CA, USA[1]) was used to normalize and genotype the samples.

Rs10462028 SNP was selected as a haplotype tag of the 3′-UTR region of the *CLOCK* gene (Haploview[2]). Genotyping was performed according to the ISO 9001:2000 requirements and kept blinded with regard to phenotypic data.

The minor allele frequencies of the selected single nucleotide polymorphism (SNP) can be seen in **Table 1B**.

Functional Prediction of rs10462028

According to the 1,000 Genomes database[3] rs10462028 is in high linkage disequilibrium (LD; $r^2 > 0.8$) with 70 SNPs covering

[1]https://www.gene-quantification.de/sequenom/
[2]https://www.broadinstitute.org/haploview/haploview
[3]http://www.internationalgenome.org/data

TABLE 1 | Details of the investigated samples and statistical results of the comparison between Manchester and Budapest subsamples.

	Total sample	Manchester	Budapest	Difference (Manchester vs. Budapest)
A. Phenotypic description				
Demographics				
Participant number (*n*)	2,157	1,277	880	
Female (*n*, %)	1,503 (69.7%)	893 (69.9%)	610 (69.3%)	$\chi^2 = 0.092$, $p = 0.761$
Age (mean ± SEM)	32.9 (±0.22)	34.02 (±0.29)	31.3 (±0.36)	**T = −5.982, $p < 0.0001$**
Migraine status				
migraineID (*n*, %)	600 (27.8%)	399 (31.2%)	201 (22.8%)	**$\chi^2 = 18.326$, $p < 0.0001$**
Depression				
Reported lifetime depression (*n*, %)	907 (42%)	713 (55.8%)	194 (22%)	**$\chi^2 = 244.087$, $p < 0.0001$**
Bipolar disorder				
Reported lifetime bipolar disorder (*n*, %)	69 (3.2%)	51 (4%)	18 (2%)	**$\chi^2 = 6.386$, $p = 0.012$**
Stress factors				
Recent negative life events categories (*n*, %)				
No or mild	1,435 (66.5%)	821 (64.3%)	614 (69.8%)	**$\chi^2 = 14.654$, $p < 0.0001$**
Moderate	400 (18.5%)	237 (18.6%)	163 (18.5%)	
Severe	318 (14.7%)	219 (17.1%)	99 (11.3%)	
Missing data	4 (0.2%)	-	4 (0.5%)	
Childhood adversity categories (*n*, %)				
No or mild	1,398 (64.8%)	780 (61.1%)	618 (70.2%)	**$\chi^2 = 29.375$, $p < 0.0001$**
Moderate	394 (18.3%)	238 (18.6%)	156 (17.7%)	
Severe	355 (16.5%)	254 (19.9%)	101 (11.5%)	
Missing data	10 (0.5%)	5 (0.4%)	5 (0.6%)	
Financial hardship categories (*n*, %)				
Living very/quite comfortably	1,267 (58.7%)	689 (54%)	578 (65.7%)	**$\chi^2 = 50.215$, $p < 0.0001$**
Just getting by	656 (30.4%)	409 (32%)	247 (28.1%)	
Finding it difficult/not able to make ends meet	225 (10.4%)	177 (13.9%)	48 (5.5%)	
Missing data	9 (0.4%)	2 (0.2%)	7 (0.8%)	
B. Genetic data				
Minor allele frequencies (MAF)				
rs10462028 (A/G)	33.01%	33.27%	32.66%	

Table 1A *shows the phenotypic description of our sample and the statistical results of the comparison between subsamples while* ***Table 1B*** *summarizes data of the genetic variable. migraineID: positive for migraine, data derived from the ID-Migraine questionnaire. SEM, standard error of mean. Childhood adversity categories: (1) no or mild (score: 0–3); (2) moderate (score: 4–6); and (3) severe (score: 7 or more). Recent negative life events categories: (1) no or mild (score: 0 or 1); (2) moderate (score: 2); and (3) severe (score: 3 or more). χ^2: Pearson χ^2; p: significance—bold: significant effects.*

a region of 132,043 base pairs (from base position 56,288,743 to 56,420,786).

The investigated SNP potentially affects microRNA (miRNA) binding—therefore here, we aim to predict the possible effects of rs10462028 on miRNA-binding and regulation of the *CLOCK* gene. Thus, we have identified miRNAs with seed regions containing rs10462028, and one of the alternative alleles possibly alters the binding affinity. Further miRNA binding sites were predicted and examined near the SNP (as the altered mRNA sequence/structure can affect the accessibility of the region) and additionally around rs1801260 polymorphism that is in high LD (r^2 = 0.9, in the same LD-block—according to the 1,000 Genomes database; and r^2 = 0.802 in the CEU population according to SNP Function Prediction)[4] with rs10462028. Rs1801260 is a frequently examined SNP of *CLOCK* because of its proposed effect on activity, sleep onset, and sleep quantity (Katzenberg et al., 1998; Mishima et al., 2005; Benedetti et al., 2007).

The sequence of the *Homo sapiens* CLOCK 3-UTR (NM_001267843.1) transcript variant was obtained from the Nucleotide database of NCBI[5]. SNPs in LD with rs10462028 and rs1801260 have been collected using NIH SNP Function Prediction[4] with the following parameters: LD ≥0.8 in Population CEU, based on Genotype Data from HapMap CEU, based on Genotype Data from dbSNP: European. We only included 3′-UTR polymorphisms in our further investigation and focused on the *CLOCK* gene in this study.

MiRNA binding sites around polymorphisms were predicted using TargetScan[6] (Lewis et al., 2003), miRanda predictions on NIH SNP Function Prediction, and MicroSNiPer[7] (Barenboim et al., 2010). Conserved and poorly conserved sites for miRNA families were both examined. We used genecards.org/ website and miRiAD[8] (Hinske et al., 2010) database to include only miRNAs with known expression in the CNS by both sources. MiRNA-binding predictions were performed with both the reference and alternative alleles of the polymorphism.

[4]https://snpinfo.niehs.nih.gov/snpinfo/snpfunc.html

[5]https://www.ncbi.nlm.nih.gov/nucleotide/

[6]http://www.targetscan.org

[7]http://vm24141.virt.gwdg.de/services/microsniper/

[8]https://bmi.ana.med.uni-muenchen.de/miriad/downloads

Statistical Analysis

To calculate Hardy-Weinberg equilibrium (HWE) p and LD r^2-values, to run logistic and linear regression analysis with additive, dominant, and recessive genetic models, PLINK v1.07[9] analysis program was used.

In the *main analyses* we tested the main effect of rs10462028, then the SNP × stress interactions with each of the stress factors (CHA, RLE, FINANC) on migraineID in the total sample. Age and gender were covariates in all analyses. To handle possible ancestral differences, subjects with European white origin (determined by self-reported data derived from the Background questionnaire) were included in the analysis, and population (study sites) was a covariate in those analysis where combined samples were used. To assess our nominally significant findings we used three methods: (a) the gold standard Bonferroni correction to adjust p-values for multiple testing in our 12 main analyses [additive, dominant and recessive models of *CLOCK* SNP main effects and SNP × stress factor (CHA, RLE, or FINANC) interactions on migraineID in the total sample] with a Bonferroni-corrected threshold of $p \leq 0.004$ (0.05/12); (b) as Bonferroni correction is overly conservative and does not take into account the interdependences between the three genetic models of the same SNP, we used another more lenient corrected p-value taking into account our four hypotheses $p \leq 0.0125$ (0.05/4); and (c) finally effects were considered statistically significant in case of reaching a significance value below 0.05 not only in the total sample but also in the two subsamples (Budapest and Manchester separately).

In case of significant results we also ran *additional analyses*. Lifetime bipolar disorder (MANIC) and lifetime depression (DEPR) were added separately to models as covariates—to control for their potential confounding effect.

Furthermore, we tested the main effects of the *CLOCK* SNP on the stress factors (FINANC, CHA, RLE), MANIC, and DEPR—to recognize its potential effect on these components that may contribute to the connection between the SNP and migraine.

For displaying purposes, we calculated positive likelihood ratios (LR+) by dividing the frequency of migraine cases (symptom carriers) by the frequency of control subjects (non-carriers) in each category of each stress variable which showed significant interaction effects with the SNP. Further statistical analyses were performed with IBM SPSS Statistics 23. All statistical testing adopted a two-tailed $p = 0.05$ threshold. As *post hoc* tests, we measured the association of migraine frequencies and the SNP in the categories of stress factors with chi-squared test. To measure differences between our two subsamples in the phenotypic data, we used chi-squared test or independent sample t-test. Logistic regression models (with covariates: gender, age, population) were used to replicate the previously identified main effect of the measured stress factors on migraine.

Quanto 1.2 version[10] was used to calculate the statistical power of our study. Assuming a case-control design (three controls/case) and an additive genetic model with a minor allele frequency between 32 and 33% in our study (n = 2,157), we have 96% power to detect genetic main effects associated with a 1.3 odds ratio (OR) for a disease and 80% power to detect a gene × environment interaction ($p = 0.05$ two-tailed) that is associated with 1.5 OR for a disease.

[9]http://pngu.mgh.harvard.edu/ purcell/plink/

[10]https://preventivemedicine.usc.edu/download-quanto/

RESULTS

Sample

A detailed description of our study sample is described in **Table 1A**. Females represented approximately 70% of our sample, and the average age (±SEM) was 32.9 (±0.22) years. 27.8% of the participants reported two or three symptoms of migraine type headache based on the ID-Migraine questionnaire and were assigned migraineID. There were significant differences in each phenotypic variable except gender between the two subsamples. Subjects from Manchester showed higher age and higher prevalence of migraine headache, lifetime depression, lifetime bipolar disorder in comparison with the Budapest subsample. They also represented higher percentages in more stressful categories regarding every stress factors (CHA, RLE, FINANC). For detailed results see **Table 1A**.

CLOCK rs10462028

Rs10462028 was in HWE in the total sample ($p = 0.36$) and in both subsamples (in Manchester: $p = 0.57$; in Budapest: $p = 0.6$).

Main Effects of Stress Factors on MigraineID

All three stress factors (CHA, RLE, FINANC) showed highly significant ($p < 0.0001$) main effects on migraineID with more severe stress increasing the prevalence of migraineID. For detailed results see **Supplementary Table S1**. These results legitimize the use of the measured stress factors in our study.

Main Effect of *CLOCK* rs10462028 on MigraineID

The SNP showed no significant main effect on migraineID. For detailed results see **Table 2**.

Rs10462028 × Stress Factors Interaction on MigraineID

The investigated SNP was tested in separate analyses in interaction with the measured stress factors on migraineID in the total sample. Results of the regression models are summarized in **Table 2**.

The SNP showed no significant interaction either with CHA or with RLE.

There was a significant interaction effect between SNP and FINANC on migraineID in the total sample (in additive and recessive models).

Figure 2 shows that subjects with AA genotype have lower degree of migraine LR+ at the most severe but a higher degree of migraine LR+ in the least severe financial hardship category. *Post hoc* chi-squared tests validated that at the most severe FINANC category there was a significantly lower frequency of migraineID among those with AA genotype vs. GG ($\chi^2 = 3.916$, $p = 0.048$) and AG ($\chi^2 = 5.259$, $p = 0.022$) genotypes. In addition,

TABLE 2 | Statistical results of main genetic effects and interaction effects between rs10462028 and stress factors on migraineID in the total sample.

			Total sample			
Main effect						
SNP	A1	Model	OR	L95	U95	*p*
rs10462028	A	ADD	1.109	0.962	1.278	0.152
		DOM	1.144	0.942	1.389	0.175
		REC	1.146	0.854	1.538	0.364
Interaction						
SNP × CHA		Model	OR	L95	U95	*p*
		ADD	1.011	0.971	1.053	0.589
		DOM	1.026	0.971	1.084	0.363
		REC	0.988	0.909	1.075	0.784
SNP × RLE		Model	OR	L95	U95	*p*
		ADD	0.942	0.849	1.044	0.255
		DOM	0.930	0.805	1.076	0.332
		REC	0.908	0.738	1.117	0.361
SNP × FINANC		Model	OR	L95	U95	*p*
		ADD	**0.779**	**0.634**	**0.956**	**0.017**
		DOM	0.815	0.617	1.075	0.148
		REC	**0.54**	**0.348**	**0.836**	**0.006**

Table 2 *shows the statistical results of main genetic effects of CLOCK rs10462028 and interaction effects between the SNP and stress factors on migraineID in the total sample. SNP, single nucleotide polymorphism; A1, minor (and effect) allele; CHA, childhood adversity; RLE, recent negative life events; FINANC, financial hardship; OR, odds ratio; L95-U95, 95% confidence interval; ADD, additive model; DOM, dominant model; REC, recessive model; p, significance—bold: significant effects. Covariates in the model: age, gender and population.*

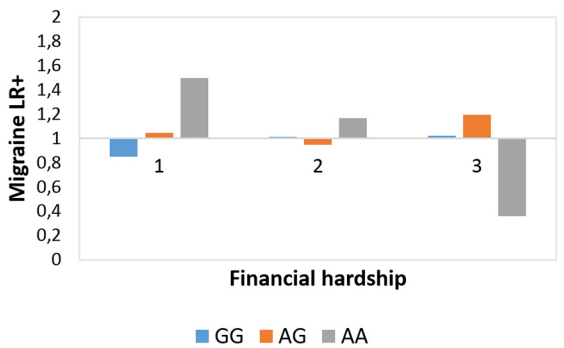

FIGURE 2 | Rs10462028 × financial hardship effect on migraineID. The interaction effect between *CLOCK* rs10462028 and financial hardship on migraineID is shown. FINANC, financial hardship; LR+, positive likelihood ratio. Number of cases in FINANC_1 (*living very/quite comfortably*) group: GG = 575, AG = 550, AA = 142. Number of cases in FINANC_2 (*just getting by*) group: GG = 294, AG = 282, AA = 80. Number of cases in FINANC_3 (*finding it difficult/not able to make ends meet*) group: GG = 102, AG = 100, AA = 23.

at the *living very/quite comfortably* level of financial difficulties those with AA genotype showed significantly higher migraineID frequency vs. GG genotype ($\chi^2 = 7.279$, $p = 0.007$) and vs. AG genotype at a tendency level ($\chi^2 = 2.98$, $p = 0.084$).

The interaction effect between rs10462028 and FINANC on migraineID was also tested in both subsamples (see **Table 3**). In Budapest both significant results were replicated (**Figure 3**). However, in Manchester only the recessive model showed a significant effect, and the additive model was not significant (**Figure 4**). So, only the recessive model was significant in all three samples—our main result with a $p = 0.006$ (see **Table 2**) is nominally significant, but only a trend effect was reached after Bonferroni-correction. However, considering the interdependence of the genetic models, it would survive the corrected significance threshold when only different hypotheses were corrected.

When MANIC and DEPR were added separately to the models as covariates (to control for their potential effect on migraineID) the SNP × FINANC interaction remained significant both in the additive and recessive models (and not significant in the dominant model)—with OR-values very similar to the original ones (for results see **Supplementary Table S2**).

Rs10462028 × FINANC Interaction on MigraineID According to Alternative Groupings of FINANC

Because the relatively low number of subjects at the most serious financial hardship level could potentially bias our results, we decided to run additional analyses with a financial difficulties variable that contains only two levels: (1) living very/quite comfortably ($n = 1{,}309$); and (2) just getting by/finding it difficult or not able to make ends meet ($n = 904$). These analyses also gave us the opportunity to test the differential effects of the SNP at the favorable and at the adverse end of the financial status spectrum that was suggested at the *a priori* level. Significant additive interaction effects between the SNP and financial hardship on migraineID were replicated in the total sample and in the Budapest subsample, but only a tendency was found in the Manchester subsample (**Supplementary Table S3**). Additionally, the original five-level financial hardship variable was also tested—showing significant interaction effects with the SNP on migraineID in the total sample and in both subsamples with very similar OR-values (**Supplementary Table S3**).

Main Effects of rs10462028 on Stress Factors, Bipolar and Unipolar Depression

The SNP showed no significant main effects on any of the measured variables (FINANC, CHA, RLE, MANIC, and DEPR) in the total sample (for detailed results see **Supplementary Table S4**). Thus, our significant interaction results are not due to gene-environment correlations.

In Silico Functional Analysis of the Genetic Region Tagged by rs10462028

We found several potential miRNA binding sites around rs10462028 and rs1801260 (in LD with the candidate SNP) with predicted change in binding due to the polymorphisms. The miRNA names, SNP allele effects, and prediction algorithms are summarized in **Supplementary Table S5**. Significantly predicted miRNAs were: miR-409-5p for rs10462028; miR-365b-3p, miR-365a-3p, and miR-664a-5p for rs1801260.

DISCUSSION

Our exploratory study demonstrated a connection between a circadian gene variant and migraine: *CLOCK* rs10462028 was

TABLE 3 | Statistical results of interaction effects between rs10462028 and financial hardship on migraineID in the subsamples.

Interaction		Manchester				Budapest			
SNP × FINANC	Model	OR	L95	U95	*p*	OR	L95	U95	*p*
	ADD	0.811	0.632	1.042	0.101	**0.612**	**0.408**	**0.916**	**0.017**
	DOM	0.9	0.643	1.26	0.539	*0.596*	*0.353*	*1.006*	*0.053*
	REC	**0.525**	**0.312**	**0.88**	**0.015**	**0.279**	**0.083**	**0.939**	**0.039**

Table 3 *shows the statistical results of interaction effects between CLOCK rs10462028 and financial hardship on migraineID in the subsamples separately (Manchester and Budapest)—to test the replicability of the significant SNP × FINANC effect found in the total sample. SNP, single nucleotide polymorphism; FINANC, financial hardship; OR, odds ratio; L95-U95, 95% confidence interval; ADD, additive model; DOM, dominant model; REC, recessive model; p, significance—bold: significant effects, italic: trend effects. Covariates in the model: age, gender.*

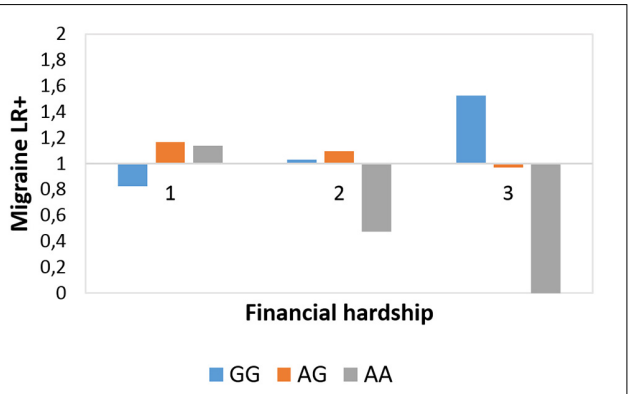

FIGURE 3 | Rs10462028 × financial hardship effect on migraineID in the Budapest subsample. The interaction effect between CLOCK rs10462028 and financial hardship on migraineID in the Budapest subsample is shown. FINANC, financial hardship; LR+, positive likelihood ratio. Number of cases in FINANC_1 (*living very/quite comfortably*) group: GG = 269, AG = 242, AA = 67. Number of cases in FINANC_2 (*just getting by*) group: GG = 106, AG = 117, AA = 24. Number of cases in FINANC_3 (*finding it difficult/not able to make ends meet*) group: GG = 23, AG = 19, AA = 6.

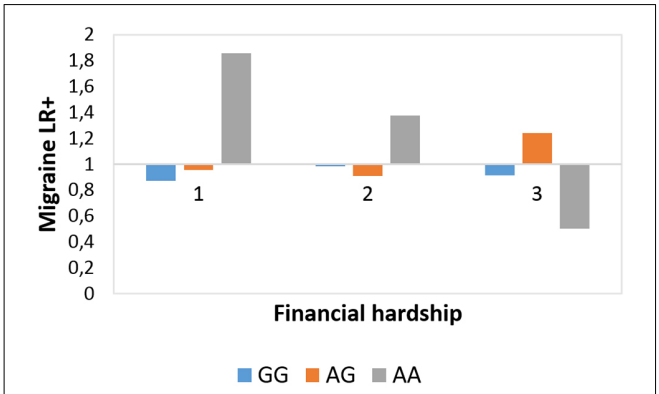

FIGURE 4 | Rs10462028 × financial hardship effect on migraineID in the Manchester subsample. The interaction effect between *CLOCK* rs10462028 and financial hardship on migraineID in the Manchester subsample is shown. FINANC, financial hardship; LR+, positive likelihood ratio. Number of cases in FINANC_1 (*living very/quite comfortably*) group: GG = 306, AG = 308, AA = 75. Number of cases in FINANC_2 (*just getting by*) group: GG = 188, AG = 165, AA = 56. Number of cases in FINANC_3 (*finding it difficult/not able to make ends meet*) group: GG = 79, AG = 81, AA = 17.

associated with a migraine phenotype in interaction with financial difficulties in a European cohort from Manchester and Budapest. Similarly to our results previous meta-analyses of migraine GWASs did not show a significant main effect of *CLOCK* (Anttila et al., 2013; Gormley et al., 2016). However, our integration of a chronic stress factor, specifically financial difficulties, pointed out the involvement of rs10462028 in migraine. Interestingly, childhood stress or RLE have not shown the same effect. Our results emphasize the importance to involve different stressors to identify genetic vulnerability to migraine.

Rs10462028 Selectively Interacts With Financial Hardship but Not Childhood Adversity and Recent Negative Events in Migraine

Circadian rhythms are organized on a daily basis, and stressors might express their influences through different pathways based on their genesis and timing. CHA represents negative effects from the earlier past, while the other two stressors are recent ones. RLE might have a better chance to contribute to the disturbance of circadian rhythms, but they are temporary situations, and that seems to be a significant difference from financial hardship. It is also a much diverse construct (in contrast to financial difficulties) representing multiple stressors.

Financial hardship is a variable of chronic stress—a proxy for deprivations and social difficulties (Sarginson et al., 2014). Its effect is reminiscent of the chronic mild stress model often used in animal studies of depression (Willner, 2017). Both situations can cause a permanent feeling of vulnerability and insecurity. Socioeconomic inequalities are major contributors to multimorbidity and mortality according to a prospective longitudinal study (Katikireddi et al., 2017), and even perceived financial strain which can be experienced at any level of socioeconomic status has been connected to earlier disability and increased mortality (Epel et al., 2018). Previously, our research group presented that different financial difficulties' variables showed a specific interacting role with polymorphisms of *NOS1* (Sarginson et al., 2014) and *5-HTTLPR* (Gonda et al., 2016) to affect depression, similarly as rs10462028 of *CLOCK* affected migraineID in the present study. Interestingly, our identified SNP × financial difficulties interaction seems to affect specifically migraine—our results were not confounded by lifetime bipolar and unipolar depression. Furthermore, we were able to replicate our main result in both subsamples despite significant differences in phenotypic data.

A previous study (Alstadhaug et al., 2008) suggested that social, work-related stress, and restorative effects of sleep might have a bigger role in the temporal patterns of migraine attacks than the actual biological circadian rhythms. However, other authors (Gori et al., 2005) highlighted that a desynchronization between the circadian clock mechanism and lifestyle might contribute to stress and migraine severity. According to our results, chronic stress and the circadian clock may interact in migraine pathophysiology.

Crossover Interaction Between rs10462028 and Financial Hardship

Our results suggest a crossover interaction between rs10462028 and financial difficulties on migraine: AA genotype seems to be a risk factor at a more favorable financial status and a protective factor at a more adverse financial stress level. This crossover type of interaction between genes and environmental factors in the background of diseases is not unprecedented. A review (Belsky et al., 2009) that discusses the environmental sensitivity hypothesis suggested that in gene × environment studies, instead of simply looking for genetic vulnerability, we should see these genetic variants as they make individuals more susceptible to both positive and negative environmental situations. This perspective can explain those results when the same genes seem to cause vulnerability to adversity and simultaneously promote an advantage in the lack of adversity—including evidence showing crossover interactions between different environmental effects on psychopathologies and *MAOA*, *5-HTTLPR*, and *DRD4* genes (Belsky et al., 2009). Our research group previously found that a variant of interleukin-1β gene (*IL1*β) had protective effect against depressive symptoms at a low degree of stressors, but it was a risk factor at high stress exposure (Kovacs et al., 2016). So, rs10462028 could also represent a so-called "plasticity gene" effect (Belsky et al., 2009) instead of a simple "vulnerability gene" effect.

In this kind of interaction the effects could statistically "obliterate" each other if we only test the main effect of the gene. Consequently, we should not expect to see these genetic effects in GWASs. These considerations highlight the importance of measuring the impact of relevant stress factors in genetic studies. Gene × environment studies can provide significant contribution to the "missing heritability" found in GWASs (Manolio et al., 2009; Juhasz et al., 2014).

Molecular Biology and Function of rs10462028

As we showed, rs10462028 (and rs1801260 in LD with it) affects miRNA binding. The most relevant predicted miRNAs have been mostly connected to different cancer types (Wang et al., 2013; Geng et al., 2016; Sahin et al., 2017; Yu et al., 2017). Migraine has not been associated with these miRNAs; the presence of chronic stress, however, might trigger this connection. Circadian genes might have an important role in cancer development through the disruption of circadian control of energy balance, immune function, and aging (Fu and Kettner, 2013). Similarly, these processes lead to functional decline in the brain (Kondratova and Kondratov, 2012). A recent study also suggested that *CLOCK* regulates brain plasticity during key developmental periods (Kobayashi et al., 2015) and thus may contribute to several brain disorders, such as migraine. However, our study did not confirm a possible interaction effect between *CLOCK* and CHA on migraine.

Functional polymorphisms in miRNAs or in their target sequences may alter regulation of gene expression (Mishra et al., 2008). Several miRNAs appear to regulate neural protein expressions, and various diseases have been connected to the altered translational regulation by the miRNA system (Dwivedi, 2011). Evidence also suggests that miRNAs are significant factors in circadian clock timing, presenting novel therapeutic targets for diseases related to circadian rhythms (Hansen et al., 2011). MiRNAs are also important in mediating environmental effects that modify gene expression (Lopizzo et al., 2015).

Our results showed allele effects impairing miRNA binding which can contribute to higher production of CLOCK protein—based on the assumption that weakened mRNA-miRNA interactions can increase protein levels (Moszynska et al., 2017). Higher level of CLOCK can contribute to an extensive disturbance in the main circadian pacemaker because of the strong interactions inside and between transcriptional/post-translation feedback loops. This confusion at the SCN may lead to a higher susceptibility for environmental effects which might explain the crossover interaction we found. A desynchronization between lifestyle and the circadian clock caused by financial difficulties may enhance the described process—finally leading to migraine susceptibility. In the case of *CLOCK* variants the C allele (in **Supplementary Table S5** the G allele on the complementary strand) of rs1801260 was associated with eveningness, delayed sleep onset, and reduced sleep (Katzenberg et al., 1998; Mishima et al., 2005; Benedetti et al., 2007), and this allele is in linkage with rs10462028 A allele[11]. Thus, eveningness, delayed sleep onset, and reduced sleep might be advantageous during financial hardship to prevent migraine type headaches while disadvantageous during financial stability. These assumptions are hypothetical at the moment and need to be tested in future studies, but they could provide a pathway that integrates chronic stress, the circadian clock, and potential epigenetic processes in migraine pathophysiology.

LIMITATIONS

The main advantage of our study: the use of detailed phenotypic data allowed us to identify a specific gene × stressor interaction which might be relevant in migraine. However, our work has some limitations. We demonstrated a relationship between a circadian gene and migraine for the first time in a relatively small sample. Nevertheless, power analyses revealed enough power to detect the investigated genetic effects. Our main result was nominally significant, but only a trend effect was reached after the gold standard Bonferroni correction of multiple testing—therefore, our findings should be interpreted with

[11] https://ldlink.nci.nih.gov/?tab=ldhap

caution and independent replications are needed to confirm our results. We used a cross-sectional design, therefore, the causative role of stressors and the temporal relationship between stress and migraine could not be investigated. Our migraine screening tool was a short questionnaire which did not provide proper medical diagnosis although it is a widely used method (Anttila et al., 2013). The ID-migraine questionnaire does not provide information regarding migraine subtypes (for example migraine with and without aura). Future studies focusing on possible differences in the role of circadian rhythmicity between migraine subtypes are needed. Nearly 70% of our sample consisted of females who are affected by migraine three times more often than men (Goadsby et al., 2017). Female gender is also a risk factor for sleeping problems, including insomnia and obstructive sleep apnea (Rains, 2018), and sex differences in circadian timing systems may be important in circadian-related diseases (for a review see Bailey and Silver, 2014). Future studies involving more male subjects are needed to gain knowledge about the possible role of gender in the association of migraine and circadian mechanisms. Finally, we need to mention that the circadian clock mechanism is far more complex—we only focused on one variant of one circadian gene. With this strategy we were able to identify a possible role of the circadian mechanism in the pathophysiology of migraine which suggests a need to further investigate the connection of circadian rhythms and migraine in a broader context.

CONCLUSIONS

In conclusion, our results show that genetic variation in the *CLOCK* gene is associated with migraine depending on the level of perceived financial stress. This could be explained most likely through a process where persistent stress disturbs the physiological function of the circadian clock mechanism, possibly *via* epigenetic regulation, specifically miRNA binding.

DATA AVAILABILITY STATEMENT

The datasets generated for this study are available on request to the corresponding author.

ETHICS STATEMENT

Our study was approved by local Ethics Committees (Scientific and Research Ethics Committee of the Medical Research Council, Budapest, Hungary, ad.225/KO/2005; ad.323-60/2005-1018EKU and ad.226/KO/2005; ad.323-61/2005-1018 EKU; North Manchester Local Research Ethics Committee, Manchester, UK REC reference number: 05/Q1406/26) and was carried out in accordance with the Declaration of Helsinki. All participants provided their written informed consent to participate in this study.

AUTHOR CONTRIBUTIONS

GB, GJ, and JD designed the study and wrote the protocol. DB undertook the statistical analysis and managed the literature search. DB, XG, NE, PP, VA, and LK wrote the first draft of the manuscript. All authors contributed to and have approved the final manuscript.

FUNDING

The study was supported by the Hungarian Brain Research Program (KTIA_13_NAP-A-II/14, 2017-1.2.1-NKP-2017-00002); by the National Development Agency (KTIA_NAP_13-1-2013-0001); by the Sixth Framework Program of the European Union, NewMood (Grant No. LSHM-CT-2004-503474); by the Hungarian Academy of Sciences, Semmelweis University and the Hungarian Brain Research Program (MTA-SE-NAP B Genetic Brain Imaging Migraine Research Group, Grant KTIA_NAP_13-2-2015-0001); by the National Institute for Health Research Manchester Biomedical Research Centre; by the Hungarian Academy of Sciences (MTA-SE Neuropsychopharmacology and Neurochemistry Research Group) and New National Excellence Program of The Ministry of Human Capacities (UNKP-16-3, UNKP-17-3-III-SE-2, UNKP-17-4-I-SE-8), and by the ITM/NKFIH Thematic Excellence Programme, Semmelweis University; and by the SE-Neurology FIKP grant of EMMI. XG is a recipient of the Janos Bolyai Research Scholarship of the Hungarian Academy of Sciences and supported by the UNKP-19-4 New National Excellence Program of the Ministry for Innovation and Technology. The sponsors had no further role in the study design; in the collection, analysis and interpretation of data; in the writing of the report; and in the decision to submit the article for publication.

ACKNOWLEDGMENTS

We thank Diana Chase, Darragh Downey, Kathryn Lloyd-Williams, Emma J. Thomas and Zoltan G. Toth for their assistance in the recruitment and data acquisition processes. We also thank the Heaton Mersey and the Cheadle Medical Practices for their assistance in recruitment.

SUPPLEMENTARY MATERIAL

The Supplementary Material for this article can be found online at: https://www.frontiersin.org/articles/10.3389/fnbeh.2019.00284/full#supplementary-material.

REFERENCES

Alstadhaug, K., Salvesen, R., and Bekkelund, S. (2008). 24-hour distribution of migraine attacks. *Headache* 48, 95–100. doi: 10.1111/j.1526-4610.2007.00779.x

Anttila, V., Winsvold, B. S., Gormley, P., Kurth, T., Bettella, F., McMahon, G., et al. (2013). Genome-wide meta-analysis identifies new susceptibility loci for migraine. *Nat. Genet.* 45, 912–917. doi: 10.1038/ng.2676

Bailey, M., and Silver, R. (2014). Sex differences in circadian timing systems: implications for disease. *Front.*

Neuroendocrinol. 35, 111–139. doi: 10.1016/j.yfrne.2013.11.003

Barenboim, M., Zoltick, B. J., Guo, Y., and Weinberger, D. R. (2010). MicroSNiPer: a web tool for prediction of SNP effects on putative microRNA targets. *Hum. Mutat.* 31, 1223–1232. doi: 10.1002/humu.21349

Belsky, J., Jonassaint, C., Pluess, M., Stanton, M., Brummett, B., and Williams, R. (2009). Vulnerability genes or plasticity genes? *Mol. Psychiatry* 14, 746–754. doi: 10.1038/mp.2009.44

Benedetti, F., Dallaspezia, S., Fulgosi, M. C., Lorenzi, C., Serretti, A., Barbini, B., et al. (2007). Actimetric evidence that CLOCK 3111 T/C SNP influences sleep and activity patterns in patients affected by bipolar depression. *Am. J. Med. Genet. B Neuropsychiatr. Genet.* 144B, 631–635. doi: 10.1002/ajmg.b.30475

Bernstein, D. P., Ahluvalia, T., Pogge, D., and Handelsman, L. (1997). Validity of the Childhood Trauma Questionnaire in an adolescent psychiatric population. *J. Am. Acad. Child Adolesc. Psychiatry* 36, 340–348. doi: 10.1097/00004583-199703000-00012

Borsook, D., Maleki, N., Becerra, L., and McEwen, B. (2012). Understanding migraine through the lens of maladaptive stress responses: a model disease of allostatic load. *Neuron* 73, 219–234. doi: 10.1016/j.neuron.2012.01.001

Brennan, K. C., Bates, E. A., Shapiro, R. E., Zyuzin, J., Hallows, W. C., Huang, Y., et al. (2013). Casein kinase idelta mutations in familial migraine and advanced sleep phase. *Sci. Transl. Med.* 5:183ra156. doi: 10.1126/scitranslmed.3005784

Breslau, N., Lipton, R. B., Stewart, W. F., Schultz, L. R., and Welch, K. M. (2003). Comorbidity of migraine and depression: investigating potential etiology and prognosis. *Neurology* 60, 1308–1312. doi: 10.1212/01.wnl.0000058907.41080.54

Brugha, T., Bebbington, P., Tennant, C., and Hurry, J. (1985). The List of Threatening Experiences: a subset of 12 life event categories with considerable long-term contextual threat. *Psychol. Med.* 15, 189–194. doi: 10.1017/s003329170002105x

Chasman, D. I., Schurks, M., and Kurth, T. (2016). Population-based approaches to genetics of migraine. *Cephalalgia* 36, 692–703. doi: 10.1177/0333102416638519

Dwivedi, Y. (2011). Evidence demonstrating role of microRNAs in the etiopathology of major depression. *J. Chem. Neuroanat.* 42, 142–156. doi: 10.1016/j.jchemneu.2011.04.002

Epel, E. S., Crosswell, A. D., Mayer, S. E., Prather, A. A., Slavich, G. M., Puterman, E., et al. (2018). More than a feeling: a unified view of stress measurement for population science. *Front. Neuroendocrinol.* 49, 146–169. doi: 10.1016/j.yfrne.2018.03.001

Fu, L., and Kettner, N. M. (2013). The circadian clock in cancer development and therapy. *Prog. Mol. Biol. Transl. Sci.* 119, 221–282. doi: 10.1016/B978-0-12-396971-2.00009-9

Geng, J., Liu, Y., Jin, Y., Tai, J., Zhang, J., Xiao, X., et al. (2016). MicroRNA-365a-3p promotes tumor growth and metastasis in laryngeal squamous cell carcinoma. *Oncol. Rep.* 35, 2017–2026. doi: 10.3892/or.2016.4617

Goadsby, P. J., Holland, P. R., Martins-Oliveira, M., Hoffmann, J., Schankin, C., and Akerman, S. (2017). Pathophysiology of migraine: a disorder of sensory processing. *Physiol. Rev.* 97, 553–622. doi: 10.1152/physrev.00034.2015

Gonda, X., Eszlari, N., Kovacs, D., Anderson, I. M., Deakin, J. F., Juhasz, G., et al. (2016). Financial difficulties but not other types of recent negative life events show strong interactions with 5-HTTLPR genotype in the development of depressive symptoms. *Transl. Psychiatry* 6:e798. doi: 10.1038/tp.2016.57

Gori, S., Lucchesi, C., Morelli, N., Maestri, M., Bonanni, E., and Murri, L. (2012). Sleep-related migraine occurrence increases with aging. *Acta Neurol. Belg.* 112, 183–187. doi: 10.1007/s13760-012-0049-6

Gori, S., Morelli, N., Maestri, M., Fabbrini, M., Bonanni, E., and Murri, L. (2005). Sleep quality, chronotypes and preferential timing of attacks in migraine without aura. *J. Headache Pain* 6, 258–260. doi: 10.1007/s10194-005-0201-2

Gormley, P., Anttila, V., Winsvold, B. S., Palta, P., Esko, T., Pers, T. H., et al. (2016). Meta-analysis of 375,000 individuals identifies 38 susceptibility loci for migraine. *Nat. Genet.* 48, 856–866. doi: 10.1038/ng.3598

Hansen, K. F., Sakamoto, K., and Obrietan, K. (2011). MicroRNAs: a potential interface between the circadian clock and human health. *Genome Med.* 3:10. doi: 10.1186/gm224

Hinske, L. C., Galante, P. A., Kuo, W. P., and Ohno-Machado, L. (2010). A potential role for intragenic miRNAs on their hosts' interactome. *BMC Genomics* 11:533. doi: 10.1186/1471-2164-11-533

Johnston, J. D. (2014). Physiological links between circadian rhythms, metabolism and nutrition. *Exp. Physiol.* 99, 1133–1137. doi: 10.1113/expphysiol.2014.078295

Juhasz, G., Chase, D., Pegg, E., Downey, D., Toth, Z. G., Stones, K., et al. (2009). CNR1 gene is associated with high neuroticism and low agreeableness and interacts with recent negative life events to predict current depressive symptoms. *Neuropsychopharmacology* 34, 2019–2027. doi: 10.1038/npp.2009.19

Juhasz, G., Csepany, E., Magyar, M., Edes, A. E., Eszlari, N., Hullam, G., et al. (2017). Variants in the CNR1 gene predispose to headache with nausea in the presence of life stress. *Genes Brain Behav.* 16, 384–393. doi: 10.1111/gbb.12352

Juhasz, G., Dunham, J. S., McKie, S., Thomas, E., Downey, D., Chase, D., et al. (2011). The CREB1-BDNF-NTRK2 pathway in depression: multiple gene-cognition-environment interactions. *Biol. Psychiatry* 69, 762–771. doi: 10.1016/j.biopsych.2010.11.019

Juhasz, G., Hullam, G., Eszlari, N., Gonda, X., Antal, P., Anderson, I. M., et al. (2014). Brain galanin system genes interact with life stresses in depression-related phenotypes. *Proc. Natl. Acad. Sci. U S A* 111, E1666–E1673. doi: 10.1073/pnas.1403649111

Katikireddi, S. V., Skivington, K., Leyland, A. H., Hunt, K., and Mercer, S. W. (2017). The contribution of risk factors to socioeconomic inequalities in multimorbidity across the lifecourse: a longitudinal analysis of the Twenty-07 cohort. *BMC Med.* 15:152. doi: 10.1186/s12916-017-0913-6

Katzenberg, D., Young, T., Finn, L., Lin, L., King, D. P., Takahashi, J. S., et al. (1998). A CLOCK polymorphism associated with human diurnal preference. *Sleep* 21, 569–576. doi: 10.1093/sleep/21.6.569

Kishi, T., Kitajima, T., Ikeda, M., Yamanouchi, Y., Kinoshita, Y., Kawashima, K., et al. (2009). Association study of clock gene (CLOCK) and schizophrenia and mood disorders in the Japanese population. *Eur. Arch. Psychiatry Clin. Neurosci.* 259, 293–297. doi: 10.1007/s00406-009-0869-4

Kobayashi, Y., Ye, Z., and Hensch, T. K. (2015). Clock genes control cortical critical period timing. *Neuron* 86, 264–275. doi: 10.1016/j.neuron.2015.02.036

Koch, C. E., Leinweber, B., Drengberg, B. C., Blaum, C., and Oster, H. (2017). Interaction between circadian rhythms and stress. *Neurobiol. Stress* 6, 57–67. doi: 10.1016/j.ynstr.2016.09.001

Kondratova, A. A., and Kondratov, R. V. (2012). The circadian clock and pathology of the ageing brain. *Nat. Rev. Neurosci.* 13, 325–335. doi: 10.1038/nrn3208

Kovacs, D., Eszlari, N., Petschner, P., Pap, D., Vas, S., Kovacs, P., et al. (2016). Effects of IL1B single nucleotide polymorphisms on depressive and anxiety symptoms are determined by severity and type of life stress. *Brain Behav. Immun.* 56, 96–104. doi: 10.1016/j.bbi.2016.02.012

Lazary, J., Lazary, A., Gonda, X., Benko, A., Molnar, E., Hunyady, L., et al. (2009). Promoter variants of the cannabinoid receptor 1 gene (CNR1) in interaction with 5-HTTLPR affect the anxious phenotype. *Am. J. Med. Genet. B Neuropsychiatr. Genet.* 150B, 1118–1127. doi: 10.1002/ajmg.b.31024

Lewis, B. P., Shih, I. H., Jones-Rhoades, M. W., Bartel, D. P., and Burge, C. B. (2003). Prediction of mammalian microRNA targets. *Cell* 115, 787–798. doi: 10.1016/s0092-8674(03)01018-3

Lipton, R. B., Dodick, D., Sadovsky, R., Kolodner, K., Endicott, J., Hettiarachchi, J., et al. (2003). A self-administered screener for migraine in primary care: the ID Migraine validation study. *Neurology* 61, 375–382. doi: 10.1212/01.wnl.0000078940.53438.83

Lopizzo, N., Bocchio Chiavetto, L., Cattane, N., Plazzotta, G., Tarazi, F. I., Pariante, C. M., et al. (2015). Gene-environment interaction in major depression: focus on experience-dependent biological systems. *Front. Psychiatry* 6:68. doi: 10.3389/fpsyt.2015.00068

Manolio, T. A., Collins, F. S., Cox, N. J., Goldstein, D. B., Hindorff, L. A., Hunter, D. J., et al. (2009). Finding the missing heritability of complex diseases. *Nature* 461, 747–753. doi: 10.1038/nature08494

Mishima, K., Tozawa, T., Satoh, K., Saitoh, H., and Mishima, Y. (2005). The 3111T/C polymorphism of hClock is associated with evening preference and delayed sleep timing in a Japanese population sample. *Am. J. Med. Genet. B Neuropsychiatr. Genet.* 133B, 101–104. doi: 10.1002/ajmg.b.30110

Mishra, P. J., Mishra, P. J., Banerjee, D., and Bertino, J. R. (2008). MiRSNPs or MiR-polymorphisms, new players in microRNA mediated regulation of the cell: introducing microRNA pharmacogenomics. *Cell Cycle* 7, 853–858. doi: 10.4161/cc.7.7.5666

Moore-Ede, M. C. (1986). Physiology of the circadian timing system: predictive versus reactive homeostasis. *Am. J. Physiol.* 250, R737–R752. doi: 10.1152/ajpregu.1986.250.5.r737

Moszyńska, A., Gebert, M., Collawn, J. F., and Bartoszewski, R. (2017). SNPs in microRNA target sites and their potential role in human disease. *Open Biol.* 7:170019. doi: 10.1098/rsob.170019

Oedegaard, K. J., Greenwood, T. A., Lunde, A., Fasmer, O. B., Akiskal, H. S., and Kelsoe, J. R. (2010). A genome-wide linkage study of bipolar disorder and co-morbid migraine: replication of migraine linkage on chromosome 4q24 and suggestion of an overlapping susceptibility region for both disorders on chromosome 20p11. *J. Affect. Disord.* 122, 14–26. doi: 10.1016/j.jad.2009.06.014

Rains, J. C. (2018). Sleep and migraine: assessment and treatment of comorbid sleep disorders. *Headache* 58, 1074–1091. doi: 10.1111/head.13357

Sahin, Y., Altan, Z., Arman, K., Bozgeyik, E., Koruk Ozer, M., and Arslan, A. (2017). Inhibition of miR-664a interferes with the migration of osteosarcoma cells *via* modulation of MEG3. *Biochem. Biophys. Res. Commun.* 490, 1100–1105. doi: 10.1016/j.bbrc.2017.06.174

Sarginson, J. E., Deakin, J. F., Anderson, I. M., Downey, D., Thomas, E., Elliott, R., et al. (2014). Neuronal nitric oxide synthase (NOS1) polymorphisms interact with financial hardship to affect depression risk. *Neuropsychopharmacology* 39, 2857–2866. doi: 10.1038/npp.2014.137

Sauro, K. M., and Becker, W. J. (2009). The stress and migraine interaction. *Headache* 49, 1378–1386. doi: 10.1111/j.1526-4610.2009.01486.x

Schwedt, T. J., and Chong, C. D. (2015). Functional imaging and migraine: new connections? *Curr. Opin. Neurol.* 28, 265–270. doi: 10.1097/wco.0000000000000194

Soria, V., Martínez-Amorós, E., Escaramis, G., Valero, J., Pérez-Egea, R., García, C., et al. (2010). Differential association of circadian genes with mood disorders: CRY1 and NPAS2 are associated with unipolar major depression and CLOCK and VIP with bipolar disorder. *Neuropsychopharmacology* 35, 1279–1289. doi: 10.1038/npp.2009.230

Stewart, W. F., Roy, J., and Lipton, R. B. (2013). Migraine prevalence, socioeconomic status, and social causation. *Neurology* 81, 948–955. doi: 10.1212/wnl.0b013e3182a43b32

Swanson, S. A., Zeng, Y., Weeks, M., and Colman, I. (2013). The contribution of stress to the comorbidity of migraine and major depression: results from a prospective cohort study. *BMJ Open* 3:e002057. doi: 10.1136/bmjopen-2012-002057

Tietjen, G. E. (2016). Childhood maltreatment and headache disorders. *Curr. Pain Headache Rep.* 20:26. doi: 10.1007/s11916-016-0554-z

van Oosterhout, W., van Someren, E., Schoonman, G. G., Louter, M. A., Lammers, G. J., Ferrari, M. D., et al. (2018). Chronotypes and circadian timing in migraine. *Cephalalgia* 38, 617–625. doi: 10.1177/0333102417698953

Vogler, B., Rapoport, A. M., Tepper, S. J., Sheftell, F., and Bigal, M. E. (2006). Role of melatonin in the pathophysiology of migraine: implications for treatment. *CNS Drugs* 20, 343–350. doi: 10.2165/00023210-200620050-00001

Wang, J., Wang, X., Wu, G., Hou, D., and Hu, Q. (2013). MiR-365b-3p, down-regulated in retinoblastoma, regulates cell cycle progression and apoptosis of human retinoblastoma cells by targeting PAX6. *FEBS Lett.* 587, 1779–1786. doi: 10.1016/j.febslet.2013.04.029

Willner, P. (2017). The chronic mild stress (CMS) model of depression: history, evaluation and usage. *Neurobiol. Stress* 6, 78–93. doi: 10.1016/j.ynstr.2016.08.002

Yu, H., Xing, H., Han, W., Wang, Y., Qi, T., Song, C., et al. (2017). MicroRNA-409–5p is upregulated in breast cancer and its downregulation inhibits cancer development through downstream target of RSU1. *Tumour Biol.* 39:1010428317701647. doi: 10.1177/1010428317701647

Conflict of Interest: Preliminary data from this study were presented at the following events: *Conference of Hungarian Clinical Neurogenetic Society*, 1–2 December 2017, Kecskemet, Hungary (lecture); *30th ECNP Congress*, 2–5 September 2017, Paris, France (poster presentation); *13th World Congress of Biological Psychiatry*, 18–22 June 2017, Copenhagen, Denmark (poster presentation); *24th Congress of the Hungarian Headache Society*, 5–6 May 2017, Siofok, Hungary (lecture); *XXVI World Congress of Psychiatric Genetics*, 11–15 October 2018, Glasgow, Scotland (poster presentation); *Semmelweis University PhD Scientific Days*, 25–26 April 2019, Budapest, Hungary (poster presentation). JD variously performed consultancy, speaking engagements and research for Bristol-Myers Squibb, AstraZeneca, Eli Lilly, Schering Plough, Janssen-Cilag and Servier (all fees are paid to the University of Manchester to reimburse them for the time taken); he also has share options in P1vital.

The remaining authors declare that the research was conducted in the absence of any commercial or financial relationships that could be construed as a potential conflict of interest.

frontiers in Behavioral Neuroscience

ORIGINAL RESEARCH
published: 22 April 2020
doi: 10.3389/fnbeh.2020.00057

Astrocytic Glutamate Transporter 1 (GLT1) Deficiency Reduces Anxiety- and Depression-Like Behaviors in Mice

Yun-Fang Jia[1†], Katheryn Wininger[2†], Ada Man-Choi Ho[3], Lee Peyton[1], Matthew Baker[1] and Doo-Sup Choi[1,2,3]*

[1] Department of Molecular Pharmacology and Experimental Therapeutics, Mayo Clinic, Rochester, MN, United States, [2] Neuroscience Program, Mayo Clinic, Rochester, MN, United States, [3] Department of Psychiatry & Psychology, Mayo Clinic, Rochester, MN, United States

OPEN ACCESS

Edited by:
Carsten T. Wotjak,
Max Planck Institute of Psychiatry (MPI), Germany

Reviewed by:
Edgar Soria-Gomez,
University of the Basque Country, Spain
Barbara Di Benedetto,
University of Regensburg, Germany

***Correspondence:**
Doo-Sup Choi
choids@mayo.edu

[†] These authors have contributed equally to this work

Specialty section:
This article was submitted to Emotion Regulation and Processing, a section of the journal Frontiers in Behavioral Neuroscience

Received: 06 February 2020
Accepted: 25 March 2020
Published: 22 April 2020

Citation:
Jia Y-F, Wininger K, Ho AM-C, Peyton L, Baker M and Choi D-S (2020) Astrocytic Glutamate Transporter 1 (GLT1) Deficiency Reduces Anxiety- and Depression-Like Behaviors in Mice. Front. Behav. Neurosci. 14:57. doi: 10.3389/fnbeh.2020.00057

Glutamatergic dysregulation is known to contribute to altered emotional regulation. Astrocytic glutamate transporter 1 (GLT1) is responsible for the majority of glutamate clearance from synapse. However, the role of astrocytic GLT1 in affective processes such as anxiety- and depression-like behavior is not fully understood. Here, we found that astrocytic GLT1 deficient mice entered more frequently, and spent more time in the open arms of elevated plus maze without difference in overall distance traveled in the open field, nor were there any metabolic changes observed in the metabolic chamber compared to wildtype mice. Moreover, mice lacking astrocytic GLT1 exhibited less immobile time and moved greater area in the tail suspension test. Similarly, in the forced swim test, they showed less immobile time and moved greater area. In addition, we found that astrocytic GLT1 deficiency reduced freezing responses in the fear contextual and cued tests. Taken together, our findings suggest that astrocytic GLT1 deficiency decreases anxiety and depression-like behaviors.

Keywords: glutamate transporter 1 (GLT1), anxiety, depression, astrocyte, behaviors, fear conditioning

INTRODUCTION

Major depressive disorder (MDD) is a mental health disorder that displays a combination of symptoms, including reduced motivation and activities, helplessness, loss of appetite or interest, and sleep disturbance (Kessler et al., 2003; Cui et al., 2014), causing significant impairment in daily life. Because of heterogeneity of depressive symptoms, it is difficult to identify molecular and cellular mechanisms underlying clinical symptoms. Generalized anxiety disorder (GAD) is one of the most common psychiatric disorders and co-occurring illness with MDD (Sunderland et al., 2010). This co-occurrence may indicate a similar etiology and pathophysiological abnormalities in MDD and GAD (Mineka et al., 1998). High rates of comorbidity (Zbozinek et al., 2012), and similar brain abnormalities are possibly attributed to both anhedonia and anxiogenesis (John et al., 2015).

In addition, since the behavioral manifestations were similar between anxiety and fear, they may have overlapping neural basis of phenotypes (Tovote et al., 2015).

Glutamate homeostasis is critical for normal brain physiology. The precisely balanced control of glutamate release and uptake assure the physiological optimum (Kiryk et al., 2008). Glutamatergic dysregulation is known to be involved in psychiatric disorders including depression, anxiety, and fear-related disorders (Davis and Myers, 2002; Walker and Davis, 2002; Bergink et al., 2004; Cortese and Phan, 2005; Mathews et al., 2012; Murrough et al., 2017). In the central nervous system (CNS), extracellular and synaptic glutamate is regulated by a family of glutamate transporters, which removes glutamate from the synaptic cleft. Among five well-identified glutamate transporters, glutamate transporter 1 (GLT1) is responsible for the majority (90%) of glutamate clearance (Su et al., 2003).

Notably, multiple brain regions including the prefrontal frontal cortex, striatum, and hippocampus are important regulators of mood disorders. Abnormal gene expression and glial loss were found in a discrete region of postmortem prefrontal cortex of MDD (Kang et al., 2007; Di Benedetto et al., 2016; Ho et al., 2019). A significant decrease in total hippocampal volume was reported in recurrent or chronic MDD (Cobb et al., 2013). Moreover, GLT1 is differentially expressed across anatomical brain. For example, altered hippocampal GLT1 expression was found in rodent depression models (Pines et al., 1992; Blacker et al., 2019; Ho et al., 2019).

As GLT1 plays a critical role in glutamate homeostasis, mice deficient of GLT1 could elucidate the impact of glutamatergic disturbances. Global GLT1 null mice display excessive glutamate levels, and exhibit severe seizure activity including spontaneous seizures and increased susceptibility to acute cortical injury (Tanaka et al., 1997). Since astrocytes participate in the uptake, metabolism, and recycling of glutamate (Rajkowska and Miguel-Hidalgo, 2007), the loss of GLT1 in astrocytes may account for the alterations in glutamate neurotransmission in depression (Rajkowska and Stockmeier, 2013). In rodents, glial loss in the prefrontal cortex was demonstrated to be sufficient to induce depressive-like behaviors (Banasr and Duman, 2008). Post-mortem studies reported a loss of glial cell number in depressed patients, indicating together with abnormal functioning could contribute to the pathophysiology of mood disorders (Czeh and Di Benedetto, 2013; Di Benedetto et al., 2016). Notably, astrocytic-, but not neuronal-specific deletion of GLT1 induced fatal epilepsy, suggesting that astrocytic GLT1 performs critical functions (Petr et al., 2015). Further, recent data indicated that selective deletion of GLT1 in the diencephalon, brainstem and spinal cord was sufficient to reproduce the phenotypes (excess mortality, decreased body weight, and lethal spontaneous seizure) (Sugimoto et al., 2018). Deletion of GLT1 in habenula astrocytes increased neuronal excitability and depression-like behaviors (Cui et al., 2014). The blockade of GLT1 by administration of its inhibitor (DHK) in the central amygdala induced both depression and anxiety (John et al., 2015). In contrast, downregulation of GLT1 by administration with the DHK acutely increased glutamatergic neurotransmission, which triggers immediate antidepressant-like responses in rats (Gasull-Camos et al., 2017).

Overall, the contribution of GLT1 in regard to emotional regulation such as anxiety- and depressive-like behavior, as well as fear remains highly controversial. These studies together conclude that GLT1 exerts specific, and sometimes even opposite roles depending on cell type and regional specifically. Therefore, this study aimed to investigate the behavioral alterations of anxiety- and depression-like behaviors in astrocytic GLT1 deficient mice.

MATERIALS AND METHODS

Animals

Mice were group-housed (4,5 animals per cage) in standard Plexiglas cages in a 12 h light/dark cycle (lights on at 6 AM and off at 6 PM) with a temperature (22–24°C) and humidity (50%) regulated environment with access to standard lab food and water ad libitum. The floxed-GLT1 mice ($GLT1^{F/F}$) mice were obtained from Niels C. Danbolt's laboratory (University of Oslo, Norway) (Gregorian et al., 2009) and the $GFAP^{cre/+}$ line was purchased from the Jackson laboratory (Cat no., 024098 – B6.Cg-Tg(Gfap-cre)77.6Mvs/2J). To generate astrocyte-specific GLT1 knockout mice, we crossed the $GLT1^{F/F}$ mice with the $GFAP^{cre/+}$ line, in which Cre recombinase is expressed selectively in the astrocytes. All mice in this study had C57BL/6J genetic background. All animal care, handling procedures and experimental protocols were approved by the Mayo Clinic Institutional Animal Care and Use Committee (IACUC) in accordance with the guidelines set forth by the National Institutes of Health.

Immunohistochemistry

Immunohistochemistry was done as previously described (Jia et al., 2019). Briefly, mice were euthanized by CO_2 asphyxiation followed by rapid brain removal. Brains were fixed in 4% paraformaldehyde (Sigma Aldrich) for 24 h and then immersed in 30% (w/v) sucrose in 0.1 M PBS at 4°C for 48 h until the tissue sunk. Coronal sections (40 μm) were cut by a cryostat for the following brain regions: medial prefrontal cortex (mPFC), striatum, and hippocampus (Hip), and incubated as free-floating sections in 0.5% Triton-PBS for 15 min and then in 5% (w/v) bovine serum albumin (BSA)-PBS for 4 h at room temperature. Sections were then incubated with guinea pig anti-GLT1 primary antibody (1:2000, Cat No.: Ab1783, Millipore), or rabbit anti-GFAP primary antibody (1:500, Cat No.: Ab68428, Abcam), or rabbit anti-Iba1 primary antibody (1:500, Cat No.: Ab178846, Abcam), or rabbit anti-NeuN primary antibody (1:500, Cat No.: Ab177487, Abcam), at 4°C for overnight. After washing with PBS, slices were incubated with secondary antibody Alexa 568-conjugated goat anti-guinea pig (1:1000, Thermo Fischer Scientific), or Alexa 488-conjugated goat anti-rabbit (1:1000, Thermo Fischer Scientific), or Alexa 594-conjugated goat anti-rabbit (1:1000, Thermo Fischer Scientific) for 3 h at room temperature. Nuclei were visualized with DAPI (1:2000, sigma) added to the mounting solution. Images from the brain regions

of interest were obtained on an LSM 510 confocal laser scanning microscope (Carl Zeiss).

Stereotaxic Viral Injection

In order to visualize the GFAP-Cre positive cells, we purchased GFAP promoter driven Cre recombinase virus fused to eGFP (enhanced green fluorescence protein) tag from Vector Biolabs. A mixture of ketamine (100 mg/kg) and xylazine (10 mg/kg) were used for anesthesia. Eight-week old male C57BL/6J mice were positioned in a stereotaxic instrument (KOPF Instruments). A 35−gage syringe needle (World Precision Instruments) was used to deliver GFAP-Cre virus (AAV9−GFAP−Cre/eGFP; 1.4×10^{13} GC/mL, 1.0 μL, Vector Biolabs) into the NAc (AP: +1.3 mm, ML: +1.0 mm, DV: −4.25 mm) at a rate of 0.1 μL/min for 10 min. At the end of injection, needles remained in place for 5 min to ensure complete delivery of the viral bolus and were then slowly retracted to minimize trauma and viral spreading. The scalp was sutured with 5−0 polyviolene sutures (Sharpoint). To allow for sufficient viral expression, immunohistochemical staining began 3 weeks after surgery.

Western Blot

Mice were euthanized by CO_2 asphyxiation and rapidly decapitated. The mPFC, striatum, and Hip were immediately isolated under a surgical microscope. The extracted tissue was weighed and snap-frozen on dry ice for storage at −80°C until processing for WB. Each brain region was homogenized in a Storm 24 magnetic Bullet Blender for 4 min at a speed setting of 4 (Next Advance Inc., Averill Park NY, United States), with 0.5 mm zirconium oxide beads in combination with 50–70 μl of Cell-lytic MT mammalian tissue extraction reagent (Sigma-Aldrich) containing 50 mM Tris buffer (pH 7.4), 2 mM EDTA, 5 mM EGTA, and 0.1% SDS. The homogenization buffer contained Complete (Roche) protease inhibitor cocktail and phosphatase inhibitor cocktails Type II and III (Sigma-Aldrich). Homogenates were then centrifuged at 16,400 rpm (4°C) for 15 min and supernatants were collected for subsequent SDS PAGE and WB analysis. For western blot analysis, homogenates were loaded at 20 μg for all brain regions. Brain samples were separated on a 4–12% Nu-Page Bis-Tris gel in MOPS buffer (Invitrogen, Carlsbad, CA) at 80 V for about 1 h followed by 150 V for the remaining 1 h. This was followed by transfer to a PVDF membrane (Invitrogen) at 30 V for 1 h. Samples were blocked at room temperature for 1 h (5% BSA in 1× TBST), then immunoblotted overnight at 4°C (5% BSA in 1× TBST) with primary antibodies specific to GLT1 (1:1000; Millipore), GS (1:2000; Abcam), and GAPDH (1:2000; Millipore). Following three washes (1× TBST), immunoblots were incubated with respective anti-guinea pig, anti-rabbit, and anti-mouse secondary antibodies (1:2000, Millipore) for 1 h at room temperature. Blots were visualized with the Radiance Peroxide Substrate (Azure Biosystems, Dublin, CA, United States), developed on a Azure Image Station scanner (Azure Biosystems, Dublin, CA, United States), and band optical density quantification was performed using NIH ImageJ software.

Quantitative Real-Time PCR (qRT-PCR)

Mice were euthanized by CO_2 asphyxiation and rapidly decapitated. The mPFC, striatum, and Hip were immediately isolated under a surgical microscope. Total RNA was isolated using the RNeasy Plus Mini kit (Qiagen; Cat No. 74134) and then reverse-transcribed by the Life Technologies Superscript III First-Strand Synthesis SuperMix kit (Cat No. 18080400) to obtain cDNA. The thermal cycling protocol for reverse transcription was 30 min at 50°C followed by 15 min at 95°C. Quantitative RT-PCR was performed on CFX 96 Touch^{TM} Real-Time System, C1000 Touch Thermal Cycler (Bio-Rad) using QuantiTect SYBR Green RT-PCR Kit (Qiagen; Cat No. 204143) and gene-specific primers (GLT1, Gls, GS, xCT, and GAPDH; Qiagen). The thermal cycling protocol for qRT-PCR was 40 amplification quantification cycles of 15 s at 94°C, followed by 10 s at 55°C, and then 30 s at 72°C. The targeted gene mRNA expression was normalized to GAPDH. Percentage changes were calculated by subtracting GAPDH Ct values from Ct values for the gene of interest using the $2^{-\Delta\Delta Ct}$ method (Livak and Schmittgen, 2001).

Behavioral Tests

Eight-week old male mice were used in the following behavioral observations. The behavioral experiments were performed between 9 AM and 5 PM. Mice were acclimated to the testing room for 30 min prior to each behavioral test. We used three independent batches of mice to avoid potential influences of behavioral tests while minimizing the use of animals. The batches are for (1) OFT, EPM, and metabolic chamber only, (2) TST and FST only, and (3) fear conditioning test. Within each batch, the behavioral tests were performed one week apart between tests.

Open Field Test

The ENV-510 test environment equipped with infrared beams and Activity Monitor (Med Associates) were used to evaluate motor activity in the open field test (OFT). Mice were placed in a Plexiglas box (27 cm × 27 cm × 20.3 cm) and allowed to explore the chamber for 1 h. The data was recorded by each beam break as one unit of exploratory activity using the activity monitoring software (Med Associates).

Elevated Plus Maze

Elevated plus maze (EPM) (Med Associates) was elevated 74 cm above the floor, which consisted of two open (35 cm × 6 cm) and two closed (35 cm × 6 cm × 22 cm) arms and a connecting central zone (6 cm × 6 cm) (Jia et al., 2014). Mice were placed in the center of the EPM, facing an open arm. Mice were allowed to freely explore the maze for 5 min. The amount of time spent in the open arms and the frequency of transitions between the open and closed arms were recorded and analyzed by the monitor software (Ethovision-XT, Noldus).

Metabolic Chamber

Mice were placed in the metabolic cages (Oxylet Pro, PanLab) for 24 h for habituation, followed by 48 h to measure oxygen consumption and energy expenditure. Mice were maintained at a

12 h light/dark cycle with lights on at 6 AM and off at 6 PM. Mice were free to access food and water. Energy expenditure, vCO_2, and vO_2 were obtained using a gas analyzer (Panlab, LE 405 Gas Analyzer) and metabolism software (Panlab, Metabolism).

Tail Suspension Test

Mice were suspended by the tail using adhesive Scotch tape, to a bar suspended 20 cm above the table (Jia et al., 2014). Individual mice were separated by a barrier and tests lasted for a total of 6 min. All sessions were video recorded. The total area moved, activity duration, and duration of time spent immobile were analyzed by Panlab Smart video tracking software (Harvard apparatus, Spain). Mice were considered immobile when they hung passively without any movement.

Forced Swim Test

Each mouse was placed in a 2-liter beaker filled with water (depth = 30 cm; temperature 24–25°C) (Jia et al., 2014). Mice were forced to swim 6 min, and the time spent immobile during the last 4 min was video recorded. The total area moved, activity duration, and duration of time spent immobile were analyzed by Panlab Smart video tracking software (Harvard apparatus, Spain). They were considered immobile when they stopped struggling, only moved slightly and occasionally to keep their nose above the water surface.

Fear Conditioning Test

The fear conditioning test was performed in four identical near infrared (NIR) Video Fear Conditioning Chambers (Med Associates, Fairfax, VT, United States), housed in a sound attenuating box. A speaker was located at the top of the right aluminum wall, and a house light at the top left aluminum wall. The floor grid was connected to an aversive stimulus. The behavior was recorded using a high speed firewire monochrome video camera with a near infrared pass filter on an 8 mm lens and analyzed using Video Freeze® software (Med Associates). On day 1, mice were trained with 2 min of habituation to the chamber followed by 5 pairings of 30 s tone (75 dB, 3000 kHz) with a shock occurring the last 2 s of the tone (0.4 mA) and a 2-min inter-trial interval (ITI 2 min). On day 2 for the contextual test, mice were only presented the same context (no sound, no shock) used on day 1 for training for identical duration as day 1. On day 3 for the cued test, a white floor grid cover and a black A-frame chamber insert were added to the chamber. Mice were subjected to 2 min of habituation to the chamber followed by five presentations of 30 s tones (75 dB, 3000 kHz) without a shock at a 2-min inter-trial interval (ITI 2 min). Freezing response (%) was measured for all training and testing days by Video Freeze® software (Med Associates). The chamber was cleaned with 70% ethanol and allowed to dry completely prior to testing in between each animal.

Statistical Analysis

All data are expressed as mean ± SEM (standard error of the mean). Analyses were conducted using GraphPad Prism (version 6.0). Unpaired two-tailed Student's *t*-test was used to compare the difference between two groups. Two-way repeated measures ANOVA was used to detect the effects of time and genotypes. ANOVA were followed by Tukey *post hoc* tests where interactions were found. Statistical significance was set at $p < 0.05$.

RESULTS

GFAP-Positive Astrocyte-Specific Deletion of GLT1

We generated GFAP-positive astrocyte-specific GLT1 knockout mice (**Figure 1A**) by crossing the floxed-GLT1 mice ($GLT1^{F/F}$) with the $GFAP^{cre/+}$ line, in which Cre recombinase was expressed selectively in the astrocytes. Control mice had a genotype of $GFAP^{cre/-}$; $GLT1^{F/F}$.

Among multiple brain regions, preclinical and clinical studies have identified three main brain regions, prefrontal frontal cortex, striatum, and hippocampus, as cores of emotional regulation (Kang et al., 2007; Di Benedetto et al., 2016; Ho et al., 2019). Thus, we sought to examine the GLT1 mRNA and protein expression in these three brain regions. Both Western blot (two−tailed unpaired *t*-test; mPFC: $t_5 = 6.619$, $p = 0.001$; Striatum: $t_5 = 9.264$, $p = 0.0002$; Hip: $t_5 = 13.19$, $p < 0.0001$; **Figures 1B,C**) and qRT-PCR (two−tailed unpaired *t*-test; mPFC: $t_5 = 4.890$, $p = 0.005$; Striatum: $t_5 = 9.794$, $p = 0.0002$; Hip: $t_6 = 18.52$, $p < 0.0001$; **Figure 1D**) analyses of GLT1 revealed a significant reduction of GLT1 protein and mRNA in the medial prefrontal cortex (mPFC), striatum, and hippocampus (Hip) of $GFAP^{cre/+}$; $GLT1^{F/F}$ mice. Immunohistochemical analysis confirmed astrocytic GLT1 deletion in mPFC, striatum, and Hip of 8-week-old $GFAP^{cre/+}$; $GLT1^{F/F}$ mice (**Figure 1E** and **Supplementary Figure S1**). To validate the specificity of Cre expression in the GFAP positive astrocyte, we employed GFAP-Cre virus to visualize the co-localization with different cell-markers with eGFP markers since Cre recombinase itself is difficult to detect with antibodies. We injected GFAP-Cre viruses to C57BL6/J mice and analyzed co-localization with astrocytic (GFAP)-, microglia (Iba1)-, and neuronal (NeuN)-antibodies, respectively. Our results demonstrated that Cre expression is uniquely co-localized with GFAP antibody (**Supplementary Figure S2A**), without noticeable co-localization with either Iba1 (**Supplementary Figure S2B**) or NeuN antibodies (**Supplementary Figure S2C**), supporting the specificity of Cre expression in GFAP-positive astrocytes.

In addition, we examined the expression of genes related to glutamate metabolism including glutaminase (GLS), glutamine synthetase (GS), and cystine-glutamate exchanger (xCT) in the mPFC, striatum and hippocampus brain regions by qRT-PCR. We found that the mRNA expression of these genes was similar between groups in the mPFC (two−tailed unpaired *t*-test; GLS: $t_6 = 0.308$, $p = 0.768$; GS: $t_6 = 1.267$, $p = 0.252$; xCT: $t_6 = 1.343$, $p = 0.228$; **Figure 2A**), striatum (two−tailed unpaired *t*-test; GLS: $t_6 = 0.394$, $p = 0.707$; GS: $t_6 = 0.897$, $p = 0.404$; xCT: $t_6 = 0.018$, $p = 0.986$; **Figure 2B**), and Hip (two−tailed unpaired *t*-test; GLS: $t_6 = 0.910$, $p = 0.398$; GS: $t_6 = 1.646$, $p = 0.151$; xCT: $t_6 = 0.355$, $p = 0.735$; **Figure 2C**). Following this, we confirmed the protein expression of GS using Western blot since GS is used as a astrocyte marker (Anlauf and Derouiche, 2013), which also

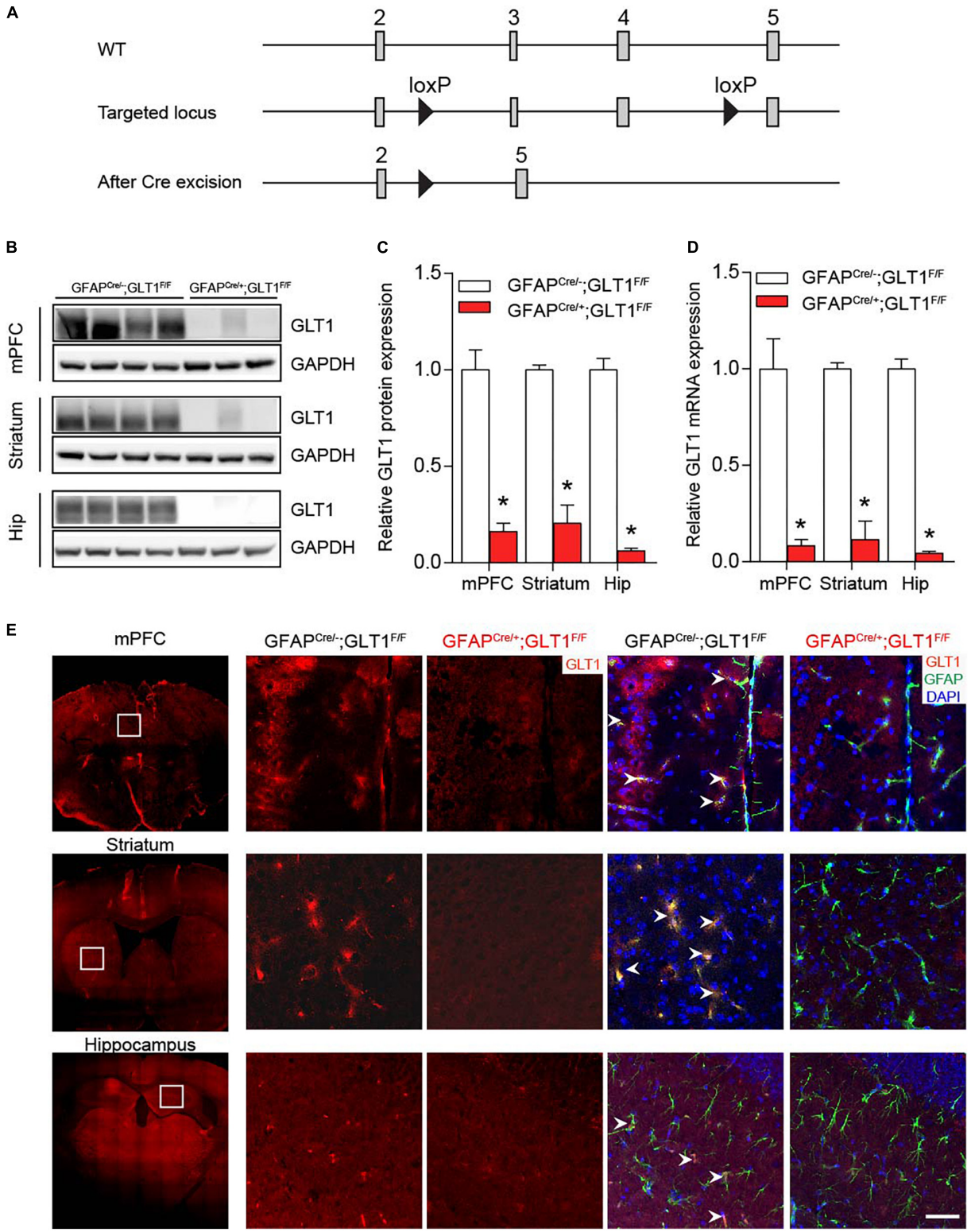

FIGURE 1 | Ablation of GLT1 in astrocytes. **(A)** Generation of astrocytic- GFAP$^{cre/+}$; GLT1$^{F/F}$ mice. **(B)** Western blot analysis of GLT1 in the medialprefrontal cortex (mPFC), striatum, and Hippocampus (Hip). GLT1 band intensities were normalized with those of GAPDH. **(C)** The quantitative analysis of western blot of 1B (n = 3,4). **(D)** Quantitative real-time PCR analysis of GLT1 in the mPFC, striatum, and Hip (n = 3,4). GLT1 mRNA level were normalized with those of GAPDH. **(E)** GLT1 immunohistochemistry for three brain regions including the mPFC, striatum, and hippocampus. Scale bar = 20 μm. All data are presented as mean ± SEM. Student's t-tests were used to compare GLT1 protein or mRNA levels of GFAP$^{cre/+}$; GLT1$^{F/F}$ mice and controls for each brain region. $^{*}p < 0.05$.

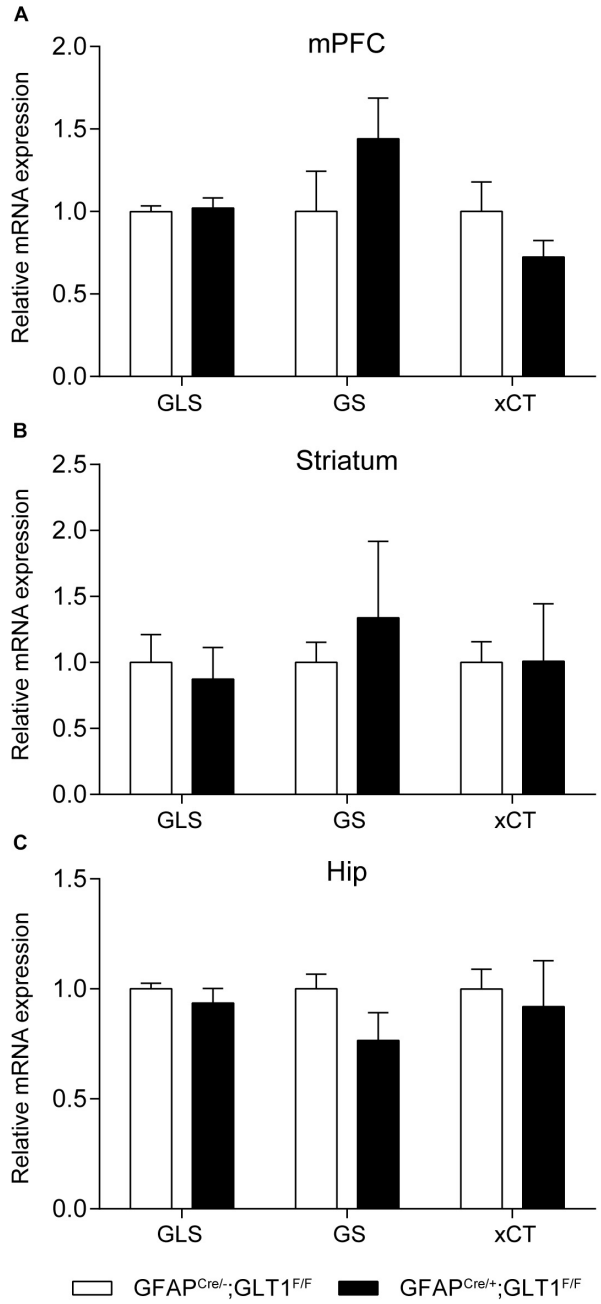

FIGURE 2 | Expression of glutamate-related genes in GFAP$^{cre/+}$; GLT1$^{F/F}$ mice. Glutamate-related genes expression including glutaminase (GLS), glutamine synthetase (GS), Cystine/glutamate antiporter (xCT) in GFAP$^{cre/+}$; GLT1$^{F/F}$ mice in mPFC **(A)**, striatum **(B)**, and Hip **(C)** by Quantitative real-time PCR analysis (n = 3,4). The interested mRNA levels were normalized with those of GAPDH. All data are presented as mean ± SEM. Student's t-tests were used to compare mRNA levels of GFAP$^{cre/+}$; GLT1$^{F/F}$ mice and controls for individual gene in each brain region. *$p < 0.05$.

revealed no difference between groups in the mPFC, striatum and Hip (two−tailed unpaired t-test; mPFC: t_5 = 1.148, p = 0.303; Striatum: t_5 = 0.565, p = 0.596; Hip: t_5 = 1.846, p = 0.124; **Supplementary Figures S3A,B**).

GFAP-Positive Astrocytic GLT1 Deficiency Showed Decreased Anxiety- and Depression-Like Behaviors

In order to investigate the basal locomotor activity, we employed the OFT. We revealed that the total distance traveled in the OFT was not different between GFAP$^{cre/+}$; GLT1$^{F/F}$ mice and controls (two−tailed unpaired t-test; t_{16} = 0.191, p = 0.851; **Figure 3A**). Two-way ANOVA analysis showed no significant difference between groups (two−way ANOVA; group effect: $F_{1,19}$ = 0.038, p = 0.848; **Supplementary Figure S4A**). To assess the performance of astrocytic GLT1 deficient mice under stress factor, we sought to investigate the anxiety-like behaviors. In the EPM, we found that the GFAP$^{cre/+}$; GLT1$^{F/F}$ mice spent more time in the open arms (two−tailed unpaired t-test; t_{25} = 2.492, p = 0.02; **Figure 3B**), and entered the open arms more frequently (two−tailed unpaired t-test; t_{22} = 2.284, p = 0.032; **Figure 3C**). In addition, we showed no significant difference between GFAP$^{cre/+}$; GLT1$^{F/F}$ mice and controls in closed arms entries (two−tailed unpaired t-test; t_{23} = 0.105, p = 0.918; **Supplementary Figure S4B**) and total entries (two−tailed unpaired t-test; t_{23} = 1.347, p = 0.191; **Supplementary Figure S4C**). Next, we examined whether the basal metabolic activity was affected by the deletion of GLT1 in astrocytes, as assessed by the metabolic chamber for a continuous 48 h. We found that GFAP$^{cre/+}$; GLT1$^{F/F}$ mice exhibited normal energy expenditure (two−tailed unpaired t-test; t_8 = 0.227, p = 0.826; **Figure 3D**), volume of CO_2 (two−tailed unpaired t-test; t_4 = 0.161, p = 0.880; **Figure 3E**), and volume of O_2 (two−tailed unpaired t-test; t_4 = 0.32, p = 0.736; **Figure 3F**) metabolism. Taken together, our results showed a decrease in anxiety-like behavior of astrocytic GLT1 deficiency without altering basal locomotion and caloric consumption.

Additionally, in the tail suspension test (TST), GFAP$^{cre/+}$; GLT1$^{F/F}$ mice showed less immobile time (two−tailed unpaired t-test; t_{22} = 2.823, p = 0.01; **Figure 4A**), had a longer activity duration (two−tailed unpaired t-test; t_{22} = 2.82, p = 01; **Figure 4B**), and also moved a greater area (two−tailed unpaired t-test; t_{22} = 3.319, p = 0.003; **Figure 4C**) compared to controls. Similarly, in the forced swim tests (FSTs), GFAP$^{cre/+}$; GLT1$^{F/F}$ mice exhibited less immobile time (two−tailed unpaired t-test; t_{24} = 4.668, $p < 0.0001$; **Figure 4D**), had a longer activity duration (two−tailed unpaired t-test; t_{24} = 4.691, $p < 0.0001$; **Figure 4E**), and also moved a greater area (two−tailed unpaired t-test; t_{24} = 2.379, p = 0.026; **Figure 4F**) compared to controls. Therefore, we conclude that reduced anxiety- or depression-like behaviors were found in GFAP$^{cre/+}$; GLT1$^{F/F}$ mice.

Reduced Freezing Response in the Fear Contextual and Cued Tests of GFAP-Positive Astrocytic GLT1 Deficient Mice

To examine the role of GFAP-positive astrocytic GLT1 in anxiety-related fear, we trained mice with five tone and foot shock pairing on day 1, and then we performed the contextual and cued fear memory tests on day 2 and day 3, respectively (**Figure 5A**).

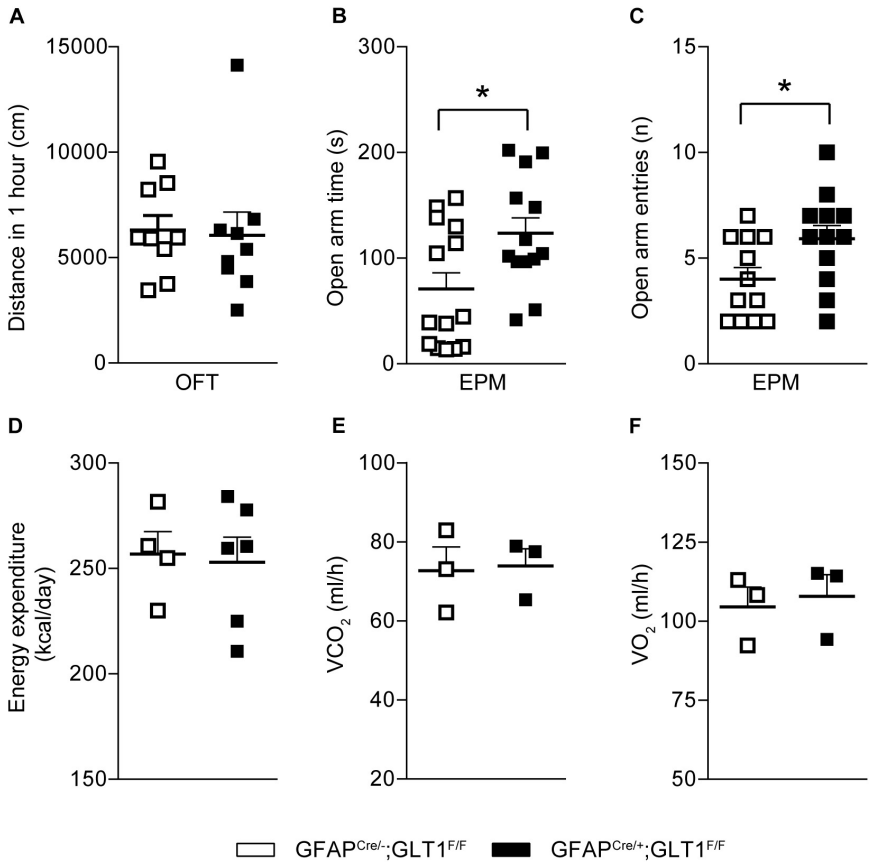

FIGURE 3 | Decreased anxiety-like behaviors in GFAP$^{cre/+}$; GLT1$^{F/F}$ mice. **(A)** Total distance (cm) moved in the open field of the 1 h in GFAP$^{cre/+}$; GLT1$^{F/F}$ mice and controls (n = 10–14). **(B)** Time spent in open arms of GFAP$^{cre/+}$; GLT1$^{F/F}$ and control mice in elevated plus maze (EPM) (n = 13,14). **(C)** Open arm entries of GFAP$^{cre/+}$; GLT1$^{F/F}$ mice and controls in EPM (n = 13,14). **(D)** Energy expenditure of GFAP$^{cre/+}$; GLT1$^{F/F}$ mice and controls in the metabolic chamber (n = 3). **(E)** Volume of CO_2 of GFAP$^{cre/+}$; GLT1$^{F/F}$ mice and controls in the metabolic chamber (n = 3). **(F)** Volume of O_2 of GFAP$^{cre/+}$; GLT1$^{F/F}$ mice and controls in the metabolic chamber (n = 3). All data are presented as mean ± SEM. Statistical significance was calculated by Student's t-test. *$p < 0.05$.

We revealed that GFAP$^{cre/+}$; GLT1$^{F/F}$ mice had comparable freezing responses across the training trials (Two way ANOVA; Interaction: $F_{4,26} = 0.368$, $p = 0.831$; **Figure 5B**. Two−tailed unpaired t-test; $t_{26} = 0.599$, $p = 0.554$; **Figure 5C**). Interestingly, in contextual test, we found significantly decreased freezing response in GFAP$^{cre/+}$; GLT1$^{F/F}$ mice compared to that of control mice (Two way ANOVA; group effect: $F_{1,26} = 9.265$, $p = 0.005$; **Figure 5D**. Two−tailed unpaired t-test; $t_{26} = 3.099$, $p = 0.005$; **Figure 5E**). Similarly, in cued test, GFAP$^{cre/+}$; GLT1$^{F/F}$ mice showed less freezing response compared to control (Two way ANOVA; group effect: $F_{1,24} = 5.771$, $p = 0.024$; **Figure 5F**. Two−tailed unpaired t-test; $t_{24} = 2.472$, $p = 0.021$; **Figure 5G**). These results suggested that the deletion of astrocytic GLT1 decreased response to fear memory without affecting fear memory acquisition, which may be associated with reduced anxiety.

DISCUSSION

This study demonstrates that GFAP-positive astrocyte-specific deletion of GLT1 reduced anxiety- and depression-like behaviors using a comprehensive array of behavioral tests including EPM, TST and FST. In addition, the freezing response in fear conditioning test was also reduced in GFAP-positive astrocytic GLT1 deficient mice. These results suggest that GFAP-positive astrocytic GLT1 is associated with emotional regulation such as anxiety, depression, and fear expression.

Previous studies have also demonstrated the association of GLT1 with emotional regulation including depression and anxiety. Chronic unpredictable stress associated with depressive behaviors, was found to decrease hippocampal GLT1 protein (Zhu et al., 2017). In stressed rodents, reduced GLT1 protein was found in the PFC of females, while reduced GLT1 was found in the striatum of males (Rappeneau et al., 2016). Hippocampal glial numbers show sex differences as well, and are reduced with prenatal stress and associated with emotional regulation and cognitive function in humans and rodents (Behan et al., 2011; Blacker et al., 2019). These studies together showed a reduction of GLT1 in PFC, striatum, and hippocampus associated with depressed status complicated by sex factors too. The administration of GLT1 selective inhibitor DHK induces robust antidepressant-like responses (Gasull-Camos et al., 2017),

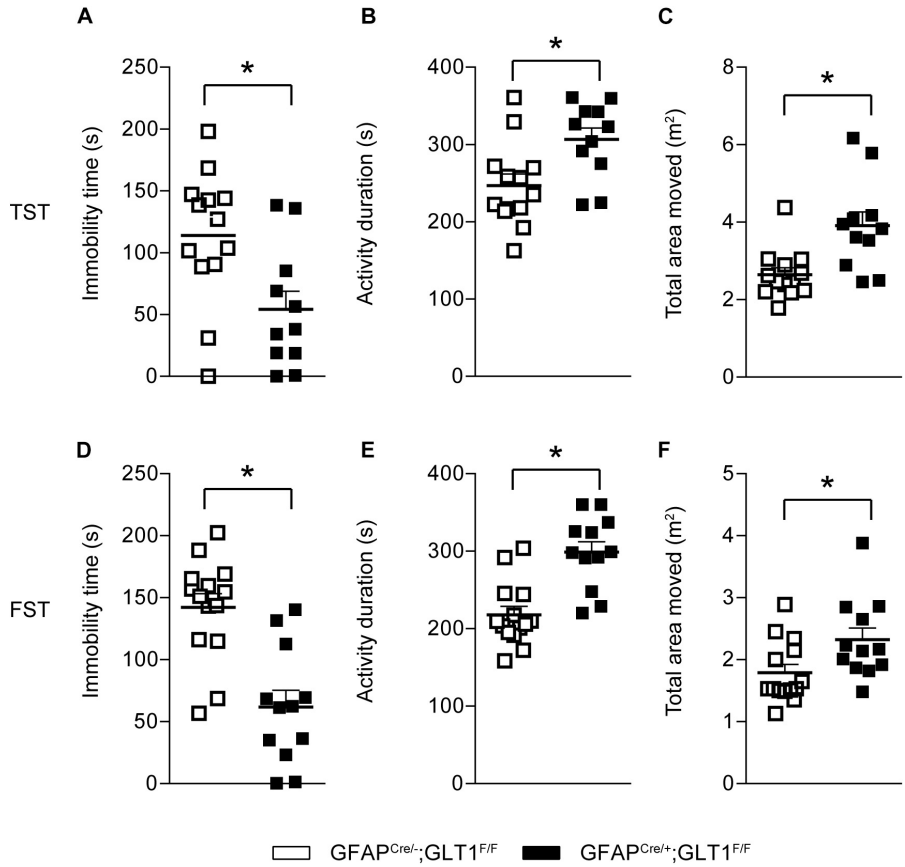

FIGURE 4 | Decreased depression-like behaviors in GFAP$^{cre/+}$; GLT1$^{F/F}$ mice. **(A)** Immobility time of GFAP$^{cre/+}$; GLT1$^{F/F}$ mice and controls in tail suspension test (TST) (n = 12–14). **(B)** Total activity duration in TST of GFAP$^{cre/+}$; GLT1$^{F/F}$ and control mice (n = 12–14). **(C)** Total area (m^2) moved in TST of GFAP$^{cre/+}$; GLT1$^{F/F}$ and control mice (n = 12–14). **(D)** Immobility time of GFAP$^{cre/+}$; GLT1$^{F/F}$ mice and controls in forced swim test (FST) (n = 12–14). **(E)** Total activity duration in FST of GFAP$^{cre/+}$; GLT1$^{F/F}$ mice and controls (n = 12–14). **(F)** Total area (m^2) moved in FST of GFAP$^{cre/+}$; GLT1$^{F/F}$ mice and controls (n = 12–14). All data are presented as mean ± SEM. Statistical significance was calculated by Student's t-test. *$p < 0.05$.

which is consistent with our findings of tail suspension and FSTs with the astrocytic GLT1 KO mice displaying a shorter immobile time. However, administration of DHK in the central amygdala induced depression and anxiety (John et al., 2015). Similarly, the deletion of GLT1 in habenula astrocytes was found to exacerbate depression-like behaviors (Cui et al., 2014). These studies suggest behavioral effects different from global GLT1 inhibition, which is expected since multiple brain regions and their interactions regulate depression and anxiety behaviors.

In addition, global GLT1 KO mice exhibited severe seizure activity with lethal spontaneous seizures and high glutamate levels (Tanaka et al., 1997). Petr et al. (2015) reported that only astrocytic but not neuronal deletion of GLT1 induced seizure activity, suggesting that the function of an astrocytic membrane protein is particularly important in the pathophysiology of multiple behaviors related to glutamatergic system. Furthermore, brain-region-specific deletion of GLT1 in the diencephalon, brainstem, and spinal cord could result in excess mortality and lethal spontaneous seizure (Sugimoto et al., 2018). Likewise, GLT1 dysfunction in the dorsal forebrain is involved in the pathogenesis of infantile epilepsy (Sugimoto et al., 2018). Overall, brain regional GLT1 plays individual roles, respectively, which might be an important future study direction.

As reported, we also observed a severe seizure phenotype for some mice starting around 3 months of age. Thus, to avoid confounding effects on our behavioral analysis, we exclude those mice showing seizure behaviors. The early stage of spontaneous seizures behavior in mice including grooming, jumping, and nodding etc. can be recognized as a type of repetitive behavior, which is highly correlated with anxiety (Crawley, 2007). It is believed that a slight elevation to glutamate levels may promote repetitive behaviors, whereas greater glutamate elevations more readily induce stereotypies and limbic seizure behaviors (McGrath et al., 2000; Chakrabarty et al., 2005).

In human studies, patients with anxiety and/or depression displayed enhanced fear memory and extinction (Cuthbert et al., 2003; Dibbets et al., 2015). In this study, astrocytic GLT1 deficiency did not affect the fear memory acquisition, suggesting that mice were able to adapt to the potential dangerous stimuli. In both contextual and cued fear memory tests, astrocytic GLT1 deficient mice showed less freezing response, indicating

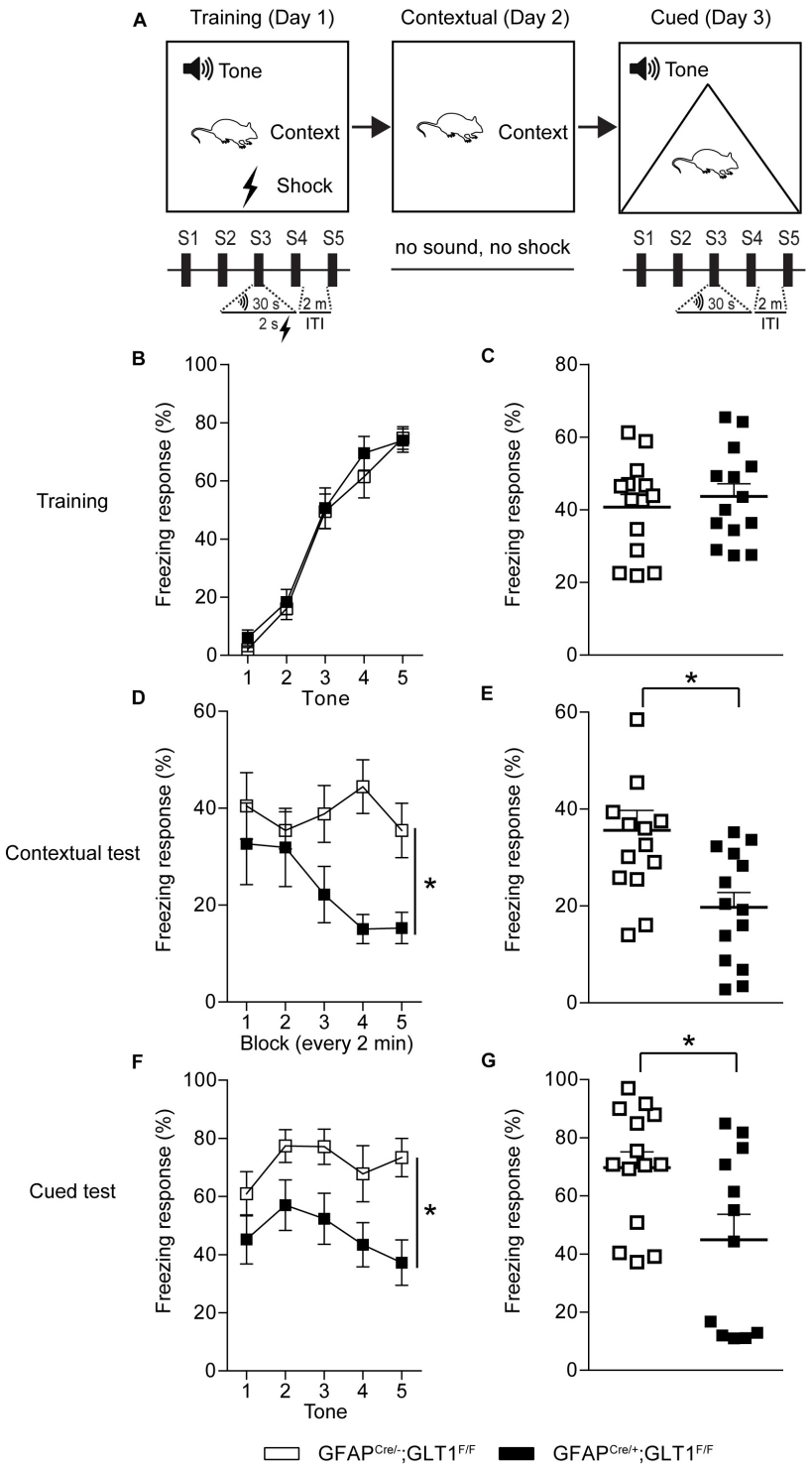

FIGURE 5 | Reduced freezing time of GFAP$^{cre/+}$; GLT1$^{F/F}$ mice in contextual and cued fear memory tests. **(A)** The experimental schedule for performing fear conditioning test. **(B)** The learning curve of fear conditioning showed the freezing response for each tone of GFAP$^{cre/+}$; GLT1$^{F/F}$ mice and controls during the training day 1 (n = 14). **(C)** The total freezing response of GFAP$^{cre/+}$; GLT1$^{F/F}$ mice and controls during the training day 1 (n = 10–14). **(D)** The curve of fear conditioning showed the freezing response for each block (every 2 min) of GFAP$^{cre/+}$; GLT1$^{F/F}$ mice and controls on day 2 during the contextual test (n = 14). **(E)** The freezing response of GFAP$^{cre/+}$; GLT1$^{F/F}$ mice and controls during the contextual test day 2 (n = 14). **(F)** The curve of fear conditioning showed the freezing response for each tone of GFAP$^{cre/+}$; GLT1$^{F/F}$ mice and controls on day 3 during the cued test (n = 14). **(G)** The freezing response of GFAP$^{cre/+}$; GLT1$^{F/F}$ mice and controls during cued test day 3 (n = 12–14). All data are presented as mean ± SEM. Statistical significance was calculated by Student's t-test in (C, E, and G), and by two-way repeated measures ANOVA with *post hoc* t-test for multiple comparisons in (B, D, and F). $^*p < 0.05$.

less fear toward the stimulus, which was also reflected by less anxiety-like behaviors in the EPM of astrocytic GLT1 deficient mice. Notably, similar decrement of anxiety was also found in a SPRED2-deficient mouse model of obsessive compulsive disorder (OCD) (Ullrich et al., 2018). However, the reduced anxiety-like behaviors in OCD mice is controversial to traditional knowledge that anxiety or depression is commonly comorbid with OCD. Interestingly, previous investigations reported that astrocytic GLT1 deficiency also showed excessive repetitive behaviors in astrocytic GLT1 deficiency, which might be caused by glutamatergic hyperactivity (Aida et al., 2015; Katz et al., 2019) since the high glutamate level was found in mice with both global and astrocytic deletion of GLT1 (Tanaka et al., 1997; Petr et al., 2015). In current study, we also do not exclude a possibility that GLT1 deletion in astrocyte might induce repetitive behavior since we saw the slightly increased locomotor activity in first 10 min of the OFT, and also the total entries in the EPM, which might be a sign of that they were repetitively checking the new environment. Overall, we concluded that the less anxious and excessive repetitive behavior might be revealed in GFAP-positive astrocytic GLT1 deficient mice. However, the contribution of GLT1 in regard to OCD, anxiety, and depressive behavior remains highly controversial.

In summary, this investigation suggests that GFAP-positive astrocyte-specific deletion of GLT1 decreased anxiety- and depression-like behaviors, which may provide novel insights toward the underlying mechanisms of mood related psychiatric disorders.

DATA AVAILABILITY STATEMENT

The datasets generated for this study are available on request to the corresponding author.

ETHICS STATEMENT

The animal study was reviewed and approved by the Mayo Clinic Institutional Animal Care and Use Committee.

AUTHOR CONTRIBUTIONS

D-SC was responsible for the study concept and design and drafted the manuscript. Y-FJ performed all the data analysis, also helped draft the manuscript and interpret the findings. Y-FJ and KW contributed to the acquisition of animal data. AH and LP assisted with the data analysis and interpretation of findings. Y-FJ, KW, AH, LP, MB, and D-SC provided critical revision of the manuscript for important intellectual content. All authors critically reviewed content and approved final version for publication.

FUNDING

This work was funded by the Samuel C. Johnson for Genomics of Addiction Program at Mayo Clinic, the Ulm Foundation, the Godby Foundation, and National Institute on Alcohol Abuse and Alcoholism (AA018779).

ACKNOWLEDGMENTS

We thank all members of the D-SC's laboratory for interest, help and comments. We thank Dr. Niels C. Danbolt for providing $GLT^{F/F}$ mice. We also thank Dr. Seungwoo Kang, and summer undergraduate students, Joyce Yang and Nicoli Carneiro. This work was funded by the Samuel C. Johnson for Genomics of Addiction Program at Mayo Clinic, the Ulm Foundation, the Godby Foundation, and National Institute on Alcohol Abuse and Alcoholism (AA018779).

SUPPLEMENTARY MATERIAL

The Supplementary Material for this article can be found online at: https://www.frontiersin.org/articles/10.3389/fnbeh.2020.00057/full#supplementary-material

FIGURE S1 | The specificity of GFAP-Cre line. **(A)** GLT1 immunohistochemistry for three brain regions including the mPFC, striatum, and hippocampus. Higher magnification of images showed from white boxes in **(B)**. Scale bar = 20 μm. **(B)** A higher magnification of GLT1 immunohistochemistry for three brain regions including the mPFC, striatum, and hippocampus. Scale bar = 10 μm.

FIGURE S2 | The specificity of GFAP-Cre line. **(A)** The mapping of GFAP-Cre-positive cells in the striatum using astrocytic (anti-GFAP antibody), **(B)** microglia (anti-Iba1 antibody), **(C)** and neuronal (anti-NeuN antibody) markers, respectively. White arrows indicate the typical co-localization or no co-localization. Scale bar = 50 μm.

FIGURE S3 | The protein expression of GS in $GFAP^{cre/+}$; $GLT1^{F/F}$ mice. **(A)** Western blot analysis of GS in the mPFC, striatum, and Hippocampus. GS band intensities were normalized with those of GAPDH. **(B)** The quantitative analysis of western blot of **(A)** (n = 3,4). All data are presented as mean ± SEM. Statistical significance was calculated by Student's t-test in **(B)**.

FIGURE S4 | No difference in total locomotion of $GFAP^{cre/+}$; $GLT1^{F/F}$ mice in open field and elevated plus maze tests. **(A)** Distance moved (cm) in the open field of every 10 min in $GFAP^{cre/+}$; $GLT1^{F/F}$ mice and controls (n = 9,12). **(B)** Closed arm entries of $GFAP^{cre/+}$; $GLT1^{F/F}$ mice and controls in EPM (n = 12,13). **(C)** Total entries of $GFAP^{cre/+}$; $GLT1^{F/F}$ mice and controls in EPM (n = 12,13). All data are presented as mean ± SEM. Statistical significance was calculated by Student's t-test in **(B,C)**, and by two-way repeated measures ANOVA with *post hoc* t-test for multiple comparisons in **(A)**.

REFERENCES

Aida, T., Yoshida, J., Nomura, M., Tanimura, A., Iino, Y., Soma, M., et al. (2015). Astroglial glutamate transporter deficiency increases synaptic excitability and leads to pathological repetitive behaviors in mice. *Neuropsychopharmacol. Offi. Pub. Am. Coll. Neuropsychopharmacol.* 40, 1569–1579. doi: 10.1038/npp.2015.26

Anlauf, E., and Derouiche, A. (2013). Glutamine synthetase as an astrocytic marker: its cell type and vesicle localization. *Front. Endocrinol. (Lausanne)* 4:144. doi: 10.3389/fendo.2013.00144

Banasr, M., and Duman, R. S. (2008). Glial loss in the prefrontal cortex is sufficient to induce depressive-like behaviors. *Biol. Psychiatry* 64, 863–870. doi: 10.1016/j.biopsych.2008.06.008

Behan, A. T., van den Hove, D. L., Mueller, L., Jetten, M. J., Steinbusch, H. W., Cotter, D. R., et al. (2011). Evidence of female-specific glial deficits in the hippocampus in a mouse model of prenatal stress. *Eur. Neuropsychopharmacol.* 21, 71–79. doi: 10.1016/j.euroneuro.2010.07.004

Bergink, V., van Megen, H. J. G. M., and Westenberg, H. G. M. (2004). Glutamate and anxiety. *Eur. Neuropsychopharmacol.* 14, 175–183. doi: 10.1016/S0924-977x(03)00100-107

Blacker, C. J., Millischer, V., Webb, L. M., Ho, A. M. C., Schalling, M., Frye, M. A., et al. (2019). EAAT2 as a research target in bipolar disorder and unipolar depression: a systematic review. *Mol. Neurops.* 1–16. doi: 10.1159/000501885 *Vol Q*.

Chakrabarty, K., Bhattacharyya, S., Christopher, R., and Khanna, S. (2005). Glutamatergic dysfunction in OCD. *Neuropsychopharmacol. Off. Pub. Am. Coll. Neuropsychopharmacol.* 30, 1735–1740. doi: 10.1038/sj.npp.1300733

Cobb, J. A., Simpson, J., Mahajan, G. J., Overholser, J. C., Jurjus, G. J., Dieter, L., et al. (2013). Hippocampal volume and total cell numbers in major depressive disorder. *J. Psychiatr. Res.* 47, 299–306. doi: 10.1016/j.jpsychires.2012.10.020

Cortese, B. M., and Phan, K. L. (2005). The role of glutamate in anxiety and related disorders. *CNS Spectr.* 10, 820–830. doi: 10.1017/s1092852900010427

Crawley, J. N. (2007). Mouse behavioral assays relevant to the symptoms of autism. *Brain Pathol.* 17, 448–459. doi: 10.1111/j.1750-3639.2007.00096.x

Cui, W., Mizukami, H., Yanagisawa, M., Aida, T., Nomura, M., Isomura, Y., et al. (2014). Glial dysfunction in the mouse habenula causes depressive-like behaviors and sleep disturbance. *J. Neurosci. Off. J. Soc. Neurosci.* 34, 16273–16285. doi: 10.1523/JNEUROSCI.1465-14.2014

Cuthbert, B. N., Lang, P. J., Strauss, C., Drobes, D., Patrick, C. J., and Bradley, M. M. (2003). The psychophysiology of anxiety disorder: fear memory imagery. *Psychophysiology* 40, 407–422. doi: 10.1111/1469-8986.00043

Czeh, B., and Di Benedetto, B. (2013). Antidepressants act directly on astrocytes: evidences and functional consequences. *Eur. Neuropsychopharmacol.* 23, 171–185. doi: 10.1016/j.euroneuro.2012.04.017

Davis, M., and Myers, K. M. (2002). The role of glutamate and gamma-aminobutyric acid in fear extinction: clinical implications for exposure therapy. *Biol. Psychiatry* 52, 998–1007. doi: 10.1016/s0006-3223(02)01507-x

Di Benedetto, B., Malik, V. A., Begum, S., Jablonowski, L., Gomez-Gonzalez, G. B., Neumann, I. D., et al. (2016). Fluoxetine requires the endfeet protein aquaporin-4 to enhance plasticity of astrocyte processes. *Front. Cell Neurosci.* 10:8. doi: 10.3389/fncel.2016.00008

Dibbets, P., van den Broek, A., and Evers, E. A. (2015). Fear conditioning and extinction in anxiety- and depression-prone persons. *Memory* 23, 350–364. doi: 10.1080/09658211.2014.886704

Gasull-Camos, J., Tarres-Gatius, M., Artigas, F., and Castane, A. (2017). Glial GLT-1 blockade in infralimbic cortex as a new strategy to evoke rapid antidepressant-like effects in rats. *Trans. Psychiatry* 7:e1038. doi: Artn E103810.1038/Tp.2017.7

Gregorian, C., Nakashima, J., Le Belle, J., Ohab, J., Kim, R., Liu, A., et al. (2009). Pten deletion in adult neural stem/progenitor cells enhances constitutive neurogenesis. *J. Neurosci.* 29, 1874–1886. doi: 10.1523/Jneurosci.3095-08.2009

Ho, A. M., Winham, S. J., Armasu, S. M., Blacker, C. J., Millischer, V., Lavebratt, C., et al. (2019). Genome-wide DNA methylomic differences between dorsolateral prefrontal and temporal pole cortices of bipolar disorder. *J. Psychiatr. Res.* 117, 45–54. doi: 10.1016/j.jpsychires.2019.05.030

Jia, Y. F., Song, N. N., Mao, R. R., Li, J. N., Zhang, Q., Huang, Y., et al. (2014). Abnormal anxiety- and depression-like behaviors in mice lacking both central serotonergic neurons and pancreatic islet cells. *Front. Behav. Neurosci.* 8:325. doi: Artn32510.3389/Fnbeh.2014.00325

Jia, Y. F., Vadnie, C. A., Ho, A. M., Peyton, L., Veldic, M., Wininger, K., et al. (2019). Type 1 equilibrative nucleoside transporter (ENT1) regulates sex-specific ethanol drinking during disruption of circadian rhythms. *Addict. Biol.* e12801. doi: 10.1111/adb.12801

John, C. S., Sypek, E. I., Carlezon, W. A., Cohen, B. M., Ongur, D., and Bechtholt, A. J. (2015). Blockade of the GLT-1 transporter in the central nucleus of the amygdala induces both anxiety and depressive-like symptoms. *Neuropsychopharmacology* 40, 1700–1708. doi: 10.1038/npp.2015.16

Kang, H. J., Adams, D. H., Simen, A., Simen, B. B., Rajkowska, G., Stockmeier, C. A., et al. (2007). Gene expression profiling in postmortem prefrontal cortex of major depressive disorder. *J. Neurosci.* 27, 13329–13340. doi: 10.1523/JNEUROSCI.4083-07.2007

Katz, M., Corson, F., Keil, W., Singhal, A., Bae, A., Lu, Y., et al. (2019). Glutamate spillover in *C. elegans* triggers repetitive behavior through presynaptic activation of MGL-2/mGluR5. *Nat. Commun.* 10:1882.

Kessler, R. C., Berglund, P., Demler, O., Jin, R., Koretz, D., Merikangas, K. R., et al. (2003). The epidemiology of major depressive disorder - Results from the national comorbidity survey replication (NCS-R). *JAMA J. Am. Med. Assoc.* 289, 3095–3105. doi: 10.1001/jama.289.23.3095

Kiryk, A., Aida, T., Tanaka, K., Banerjee, P., Wilczynski, G. M., Meyza, K., et al. (2008). Behavioral characterization of GLT1 (+/−) mice as a model of mild glutamatergic hyperfunction. *Neurotox. Res.* 13, 19–30. doi: 10.1007/Bf03033364

Livak, K. J., and Schmittgen, T. D. (2001). Analysis of relative gene expression data using real-time quantitative PCR and the $2^{-\Delta\Delta C_T}$ method. *Methods* 25, 402–408. doi: 10.1006/meth.2001.1262

Mathews, D. C., Henter, I. D., and Zarate, C. A. (2012). Targeting the glutamatergic system to treat major depressive disorder: rationale and progress to date. *Drugs* 7, 1313–1333. doi: 10.2165/11633130-000000000-00000

McGrath, M. J., Campbell, K. M., Parks, C. R., and Burton, F. H. (2000). Glutamatergic drugs exacerbate symptomatic behavior in a transgenic model of comorbid Tourette's syndrome and obsessive-compulsive disorder. *Brain Res.* 877, 23–30. doi: 10.1016/s0006-8993(00)02646-9

Mineka, S., Watson, D., and Clark, L. A. (1998). Comorbidity of anxiety and unipolar mood disorders. *Annu. Rev. Psychol.* 49, 377–412. doi: 10.1146/annurev.psych.49.1.377

Murrough, J. W., Abdallah, C. G., and Mathew, S. J. (2017). Targeting glutamate signalling in depression: progress and prospects. *Nat. Rev. Drug Discov.* 16, 472–486. doi: 10.1038/nrd.2017.16

Petr, G. T., Sun, Y., Frederick, N. M., Zhou, Y., Dhamne, S. C., Hameed, M. Q., et al. (2015). Conditional deletion of the glutamate transporter GLT-1 reveals that astrocytic GLT-1 protects against fatal epilepsy while neuronal GLT-1 contributes significantly to glutamate uptake into synaptosomes. *J. Neurosci. Off. J. Soc. Neurosci.* 35, 5187–5201. doi: 10.1523/JNEUROSCI.4255-14.2015

Pines, G., Danbolt, N. C., Bjoras, M., Zhang, Y. M., Bendahan, A., Eide, L., et al. (1992). Cloning and expression of a rat-brain L-glutamate transporter. *Nature* 360, 464–467. doi: 10.1038/360464a0

Rajkowska, G., and Miguel-Hidalgo, J. J. (2007). Gliogenesis and glial pathology in depression. *CNS Neurol. Disord. Drug Targets* 6, 219–233. doi: 10.2174/187152707780619326

Rajkowska, G., and Stockmeier, C. A. (2013). Astrocyte pathology in major depressive disorder: insights from human postmortem brain tissue. *Curr. Drug Targets* 14, 1225–1236. doi: 10.2174/13894501131349990156

Rappeneau, V., Blaker, A., Petro, J. R., Yamamoto, B. K., and Shimamoto, A. (2016). Disruption of the glutamate-glutamine cycle involving astrocytes in an animal model of depression for males and females. *Front. Behav. Neurosci.* 10:231. doi: 10.3389/fnbeh.2016.00231

Su, Z. Z., Leszczyniecka, M., Kang, D. C., Sarkar, D., Chao, W., Volsky, D. J., et al. (2003). Insights into glutamate transport regulation in human astrocytes: Cloning of the promoter for excitatory amino acid transporter 2 (EAAT2). *Proc. Natl. Acad. Sci. U.S.A.* 100, 1955–1960. doi: 10.1073/pnas.0136555100

Sugimoto, J., Tanaka, M., Sugiyama, K., Ito, Y., Aizawa, H., Soma, M., et al. (2018). Region-specific deletions of the glutamate transporter GLT1 differentially affect seizure activity and neurodegeneration in mice. *Glia* 66, 777–788. doi: 10.1002/glia.23281

Sunderland, M., Mewton, L., Slade, T., and Baillie, A. J. (2010). Investigating differential symptom profiles in major depressive episode with and without generalized anxiety disorder: true co-morbidity or symptom similarity? *Psychol. Med.* 40, 1113–1123. doi: 10.1017/S0033291709991590

Tanaka, K., Watase, K., Manabe, T., Yamada, K., Watanabe, M., Takahashi, K., et al. (1997). Epilepsy and exacerbation of brain injury in mice lacking the glutamate transporter GLT-1. *Science* 276, 1699–1702. doi: 10.1126/science.276.5319.1699

Tovote, P., Fadok, J. P., and Luthi, A. (2015). Neuronal circuits for fear and anxiety. *Nat. Rev. Neurosci.* 16, 317–331. doi: 10.1038/nrn3945

Ullrich, M., Weber, M., Post, A. M., Popp, S., Grein, J., Zechner, M., et al. (2018). OCD-like behavior is caused by dysfunction of thalamo-amygdala circuits and

upregulated TrkB/ERK-MAPK signaling as a result of SPRED2 deficiency. *Mol. Psychiatry* 23, 444–458. doi: 10.1038/mp.2016.232

Walker, D. L., and Davis, M. (2002). The role of amygdala glutamate receptors in fear learning, fear-potentiated startle, and extinction. *Pharmacol. Biochem. Behav.* 71, 379–392. doi: 10.1016/s0091-3057(01)00698-690

Zbozinek, T. D., Rose, R. D., Wolitzky-Taylor, K. B., Sherbourne, C., Sullivan, G., Stein, M. B., et al. (2012). Diagnostic overlap of generalized anxiety disorder and major depressive disorder in a primary care sample. *Depress. Anxiety* 29, 1065–1071. doi: 10.1002/da.22026

Zhu, X., Ye, G., Wang, Z., Luo, J., and Hao, X. (2017). Sub-anesthetic doses of ketamine exert antidepressant-like effects and upregulate the expression of glutamate transporters in the hippocampus of rats. *Neurosci. Lett.* 639, 132–137. doi: 10.1016/j.neulet.2016.12.070

Conflict of Interest: D-SC is a scientific advisory board member to Peptron Inc. and Peptron Inc. had no role in the preparation, review, or approval of the manuscript; nor the decision to submit the manuscript for publication.

The remaining authors declare no biomedical financial interests or potential conflicts of interest.

Advantages of publishing in Frontiers

OPEN ACCESS
Articles are free to read for greatest visibility and readership

FAST PUBLICATION
Around 90 days from submission to decision

HIGH QUALITY PEER-REVIEW
Rigorous, collaborative, and constructive peer-review

TRANSPARENT PEER-REVIEW
Editors and reviewers acknowledged by name on published articles

Frontiers
Avenue du Tribunal-Fédéral 34
1005 Lausanne | Switzerland

Visit us: www.frontiersin.org
Contact us: frontiersin.org/about/contact

REPRODUCIBILITY OF RESEARCH
Support open data and methods to enhance research reproducibility

DIGITAL PUBLISHING
Articles designed for optimal readership across devices

FOLLOW US
@frontiersin

IMPACT METRICS
Advanced article metrics track visibility across digital media

EXTENSIVE PROMOTION
Marketing and promotion of impactful research

LOOP RESEARCH NETWORK
Our network increases your article's readership